INTERNATIONAL SCIENTIFIC JOURNAL

GEOGRAPHICA PANNONICA

Impact factor: 1.2 | CiteScore: 2.8

Volume 29, Issue 2 (June 2025)

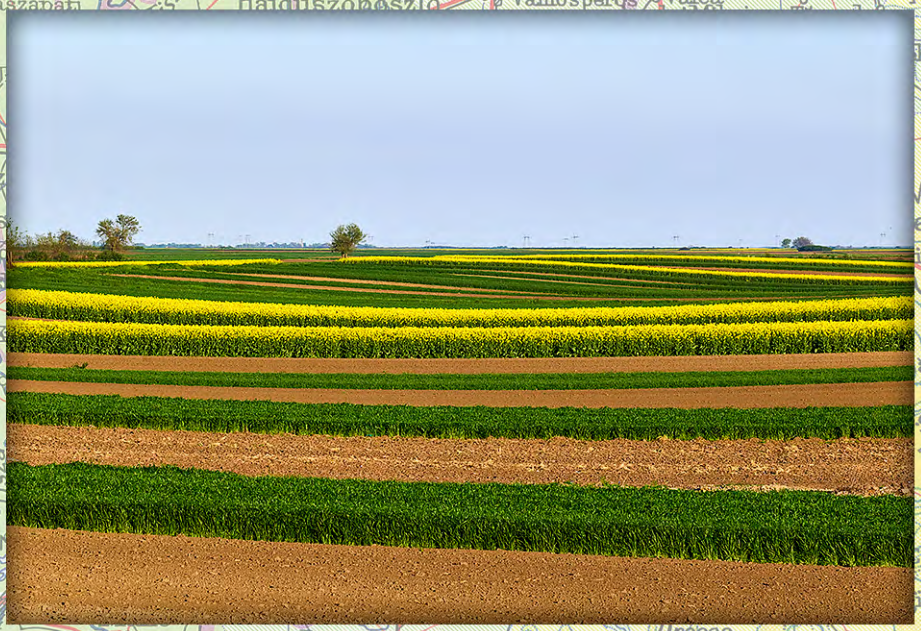

UNIVERSITY OF NOVI SAD, FACULTY OF SCIENCES

DEPARTMENT OF GEOGRAPHY, TOURISM AND HOTEL MANAGEMENT

UNIVERSITY OF NOVI SAD | FACULTY OF SCIENCES
DEPARTMENT OF GEOGRAPHY, TOURISM & HOTEL MANAGEMENT

INTERNATIONAL SCIENTIFIC JOURNAL

GEOGRAPHICA PANNONICA

Impact factor: 1.2 | CiteScore: 2.8

Volume 29, Issue 2, June 2025

ISSN 0354-8724 (hard copy) | ISSN 1820-7138 (online) | UDC 05:91(497.1)=20

ISSN 0354-8724 (hard copy) | ISSN 1820-7138 (online) | UDC 05:91(497.1)=20

INTERNATIONAL SCIENTIFIC JOURNAL

GEOGRAPHICA PANNONICA

UNIVERSITY OF NOVI SAD | FACULTY OF SCIENCES | DEPARTMENT OF GEOGRAPHY, TOURISM & HOTEL MANAGEMENT

EDITORIAL OFFICE

Faculty of Sciences
Department of Geography, Tourism and Hotel Management
Trg Dositeja Obradovića 3, 21000 Novi Sad, Serbia
tel. +381 21 450-105
fax +381 21 459-696
Official site: www.dgt.uns.ac.rs

CONTACTS

Lazar Lazić, PhD, full professor
Department of Geography, Tourism and Hotel Management, Serbia, lazar.lazic@dgt.uns.ac.rs

Dragan Milošević, teaching assistant
Department of Geography, Tourism and Hotel Management, Serbia, dragan.milosevic@dgt.uns.ac.rs

Official mail of the Journal
gpscijournal@dgt.uns.ac.rs

Internet portal
www.dgt.uns.ac.rs/pannonica.html

Instructions to authors
www.dgt.uns.ac.rs/pannonica/instructions.htm

Contents

INTERNATIONAL SCIENTIFIC JOURNAL
GEOGRAPHICA PANNONICA
Volume 29, Issue 2, 65–83 (June 2025)
Journal homepage: http://www.dgt.uns.ac.rs/en/homepage/pannonica/

Spatio-temporal Analysis of Drought Trends Recorded during the Wettest Months in the Mouhoun-Comoé Basin in Burkina Faso (Africa): an Analysis using Z-score and Linear Regression

Joseph Yameogo[A]

[A] *Ziniaré University Center/ Joseph Ki-ZERBO University: Ouagadougou, Burkina Faso; ORCID JY: 0000-0001-5879-2723*

KEYWORDS

- drought
- soil moisture
- z-score
- linear regression
- correlation
- Mouhoun-Comoé basin
- Africa

ABSTRACT

Meteorological drought is a natural phenomenon that occurs when there is insufficient rainfall over a more or less prolonged period. In West African countries, and particularly in Burkina Faso, this situation undermines agricultural systems. Knowledge of the spatio-temporal trends of drought is essential for optimal management of water resources and effective planning of sustainable agricultural activities. The aim of this study is the analysis of the spatio-temporal trends of drought in the Mouhoun-Comoé basin in Burkina Faso. To this end, the study used CHIRPS rainfall data in raster and CSV file form for July and August, as well as soil moisture (0-10 cm) at 1-, 2- and 3-month scales for the period 1994-2024. The data were analysed using the z-score index, linear regression and correlation. The study shows that the upward trend in drought oscillates between extreme drought and mild drought. The decade 1994-2004 was characterised by extreme drought, followed by a decrease in drought throughout the basin during the decade 2005-2014. Finally, in the decade 2015-2024, a phase of high humidity was observed throughout the basin. Drought trends have had an impact on soil moisture levels, particularly in the valleys of the basin. This situation has a negative impact on agricultural production in the basin. This situation is forcing farmers to use crops that have more or less water tolerance in order to cope with the drought.

Introduction

Climate change is the most pressing global threat (Sharma et al., 2021). It directly or indirectly affects our ecosystem (Kulikov et al., 2014). Sea ice, lakes and coastal ecosystems are severely affected (Grimm et al., 2013). Agriculture, livestock systems and human livelihoods are also being undermined globally (Ghahramani & Moore, 2016; Habtemariam et al., 2017; Duku et al., 2018; Batool et al., 2019). Watersheds and their ecosystems are not spared. Indeed, a change in the services provided by watershed ecosystems has been observed in the Po basin (Italy) and the Red basin (Vietnam), as shown by Pham et al. (2019). In Iran, in the Sirvan basin, the cumulative effect of land use changes, reduced rainfall and increased temperatures has affected the amount of water in the basin. The same is true for the Yellow River basin in China (Yang et al., 2021). In the alpine basin of the Tibetan Plateau in China, vegetation dynamics

* Corresponding author: Joseph Yameogo; josephyameogo10@gmail.com

doi: 10.5937/gp29-56313

Received: January 27, 2025| Revised: May 6, 2025| Accepted: May 20, 2025

around the basin have been observed as a result of climate change and drought (D'uo et al., 2021). The Heihe basin is more affected by rainfall variability, which causes variations in water runoff (Liu et al., 2024). Xiong et al. (2024) finds that 168 of the world's basins are experiencing spatio-temporal changes. According to the authors, the upward trends in the standardised precipitation index (PSI) are more pronounced in basins in arid zones than in those in humid zones. At the same time, six basins are identified as hot spots with an increase in PSI between 2003 and 2021: the Don, Yellow, Haihe, Rio Grande, Sao Francisco and Ganges basins.

In Africa, watersheds and their ecosystems are the economic lungs of vulnerable populations. However, they are also subject to the vagaries of climate variability, which has a negative impact on the water resources of these catchments (Séne et al., 2024). In southern Africa, basins such as the Limpopo, the Orange, the Okavango and the Zambezi have been severely affected by the level of drought (Abiodun et al., 2019). Burkina Faso has four of them. Most hydro-agricultural and hydro-electric schemes depend directly on them. However, two of them are of vital importance: the Mouhoun and Nakambè basins. All the country's dams, large and small, have been built on these two basins. For this reason, several studies have been carried out on these two basins. For example, studies have focused on climate variability in the Vranso sub-basin, where climate variability has affected surface water levels (Yameogo & Sawadogo, 2024), and on its consequences for water flow in the Mouhoun sub-basin (Zouré et al., 2023), as well as in the Nakambè basin (Gbohoui et al., 2020). Other studies are looking at the dynamics of land use, which is reducing water resources in the Nakambè basin.

In the Sudano-Sahelian and Sudanese zones of Burkina Faso, rainfall remains the main source of water. Climatic variability, reflected in both increasing and decreasing rainfall (Yameogo, 2025), causes frequent droughts, and the basins are not spared. The wettest periods, particularly July and August, record an average rainfall of 130 mm per year, while August records an average of 230 mm per year. However, most studies focus on the Nakambè basin and use the Standardised Precipitation Index (SPI) and the Standardised Precipitation Evapotranspiration Index (SPEI) (Fowé et al., 2023). Some studies compare the SPI and SPEI to assess the level of drought in the Massili (Nakambè) basin (Guira et al., 2022; Bontogho et al., 2023), while others use the Effective Reconnaissance Drought Index to assess the level of drought in the Massili basin (Bontogho et al., 2024). The Mouhoun-Comoé is the largest watershed in Burkina Faso and its surface water resources are used by millions of people for socio-economic activities and food production. However, few studies have been carried out in this basin to understand the spatio-temporal evolution of droughts and their impact on soil moisture. Analysis of spatial and temporal trends in drought provides useful information for effective planning and management of water resources. Therefore, studying the evolution of these phenomena during the wettest months is essential for identifying the negative effects of climate change.

The aim of this study is to analyze the spatio-temporal trends of droughts during the two wettest months (July and August) in the Mouhoun-Comoé watershed in Burkina Faso. Its uniqueness lies in the use of CHIRPS data, which are used for drought monitoring by the Famine Early Warning Systems Network (FEWS NET) of the United States Agency for International Development (USAID).

Materials and methods

Study area

The Mouhoun-Comoé basin was selected for this study. The Mouhoun basin covers an area of 113,896 km^2 and includes all or part of the Boucle du Mouhoun, Cascades, Centre-West, Hauts-Bassins, North and South-West regions. Figure 1 shows the location of the study area.

According to the Köppen classification, the Mouhoun-Comoé basin is divided into two climatic zones: the hot semi-arid climate and the tropical savanna climate (Figure 2).

The average rainfall is 240 mm per year in August and 178 mm per year in July. Temperatures vary from July to August. In August, the maximum temperature is 35.45°C, the average temperature is 27.23°C, and the minimum temperature is 23°C. In July, maximum temperatures are 32°C, average temperatures are 28°C, and minimum temperatures are 23.72°C. Figure 3 below shows rainfall and temperatures in the Mouhoun-Comoé watershed.

Climate data and Normality

Monthly rainfall (for July and August) and soil moisture data for July and August for the study area were obtained from the Climate Hazards Group InfraRed Precipitation with Stations (CHIRPS) database on the US Agency for International Development Famine Early Warning Systems Network (FEWS NET) website. CHIRPS was developed by the Climate Hazards Group at the University of California, Santa Barbara (UCSB) and the US Geological Survey (USGS) (Aksu & Akgul, 2020).

The data and products will be available for download from the Famine Early Warning Systems Network (FEWS NET) data portal (Senay et al., 2023; Senay et al., 2015). The latter provides z-score data and soil moisture in the form

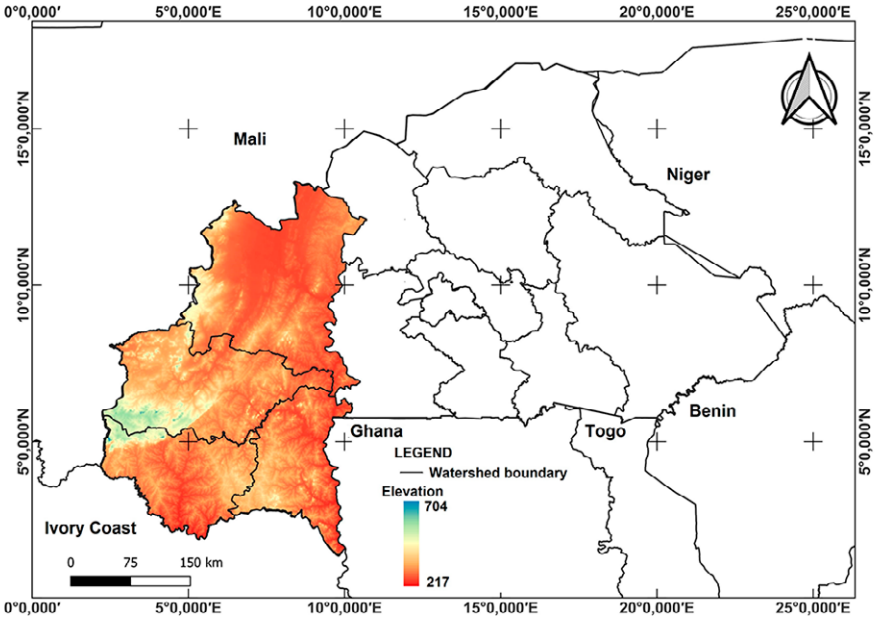

Figure 1. Geographical location of the Mouhoun-Comoé basin

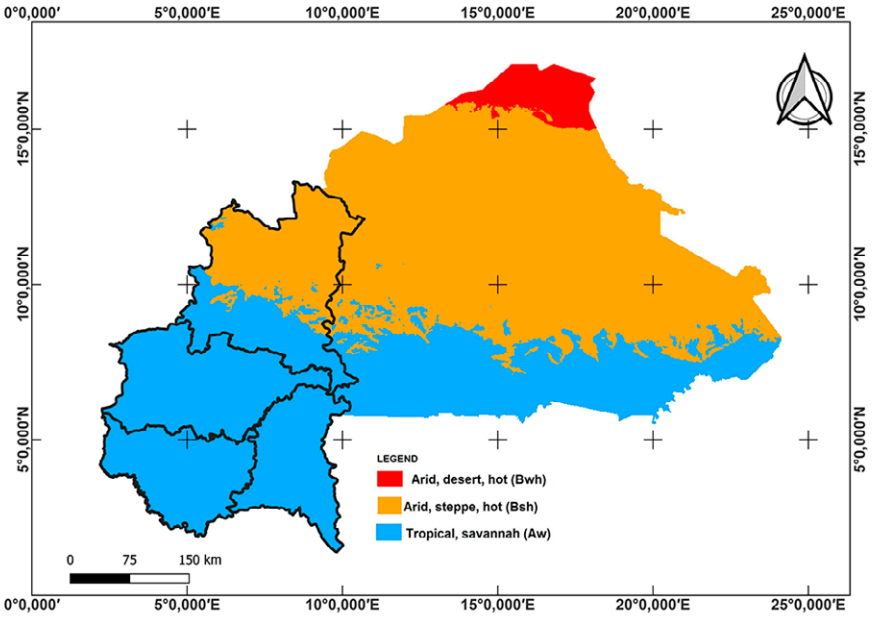

Figure 2. Watershed climate zone according to Köppen classification 1991-2020

of raster and CSV files for the Excel spreadsheet for the period 1994-2024, with time steps of one month, two months and three months. CHIRPS extends from 50° South latitude to 50° North latitude (and all longitudes) and covers the period from 1981 to the present, integrating satellite imagery at 0.05° resolution and in situ station data to produce gridded precipitation time series (Funk et al., 2015).The CHIRPS data have undergone a rigorous evaluation procedure that integrates satellite records and in situ station data, making them highly reliable for scientific research, including climate studies, hydrological modelling and agricultural assessments (Poste et al., 2024). As a result, several studies have used them, notably to characterise the spatio-temporal variability of drought in the Cauto basin in Cuba (Tran et al., 2024) or the Seyhan basin in southern Turkey (Orieschnig & Cavus, 2024). In Ethiopia, Alemu and Bawoke (2020) used CHIRPS data to analyse spatio-temporal rainfall trends in the Amhara region. The same is true for the study in Iraq (Ahmad et al., 2021) and Congo (Ahana et al., 2024). The z-score statistics are on a monthly scale, for the

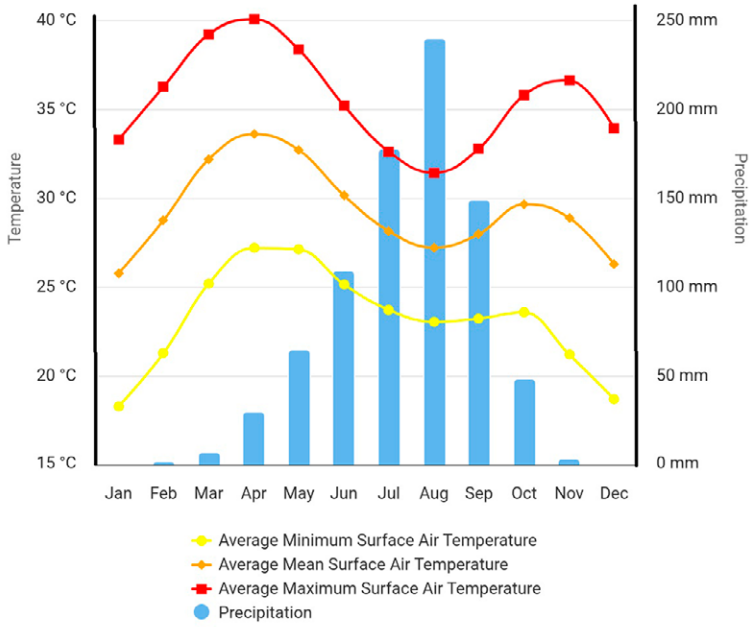

Figure 3. Precipitation and temperatures in the Mouhoun-Comoé basin

period 1994-2024, and are time series data. Checking the normality of the data therefore makes it possible to indicate the appropriate method of analysis. To this end, three normality tests have been used, as follows Shapiro-Wilk, Anderson-Darling and Lilliefors. The null hypothesis (H_0) of these tests is that the data follow a normal distribution. The alternative hypothesis (H_a) is that the data do not follow a normal distribution.

Method of trend analysis

In this study, linear regression was used to analyze the trend of the Z-score over the period from 1994 to 2024.

Linear regression

Linear regression is a parametric method that requires normality of the data and can be used to identify a linear trend and estimate its magnitude (U.S. Environmental Protection Agency, 2009). Linear regression analysis is commonly used to identify trends in climate variables over long periods of time (Feidas et al., 2004; Ghebrezgabher et al., 2016; Yaméogo & Sawadogo, 2024; Yanogo & Yameogo, 2023). Regression is based on the assumption that there is a linear relationship between the dependent variable (Y) and the independent variable (X). The linear regression equation is defined as follows (Rawlings et al., 1998):

$$Y = Ax + b \tag{1}$$

Where, Y indicates a dependent variable, x indicates an independent variable, and A is the slope of the line and b is the Y-intercept constant (Compaoré & Yaméogo, 2024).

If the direction coefficient of the trend equation is greater than zero, less than zero or equal to zero, then the sign of the trend is positive (increasing), negative (decreasing) or there is no trend (no change) respectively (Gavrilov et al., 2015).

Pearson's correlation coefficient

Pearson's correlation coefficient measures the strength of the linear relationship between two variables. If there is a strong linear relationship, the correlation coefficient is close to 1 or –1, and 0 means no linear relationship (U.S. Environmental Protection Agency, 2009, Athanasiou et al., 2017). It indicates the direction and 'strength' of the trend. A positive value of r indicates an increasing linear trend and a negative value indicates a decreasing linear trend. The trend is 'strong' if the absolute value of r varies between 0.6 and 0.8. The correlation coefficient r between the two variables X and Y is called the Pearson correlation and is calculated as follows (Athanasiou et al., 2017):

$$r = \frac{\sum_{i=1}^{n}\left(x_i - \bar{x}\right) - \left(y_i - \bar{y}\right)}{\sqrt{\sum_{i=1}^{n}\left(x_i - \bar{x}\right)^2}\sqrt{\sum_{i=1}^{n}\left(y_i - \bar{y}\right)^2}} \tag{2}$$

$$\text{Where, } \bar{y} = (1/n)\left(\sum_{i=1}^{n} y_i\right), \text{ and } \bar{x} = (1/n)\left(\sum_{i=1}^{n} x_i\right)$$

Statistical Z-Score (Z-Score)

The statistical Z score, or standard score, is used as another drought index (Wu et al., 2001). The standard score method is a simple approach that is used to standardise

a set of data on the basis of its mean value and its standard deviation (Careto et al., 2024). It can be calculated by subtracting the long-term mean from an individual rainfall value, then dividing the difference by the standard deviation (Noor et al., 2020). The Z-score indicates the number of standard deviations that a rainfall value is above or below the mean (Dogan et al., 2012). The calculations are straightforward and can be performed on a variety of time scales. The Z-score applies to both dry and wet periods and, like the SPI, tolerates gaps in the data (WMO, 2016). Its mathematical formula is as follows (Wu et al., 2001):

$$Z_{score} = \frac{x_{ij} - \mu_i}{\sigma_i} \quad (3)$$

where Z is the symbol for the standard score, xij is precipitation of j month for period i, is mean, is standard deviation. Table 1 below shows the different interpretations of Z-score.

Table 1. Different interpretations of Z-score

Z-score value	Drought/wetness condition
≤-2.0	Extreme drought
-1.90 to -1.50	Severe drought
-1.49 to -1.00	Moderate drought
-0.99 to 0.99	Mild drought
≥1.0	Normal wet condition

Source: Noor et al. (2020)

In addition, the raster z-score data were interpolated using QGIS 3.4 software to obtain the spatial evolution of z-scores in the Mouhoun-Comoé basin. Figure 4 below provides a summary of the data and methods used in the study.

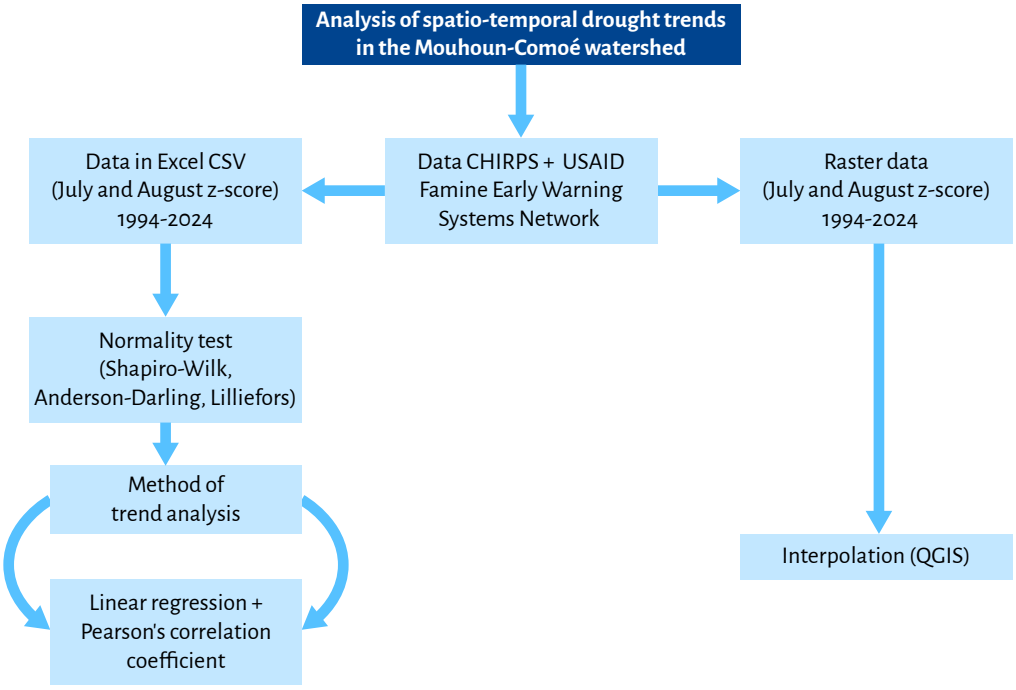

Figure 4. Outline the Data and Methods Used in the Study

Results and Discussion

Data normality over the 1994-2024 period

Overall, the data show a normal distribution over the period 1994-2024 (Table 2).

Temporal analysis of annual drought trends in the Mouhoun-Comoé basin

The analysis of drought in the wettest months of the basin shows an increasing trend over the period 1994-2024, as indicated by the positive leading coefficients (Figure 5).

Figure 5 shows an upward trend in the z-score, which indicates that conditions have become wetter and less dry over time. However, the trend remains weak and very weak. In fact, July and August in 1 month, 2 months and 3 months have very high correlation coefficients r=0.301, which shows a weak trend.

Table 2. Normality of data extracted from CHIRPS over the period 1994-2024

Test of normality	July			August		
	1month	2month	3month	1month	2month	3month
Shapiro-Wilk test	0.937	0.933	0.960	0.986	0.971	0.972
P-value	0.07	0.054	0.284	0.948	0.545	0.585
Alpha threshold	5%	5%	5%	5%	5%	5%
null hypothesis (H_0)	X	X	X	X	X	X
Alternative hypothesis (H_a)	-	-	-	-	-	-
Anderson-Darling	0.522	0.688	0.455	0.194	0.267	0.222
P-value	0.142	0.065	0.251	0.886	0.663	0.812
Alpha threshold	5%	5%	5%	5%	5%	5%
null hypothesis (H_0)	X	X	X	X	X	X
Alternative hypothesis (H_a)	-	-	-	-	-	-
Lilliefors test	0.125	0.140	0.112	0.092	0.090	0.077
P-value	0.250	0.778	0.626	0.731	0.502	0.914
Alpha threshold	5%	5%	5%	5%	5%	5%
null hypothesis (H_0)	X	X	X	X	X	X
Alternative hypothesis (H_a)	-	-	-	-	-	-

Source: CHIRPS, 1994-2024, X=Accepted, - : no Accepted

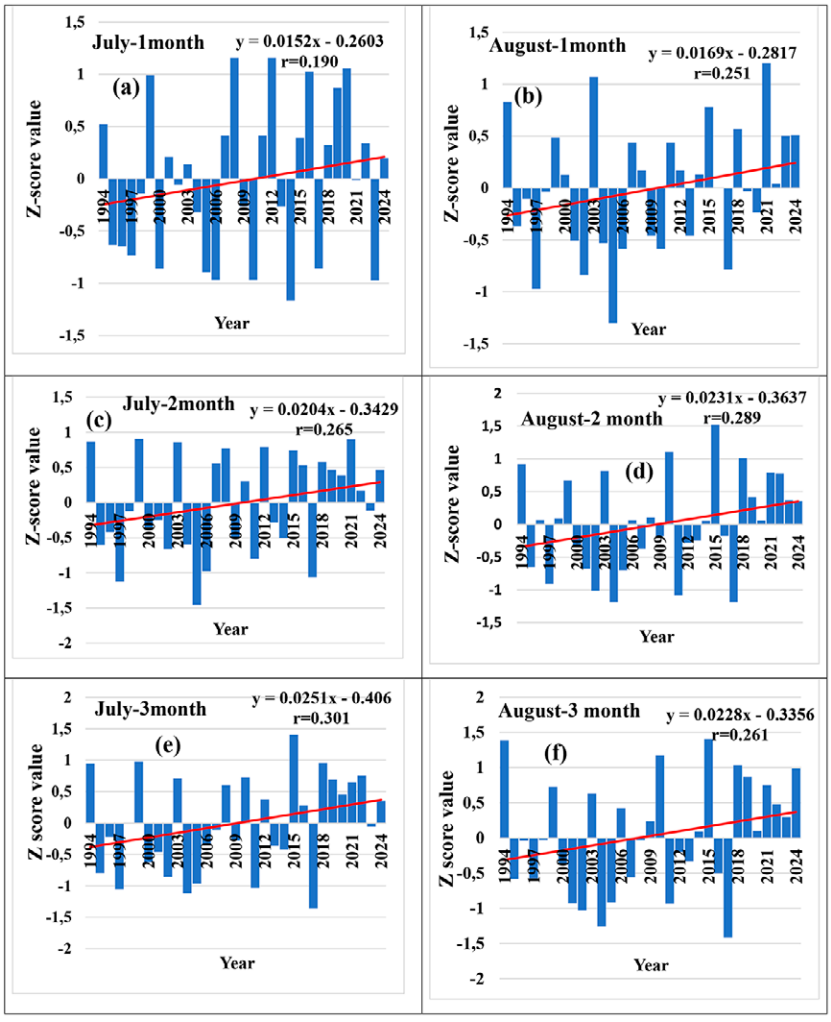

Figure 5. Time trend of z-score at different scales between 1994 and 2024

Temporal analysis of the ten-year trend of drought in the Mouhoun-Comoé basin

In Figure 6a, the decade 1994-2004 shows a decreasing z-score trend in August and an increasing trend in July. Conversely, the 2005-2014 decade shows an upward trend in both wet months. However, the decade 2015-2024 shows a differentiated trend, with an upward trend in August and a downward trend in July. Figure 6b shows an upward trend in the Z-score over 2 and 3 months in the decades 1994-2004 and 2005-2014 (in appendix). However, a downward trend is observed at the 1-month, 2-month and 3-month scales for the 1994-2004, 2005-2014 and 2015-2024 periods. The correlation coefficient r remains very low, indicating a slight increase. Overall, the 1994-2004 decade saw a period of moderate drought in the basin during the rainy months (July and August). In contrast, the 2005-2014 decade was characterised by a normal wet phase in the area. This situation continued during the decade 2015-2024.

Spatial analysis of drought trends in the Mouhoun-Comoé basin

- Annual spatial trend of drought in the two wettest months

Figure 7a below shows a significant change in droughts in the Mouhoun-Comoé basin between 1994 and 2024. On a 1-month scale, extreme drought is observed in July in the south-eastern part of the basin and wetness in the north-western part. In August, however, the north-western zone remains wet (z-score = 1.87) in 2015-2024, while the rest of the basin experiences moderate drought (z-score = -0.95). On a two-month scale, a zone of severe drought is marked from the south-east to the centre of the basin in July (figure b in appendix). A wet phase was also observed towards the far north-west of the basin. In August, the moisture continued to spread from the far north-west to the west. The rest of the basin also experienced a period of light to moderate drought. Over a three-month

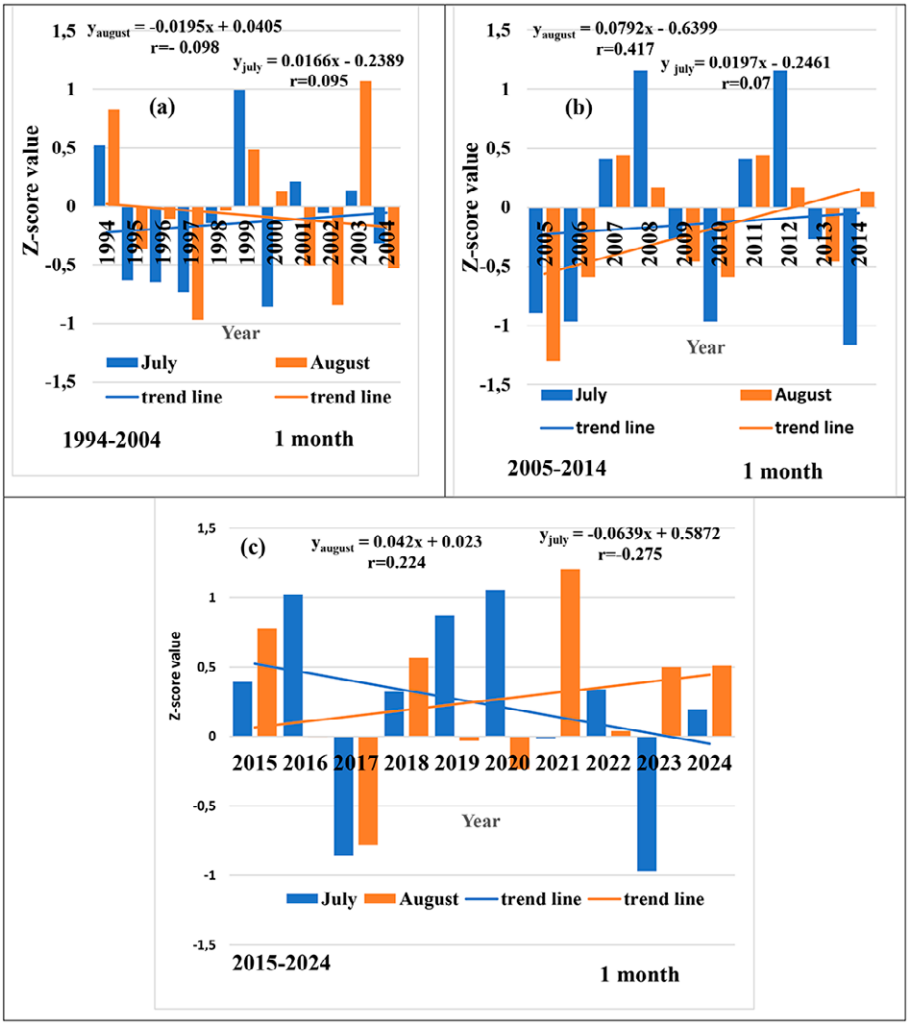

Figure 6a. Decadal evolution of Z-score on a one-month scale

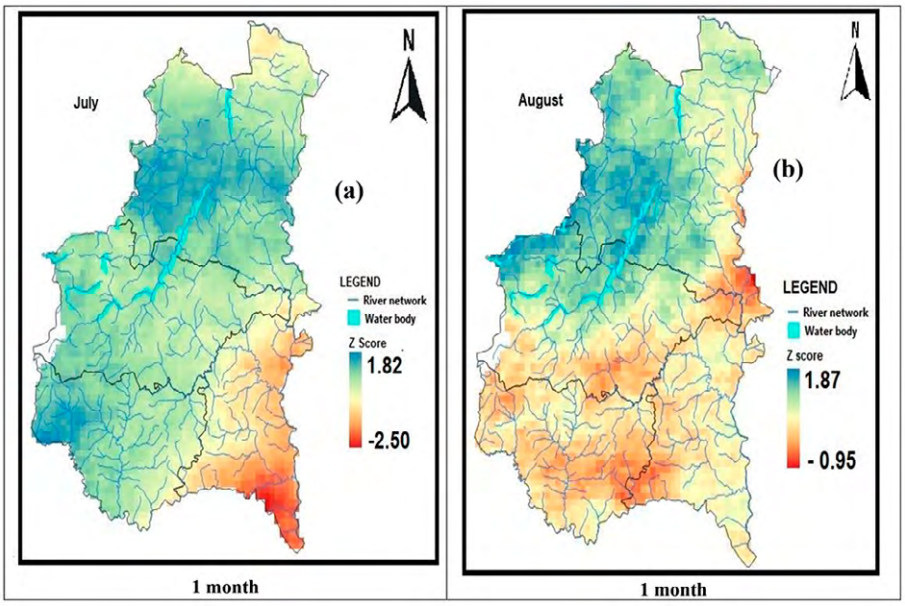

Figure 7a. Spatial trend in drought on a monthly scale over the period 1994-2024

period, the basin is almost completely dry, with the exception of the northern zone (in appendix). In August, an area of high humidity moves westwards and moderate to extreme drought affects the rest of the basin.

Spatial analysis of drought trends in the Mouhoun-Comoé basin over a ten-year period

- the case of July on a 1-month, 2-month and 3-month scale

July's drought was highly variable in the Mouhoun-Comoé basin. On a monthly scale, the spatial evolution of the drought is oriented towards the south-west of the basin. The decade 1994-2004 was characterised by extreme drought (z-score of -2.06 in Figure 8a.g) in the west and centre of the basin. Only the extreme southwest of the basin was wet. In Figure 8a.h, mild drought prevailed over most of the basin, except in the north. Figure 8a.i shows a trend towards normalisation of moisture across the basin. However, there is a slight drought in the southwest.

Figure 8b.j shows that over a two-month period, drought occurs in the west and centre of the basin. Other areas of the basin fluctuate between mild and moderate drought. Figure 8b.k shows a drought zone with a z-score between 0.80 and -1.8. The areas that were in extreme drought in Figure 8b.j have become wetter in Figure 8b.k (in appendix). This trend continues in Figure 8b.l, but with a slight

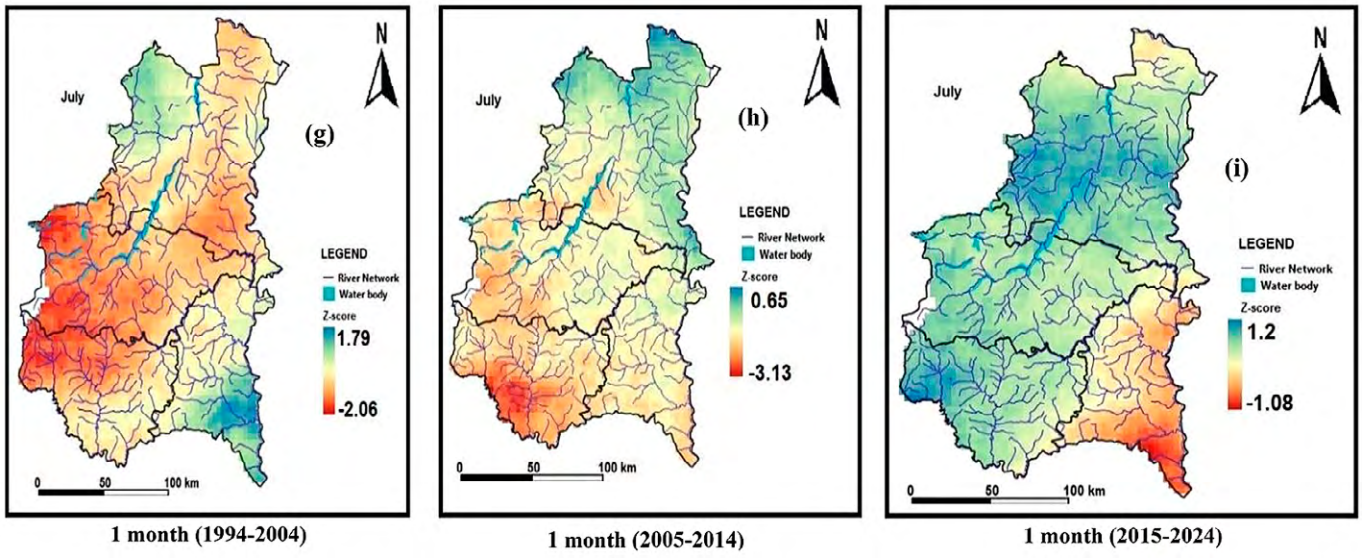

Figure 8a. Ten-year spatial trend in July drought for the period 1994-2024

concentration of drought in the south-western part of the basin (in appendix).

Figure 8b.m shows that over a three-month period, the western and central parts of the basin are in a dry phase. However, the south-western zone is in a wet phase. The drought is receding, with only one occurrence in the southwestern part of the basin (Figure 8b.n) (in appendix). The wet phase is observed towards the west and northwest of the basin, while a moderate drought phase is observed in the south-western part of the basin during the period 2015-2024.

- the case of August on a 1-month, 2-month and 3-month scale

Figures 9a.p, q and r show the spatial evolution of drought in August, the wettest month in Burkina Faso. During the decade 1994-2004, the western, northern and central parts of the basin experienced moderate to extreme drought. In the decade 2005-2014, these drought zones decreased and are now located in the north and south-west of the basin. Finally, in the period 2015-2024, drought, which has become moderate, continues to decrease and is now located in the south and extreme southwest of the basin.

Careto et al., 2024; Ogunrinde et al., 2025). It varies considerably in space and time across the basin. The work of Ndehedehe et al. (2016) confirms the same trends. The authors found a variable trend in the SPI index over the period 1979-2013 in the Volta basin, which includes the Mouhoun-Comoé basin. This temporal trend is punctuated by periods of more or less severe wetness and drought. Other studies carried out in the Mouhoun sub-basin in Burkina Faso have found similar results. Compaoré and Yameogo (2024) and Yaméogo and Sawadogo (2024) found a temporal evolution of the SPI index characterised by wet and dry phases between 1980 and 2021.

Drought in the Mouhoun-Comoé basin and its impact on soil moisture in the valleys

Drought affects soil moisture in the basin. There is a strong correlation between z-score and soil moisture (depth 0-10 cm) in July and August for the period 1994-2024. The correlation coefficients vary between 0.85 and 0.58, with high to very high levels of significance (p-value varies between 0.002 and 0.0013). The correlations are weaker and insignificant for July on a 2-month scale and for August on a

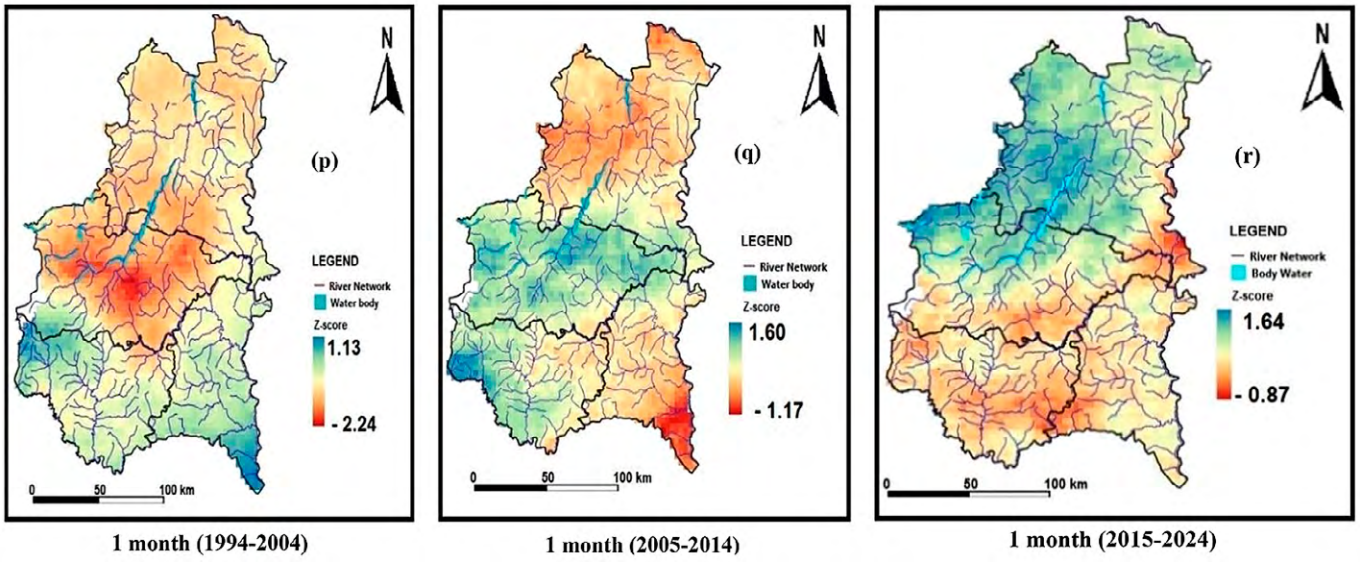

Figure 9a. Ten-year spatial trend in August drought between 1994 and 2024

A similar trend can be seen in Figures 9b.s, t, u (in appendix). The situation changes when we move to the three-month scale. Extreme drought dominates in the western and central parts of the basin, while the rest of the basin experiences moderate drought. Only the extreme southern and south-western parts of the basin experience a wet phase.

Meteorological drought is a category of long-term natural disasters that develops gradually and is caused by periods of abnormally low precipitation (Kumari et al., 2023;

3-month scale. Overall, the upward trend in drought is reflected in soil moisture in the Mouhoun-Comoé catchment. The trend lines also show an upward trend for July on a 1-month scale and for August on a 1-month, 2-month and 3-month scale. Table 3 below shows the different correlation coefficients and directional coefficients at different time scales.

Table 3 shows that drought affects the Mouhoun-Comoé basin during the wettest months (July and August). This situation affects the valleys, especially the Sourou

Table 3. Strong correlation between the z-score and the soil moisture at different scales in the catchment area for the period from 1994 to 2024

Soil moisture-z-score	correlation coefficient	p-Value	Relationship
Soil moisture 10 cm-z-score (1 month july)	0.835	**0.003**	Very significant
Soil moisture 10 cm-z-score (1 month august)	-0.69	**0.027**	Significant
Soil moisture 10 cm-z-score (2 month july)	0.163	0.65	Non-Significant
Soil moisture 10 cm-z-score (2 month august)	0.85	**0.002**	Very significant
Soil moisture 10 cm-z-score (3 month july)	0.86	**0.002**	Very significant
Soil moisture 10 cm-z-score (3 month august)	0.58	**0.078**	Weak Significant

valley in the extreme north of the watershed. In this valley, more than 3,800 ha of land have been developed out of an estimated potential of 30,000 ha. These cultivated areas are farmed by rural residents and privately by more than 3,000 producers organised in eleven agricultural cooperatives, four producer groups and seventeen agricultural entrepreneurs or agribusinesses. However, extreme to moderate droughts are common in this valley, with direct consequences for soil moisture (Figure 10a.a, b,c).

Figure 10a.a, b,c, and figure 10b.d,e,f (in appendix) shows that there is a strong change in soil moisture in the Sourou Valley. In fact, the decade 1994-2004 and 2015-2024 is interrupted by relatively positive soil moisture in the Sourou Valley for the month of July. However, in the period 2005-2014, the valley is affected by a decrease in soil moisture. This situation could affect the crops grown by the rural population. Soil moisture in August also varies from decade to decade. In 1994-2004, soil moisture in the valley was low. In the period 2005-2014, an improvement in moisture was observed. The period 2015-2024 is characterized by a high level of soil moisture in the Sourou valley, reflecting a decade in the wet phase. The other valleys in the Mouhoun-Comoé basin are also affected by drought (Figure 11a.a.b).

Figure 11a shows that the decade 1994-2004 (Figure 11a.a) and the decade 2005-2014 (Figure 11a.b) are characterized by a decrease in soil moisture in the valleys for the month of July. However, the 2015-2024 decade is charac-

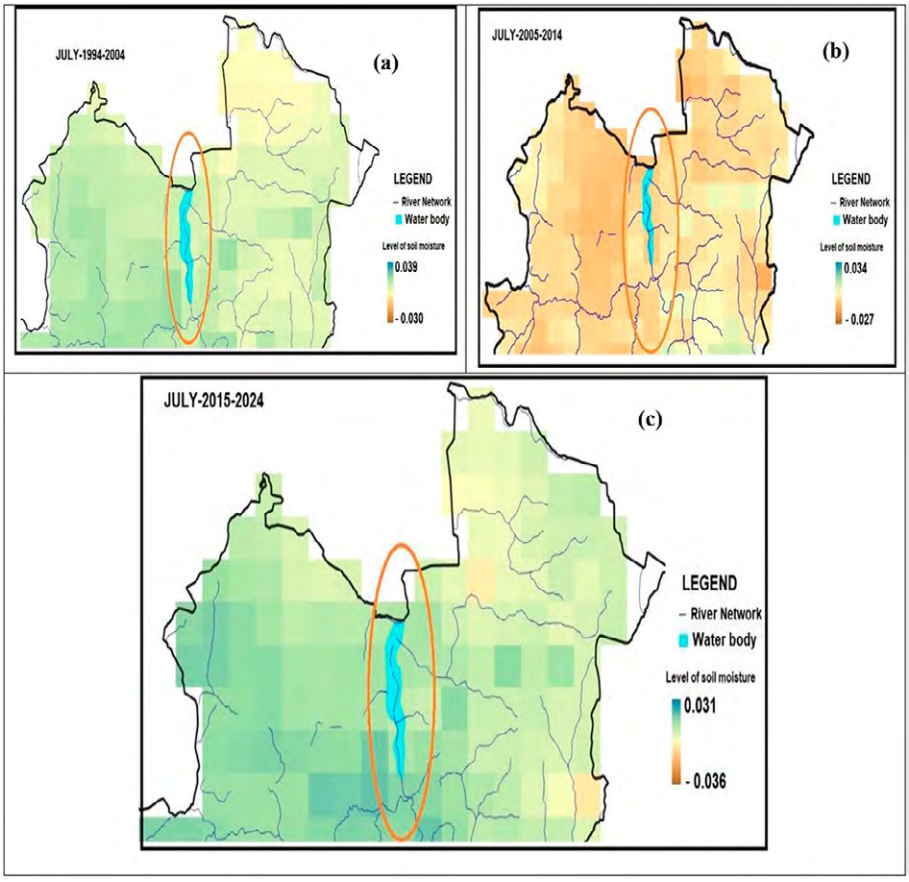

Figure 10a. Ten-year change in soil moisture in the Sourou Valley between 1994 and 2024

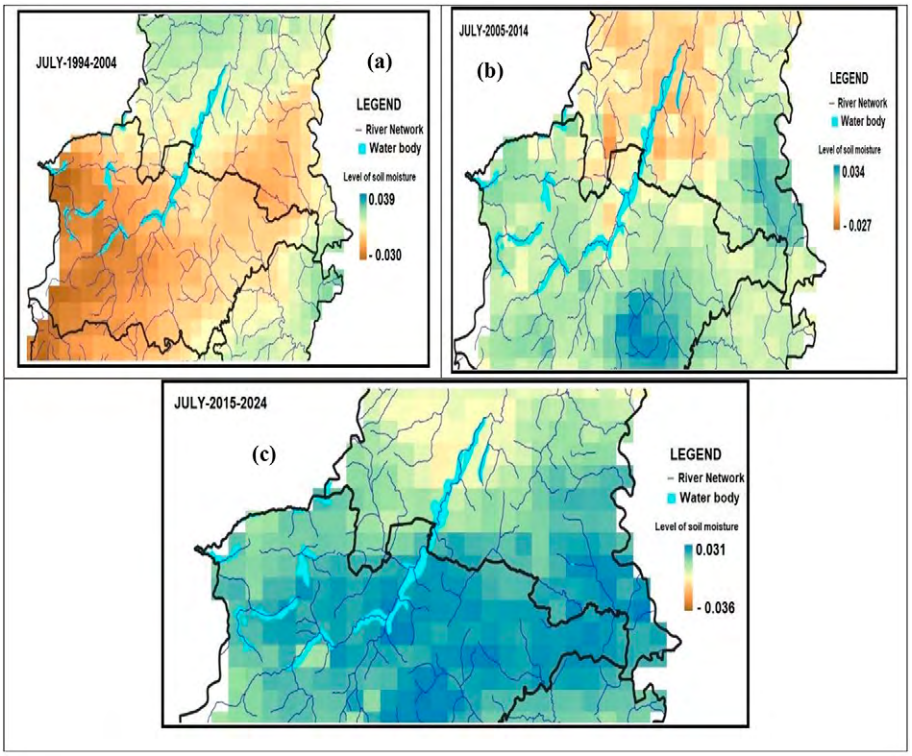

Figure 11a. Ten-year change in humidity in the other valleys of the basin between 1994 and 2024

terized by high soil moisture. For the month of August, the 1994-2024 decade (Figure 11b.d) is characterized by a significant decrease in soil moisture (in appendix). Soil moisture improved during the 2005-2014 decade (Figure 11b.e) (in appendix). The 2015-2024 decade shows significant soil moisture in July. The trend of increasing soil moisture in the basin is confirmed by the Yaméogo study (2025). The study shows an upward trend in soil moisture, but it is highly variable in the Mouhoun basin. This situation could be explained by the increase in rainfall in the country. The study by Yameogo and Rouamba (2024) shows that Burkina Faso experienced a period of flooding between 2005 and 2020. This suggests an increase in rainfall between 2005 and 2020. Several other studies in the country confirm the wet phase. Compaoré and Yaméogo (2024) observed an upward trend in rainfall in the Centre-West region between 2001 and 2021. Work by Yaméogo and Sawadogo (2024) in the Mouhoun sub-basin (vranso) over the period 1980-2014 shows an upward trend in rainfall. Another study by Yanogo and Yaméogo (2023) on the south-western region of Burkina Faso (part of the Mouhoun Basin), in the high basins, shows increasing rainfall phases over the period 2011-2020, as also observed by Karambiri and Gansaonre (2023). The study by Yanogo and Yaméogo (2023) also finds an increase in extreme rainfall, but the southwest region is less affected than the north. A general trend of increasing precipitation has also been observed across West Africa. Ilori and Ajayi (2020) note that the wet phase began on the African continent in the 1990s. Other studies, such as those by Damberg and Agha-Kouchak (2014) and Fuentes et al. (2022), show different results from previous studies at local and regional level. Indeed, Damberg and Agha-Kouchak (2014) show a significant positive trend in drought areas on Southern Hemisphere lands (Africa, Northern India and parts of the Mediterranean), while no significant trend is observed on Northern Hemisphere lands between 1980 and 2012. This means that watersheds in the southern hemisphere are more affected. These results are similar to those of Fuentes et al (2022), who show that all continents are affected by drought, particularly Africa and Southeast Asia. However, according to the same authors, drought severity is more pronounced in the Horn of Africa and East Africa, while West Africa is moderately affected. These results differ from those of the study area in that the time frame (1980-2012) of the study by Damberg and Agha-Kouchak (2014) corresponds to a dry period in West Africa, whereas this study focuses on a wet period (1994-2024). This could explain the difference in results. The results of Fuentes et al. (2022) partially support our study, since they observe a less extensive wet phase in 2019

This wet phase (positive z-score over the period 2015-2024), accompanied by an increase in soil moisture in the Mouhoun-Comoé basin, will have an impact on agricultural crops, which cannot tolerate permanent humidity. This situation is more damaging for crops located in the valleys of the basin. Bossa (2020) notes that, under

these conditions, the agricultural development of wetlands faces the risk of hydric flooding, which prevents the establishment of crops or damages them. Week and Wizor (2020) and Reed et al. (2022) add that this situation could have a negative impact on the food security of African populations.

Conclusion

Agricultural activities are dependent on water resources. In Burkina Faso, watersheds are the main areas of agricultural activity. Recent droughts caused by extreme weather conditions have highlighted the need to better understand the impact of climate change on water resources in the Mouhoun-Comoé watershed. Understanding droughts during the wettest months is essential for agricultural planning. The aim of the study was to analyse the spatio-temporal trends of droughts in this basin. It showed that the basin experienced extreme, moderate and mild droughts on the scale of one, two and three months over the period 1994-2024. The ten-year analysis shows that the period 1994-2004 is generally characterised by extreme droughts. The other periods, 2005-2014 and 2015-2024, show a phase of humidity in the basin, with a significant increase in soil moisture. This situation could be detrimental to certain crops that do not like excess moisture. It is therefore essential that strategies to adapt to this new situation take into account the increasing humidity in the basin during the decade 2015-2024. Consequently, local and state authorities must encourage the use of water-intensive crops to adapt to the basin's new humidity.

References

Abiodun, B. J., Makhanya, N., Petja, B., Abatan, A. A., & Oguntunde, P. G. (2019). Future projection of droughts over major river basins in Southern Africa at specific global warming levels. *Theoretical and Applied Climatology*, 137, 1785-1799. https://doi.org/10.1007/s00704-018-2693-0

Ahana, B. S., Posite, V. R., Maouly, D. K., Abdelbaki, C., Kantoush, S. A., Nguyen, B. Q., & Kumar, N. (2024). Changing Rainfall Patterns in the Northeastern South Kivu Region, Democratic Republic of the Congo: A Detailed Analysis Using CHIRPS Rainfall Data (1981-2023). *Earth Systems and Environment*, 8(5), 1-18. 10.1007/s41748-024-00510-0

Ahmad, H. Q., Kamaruddin, S. A., Harun, S. B., Al-Ansari, N., Shahid, S., & Jasim, R. M. (2021). Assessment of spatiotemporal variability of meteorological droughts in northern Iraq using satellite rainfall data. *KSCE Journal of Civil Engineering*, 25(11), 4481-4493. 10.1007/s12205-021-2046-x

Akhtari, R., Morid, S., Mahdian, M. H., & Smakhtin, V. (2009). Assessment of areal interpolation methods for spatial analysis of SPI and EDI drought indices. *International Journal of Climatology*, 29(1), 135. https://doi.org/10.1002/joc.1691

Aksu, H & Akgul M.A. (2020). Performance evaluation of CHIRPS satellite precipitation estimates over Turkey. *Theoretical and Applied Climatology*, 142, 71-84. https://doi.org/10.1007/s00704-020-03301-5

Aksu, H., Cavus, Y., Aksoy, H., Akgul, M. A., Turker, S., & Eris, E. (2022). Spatiotemporal analysis of drought by CHIRPS precipitation estimates. *Theoretical and Applied Climatology*, 148(1), 517-529. https://doi.org/10.1007/s00704-022-03960-6

Alemu, M. M., & Bawoke, G. T. (2020). Analysis of spatial variability and temporal trends of rainfall in Amhara region, Ethiopia. *Journal of Water and Climate Change*, 11(4), 1505-1520. https://doi.org/10.2166/wcc.2019.084

Athanasiou, L. S., Fotiadis, D. I., & Michalis, L. K. (2017). Propagation of segmentation and imaging system errors. *Atherosclerotic Plaque Characterization Methods Based on Coronary Imaging*, 151-166. Academic Press.

Batool, N., Shah, S. A., Dar, S. N., & Skinder, S. (2019). Rainfall variability and dynamics of cropping pattern in Kashmir Himalayas: a case study of climate change and agriculture. *SN Applied Sciences*, 1, 606. https://doi.org/10.1007/s42452-019-0599-9

Bontogho, T. P. E., Kansole, M. M. R., Abarike, M. A., Kabore, M. (2024). Investigating Effective Reconnaissance Drought Index Ability to Reproduce Drought Signature over the Massili Basin (Burkina Faso). *Journal of Water Resources and Ocean Science*, 13(5), 116-123. 10.11648/j.wros.20241305.11

Bontogho, T. N. P. E., Kansole, M. M. R., Kabore, M., & Guira, M. (2023). Comparative analyses of SPI and SPEI as drought characterization tools in Massili watershed, central Burkina Faso. *International Journal of Hydrology Research*, 8(1), 14-22. https://doi.org/10.18488/ijhr.v8i1.3485

Bossa, A. (2020). Introduction. In B. Sultan, A. Y. Bossa, S. Salack, & M. Sanon (Eds.), *Risques climatiques et agriculture en Afrique de l'Ouest* [Climate risks and agriculture in West Africa] (pp. 117–119). IRD Éditions. https://doi.org/10.4000/books.irdeditions.36259

Damberg, L., & AghaKouchak, A. (2014). Global trends and patterns of drought from space. *Theoretical and applied*

climatology, 117, 441-448. https://doi.org/10.1007/s00704-013-1019-5

Dogan, S., Berktay, A., & Singh, V. P. (2012). Comparison of multi-monthly rainfall-based drought severity indices, with application to semi-arid Konya closed basin, Turkey. *Journal of Hydrology*, 470-471, 255-268. https://doi.org/10.1016/j.jhydrol.2012.09.003

Duku, C., Zwart, S. J., & Hein, L. (2018). Impacts of climate change on cropping patterns in a tropical, sub-humid watershed. *PloS one*, 13(3), e0192642. https://doi.org/10.1371/journal.pone.0192642

Careto M., J. A., Cardoso, R. M., Russo, A., André Lima, D. C., & Matos Soares, P. M. (2024). Generalised drought index: a novel multi-scale daily approach for drought assessment. *Geoscientific Model Development*, 17(22), 8115-8139. https://doi.org/10.5194/gmd-17-8115-2024

Compaoré, N., & Yaméogo, J. (2024). Impact of climate smart agriculture adoption on food security: The case of urban market gardeners in the city of Réo, Burkina Faso. *Journal of Biodiversity and Environmental Sciences*, 25(3), 1-14.

Feidas, H., Makrogiannis, T., & Bora-Senta, E. (2004). Trend analysis of air temperature time series in Greece and their relationship with circulation using surface and satellite data: 1955-2001. *Theoretical and Applied Climatology*, 79(3-4), 185–208. https://doi.org/10.1007/s00704-004-0064-5

Fowé, T., Yonaba, R., Mounirou, L. A., Ouédraogo, E., Ibrahim, B., Niang, D., ... & Yacouba, H. (2023). From meteorological to hydrological drought: a case study using standardized indices in the Nakanbe River Basin, Burkina Faso. *Natural Hazards*, 119(3), 1941-1965. https://doi.org/10.1007/s11069-023-06194-5

Fuentes, I., Padarian, J., & Vervoort, R. W. (2022). Spatial and temporal global patterns of drought propagation. *Frontiers in Environmental Science*, 10, 788248. https://doi.org/10.3389/fenvs.2022.788248

Funk, C., Peterson, P., Landsfeld, M., Pedreros, D., Verdin, J., Shukla, S., & Michaelsen, J. (2015). The climate hazards infrared precipitation with stations—a new environmental record for monitoring extremes. *Scientific data*, 2, 150066 (2015). https://doi.org/10.1038/sdata.2015.66

Gavrilov, M. B., Marković, S. B., Jarad, A., & Korać, V. M. (2015). The analysis of temperature trends in Vojvodina (Serbia) from 1949 to 2006. *Thermal Science*, 19(suppl. 2), 339-350. 10.2298/TSCI150207062G

Gbohoui, Y. P., Paturel, J. E., Tazen, F., Mounirou, L. A., Yonaba, R., Karambiri, H., & Yacouba, H. (2021). Impacts of climate and environmental changes on water resources: A multi-scale study based on Nakanbé nested watersheds in West African Sahel. *Journal of Hydrology: Regional Studies*, 35, 100828. https://doi.org/10.1016/j.ejrh.2021.100828

Ghahramani, A., & Moore, A. D. (2016). Impact of climate changes on existing crop-livestock farming systems. *Agricultural Systems*, 146, 142-155. https://doi.org/10.1016/j.agsy.2016.05.011

Grimm, N. B., Chapin III, F. S., Bierwagen, B., Gonzalez, P., Groffman, P. M., Luo, Y., & Williamson, C. E. (2013). The impacts of climate change on ecosystem structure and function. *Frontiers in Ecology and the Environment*, 11(9), 474-482.

Guira, M., Kabore, M., Kansole, M. M. R., & Bontogho, T. N. P. E. (2022). Patterns of Meteorological Drought Using Standardized Precipitation Evapotranspiration Index for Massili Basin, Burkina Faso. *International Journal of Environment and Climate Change*, 12(11), 3368-3377. https://doi.org/10.9734/ijecc/2022/v12i111387

Habtemariam, L. T., Kassa, G. A., & Gandorfer, M. (2017). Impact of climate change on farms in smallholder farming systems: Yield impacts, economic implications and distributional effects. *Agricultural systems*, 152, 58-66. 10.1016/j.agsy.2016.12.006

Ilori, O. W., & Ajayi, V. O. (2020). Change detection and trend analysis of future temperature and rainfall over West Africa. *Earth systems and Environment*, 4, 493-512. https://doi.org/10.1007/s41748-020-00174-6

Karambiri B.L.C.N., & Gansaonre R.N. (2023). Variabilité Spatio-Temporelle de la Pluviométrie dans les Zones Soudaniennes, Soudano-Sahélienne et Sahélienne du Burkina Faso [Spatio-temporal variability of rainfall in the Sudanian, Sudanian-Sahelian and Sahelian zones of Burkina Faso]. *European Scientific Journal, ESJ*, 15(1). Retrieved from https://eujournal.org/index.php/esj/article/view/16506

Kumari, S., Mayoor, M., Agarwal, S., Mahapatra, S. and Bharti, B. (2023). Drought Assessment using Z-Score for Vidarbha Region, Maharashtra. *Indian Journal of Environmental Protection*, 43(5), 421-430.

Kulikov, A. I., Ubugunov, L. L., & Mangataev, A. T. (2014). Global climate change and its impact on ecosystems. *Arid ecosystems*, 4, 135-141. https://doi.org/10.1134/S2079096114030032

Ndehedehe, C. E., Awange, J. L., Corner, R. J., Kuhn, M., & Okwuashi, O. (2016). On the potentials of multiple climate variables in assessing the spatio-temporal characteristics of hydrological droughts over the Volta Basin. *Science of The Total Environment*, 557-558, 819–837. 10.1016/j.scitotenv.2016.03.004.

Noor, N. M., Noor, N. M., Alias, R., & Ideris, M. M. (2020). Drought indices monitoring using SPI and Z index score for gua musang, Kelantan. In *IOP Conference Series: Materials Science and Engineering* (Vol. 932, No. 1, p. 012050). IOP Publishing. https://doi.org/10.1088/1757-899X/932/1/012050

Ogunrinde, A. T., Adigun, P., Xue, X., Koji, D., & Jing, Q. (2025). Spatiotemporal analysis of drought patterns and trends across Africa: a multi-scale SPEI approach

(1960–2018). *International Journal of Digital Earth*, 18(1), 2447342. https://doi.org/10.1080/17538947.2024.2447342

Orieschnig, C., & Cavus, Y. (2024). Spatial characterization of drought through CHIRPS and a station-based dataset in the Eastern Mediterranean. *Proceedings of IAHS*, 385, 79-84. https://doi.org/10.5194/piahs-385-79-2024

Rawlings, J. O., Pantula, S. G., & Dickey, D. A. (1998). *Applied regression analysis: A research tool*. Springer.

Senay, G. B., Velpuri, N. M., Bohms, S., Budde, M., Young, C., Rowland, J., & Verdin, J. P. (2015). Drought monitoring and assessment: remote sensing and modeling approaches for the famine early warning systems network. In *Hydro-meteorological hazards, risks and disasters*, 233-262. https://doi.org/10.1016/B978-0-12-394846-5.00009-6

Senay, G. B., Velpuri, N. M., Bohms, S., Budde, M., Young, C., Rowland, J., & Verdin, J. P. (2023). Drought monitoring and assessment: remote sensing and modeling approaches for the famine early warning systems network. *In Hydro-meteorological hazards, risks and disasters (Second Edition)*, 247-276. https://doi.org/10.1016/B978-0-12-819101-9.00002-9

Séne, S. M. K., Faye, C., & Pande, C. B. (2024). Assessment of current and future trends in water resources in the Gambia River Basin in a context of climate change. *Environmental Sciences Europe*, 36(1), 32. https://doi.org/10.1186/s12302-024-00848-2

Sharma, S. K., Sharma, D. P., Sharma, M. K., Gaur, K., & Manohar, P. (2021). Trend analysis of temperature and rainfall of Rajasthan, India. *Journal of Probability and Statistics*, 1, 6296709. https://doi.org/10.1155/2021/6296709

Pham, H. V., Torresan, S., Critto, A., & Marcomini, A. (2019). Alteration of freshwater ecosystem services under global change–A review focusing on the Po River basin (Italy) and the Red River basin (Vietnam). *Science of the Total Environment*, 652, 1347-1365. http://dx.doi.org/10.1016/j.scitotenv.2018.10.303

Posite, V. R., Saber, M., Ahana, B. S., Abdelbaki, C., Bessah, E., Appiagyei, B. D. & Danquah, J. A. (2024). Modeling Spatio-Temporal Rainfall Distribution in Beni–Irumu, Democratic Republic of Congo: Insights from CHIRPS and CMIP6 under the SSP5-8.5 Scenario. *Remote Sensing*, 16(15), 2819. https://doi.org/10.3390/rs16152819

Reed, C., Anderson, W., Kruczkiewicz, A., Nakamura, J., Gallo, D., Seager, R., & McDermid, S. S. (2022). The impact of flooding on food security across Africa. *Proceedings of the National Academy of Sciences*, 119(43), e2119399119. https://doi.org/10.1073/pnas.2119399119

Rouamba, S., Yaméogo, J., Sanou, K., Zongo, R., & Yanogo, I. P. (2023). Trends and variability of extreme climate indices in the Boucle du Mouhoun (Burkina Faso). GEOREVIEW: Scientific Annals of Stefan cel Mare University of Suceava. *Geography Series*, 33(1), 70-84.

Tran, A. P., Tran, B. C., Campbell, S. B., Nguyen, N. A., Tran, D. H., Nguyen, T. T., & Duong, H. S. (2024). Spatio-temporal characterization of drought variability in data-scarce regions using global precipitation data: a case study in Cauto river basin, Cuba. *Scientific Reports*, 14(1), 11659. https://doi.org/10.1038/s41598-024-61709-9

U.S. Environmental Protection Agency, Office of Resource Conservation and Recovery. (2009). *Statistical analysis of groundwater monitoring data at RCRA facilities: Unified guidance* (EPA 530/R-09-007, p. 888). https://www.epa.gov/

Week, D. A., & Wizor, C. H. (2020). Effects of flood on food security, livelihood and socio-economic characteristics in the flood-prone areas of the core Niger Delta, Nigeria. *Asian Journal of Geographical Research*, 3(1), 1-17. https://doi.org/10.9734/ajgr/2020/v3i130096

World Meteorological Organization (WMO). (2016). *Handbook of drought indicators and indices* (WMO-No. 1173). Geneva: World Meteorological Organization. https://library.wmo.int/doc_num.php?explnum_id=3313

Wu, H., Hayes, M. J., Weiss, A., & Hu, Q. I. (2001). An evaluation of the Standardized Precipitation Index, the China-Z Index and the statistical Z-Score. *International Journal of Climatology: A Journal of the Royal Meteorological Society*, 21(6), 745-758. https://doi.org/10.1002/joc.658

Xiong, J., Guo, S., Kinouchi, T., & Anjaneyulu, R. (2024). Emerging trends and spatial shifts of drought potential across global river basins. *Journal of Environmental Management*, 352, 120093. https://doi.org/10.1016/j.jenvman.2024.120093

Yaméogo, J. (2025). Analysis of soil moisture trends in Burkina Faso between 1981 and 2020 using the innovative şen trend method. *Revue de Géographie du Poro*, 1, 888-910.

Yaméogo, J. (2025). Annual rainfall trends in the Burkina Faso Sahel: a comparative analysis between Mann–Kendall and innovative trend method (ITM). Discover Applied Sciences, 7, 221. https://doi.org/10.1007/s42452-025-06675-1

Yaméogo, J & Rouamba S. (2023). Climatic disasters in Burkina Faso from 1960 to 2020: Occurrence, Spatio-temporal dynamics and Socio-environmental consequences. African *Journal on Land Policy and Geospatial Sciences*, 6(5), 1022-1043. http://dx.doi.org/10.48346/IMIST.PRSM/ajlp-gs.v6i5.43074

Yaméogo, J., & Sawadogo, A. (2024). Consequences of precipitation variability and socio-economic activity on surface water in the Vranso water basin (Burkina Faso). *Glasnik Srpskog geografskog drustva*, 104(1), 255-266. https://doi.org/10.2298/GSGD2401255Y

Yang, J., Xie, B., Zhang, D., & Tao, W. (2021). Climate and land use change impacts on water yield ecosystem service in the Yellow River Basin, China. *Environmental Earth Sciences*, 80(3), 72. 10.1007/s12665-020-09277-9

Yangouliba, G. I., Zoungrana, B. J. B., Hackman, K. O., Koch, H., Liersch, S., Sintondji, L. O. & Koffi, B. (2023). Modelling past and future land use and land cover dy-

namics in the Nakambe River Basin, West Africa. *Modeling Earth Systems and Environment*, 9(2), 1651-1667. https://doi.org/10.1007/s40808-022-01569-2

Yanogo, I. P., & Yaméogo, J. (2023). Recent rainfall trends between 1990 and 2020: contrasting characteristics between two climate zones in Burkina Faso (West Africa). *Glasnik Srpskog Geografskog Drustva*, 103(1), 87-106. https://doi.org/10.2298/GSGD2301087Y

Zouré, C. O., Kiema, A., Yonaba, R., & Minoungou, B. (2023). Unravelling the Impacts of Climate Variability on Surface Runoff in the Mouhoun River Catchment (West Africa). Land, 12(11). https://doi.org/10.3390/land12112017

Appendix

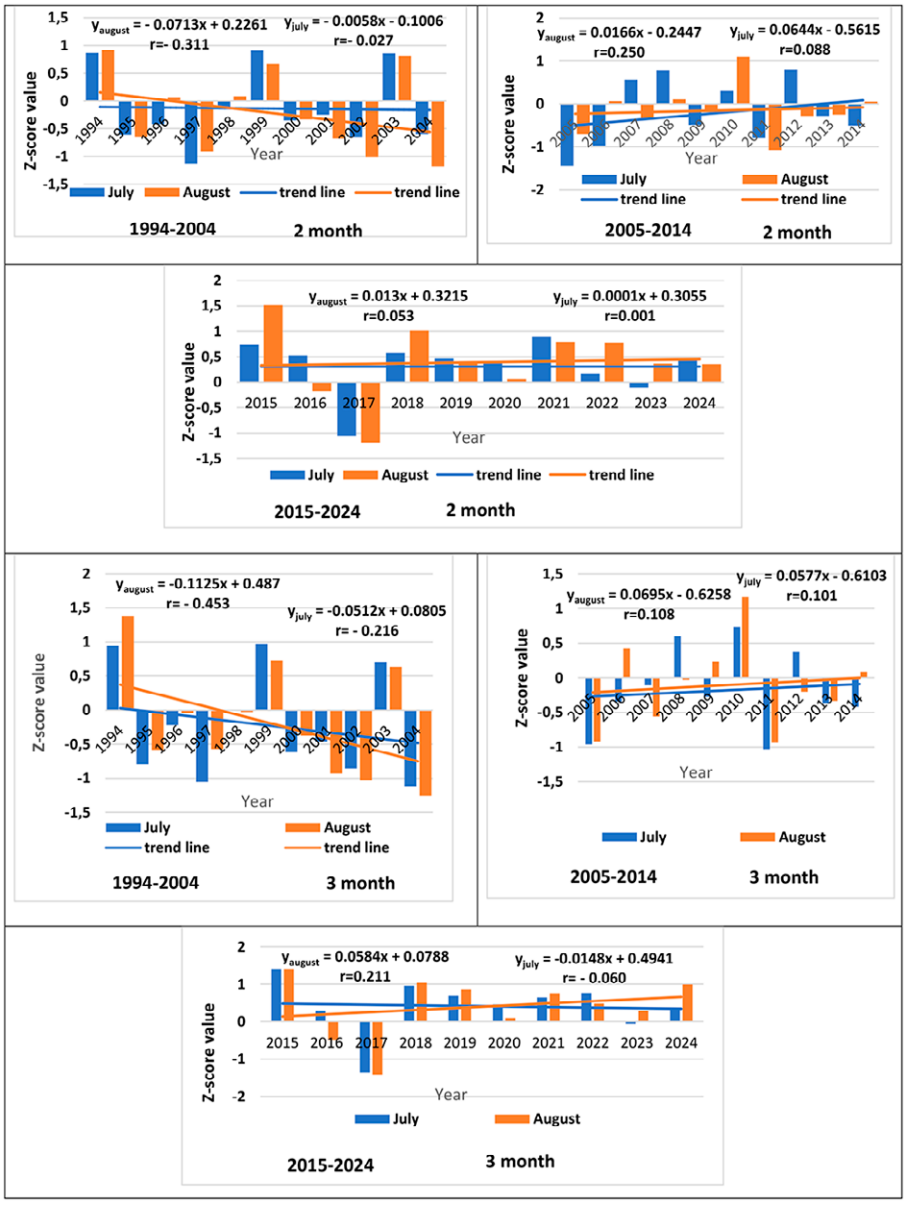

Figure 6b. Decadal evolution of Z-score on a two- and three-month scale

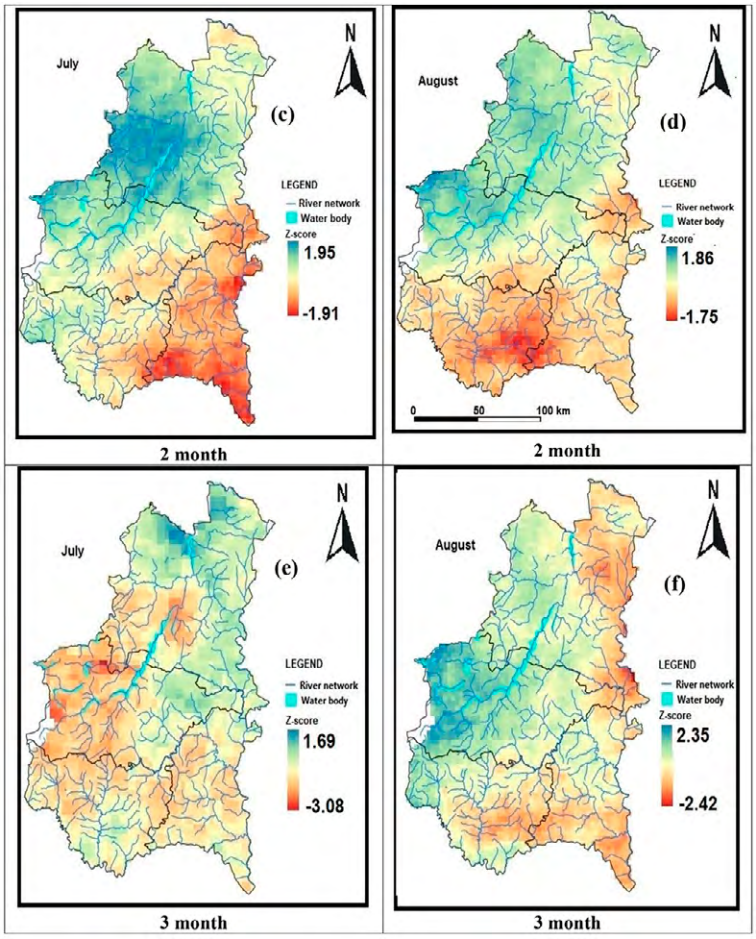

Figure 7b. Multiscale spatial trend of drought 1994-2024

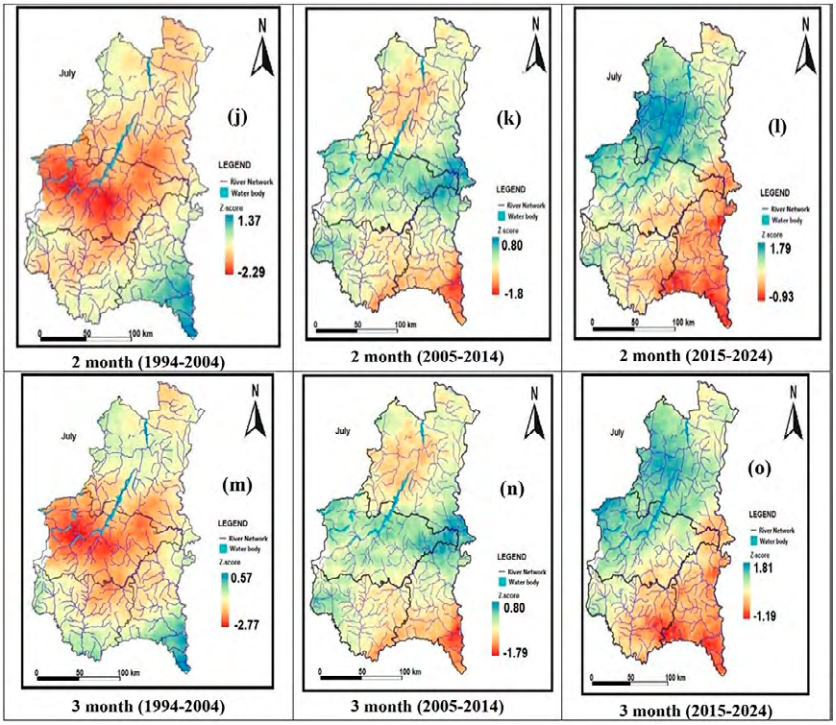

Figure 8b. Ten-year spatial trend of the July drought at different scales for the period from 1994 to 2024

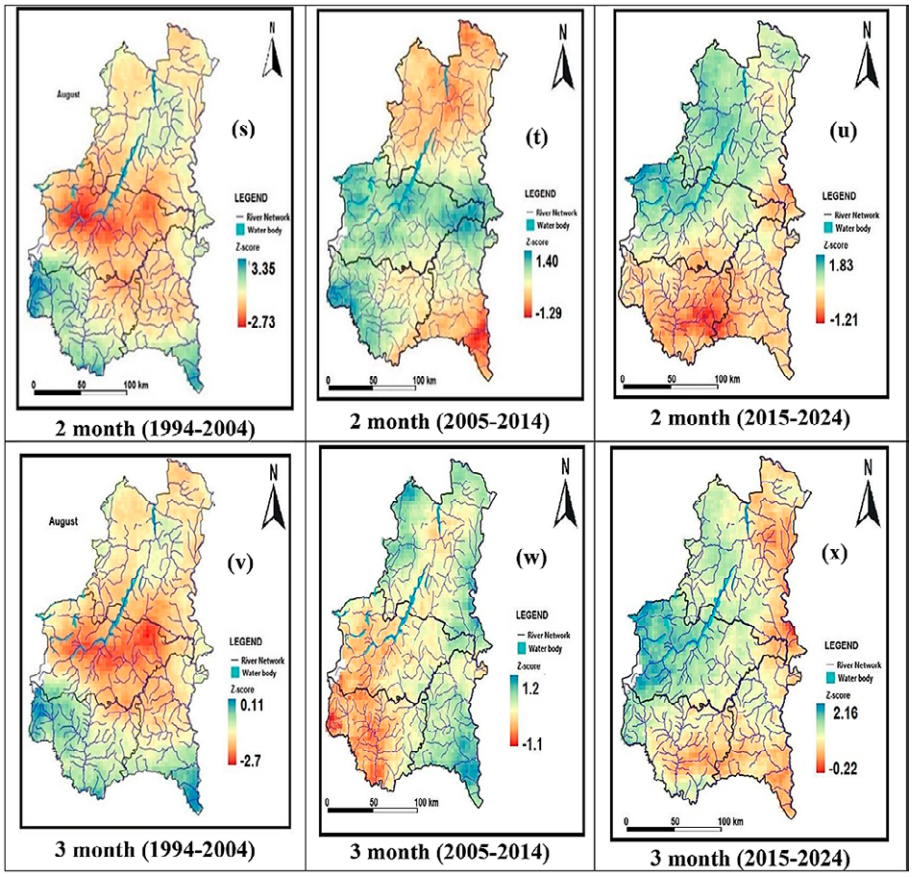

Figure 9b. Decadal spatial evolution of August drought at different scales between 1994 and 2024

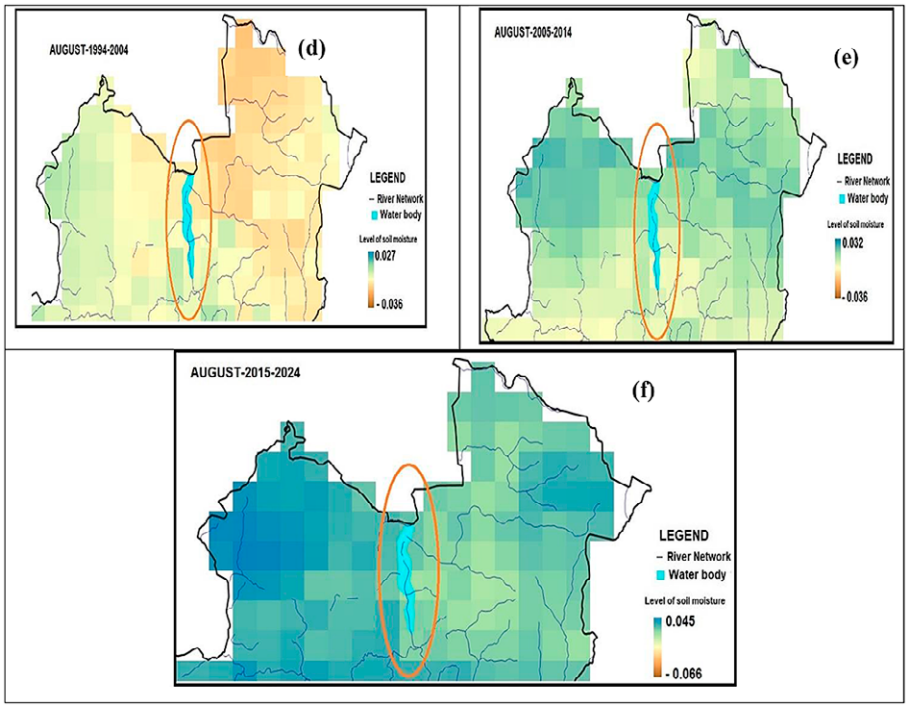

Figure 10b. Ten-year change in soil moisture in the Sourou valley at different scales between 1994 and 2024

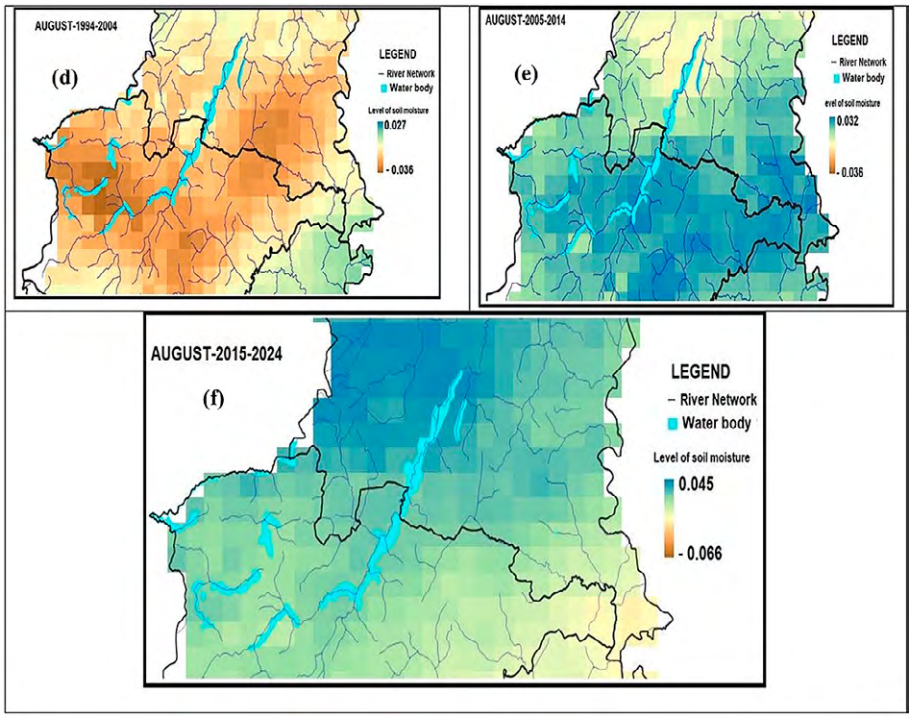

Figure 11b. Decadal trend in humidity in the other valleys of the basin on 2- and 3-month scales between 1994 and 2024

INTERNATIONAL SCIENTIFIC JOURNAL
GEOGRAPHICA PANNONICA
Volume 29, Issue 2, 84–107 (June 2025)
Journal homepage: http://www.dgt.uns.ac.rs/en/homepage/pannonica/

Fine-scale Mapping of Heat-hazard Risk and Vulnerability Using Geo-spatial Techniques: Insights from a Tropical Indian City

Rajashree Kotharkar[A*], Aveek Ghosh[A], Ravindra Keskar[A]

[A] *Visvesvaraya National Institute of Technology (VNIT), Nagpur, Maharashtra, India; ORCID RK: 0000-0002-5063-2757; AG: 0000-0002-5025-395X; RK: 0000-0002-3674-6539*

KEYWORDS

- extreme heat
- heat-hazard risk
- heat vulnerability index
- sensitivity
- exposure
- adaptive capacity
- local climate zone

ABSTRACT

Unprecedented extreme heat events (EHEs) have amplified associated health risks, but they present great differences within the urban environment. This paper aims to assess heat-hazard risk (HHR) and associated vulnerability in Nagpur, a heat-prone Indian city using remotely sensed and on-site meteorological data. HHR was generated through high resolution local climate zone (LCZ) maps via the product of hazard and vulnerability which featured census-tract socio-economic variables (sensitivity and adaptive capacity) and exposure. Principal component analysis (PCA) with equal weighting was applied to develop a composite fine-scale heat vulnerability index (HVI). Out of 136 wards, a total of 68 wards were identified to have 'high' or 'very high' HVI featuring about 49.06% of the population. LCZ-based spatial mapping showed a heterogeneous heat 'risk-scape' across the city. 'High' and 'very high' heat vulnerability/risk (HV/R) signature was observed in city core, its adjoining areas (LCZs 3 and 3_F) and urban fringes (LCZs 9 and 9_3). Conversely, open areas with moderate vegetation cover and natural classes (LCZs 6, 6B, A and B) showed 'moderate' to 'low' HHR. The findings of this research will enable the urban practitioners and policymakers to deal with explicit determinants of heat vulnerability and risk especially in regions with low adaptive capacity.

Introduction

Heat-related hazards pose major health risks in cities (Santamouris, 2019; Ebi et al., 2021) and significantly affect urban livability (Wouters et al., 2017; Kotharkar et al., 2024a, 2024b). Extreme heat events (EHEs) or heat waves (HWs), characterized as extended durations of abnormally elevated temperatures particularly result in excessive mortality rates (Gasparrini and Armstrong, 2011; Kumar & Singh, 2021). In recent past, multiple cities globally have suffered the brunt of frequent HWs including 2015 Indian and Pakistani HW (Wehner et al., 2016), 2016 South-East Asian HW (Gu et al., 2016), 2019 European HW (Pascal et al., 2021), 2020 Siberian HW (WMO, 2021) and 2021 North American HW (Keith et al., 2021). Multiple reports have predicted EHEs to be more intense, more frequent and longer-lasting, particularly in urbanized environments (IPCC, 2018, 2021). In this context, it is of paramount importance for urban practitioners to gain knowledge on heat vulnerability and associated socio-economic risks to manage and cope with EHEs.

* Corresponding author:Rajashree Kotharkar; e-mail: rskotharkar@gmail.com

doi: 10.5937/gp29-56164

Received: January 20, 2025| Revised: April 28, 2025| Accepted: May 22, 2025

In the recent past, multiple studies have conducted HV/R assessment across cities/metropolitan areas/regions with improving spatial accuracy (Maragno et al., 2020; Karanja et al., 2022). In this study, we define HV/R as a tool which can developed to identify the population or geographies that are at high risk of heat hazard (HH) using spatial socio-economic, physical and environmental data that are associated with heat-related adverse health outcomes. The external event of a HH can be referred to a dangerous condition or risk to public health caused by extreme heat episodes. This can result from high environmental temperatures, prolonged exposure to heat sources, or physical exertion in hot conditions. The knowledge of HV/R can subsequently inform urban planning policies, public health interventions, emergency measures and mitigation strategies. The wide range of studies shows concentration of research efforts in developed countries especially with tropical climates (Azhar et al., 2017; Hu et al., 2017; Rathi et al., 2021; Kotharkar et al., 2019; Li et al., 2022). Similarly, a number of research efforts have concentrated on mapping heat-health risks to evaluate intra-urban differences (Navarro-Estupiñan et al., 2020; Kotharkar & Ghosh, 2021a, 2021b; Zhou et al., 2021; Chen et al., 2022; Cheval et al., 2022; Ellena et al., 2023; Ma et al., 2023).

Urban environments exhibit significant variations in heat risks (HRs) and/or HHRs due to differences in surface morphologies and physical structures. In this paper, we define HHR as the potential harm to human health across population groups, due to exposure to extreme heat conditions in a given geographical area. To better understand the impact of different urban surfaces, Stewart and Oke (2012) introduced the concept of local climate zones (LCZs). LCZs are defined as the regions that possess similar characteristics like surface cover, material, structure, and population activity, extending from several hundred meters to a few kilometers. The framework has been extensively used to collect urban data by logically dividing the urban landscape (Lehnert et al., 2021). It has found its application in the wider assessment of heat-health risks in multiple cities (Verdonck et al., 2018; Chen et al., 2021), including Chongqing (Cai et al., 2019), Hermosillo (Navarro-Estupiñan et al., 2020), Beijing (Zhou et al., 2021; Chen et al., 2022), Turin (Ellena et al., 2023) and Changzhou (Ma et al., 2023). The wide range of assessments using spatial classification systems (e.g., LCZ maps) provides valuable input and decision support for climate adaptation planning to mitigate urban HRs. Such assessments can inform, guide and strengthen heat-health action plans (HHAPs) via extreme heat planning and management. A HHAP lays a strong foundation and serve as an effective tool for directing heat-related adaptation and mitigation efforts across spatial scales (Kotharkar & Ghosh 2021b). HHAPs aims to provide a methodical framework inclusive of public health responses, activation of alert systems and inter-agency coordination to reduce the negative impact of HWs. Hence, evidence-based local assessment of HV/R is crucial for augmenting the overall response to growing risks of HWs.

A widely used framework for assessing heat-related health risks is the 'Crichton Risk Triangle', which consists of three key components: hazard, exposure, and vulnerability (Crichton, 1999). Over the past decade, an increasing number of studies have adopted this framework for evaluating heat-related health risks (Hu et al., 2017; Estoque et al., 2020). With the advancement of research on LCZ, many studies have demonstrated that the framework is a valuable tool for analyzing various aspects of the urban thermal environment (Verdonck et al., 2018). For instance, Zhou et al. (2021) applied the LCZ system to examine heat risk in Beijing, specifically analyzing the distribution of LCZ types in relation to population heat exposure. Most previous studies assess risk at the level of administrative units (such as cities or neighborhoods) primarily due to data constraints. However, it lacks the resolution to capture the heterogeneous spatial distribution of populations within those boundaries. While such studies provide valuable insights for urban planning and management, they fall short in analyzing finer-scale relationships with urban structure, limiting their usefulness for implementing targeted planning measures (Hu et al., 2017; Zuhra et al., 2019; Chen et al., 2022). Additionally, past research has largely concentrated on heat-related hazards, with comparatively little attention given to exposure and vulnerability, which represents two critical components that shape the overall impact of hazards (Ren et al., 2022; Wu et al., 2022).

Research gap, novelty and significance of the study

The existing literature shows that the geographical distribution of HV/R assessments in Asian tropics as well as high population and development density settings (e.g., India) are not usually well known and remain less explored barring a few (Rathi et al., 2021; Shih & Mabon, 2021; Nanda et al., 2022; Ghosh et al., 2024). Moreover, due to limited availability of dense weather station data in these regions, several studies have used remotely-sensed land surface temperature (LST) to measure HH (Romero-Lankao et al., 2012). While some studies have highlighted that the UHI effect increases the extent and intensity of extreme heat stress in cities, most have focused solely on daytime temperatures, neglecting nighttime temperatures and potentially underestimating the overall HHR in urban areas. Research has shown that integrating heat exposure data with population vulnerability factors can effectively map high-risk areas and guide targeted interventions (Inostroza et al., 2016; Hu et al., 2017). Additionally, spatial frameworks enable the identification of heat risk hotspots from local to regional levels, supporting more effective climate adaptation planning and emergency management (Aubrecht & Özceylan, 2013; Ma et

al., 2023). As EHEs are predicted to increase in frequency and severity due to climate change, these spatial vulnerability assessments become increasingly important for developing targeted heatwave preparedness plans and reducing heat-related health risks (Ghosh, 2024). Hence, spatial vulnerability and risk estimation are crucial for understanding and mitigating heat-related hazards in urban areas (Karanja & Kiage, 2021; Li et al., 2022, 2024).

It has also been shown that LCZs vary in the levels of human thermal stress they experience due to extreme heat (Kotharkar et al., 2021, 2022). A study in Nagpur highlighted pedestrian discomfort and thermal stress in commercial streets, affecting walkability and public transit usage (Mohite & Surawar, 2024). Another research identified relatively high levels of thermal stress benchmarks with respect to respondent's sensation, comfort, tolerance and acceptability in Nagpur city (Kotharkar et al., 2024a). A recent comprehensive study by Kotharkar et al. (2024b) indicate that large low-rise, sparsely built, and scattered areas mixed with compact low-rise zones (i.e., LCZs 8, 9 and 9_3) present higher levels of heat stress indicating greater susceptibility to mortality. The wide variety of scientific literature constructs a possibility of different LCZs demonstrating variation in heat-related risks and implications. However, vulnerability-based research to inform extreme heat-related risks are still limited. LCZs with distinct surface morphologies and physical structures can help identify differences in HRs and provide a foundation for developing effective adaptation and mitigation strategies (Kotharkar et al., 2024c). This study uses the LCZ framework to standardize urban zones, a widely adopted method for examining spatio-temporal variations in the thermal environment. Therefore, to fill this research gap, the research conducts a comprehensive HV/R assessment combined with LCZ maps to provide valuable insights of high-risk areas at a local level with finer resolution.

The present study is first of its kind to employ a novel and hybrid approach to calculate HHR using census and local climate information (daytime and nighttime hazard analysis) in Nagpur, a heat-prone central Indian city. It attempts to spatially analyse and conduct a comprehensive heat-related health risk assessment using LCZ classification at a spatially explicit raster level. This is particularly critical in tropical and sub-tropical regions with limited adaptation solutions, low socioeconomic status and poor heat-health governance. These investigations can play a crucial role in mitigating the adverse impacts of HHs on households via easier implementation, thereby enhancing the urban thermal environment in cities.

Aim and objectives of the study

The present study aims to estimate HHR for Nagpur, a centrally located tropical Indian city. It attempts to assess local-level heat-health risk (HHR) using the LCZ classification to help inform and support decisions for the effective implementation of preventive measures in heat-health action plans (HHAPs). The objective of this paper is to explore the interaction of HH and related vulnerability at ward level. Mapping of HV involved estimating the spatial patterns of exposure, sensitivity and adaptive capacity using principal component analysis (PCA) tool and identifying the influencing variables.

Study area and climate

Nagpur (21.1458° N, 79.0882° E; 310 meters above sea level) is a tropical city located in central India. The city, administered by the municipal corporation, has a population of approximately 2.4 million and a gross population density of 110 people per hectare (pph) (MHA, 2011). Spanning an area of 217.65 km², Nagpur is the 13th largest city in India by population. The city is relatively compact, with dense core areas. In the peripheral regions, particularly in the western and southwestern parts, the population density ranges from 20 to 32 pph, while in the inner and core areas, the density can reach as high as 750 to 1,000 pph. Nine wards situated in the city center has density in the

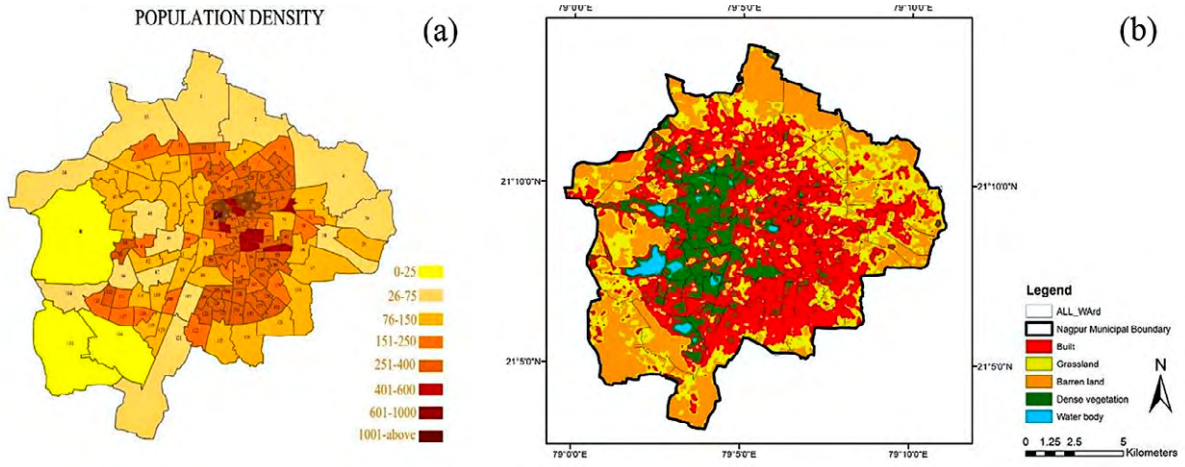

Figure 1 a, b. Population density of Nagpur city in 2011 (b) LULC map

range of 601–1000 pph while ward no. 67 has population density in excess of 1000 pph (refer Fig. 1a). In 2021, area covered under built-up, grassland, vegetation (sparse and dense), barren and water bodies were 41.2%, 12.13%, 17.31 %, 26.07% and 3.29%, respectively (see Fig. 1b). Slums are spread over an area of 17 km^2 (7.81%) while >2% of the land is officially classified as urban green spaces.

The city has a tropical savanna climate, classified as "Aw" under the Köppen climate system. It experiences four distinct seasons: summer (March to June), monsoon (July to August), post-monsoon (September to October), and winter (November to February). Historically, annual temperatures range from a record high of 48°C during summer to a low of 4°C during winter (Kotharkar et al., 2021). However, city's tropical climate experiences significant temperature variations throughout the year. Summers are exceptionally hot, often accompanied by frequent heatwave days, locally known as *'loo'*. In recent past, the city has witnessed record extreme temperatures coupled with recurrent HWs with increasing intensities. These extreme summer conditions create uncomfortable outdoor environments and pose exacerbated thermal discomfort.

Materials and methods

The HHR mapping workflow is carried out in four stages, as shown in Figure 2. The present research was aided by various software including ArcGIS v10.4, Autodesk AutoCAD v2020, HOBOware v3.7.4, MS Excel v2011, and statistical software 'R' v4.2.1. The stages of the study can be described as:

1. The first stage involved a literature review of previous HV/R assessments across geographic locations and climate zones to identify appropriate indicators which are best possible fit. The indicators from each variable to describe vulnerability were extracted from 2011 census data, which was pre-processed (conversion from vector to raster form) and normalized for further analysis. Simultaneously, LCZ mapping of Nagpur city was conducted using WUDAPT technique (Bechtel et al., 2015; Mills et al., 2015). To estimate HH, in-situ air temperature measurements (refer Fig. 3) were carried out across different LCZs covering major parts of the city.
2. In the second stage, PCA with varimax rotation was used as a dimension reduction technique to filter the actual indicators explaining majority of the variance. The HVI scores (ward-wise) were normalized on a scale of 0 to 1.

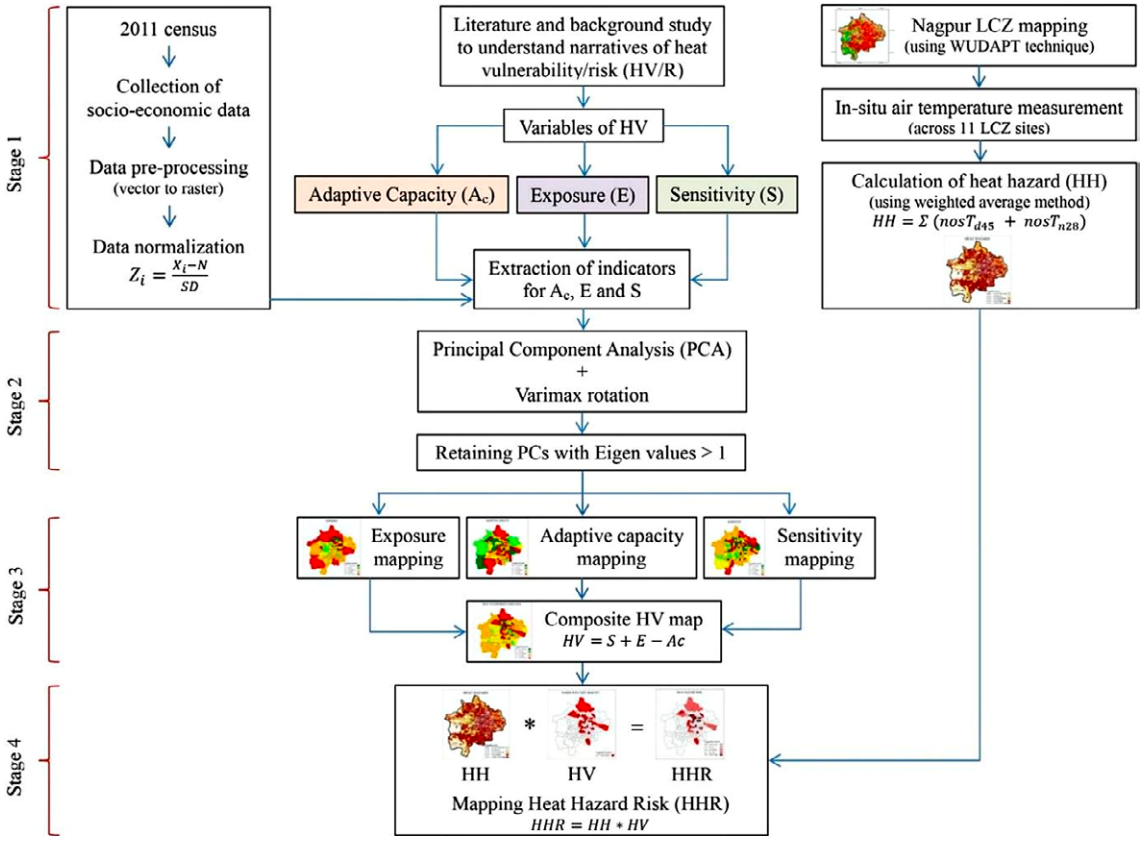

Figure 2. Workflow for HHR mapping

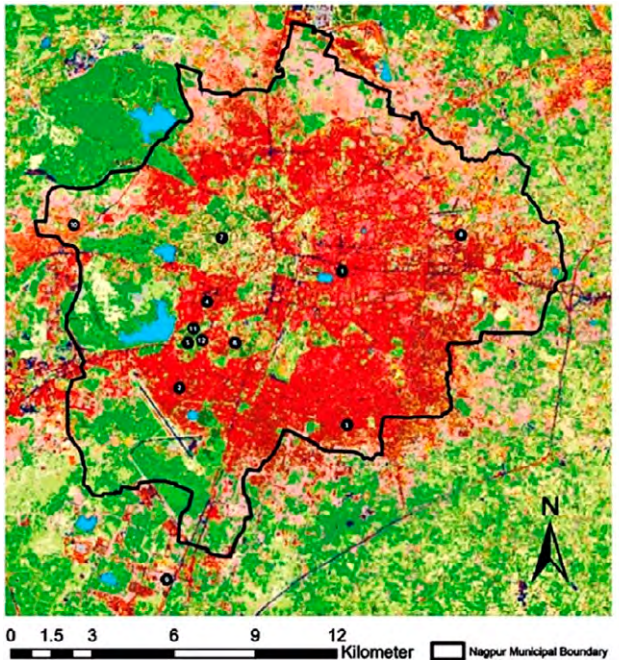

Sr	Area	Description
1	MHL LCZ 3	Densely built compact low-rise area with scarce vegetation and abundance of impervious surfaces
2	DDN LCZ 3_F	Low-rise built forms with moderately low amount of vegetation and bare soil
3	MNW LCZ 3_F	Low-rise and compact urban setting with high coverage of bare surfaces and low amount of vegetation
4	SVJN LCZ 5	Open area with midrise buildings, and moderate pervious surface
5	VNIT LCZ 6	Open low-rise blocks with abundance of vegetation and pervious surfaces
6	BJN LCZ 6_S	Mix of low-rise and mid-rise built forms with moderate amount of vegetation
7	ADT LCZ 6_B	Open low rise blocks with abundance of pervious land cover and vegetation
8	APMC LCZ 8	Large open low-rise area with moderate amount of paved surface
9	Khapri LCZ 9	Sparsely built low-rise setting with scarce vegetation and abundance of pervious surfaces
10	DBA LCZ 9_3	Sparsely built low-rise setting nested with few compact low-rise buildings
11	VNIT A LCZ A	Area with dense vegetation and wooded trees
12	VNIT Park LCZ B	Area with scattered trees, pavements and patches of grasslands

Two stations representative of LCZ 3_F were selected as the city showed a high coverage of the same

Figure 3. LCZ map of Nagpur city showing measurement locations

3. The third stage encompassed spatial mapping of HV variables (adaptive capacity, exposure and sensitivity) which led to the generation of composite HV map using eqn. 2. Wards with very high HVI as well as dominant LCZs were identified and spatial overlap and the intensity of HHR across LCZ classes were analyzed.
4. The fourth and the final stage involved the estimation of HHR using the product of HH and HV (for wards with very high HV).

HV assessment

The census at municipal ward level, developed by the Office of the Registrar General and Census Commissioner of India, Ministry of Home Affairs, Government of India was used for spatial analysis. The 2011 census data within continuous urban area of Nagpur municipality (consisting 136 wards) was obtained from https://censusindia.gov.in/census.website/data/census-tables. A composite heat vulnerability index (HVI) was developed using spatially explicit variables of sensitivity, adaptive capacity and exposure. Duplicate variables that represented similar constructs were removed and diverse indicators across demographic, social, economic, health, and environmental domains were selected. The present study encompasses a combined total of twenty-one (21) indicators including eight (8) indicators of adaptive capacity, twelve (12) indicators for sensitivity and LST as the sole indicator for exposure (refer Annexure I). It considers that HVI is triggered by sensitivity and exposure and diminished with increasing adaptive capacity (see eqn. 1 and 2), which can be represented as:

$$\text{Heat Vulnerability} = f\ (\text{Exposure, Sensitivity, Adaptive capacity}) \quad (1)$$

This can be mathematically calculated as shown in eqn. 2:

$$HV = S + E - A_c \quad (2)$$

where, HV is the composite heat vulnerability, S refers to sensitivity level, E refers to exposure level, and A corresponds to the adaptive capacity.

Adaptive Capacity

Adaptive capacity denotes the residents' capability to respond to the adverse impacts of extreme heat and rebound from any resulting losses. Eight indicators constituted adaptive capacity which included access to infrastructure and other coping mechanisms (electricity, water, communication/health/social facilities, personal vehicle and bank account) which help residents to survive periods of extreme heat (Kovats & Hajat, 2008) (see Annexure I). NDVI was included as an indicator reflecting higher proportion of vegetation and its health which reduces heat intensity (Raja et al., 2021).

Sensitivity

'Sensitivity' is the degree to which urban population is affected by heat-related stimuli (IPCC, 2014; Sharma & Ravindranath, 2019). Twelve (12) indicators obtained from census data were deduced to determine sensitivity (see Annexure I). This include illiterate population and person with disability as they are not aware of the negative effects of extreme heat (Cutter et al., 2003; Uejio et al., 2011; Raja et al.,

2021) and possess fewer resources to combat the heat exposure and thus are vulnerable to heat stress. Females, young children (below 6 years) and elderly (above 60 years) population were accounted as they are susceptible to EHEs (Wilhelmi & Hayden, 2010; Nayak et al., 2018). It also included the socioeconomically marginalized section (scheduled caste and scheduled tribes). It further considered population density, typology of dwelling units, average number of inhabitants per household and single household sizes to account for sensitive population groups.

Exposure

'Exposure' to extreme heat is referred to as the external impact of HH on the population. In the present study, exposure is represented by LST, which is considered to be one of the most influential variables to describe heat exposure (Zuhra et al., 2019), which heightens extreme heat issues (Reid et al., 2009; Aubrecht & Özceylan, 2013).

Heat-hazard estimation

HH is captured through the intensity and distribution of extreme heat. The study accounted for the nocturnal effect by integrating Tmax with daily minimum temperature (T_{min}). T_{max} and T_{min} across selected LCZs were used to represent HWs and hot nights respectively to account for its intensity and frequency. The study applied the HW criteria formulated by the India Meteorological Department (NDMA, 2019) for the plains of India. HW conditions are identified when the maximum temperature at a station reaches 45°C or higher during the day. HH was calculated by summing the instances when the daily maximum temperature exceeded 45°C during daytime ($nosT_{d45}$) and/or 28°C during nighttime ($nosT_{n28}$). These daily instances were then aggregated and normalized to create an HH index. (see eqn. 3):

$$HH = \frac{\sum\left(nosT_{d45} + nosT_{n28}\right)}{\text{Total instances}} \quad (3)$$

where, HH is the heat hazard, $nosT_{d45}$ refers to number of days with daily maximum temperature above 45°C, and $nosT_{n28}$ is the number of days with daily minimum temperature above 28°C. The total instances were estimated to be 108 (54 days * 2 instances for each day reflecting daytime and nighttime condition). The daytime conditions were considered during 06:00 – 17:59 hrs while nighttime conditions denoted 18:00 – 05:59 hrs.

A threshold 28°C was selected as an indicator of tropical night which is often used to measure extreme high nighttime temperature (nocturnal discomfort). However, the selection of threshold for indicating tropical nights is inconsistent in the scientific literature. Nocturnal thermal high is considered when T_{min} exceeding an absolute threshold such as 25-28°C or 90% or 95% percentile of its climatological series (Ha & Yun, 2012; Klok et al., 2023). The present study selected the threshold (28°C) based on the research conducted in similar tropical Asian countries (Korea and South China) (Chen et al., 2023; Klok et al., 2023).

Local climate zone mapping and collection of summertime air temperature

The LCZ mapping of Nagpur city employed the World Urban Database and Access Portal Tools (WUDAPT) method (Bechtel et al., 2015) to process remotely sensed images using ArcGIS 10.4.4. Pixel-based classification techniques for LCZ mapping have become widely used in urban areas (Verdonck et al., 2017; La et al., 2020). Each pixel was assigned to a single LCZ, and the remotely sensed data was cropped to the region of interest, defined by the Nagpur municipal boundary. The vector processing and supervised classification process involved selecting LCZ training areas from Google Earth, based on expert knowledge. LANDSAT 8 data was then used, along with the maximum likelihood classification (MLC) tool, to classify the LCZs. This process was repeated iteratively until an accurate LCZ map was produced.

Stationary surveys were conducted during the summer of 2022 to gather data across various LCZs (see Figure 2). These sites, representing urban areas with distinct microclimates, provided a 54-day dataset for analysis. The locations were chosen based on LCZ mapping covering ~ 75% area of Nagpur city. Measurements of T_{air} were taken at an elevation between 1.5 - 2 meters above ground level, and recorded at five-minute intervals. Days with abnormal and missing values were filtered. The final dataset was used for further assessment. The instrument setup featured a built-in temperature sensor housed in a radi-

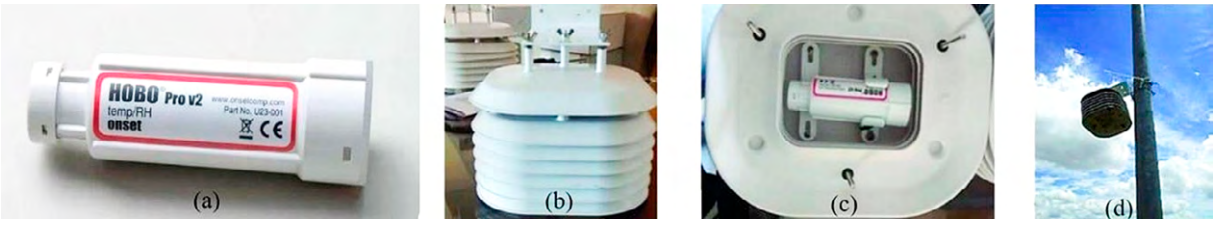

Figure 4. (a) HOBO pro V2 data logger (b) Radiation shield (c) Data logger placed inside the shield (d) Instrument placed at site

ation shield. An Onset HOBO U-23 Pro V2 weatherproof data logger, accurate to ±0.2°C within a temperature range of 0–70°C, was used for data collection (refer Fig. 4a-d). All necessary precautions and specifications were followed during the surveys (Oke, 2004; Runnalls & Oke, 2006).

Heat-hazard risk assessment

The study employed Crichton's conceptual definition of the risk triangle (Crichton, 1999) and IPCC AR4 (IPCC, 2007) to develop the HHR map. This notion offers a concise structure overlapping the layers of hazard and vulnerability. Multiple studies have demonstrated that the multiplicative principle accurately captures the intricate interaction between hazard and vulnerability (Estoque et al., 2020). The present study adopted the methodology used by Ma et al. (2023) and estimated the combined HHR as the aggregate of hazard and vulnerability (refer eqn. 4), which can be understood as:

$$HHR = HH \cdot HV \tag{4}$$

where, *HHR* is the heat-hazard risk, *HH* refers to heat hazard, and *HV* denotes heat vulnerability.

The allocation of weights to indices within the risk triangle framework has been a point of inconsistency in prior literature (Reckien, 2018). Therefore, this study opts for assigning equal weights to the layers of hazard and vulnerability in generating the *HHR*.

Statistical analysis

PCA was applied to embrace multiple factors of vulnerability (Wolf & McGregor, 2013; Inostroza et al., 2016; Nayak et al., 2018; Kotharkar et al., 2019). This approach has proven reliable as a method for reducing dimensions, creating independent principal components (PCs) that accurately represent the maximum variance. A composite PC score (z-score) was formulated to indicate the statistical deviation from the mean value (Wolf & McGregor, 2013). The variance-weighted approach (Schmidtlein et al., 2008) was applied, with the ranking of principal components (PCs) based on the amount of data variability they capture. This ranking is represented by the eigenvalues associated with the vector of each PC (Inostroza et al., 2016). The Pearson correlation matrix was used to observe relationship of individual variables. The variables was standardised as PCA is highly dependent on input vaules. This was accomplished by transforming the values into z-scores (utilizing eqn. 5):

$$Z_i = \frac{X_i - N}{SD} \tag{5}$$

where, Z_i represents the z-score for each ward, X_i denotes the original value, N signifies the mean of all indicator values, and SD represents the standard deviation of the individual indicator values.

The adequacy of the data for PCA was evaluated using the Kaiser-Meyer-Olkin (KMO) test and Bartlett's test of sphericity. For sampling adequacy, the KMO estimate should be more than 0.50 (on a scale from 0 to 1) and *p value <0.001* to pass Bartlett's test (Adnan et al., 2023). The Kaiser eigenvalue criterion (eigenvalue > 1) was employed along with orthogonal varimax rotation to extract PCs as suggested by Kaiser (1960). Varimax rotation was chosen due to its capability to extract highly independent components (Raja et al., 2021). Any component that accounted for approximately 10% of the variance, or where the cumulative percent of the retained components was at least 70%, was kept. The calculated scores from Eqn. (2) were integrated to compute the aggregated HVI score. Subsequently, Eqn. (6) was applied to standardize the HVI scores for each ward on a scale from 0 to 1 (Inostroza et al., 2016):

$$\beta = \left[\frac{x - x_{min}}{x_{max} - x_{min}} \right] \tag{6}$$

where, β represents the normalized HVI value for each ward, while x denotes the original HVI value. The terms x_{min} and x_{max} refer to the lowest and highest HVI values, respectively.

The HVI was calculated by summing the scores from each component for each ward. These normalized HVI values were then grouped into five categories—'very low', 'low', 'moderate', 'high', and 'very high'—based on the GIS methodology outlined by Raja et al. (2021).

Estimation of satellite-based LST and NDVI

The study utilized the Thermal Infrared Sensor (TIRS) and Operational Land Imager (OLI) instruments of LANDSAT 8 to acquire daytime Land Surface Temperature (LST) data. [imagery date: 22 April 2022; cloud cover: 2.97%; sun elevation: 66°; (path 144, row 45)], which overlaps with the period of data collection across LCZ sites (year 2022). The date was selected as it represents a typical hot summer day for Nagpur city. Satellite imagery for Nagpur was obtained from open-source data (https://eos.com/landviewer/?lat=21.14510&lng=79.08610&z=11). LANDSAT 8 satellite data offer several advantages, including enhanced radiometric and spectral resolution, a better signal-to-noise ratio, refined bandwidth, and two thermal infrared bands (Dube & Mutanga 2015; Karlson et al. 2015). LST was extracted by widely adopted methodology in multiple studies (Zanter, 2016; Navarro-Estupiñan; 2020).

Results and findings

The present study evaluated city-scale HH and related vulnerability to estimate HHR for Nagpur city. The findings are presented in four sub-sections which include; a) spatial distribution of LST, NDVI and LCZ classes (b) constructing a composite HVI using the indicators of adaptive capacity, sensitivity and exposure (c) mapping of HH and HHR.

Spatial distribution of LCZ classes and mapping of LST and NDVI

The LCZ mapping of Nagpur city showed a heterogeneous and uneven structure and confirmed its compact pattern (refer Fig. 5a). It has 10 built types (LCZs 1-10) and zones with few nested LCZs (LCZs 3_7, 3_F, 6_5, 6_B and 9_3). Built and natural types accounted for 72.61% and 27.39% area respectively (refer Fig. 5b). The central regions were primarily characterized by a combination of compact low-rise settings (LCZ 3) and mid-rise buildings (LCZ 2). In contrast, the peripheral areas were dominated by LCZs 9 and 9_3. LCZ 6_5 (open mid-rise nested in open low-rise zone) constitutes a significant sub-class among built zones, accounting for approximately 9.97% of the total area. LCZs 3 and 9 were the dominant zones covering 14.74% and 9.86% of the area respectively (refer Fig. 5c).

The city center comprising LCZs 3 (38.78°C) and 3_7 (38.99°C) showed lower LST_{max} values mainly due to mutual shading attributed to densely packed buildings (see Fig. 5d). Outer city limits embracing LCZs 9 (max. 41.78°C) and 9_3 (max. 41.02°C) generally showed higher LST_{max} values due to high daytime exposure. LCZs 3_F (max. 40.03°C) and F (max. 46.69°C) also showed higher values due to the presence of bare patches. Areas with lower temperatures were predominantly concentrated in water bodies and vegetated areas. These regions have the capacity to moderate temperatures through mechanisms such as heat absorption, evapotranspiration, and shading. The average LST observed for built-up areas was 35.05°C, while for vegetation it was 33.59°C, and for water bodies, it stood at 26.85°C.

The spatial pattern of Land Surface Temperature (LST) aligns with the distribution of LCZs, where areas with a higher concentration of built-up zones tend to exhibit higher LST values (refer Fig. 3d). An average LST of 35.58°C was observed while the maximum and minimum values were 53.23°C and 17.94°C respectively. The peripheral areas especially along the northern, south-western zones were characterized by higher LST values. Spatial differences in NDVI showed lack of greenness/vegetation within the city limits (refer Fig. 5e). Core areas comprising high density settings showed lower NDVI values. The pixel-based maximum and minimum NDVI values were observed to be 0.435 and -0.101 respectively. There is a notable negative correlation observed LST and NDVI, indicated by a Pearson correlation coefficient of -0.354 ($p<0.01$), suggesting a statistically significant relationship between the two variables.

Developing a composite HVI

In the next step, the Pearson correlation matrix was calculated to assess the strength and direction of the relationship between the two variables. Indicators of adaptive capacity when correlated with those of sensitivity, yielded moderate to strong relationships (see Table 1). For instance, electricity supply was positively correlated with population density (+0.48), housing typology (+0.559) and single household size (+0.648). NDVI was negatively correlated with roof material (-0.229) and LST (-0.354). Indicators of sensitivity were found to be strongly correlated with infrastructural facilities (e.g., water/electricity supply, access to communication). Communication facilities (access to landline/mobile) showed a strong positive relationship with building typology (+0.804), single household size (+0.647), average number of people/household (+0.665) and rented housing (+0.632). LST as the sole indicator of exposure was found to be positively associated with building typology (+0.407), population density (+0.496) and roof material (0.551).

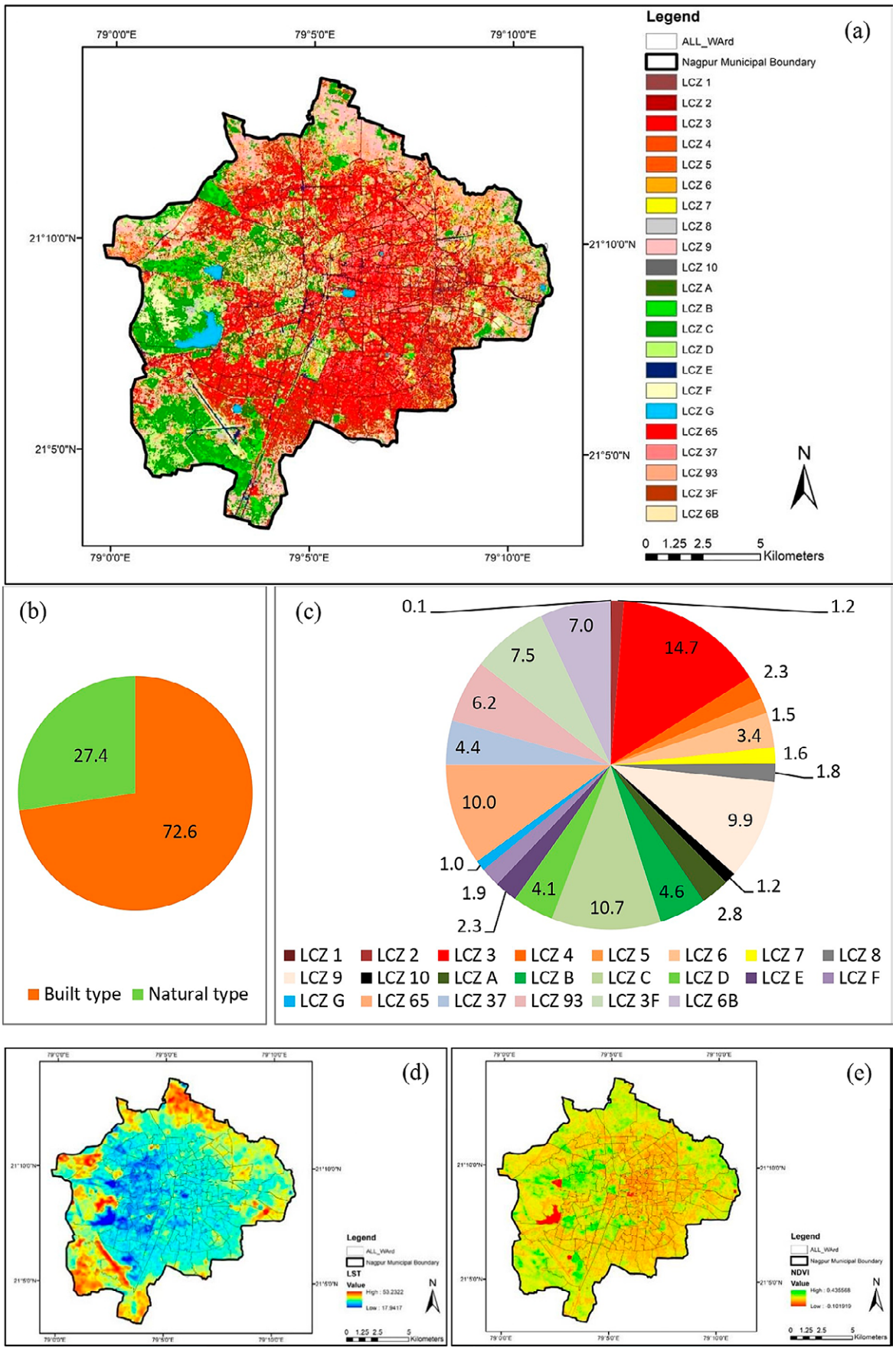

Figure 5. (a) LCZ mapping of Nagpur city (b) proportion of built and natural types (c) overall coverage of different LCZs (d) Pixel-based mapping of LST (e) spatial distribution of NDVI

Table 1. Correlation matrix (Pearson)

Indicators	ES	WS	CF	HF	SF	PV	BA	NDVI	IP	FP	YP	OP	SCST	PD	POP	TYP	SH	HH	RH	TS	RM	DIS	LST
ES	**1**	0.144	**0.492**	**0.449**	**0.593**	0.177	0.296	0.052	**0.423**	-0.095	-0.078	-0.399	0.145	**0.480**	0.170	**0.559**	**0.648**	0.392	**0.741**	**0.573**	**0.730**	-0.051	0.242
WS	0.144	**1**	0.143	0.130	-0.046	-0.128	**0.501**	-0.157	0.055	0.281	-0.084	0.296	-0.053	-0.083	-0.091	0.181	0.114	-0.013	0.106	-0.197	0.133	0.209	-0.12
CF	**0.492**	0.143	**1**	**0.856**	**0.496**	**0.518**	0.288	-0.027	**0.677**	0.287	-0.250	-0.275	0.139	-0.123	**-0.441**	**0.804**	**0.647**	**0.665**	**0.632**	0.126	-0.171	0.377	0.29
HF	**0.449**	0.130	**0.856**	**1**	0.365	**0.460**	0.308	0.184	**0.703**	0.401	-0.054	-0.287	0.025	-0.073	-0.308	**0.896**	**0.754**	**0.673**	**0.717**	0.355	**0.791**	**0.508**	-0.116
SF	**0.593**	-0.046	**0.496**	0.365	**1**	0.106	-0.078	0.096	**0.473**	-0.149	-0.094	-0.113	0.066	0.301	-0.099	**0.447**	**0.514**	**0.553**	**0.657**	**0.703**	**0.571**	0.025	0.087
PV	0.177	-0.128	**0.518**	**0.460**	0.106	**1**	-0.044	-0.162	**0.491**	0.059	-0.183	-0.089	0.156	-0.297	-0.283	**0.477**	0.299	0.273	0.266	0.326	0.396	0.032	0.085
BA	0.296	0.501	0.288	0.308	-0.078	-0.044	**1**	0.035	0.196	0.197	-0.334	0.000	-0.018	0.200	0.092	0.262	0.283	0.045	0.268	-0.233	0.244	-0.112	-0.178
NDVI	0.052	-0.157	-0.027	0.184	0.096	-0.162	0.035	**1**	0.014	-0.292	-0.171	0.037	0.168	-0.39	-0.289	**-0.408**	0.219	0.132	-0.261	-0.14	-0.229	-0.35	-0.354
IP	**0.423**	0.055	**0.677**	**0.703**	**0.473**	**0.491**	0.196	0.014	**1**	0.142	-0.368	-0.240	0.239	0.161	-0.123	**0.730**	**0.693**	**0.535**	**0.749**	**0.601**	**0.749**	-0.296	0.039
FP	-0.095	0.281	0.287	0.401	-0.149	0.059	0.197	-0.292	0.142	**1**	-0.125	0.134	**-0.442**	-0.259	-0.365	**0.445**	0.404	0.056	0.266	-0.067	0.227	-0.365	0.008
YP	-0.078	-0.084	-0.250	-0.054	-0.094	-0.183	-0.334	-0.171	-0.368	-0.125	**1**	-0.121	-0.166	0.062	0.015	-0.173	-0.140	-0.020	-0.106	-0.053	-0.057	-0.268	-0.057
OP	-0.399	0.296	-0.275	-0.287	-0.113	-0.089	0.000	0.037	-0.240	0.134	-0.121	**1**	-0.188	-0.294	-0.215	-0.271	-0.336	-0.259	-0.401	-0.361	-0.376	0.021	0.131
SCST	0.145	-0.053	0.139	0.025	0.066	0.156	-0.018	0.168	0.239	**-0.442**	-0.166	-0.188	**1**	0.008	0.004	-0.110	-0.188	0.221	-0.134	0.062	-0.051	0.103	-0.06
PD	**0.480**	-0.083	-0.123	-0.073	0.301	-0.297	0.200	-0.39	0.161	-0.259	0.062	-0.294	0.008	**1**	**0.654**	-0.001	0.193	0.190	0.376	0.291	0.370	**0.424**	**0.496**
POP	0.170	-0.091	**-0.441**	-0.308	-0.099	-0.283	0.092	-0.289	-0.123	-0.365	0.015	-0.215	0.004	**0.654**	**1**	-0.222	-0.117	-0.158	-0.022	-0.115	0.141	**0.516**	0.204
TYP	**0.559**	0.181	**0.804**	**0.896**	**0.447**	**0.477**	0.262	**-0.408**	**0.730**	**0.445**	-0.173	-0.271	-0.110	-0.001	-0.222	**1**	**0.916**	**0.500**	**0.843**	**0.508**	**0.877**	0.038	**0.407**
SH	**0.648**	0.114	**0.647**	**0.754**	**0.514**	0.299	0.283	0.219	**0.693**	0.404	-0.140	-0.336	-0.188	0.193	-0.117	**0.916**	**1**	0.314	**0.947**	**0.555**	**0.853**	-0.257	-0.175
HH	0.392	-0.013	**0.665**	**0.673**	**0.553**	0.273	0.045	0.132	**0.535**	0.056	-0.020	-0.259	0.221	0.190	-0.158	**0.500**	0.314	**1**	**0.458**	**0.510**	**0.608**	0.031	0.289
RH	**0.741**	0.106	**0.632**	**0.717**	**0.657**	0.266	0.268	-0.261	**0.749**	0.266	-0.106	-0.401	-0.134	0.376	-0.022	**0.843**	**0.947**	**0.458**	**1**	**0.689**	**0.909**	-0.274	0.23
TS	**0.573**	-0.197	0.126	0.355	**0.703**	0.326	-0.233	-0.14	**0.601**	-0.067	-0.053	-0.361	0.062	0.291	-0.115	**0.508**	**0.555**	**0.510**	**0.689**	**1**	**0.628**	0.119	-0.172
RM	**0.730**	0.133	-0.171	0.791	**0.571**	0.396	0.244	-0.229	**0.749**	0.227	-0.057	-0.376	0.051	0.370	0.141	**0.877**	**0.853**	**0.608**	**0.909**	**0.628**	**1**	0.07	**0.551**
DIS	-0.051	0.209	0.377	0.508	0.025	0.032	-0.112	-0.35	-0.296	-0.365	-0.268	0.021	0.103	**0.424**	**0.516**	0.038	-0.257	0.031	-0.274	0.119	0.07	**1**	-0.08
LST	0.242	-0.12	0.29	-0.116	0.087	0.085	-0.178	-0.354	0.039	0.008	-0.057	0.131	-0.06	**0.496**	0.204	**0.407**	-0.175	0.289	0.23	-0.172	**0.551**	-0.08	**1**

Values in bold present strong statistical relationship at a significance level alpha=0.05

A composite HVI was derived by aggregating the components with equal weight and then normalizing the result. The PCA yielded consistent outcomes with nearly constant values for the eigenvalues and loadings of PCs, as depicted in Table 4. The present study estimated KMO values in the range of 0.59-0.73 and *p-value* to be 2.2e-16 (see Table 2) which taken together proves the suitability of dataset for HV analysis.

Table 2. Measure of Kaiser-Meyer-Olkin (KMO) and Bartlett's test of sphericity

Adaptive Capacity		Sensitivity		Exposure	
KMO	Bartlett's p-value	KMO	Bartlett's p-value	KMO	Bartlett's p-value
0.73	2.2e-16	0.59	2.2e-16	0.62	2.2e-16

The results of PCA highlighted the respective contributions of various factors to the HVI (refer Table 3). Two PCs with eigenvalues > 1 collectively explained 71.38% of the variance in the dataset (PC1: 44.02% and PC2: 27.36%). According to the rotated component matrices, PC1 was mainly presented indicators of adaptive capacity which included communication facilities (-0.270), health facilities (+0.719) and sensitivity indicators comprising female population (+0.537), young population (+0.692), population density (+0.753), average number of people/household (+0.679) and roof material (+0.610). PC2 mainly featured other indicators of sensitivity illiterate population (+0.730), elderly population (+0.628), SC/ST population (+0.531) and LST (+0.520). The PC loadings indicated that infrastructural facilities act as coping solutions while demographic factors and housing conditions are major influencing indicators of HV.

The HV mapping was generated using its composite values (see Annexure II). Subsequent mapping of HV variables showed distinct variation across different wards of the city. Administrative wards in core areas showed a greater

Table 3. PC loadings for indicators

	Indicators	PC1	PC2	PC3	PC4	PC5	PC6
ADPATIVE CAPACITY	1. Electricity supply	+0.106	-0.007	+0.112	+0.032	+0.014	+0.005
	2. Water supply	+0.087	+0.806^	-0.040	+0.223	-0.020	+0.119
	3. Communication facilities	-0.270*	+0.051	+0.140	-0.051	+0.117	-0.02
	4. Health facilities	+0.719*	+0.023	+0.198	+0.157	+0.039	-0.024
	5. Social facilities: religious facilities & schools	-0.091	+0.044	-0.069	+0.56	+0.063	-0.223
	6. Personal vehicle	-0.183	+0.102	-0.027	+0.009	+0.066	-0.006
	7. Bank account	-0.113	+0.039	-0.005	-0.142	-0.096	+0.081
	8. Normalized Difference Vegetation Index	-0.234	+0.017	+0.184	-0.058	+0.104	-0.026
SENSITIVITY	9. Illiterate Population	+0.101	+0.730^	-0.146	+0.087	+0.04	+0.097
	10. Female population	+0.537*	+0.014	+0.060	+0.161	-0.126	-0.015
	11. Population aged under 6 years	+0.692*	+0.056	+0.139	+0.042	-0.003	+0.008
	12. Population aged over 60 years	+0.173	+0.628^	+0.409	+0.006	-0.144	-0.101
	13. Population of Scheduled Caste (SC)/ Scheduled Tribe (ST)	+0.060	+0.531^	-0.071	-0.018	+0.068	-0.09
	14. Population density	+0.753*	+0.181	+0.048	+0.039	-0.032	+0.142
	15. Typology of houses	+0.056	-0.109	+0.486	+0.072	+0.194	+0.055
	16. Single household size	+0.480	+0.504	+0.094	+0.091	+0.043	-0.027
	17. Average number of people per household	+0.679*	+0.091	+0.003	-0.006	-0.018	-0.031
	18. Rented housing	-0.131	+0.128	+0.152	+0.153	+0.039	+0.077
	19. Roof material	+0.610*	+0.103	-0.018	+0.068	-0.018	-0.165
	20. Population that has disability 18-64 years	-0.058	+0.158	+0.031	+0.024	+0.058	-0.084
EXPOSURE	21. Land surface temperature	+0.18	+0.520	+0.029	+0.082	-0.045	-0.02

*Note: Statistically significant ones are values > 0.5; * Statistically significant values for PC1; ^ Statistically significant values for PC2*

mix of 'very low' and 'very high' adaptive capacity. Core areas mostly represent a mix of old neighborhoods and newly developed zones. This may possibly be attributed to a difference in infrastructural facilities (water and electricity supply), urban redevelopment initiatives and presence of differential vegetation cover. Such moderations can cause change in adaptive capacity within core areas. Urban fringes in western direction had lower levels. Adaptive capacity was generally 'very high' in the wards located in far northern and southern fringes. The core and adjoining areas generally showed 'moderate and 'high' levels of exposure while majority of fringes featured in 'very high' levels. The results revealed that more than 66% of the area was in 'high' or 'very high' exposure range. For sensitivity, western fringes were found to be in 'high' range while core areas generally showed 'moderate' values. About 40% of the area was found to be with 'very low' and 'low' sensitivity levels (refer Fig. 6).

els and 24.54% were located in 'moderate' level. 33 wards in 'very high' levels of HV were used for further analysis to calculate HHR. These were mainly located towards the eastern side and distributed in the city center and fringes. A detailed assessment of HV mapping revealed that a total of 69 wards present with 'high' (0.31-0.41) and 'very high' (>0.41) HVI. A total area of 39.7 km^2 (out of total 217.65 km^2) in the city was found to have 'high' and 'very high' HVI but constituted 49.06% of the population (about 1.18 million). Majority of the 'high' and 'very high' HV areas were dominated by compact low-rise neighbourhoods, sparsely-built settings and built areas nested with bare soil.

Mapping of HH and HHR

Mapping of HH accounted for the intensity and frequency of HW event during the 2022 summer season. The hazard map revealed the distribution of high temperature days (both daytime and nighttime above a certain threshold)

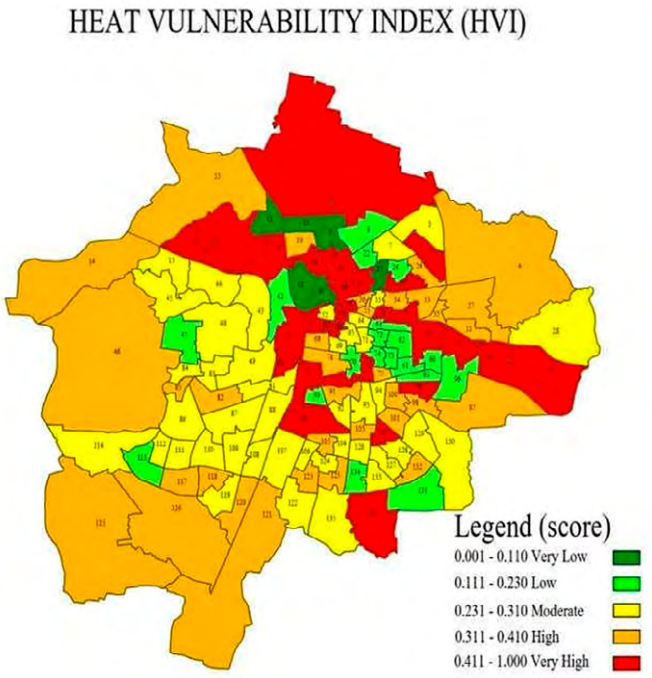

Figure 6. Spatial extent and distribution of HVI

The HV mapping was generated using eqn. (2) using its composite values 'Very high' levels of HV were found in core and urban fringes. Areas with moderate vegetation cover correspond to 'low' or 'very low' HV while most of the residential areas featured in 'moderate' level. The mapping showed a greater variation in the eastern direction while the western fringes majorly presented a consistent HV signature in 'moderate' level. The composite HV map showed a distribution of 'very low' in 5 wards; 'low' in 20 wards; 'moderate' in 42 wards; 'high' in 36 wards while 33 wards were under 'very high' category. About one-fourth of the population was found to be in 'very low' or 'low' lev-

based on on-site data collection across different LCZs (see Fig. 7a). Mapping results revealed that a high percentage (>50%) of land area is exposed to 'very high' HH. Majority of 'very high' HH areas were found to be concentrated in the central, eastern and southern parts of the city. Among the built classes, HH levels were found to be 'very high' for LCZs 3 (0.481), 3_F (0.472), 5 (0.426), 6_5 (0.444), 8 (0.454) and 9_3 (0.481) as they experienced high daytime and nocturnal heat stress. 'High' HH was observed for LCZ 6 (0.352) while LCZ 9 showed 'moderate' value (0.306). Open zones with vegetation/trees (LCZ 6_B) and natural classes (LCZs A and B) demonstrated 'low' HH values. Fringe areas in

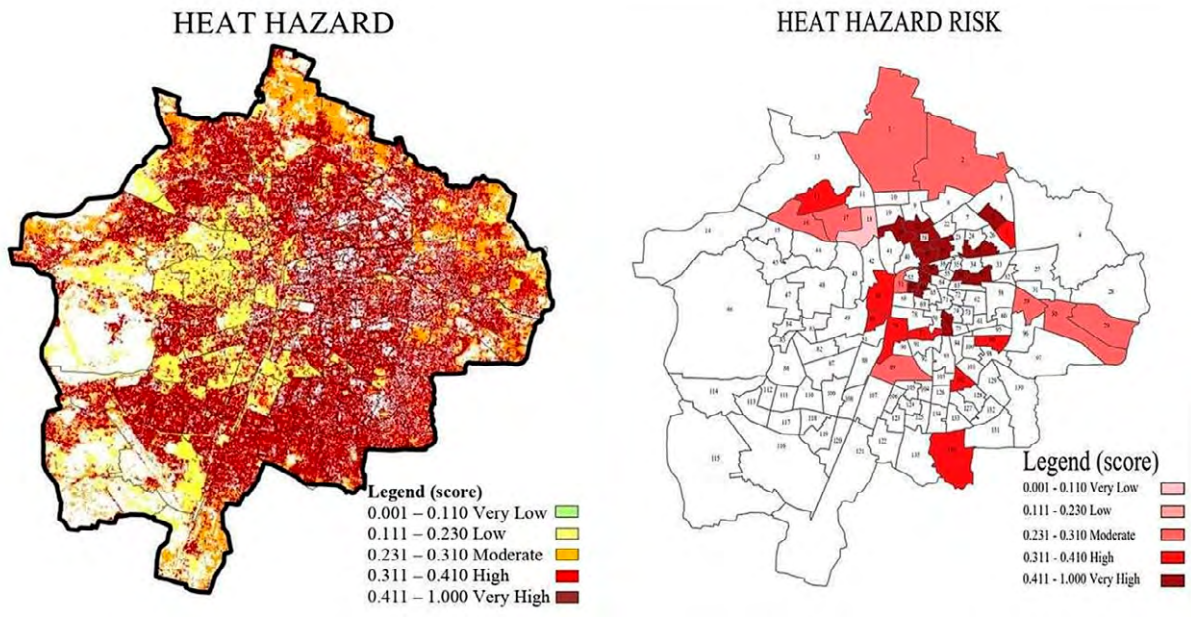

Figure 7. Spatial distribution of (a) heat hazard (b) heat hazard risk

the north-eastern direction generally showed 'moderate' HH values. The spatial distribution of HHR for wards with 'very high' HV is shown in Fig. 7 (b). HHR in the city centre of Nagpur appears to be higher compared to the suburbs. Out of the 33 wards with 'very high' HV, 14 wards were designated with 'very high' HHR (>0.411) and were located in the east-central part of the city. These constitute highly dense areas coupled with very high population density. 'High' (9 wards) and 'moderate' (9 wards) HHR constituted 18 wards and were distributed across the core areas and urban fringes.

LCZ-based HHR mapping revealed that densely built areas generally had higher values. LCZs constituting at least 75% of the wards were extracted and termed as 'dominant' ones. Due to differences in urban morphology that LCZs represent, their corresponding risk levels were found to be varied (see table 4). Spatial overlap and the intensity of heat risk across LCZ classes were analysed for 33 wards which featured with 'very high' composite HVI scores. The intersection of wards and HHR distribution mostly aligns (commonly prevalent) for LCZs 3, 3F and 9. In a few wards, there exists disagreements. 'Very high' HHR were characteristic for LCZ 3 and 3_F while 'high' HHR values corresponded for LCZs 3, 3_7, 3_F, 6_5 and 9. Natural (LCZs A and B) and built classes with vegetation cover (LCZ 6_B) showed 'moderate' and/or 'low' HHR. 'Very high' and 'high' HHR areas covered 17.43 km^2, accounting for about 8% of the total area. This shows a great deal of spatial heterogeneity in HHR even within wards with 'very high' HV. The findings reflect that compact low-rise and its variants (LCZs 3 and 3_F) and sparsely built zones and its variants (LCZ 9 and 9_3) agree with the distribution of HHR across these administrative wards. Conversely, LCZ classes (3_7, 6, 6_5, 6_B and B) disagree when wards and HHR values intersect.

Table 4. Prevalent LCZs with very high HVI and respective HHR

Ward No	HVI score	Dominant LCZs	Heat Hazard Risk (level)
1	0.483	3 & 9	0.291 (moderate)
2	0.511	3 & 9	0.294 (moderate)
5	0.616	3, 3_7 & 9	0.401 (high)
6	0.547	3_7 & 9_3	0.577 (very high)
12	0.493	3 & 6_5	0.399 (high)
16	0.441	3 & 6_5	0.305 (moderate)
17	0.529	3, 5, & 9	0.254 (moderate)
18	0.477	3, 6_5, & 6_B	0.108 (very low)
20	0.532	3 & 6	0.452 (very high)
21	0.45	3 & 9_3	0.592 (very high)
25	0.474	3 & 3_F	0.532 (very high)
29	0.776	3 & 9	0.309 (moderate)
30	0.797	3, 6 & 9	0.263 (moderate)
37	0.573	3 & 3_F	0.451 (very high)
38	0.541	3 & 3_F	0.510 (very high)
39	0.42	3	0.492 (very high)
50	0.56	3, & 6_B	0.359 (high)
51	0.444	3, 6, & 3_F	0.282 (moderate)
53	0.423	3	0.542 (very high)
54	0.479	3	0.531 (very high)
56	0.724	3	0.617 (very high)
57	0.579	3, 6 & 3_F	0.516 (very high)
59	0.495	3, 6 & 9	0.310 (moderate)
66	0.522	3	0.555 (very high)
67	0.447	3	0.618 (very high)
76	0.448	3	0.491 (very high)
77	0.428	3, 3_F & B	0.401 (high)
79	0.444	3, 6, & 6_B	0.399 (high)
80	0.416	3 & 9_3	0.352 (high)
89	0.437	3, 6, & 6_B	0.246 (moderate)
99	0.42	3, 3F, & 6_5	0.356 (high)
102	0.416	3, 6 & 3_F	0.359 (high)
136	0.642	3, 9 & 3_F	0.380 (high)

Discussion

The present study carried out a comprehensive HV/R assessment for Nagpur, a tropical and heat-prone Indian city. The city experiences extreme summertime conditions and often witness severe HW conditions, thus affecting a large and sprawling city (Mohite & Surawar, 2024). Research efforts in Nagpur have demonstrated a strong correlation between heat stress indices and all-cause mortality, with certain LCZ classes showing higher susceptibility to heat stress (Kotharkar et al., 2024a; Dutta et al., 2020). The aim was to pinpoint populations or geographic areas at elevated risk by leveraging spatial socio-economic and environmental data. PCA was utilized to assess vulnerability encompassing three underlying vulnerability components: exposure, sensitivity, and adaptive capacity. Among the indicators of adaptive capacity, infrastructural facilities (such as access to water, electricity, mobile/landline services, healthcare/social facilities, and NDVI) showed a negative correlation with HVI. Such findings

corroborate the results of previous studies (Rinner et al., 2010; Adnan et al., 2023). Social isolation was found to be another risk factor (Luber & McGeehin 2008, Uejio et al., 2011). PCA generated two PCs where the first one consisted of infrastructural facilities, specific population groups (young and females) and housing characteristics while the other one featured LST, illiterate, elderly, and SC/ST population (Cutter et al., 2003; Azhar et al., 2017; Karanja et al., 2025). Health care services provided by medical infrastructure (e.g., hospitals, clinics) were identified as crucial indicators. Education level was found to be associated with socio-economic status, as high illiteracy rates indicate a reduced ability to read and understand heat-health warnings.

Spatial distribution of HV revealed three clusters with 'very high' values. These wards, characterized by high population density, are scattered across the central part of the city and are represented by older neighbourhoods and core residential areas. This distribution aligns with the outcomes reported in previous studies (Wolf & McGregor, 2013; Raja et al., 2021). The study found LCZs 8 and 10 to be associated with higher LST but with relatively low risk similar to the findings in Changzhou, China (Ma et al., 2023). This is due to low population density as against other residential and compact zones (LCZs 3 and 3_F) (Ma et al., 2023). It proves that LST is not a good indicator for HH assessment. Additionally, differential adaptive capacity was observed within core areas owing to demographic shifts, urban redevelopment and changes in infrastructural facilities. The study also confirmed a significant negative correlation between LST and NDVI which provides strong scientific evidence for increasing urban green spaces for effective heat mitigation.

The Pearson correlation matrix revealed a statistically significant positive relationship between overall heat vulnerability and lack of adaptive capacity, aligning with the findings of Rathi et al. (2021) and Hess et al. (2012). Previous studies describe the relationship between adaptive capacity and vulnerability in three ways: (1) they are not mutually exclusive, (2) vulnerability can result from limited adaptive capacity along with other factors, and (3) they are inversely related, meaning greater adaptive capacity leads to lower vulnerability and vice versa (Brooks et al., 2005; Gaillard, 2010). In this study, vulnerability was found to be directly proportional to the lack of adaptive capacity. This suggests that municipal authorities should implement short-term measures to improve the adaptive capacity of vulnerable households, while also developing long-term strategies to reduce their exposure and sensitivity.

The present study found significant variation in HHR levels across different LCZs. It also noted that compact low-rise zones and its variants (LCZs 3 and 3_F) occupying a large proportion of area showed 'high' and 'very high' HHR. This could be attributed to closely spaced buildings coupled with minimal vegetation leading to less evapotranspiration (Li et al., 2025; Zou et al., 2025). Additionally, these zones have a high percentage of impervious surfaces with densely built areas representative of older urban neighbourhoods or inner-city residential zones. These zones reflect a higher population density and anthropogenic heat release which require urgent attention. Conversely, midrise LCZs (LCZs 2 and 5) did not exhibit high risk. This could be due a combination of factors related to urban morphology, and socioeconomic context. These zones house less vulnerable populations owing to better infrastructure facilities (water and electricity). The findings align with previous empirical evidence observed in hot-dry tropical/sub-tropical climates (Huang et al., 2023) and other cities in China (Cai et al., 2019; Li et al., 2022). Peripheral areas representative of LCZs 9 and 9_3 also featured with 'very high' HHR. Conversely, low-density and open developments (LCZ 6 and 6_B) presented lesser risks to extreme heat (Inostroza et al., 2016). Previous studies on high density and heterogeneous developments also support similar findings (Zhou et al., 2021; Chen et al., 2022; Cheval et al., 2022). These findings align with past research in Nagpur city which has shown an increasing trend in maximum temperatures, and hot nights, with heat stress indices rising over time (Kotharkar et al., 2024b).

The limitations of the study need to be acknowledged. Firstly, the present research used 2011 census data to estimate HV, as the 2021 census was postponed due to the COVID-19 pandemic. This may create some discrepancy among data collection dates and inevitably result in some temporal ambiguity in the index estimates. Secondly, ward-wise mortality data was unavailable which limits the validity of HV estimation. Lastly, equal weightage was allotted to the indicators which may not represent unique characteristics of cities. Weightings can be adjusted based on new insights into heat-related health issues or specific user needs. Future studies can include multiple instances represented by several LST imagery can enhance the accuracy and reliability of HV. Additionally, research efforts can account for biometeorological indices to better quantify the exposure.

Conclusion

Urban heat and extended periods of hot weather present a significant challenge to residents and cause heat-related health risks. The present study assessed HHR and estimated associated vulnerability using the variables of adaptive capacity, sensitivity and exposure. It used a detailed, granular approach, incorporating both remotely sensed

and on-site meteorological data to estimate the city-level HHR. The mapping of heat vulnerability revealed significant spatial asymmetry in its distribution. City centres and adjoining areas along with urban fringes were recognized with 'very high' HHR while open developments and areas with moderate vegetation cover presented lesser HRs. The HHR map for Nagpur serves as an effective tool for devising heat mitigation strategies and identifying hotspot areas, aiding in the identification of vulnerable zones or populations. This approach aids in identifying risk prevention strategies and prioritizing heat management tactics at the municipal level. Application of spatial frameworks (e.g., LCZ map used in this study) could provide crucial insights for urban planners to consider climate-based recommendations to alleviate extreme heat in specific zones in a city. The results could inform evidence-based guidelines within city-level HHAPs.

Researchers agree that urban HV/R is a complex phenomenon characterized by significant spatial and temporal variability. As a result, HV/R assessments must be dynamic, adapting to recognize evolving risks driven by changes in urban characteristics. Future research efforts could be extended to the implementation of a localized heat early warning system and can be conducted in cities which are likely to be affected by future warming. Future research could consider supplementary indicators, such as pre-existing medical or chronic conditions, access to air conditioning, income level, and other relevant data. In addition, enhancing the quality of LCZ as a spatial unit of analysis can improve the overall interpretation of results. The methodology adopted in the present study with slight adjustments can act as a guide for an accurate retrieval of HHR and allows for greater replicability across different spatial scales.

Acknowledgement

The study is under the research project "Developing framework for heat vulnerability mapping and model heat action plan for Indian cities", supported by the National Disaster Management Authority (NDMA), New Delhi, Government of India (Sanction No. 1-111/2019-PP). We thank the Department of Architecture & Planning, Visvesvaraya National Institute of Technology (VNIT), Nagpur for providing the necessary infrastructure.

References

Adnan, M. S. G., Kabir, I., Hossain, M. A., Enan, M. S., Chakma, S., Tasneem, S. N., Hassan, Q. K., & Dewan, A. (2023). Heatwave vulnerability of large metropolitans in Bangladesh: an evaluation. *Natural Hazards*. (preprint version). https://doi.org/10.21203/rs.3.rs-3093933/v1

Aubrecht, C., & Özceylan, D. (2013). Identification of heat risk patterns in the U.S. National Capital Region by integrating heat stress and related vulnerability. *Environment International*, 56, 65–77. 10.1016/j.envint.2013.03.005

Azhar, G., Saha, S., Ganguly, P., Mavalankar, D., & Madrigano, J. (2017). Heat Wave Vulnerability Mapping for India. *International Journal of Environmental Research and Public Health*, 14(4), 357. 10.3390/ijerph14040357

Bechtel, B., Alexander, P., Böhner, J., Ching, J., Conrad, O., Feddema, J., ... & Stewart, I. (2015). Mapping Local Climate Zones for a Worldwide Database of the Form and Function of Cities. *ISPRS International Journal of Geo-Information*, 4(1), 199–219. 10.3390/ijgi4010199

Brooks, N., Adger, W. N., & Kelly, P. M. (2005). The determinants of vulnerability and adaptive capacity at the national level and the implications for adaptation. *Global environmental change*, 15(2), 151-163. https://doi.org/10.1016/j.gloenvcha.2004.12.006

Cai, Z., Tang, Y., Chen, K., & Han, G. (2019). Assessing the Heat Vulnerability of Different Local Climate Zones in the Old Areas of a Chinese Megacity. *Sustainability*, 11(7), 2032. https://doi.org/10.3390/su11072032

Chen, B., Xie, M., Feng, Q., Wu, R., & Jinag, L. (2022). Diurnal heat exposure risk mapping and related governance zoning: A case study of Beijing, China. *Sustainable Cities and Society*, 81, 103831. https://doi.org/10.1016/j.scs.2022.103831

Chen, R., Wen, Z., Lin, W., & Qiao, Y. (2023). Diverse relationship between the tropical night in South China and the water vapor transport over the South China Sea and the plausible causes. *Atmospheric Research*, 296, 107080. https://doi.org/10.1016/j.atmosres.2023.107080

Chen, T-L., Lin, H., & Chiu, Y-H. (2021). Heat vulnerability and extreme heat risk at the metropolitan scale: A case study of Taipei metropolitan area, Taiwan. *Urban Climate*, 41, 101054. https://doi.org/10.1016/j.uclim.2021.101054

Cheval, S., Dumitrescu, A., Amihăesei, V., Irașoc, A., Paraschiv, M.-G., & Ghent, D. (2022). A country scale assessment of the heat hazard-risk in urban areas. *Building and Environment*, 229, 109892. https://doi.org/10.1016/j.buildenv.2022.109892

Crichton, D. (1999) The Risk Triangle. In: Ingleton, J., Ed., *Natural Disaster Management*, Tudor Rose, London, 102-103.

Cutter, S. L., Boruff, B. J., & Shirley, W. L. (2003). Social vulnerability to environmental hazards. *Social Science Quarterly*, 84(1), 242–261. https://doi.org/10.1111/1540-6237.8402002

Dube, T., & Mutanga, O. (2015). Evaluating the utility of the medium-spatial resolution Landsat 8 multispectral sensor in quantifying aboveground biomass in uMgeni catchment, South Africa. *ISPRS Journal of Photogrammetry and Remote Sensing*, 101, 36–46. https://doi.org/10.1016/j.isprsjprs.2014.11.001

Dutta, P., Sathish, L., Mavankar, D., Ganguly, P. S., & Saunik, S. (2020). Extreme Heat Kills Even in Very Hot Cities: Evidence from Nagpur, India. *The international journal of occupational and environmental medicine*, 11(4), 188–195. https://doi.org/10.34172/ijoem.2020.1991

Ebi, K. L., Capon, A., Berry, P., Broderick, C., de Dear, R., Havenith, G., ... & Jay, O. (2021). Hot weather and heat extremes: health risks. *The Lancet*, 398(10301), 698–708. https://doi.org/10.1016/S0140-6736(21)01208-3

Ellena, M., Melis, G., Zengarini, N., Di Gangi, E., Ricciardi, G., Mercogliano, P., & Costa, G. (2023). Micro-scale UHI risk assessment on the heat-health nexus within cities by looking at socio-economic factors and built environment characteristics: The Turin case study (Italy). *Urban Climate*, 49, 101514. https://doi.org/10.1016/j.uclim.2023.101514

Estoque, R. C., Ooba, M., Seposo, X. T., Togawa, T., Hijioka, Y., Takahashi, K., & Nakamura, S. (2020). Heat health risk assessment in Philippine cities using remotely sensed data and social-ecological indicators. *Nature Communications*, 11(1). https://doi.org/10.1038/s41467-020-15218-8

Gaillard, J. C. (2010). Vulnerability, capacity and resilience: Perspectives for climate and development policy. *Journal of International Development: The Journal of the Development Studies Association*, 22(2), 218-232. https://doi.org/10.1002/jid.1675

Gasparrini, A., & Armstrong, B. (2011). The impact of heat waves on mortality. *Epidemiology (Cambridge, Mass.)*, 22(1), 68–73. https://doi.org/10.1097/EDE.0b013e3181fdcd99

Ghosh, A. (2024). Smart Heat-health Action Plans: A programmatic, progressive and dynamic framework to address urban overheating. *Geographica Pannonica*, 28(3), 221-237. https://doi.org/10.5937/gp28-51694

Gu, S., Huang, C., Bai, L., Chu, C., & Liu, Q. (2016). Heat-related illness in China, summer of 2013. *International Journal of Biometeorology*, 60(1), 131–137. 10.1007/s00484-015-1011-0

Ha, K. J., & Yun, K. S. (2012). Climate change effects on tropical night days in Seoul, Korea. *Theoretical and applied climatology*, 109, 191-203. https://doi.org/10.1007/s00704-011-0573-y

Hess, J. J., McDowell, J. Z., & Luber, G. (2012). Integrating climate change adaptation into public health practice: using adaptive management to increase adaptive capacity and build resilience. *Environmental health perspectives*, 120(2), 171–179. https://doi.org/10.1289/ehp.1103515

Huang, H., Ma, J., & Yang, Y. (2023). Spatial heterogeneity of driving factors for urban heat health risk in Chongqing, China: A new identification method and proposal of planning response framework. *Ecological Indicators*, 153, 110449. https://doi.org/10.1016/j.ecolind.2023.110449

Hu, K., Yang, X., Zhong, J., Fei, F., & Qi, J. (2017). Spatially Explicit Mapping of Heat Health Risk Utilizing Environmental and Socioeconomic Data. *Environmental Science and Technology*, 51(3), 1498–1507. 10.1021/acs.est.6b04355

Inostroza, L., Palme, M., & de la Barrera, F. (2016). A Heat Vulnerability Index: Spatial Patterns of Exposure, Sensitivity and Adaptive Capacity for Santiago de Chile. PLOS ONE, 11(9), e0162464. https://doi.org/10.1371/journal.pone.0162464

IPCC. (2007). *Summary for policymakers.* In M. L. Parry, O. F. Canziani, J. P. Palutikof, P. J. van der Linden, & C. E. Hanson (Eds.), *Climate change 2007: Impacts, adaptation and vulnerability. Contribution of Working Group II to the Fourth Assessment Report of the Intergovernmental Panel on Climate Change* (pp. 7–22). Cambridge University Press.

IPCC. (2014). *Summary for policymakers.* In C. B. Field, V. R. Barros, D. J. Dokken, K. J. Mach, M. D. Mastrandrea, T. E. Bilir, ... L. L. White (Eds.), *Climate change 2014: Impacts, adaptation, and vulnerability. Part A: Global and sectoral aspects. Contribution of Working Group II to the Fifth Assessment Report of the Intergovernmental Panel on Climate Change* (pp. 1–32). Cambridge University Press.

IPCC. (2018). *Global warming of 1.5°C: An IPCC special report on the impacts of global warming of 1.5°C above pre-industrial levels and related global greenhouse gas emission pathways, in the context of strengthening the global response to the threat of climate change, sustainable development, and efforts to eradicate poverty* (V. Masson-Delmotte, P. Zhai, H.-O. Pörtner, D. Roberts, J. Skea, P. R. Shukla, et al., Eds.). In press.

IPCC. (2021). *Summary for policymakers.* In V. Masson-Delmotte, P. Zhai, A. Pirani, S. L. Connors, C. Péan, S. Berger, N. Caud, Y. Chen, L. Goldfarb, M. I. Gomis, M. Huang, K. Leitzell, E. Lonnoy, J. B. R. Matthews, T. K. Maycock, T. Waterfield, O. Yelekçi, R. Yu, & B. Zhou (Eds.), *Climate change 2021: The physical science basis. Contribution of Working Group I to the Sixth Assessment Report of the Intergovernmental Panel on Climate Change.* Cambridge University Press. In press.

Kaiser, H. F. (1960). The application of electronic computers to factor analysis. *Educational and Psycho-*

logical Measurement, 20(1), 141–151. https://doi.org/10.1177/001316446002000116

Karanja, J., & Kiage, L. (2021). Perspectives on spatial representation of urban heat vulnerability. *Science of The Total Environment*, 774, 145634. https://doi.org/10.1016/j.scitotenv.2021.145634

Karanja, J., Vanos, J., Georgescu, M., Frazier, A. E., & Hondula, D. (2025). The Imperative for Hazard and Place-Specific Assessment of Heat Vulnerability. *Environmental health perspectives*. https://doi.org/10.1289/EHP14801

Karanja, J., Wanyama, D., & Kiage, L. (2022). Weighting mechanics and the spatial pattern of composite metrics of heat vulnerability in Atlanta, Georgia, USA. *Science of The Total Environment*, 812, 151432. https://doi.org/10.1016/j.scitotenv.2021.151432

Karlson, M., Ostwald, M., Reese, H., Sanou, J., Tankoano, B., & Mattsson, E. (2015). Mapping Tree Canopy Cover and Aboveground Biomass in Sudano-Sahelian Woodlands Using Landsat 8 and Random Forest. *Remote Sensing*, 7(8), 10017–10041. https://doi.org/10.3390/rs70810017

Keith, L., Meerow, S., Hondula, D. M., Turner, V. K., & Arnott, J. C. (2021). Deploy heat officers, policies and metrics. *Nature*, 598(7879), 29–31. https://doi.org/10.1038/d41586-021-02677-2

Klok, S., Kornus, A., Kornus, O., Danylchenko, O., & Skyba, O. (2023). Tropical nights (1976–2019) as an indicator of climate change in Ukraine. *IOP Conference Series: Earth and Environmental Science*, 1126(1), 012023. https://doi.org/10.1088/1755-1315/1126/1/012023

Kotharkar, R., Aneja, S., & Ghosh, A. (2019). Heat vulnerability index for urban heat wave risk adaptation for Indian cities: A case study of Akola. *5th International Conference on Countermeasures to Urban Heat Islands (IC2UHI), 02–04 December 2019, International Institute of Information Technology – Hyderabad, India*. https://doi.org/10.37285/bsp.ic2uhi.10

Kotharkar, R., Dongarsane, P., & Ghosh, A. (2024a). Quantification of summertime thermal stress and PET range in a tropical Indian city. *Urban Climate*, 53, 101758. https://doi.org/10.1016/j.uclim.2023.101758

Kotharkar, R., Dongarsane, P., Ghosh, A. & Kotharkar, V. (2024b). Numerical analysis of extreme heat in Nagpur city using heat stress indices, all-cause mortality and local climate zone classification. *Sustainable Cities and Society*, 101, 105099. https://doi.org/10.1016/j.scs.2023.105099

Kotharkar, R., & Ghosh, A. (2021a). Review of heat wave studies and related urban policies in South Asia. *Urban Climate*, 36, 100777. https://doi.org/10.1016/j.uclim.2021.100777

Kotharkar, R., & Ghosh, A. (2021b). Progress in extreme heat management and warning systems: A systematic review of heat-health action plans (1995-2020). *Sustainable Cities and Society*, 76, 103487. https://doi.org/10.1016/j.scs.2021.103487

Kotharkar, R., Ghosh, A., Kapoor, S., & Reddy, D. G. K. (2022). Approach to local climate zone based energy consumption assessment in an Indian city. *Energy & Buildings*, 259, 111835. https://doi.org/10.1016/j.enbuild.2022.111835

Kotharkar, R., Ghosh, A., & Kotharkar, V. (2021). Estimating summertime heat stress in a tropical Indian city using Local Climate Zone (LCZ) framework. *Urban Climate*, 36, 100784. https://doi.org/10.1016/j.uclim.2021.100784

Kotharkar, R., Vidyasagar, A., & Ghosh, A. (2024). Application of LCZ to urban heat island studies. In R. Wang, M. Cai, C. Ren, & Y. Shi (Eds.), *Local climate zone application in sustainable urban development* (pp. 79-103). Springer. https://doi.org/10.1007/978-3-031-56168-9_5

Kovats, R. S., & Hajat, S. (2008). Heat stress and public health: A critical review. *Annual Review of Public Health*, 29(1), 41–55. https://doi.org/10.1146/annurev.publhealth.29.020907.0908

Kumar, A., & Singh, D. P. (2021). Heat stroke-related deaths in India: An analysis of natural causes of deaths, associated with the regional heatwave. *Journal of Thermal Biology*, 95, 102792. 10.1016/j.jtherbio.2020.102792

La, Y., Bagan, H., & Yamagata, Y. (2020). Urban land cover mapping under the local climate zone scheme using Sentinel-2 and PALSAR-2 data. *Urban Climate*, 33, 100661. https://doi.org/10.1016/j.uclim.2020.100661

Lehnert, M., Savić, S., Milošević, D., Dunjić, J., & Geletič, J. (2021). Mapping Local Climate Zones and Their Applications in European Urban Environments: A Systematic Literature Review and Future Development Trends. *ISPRS International Journal of Geo-Information*, 10(4), 260. 10.3390/ijgi10040260

Li, F., Yigitcanlar, T., Li, W., Nepal, M., Nguyen, K., & Dur, F. (2024). Understanding urban heat vulnerability: Scientometric analysis of five decades of research. *Urban Climate*, 56, 102035. https://doi.org/10.1016/j.uclim.2024.102035

Li, F., Yigitcanlar, T., Nepal, M., Thanh, K., & Dur, F. (2022). Understanding Urban Heat Vulnerability Assessment Methods: A PRISMA Review. *Energies*, 15(19), 6998. http://dx.doi.org/10.3390/en15196998

Li, F., Yigitcanlar, T., Nepal, M., Nguyen, K., Dur, F., & Li, W. (2025). Mapping heat vulnerability in Australian capital cities: A machine learning and multi-source data analysis. *Sustainable Cities and Society*, 119, 106079. https://doi.org/10.1016/j.scs.2024.106079

Luber, G., & McGeehin, M. (2008). Climate change and extreme heat events. *American journal of preventive medicine*, 35(5), 429–435. https://doi.org/10.1016/j.amepre.2008.08.021

Ma, L., Huang, G., Johnson, B. A., Chen, Z., Li, M., Yan, Z., Zhan, W., Lu, H., Hw, W., & Lian, D. (2023). Inves-

tigating urban heat-related health risks based on local climate zones: A case study of Changzhou in China. *Sustainable Cities and Society*, 91, 104402. https://doi.org/10.1016/j.scs.2023.104402

Maragno, D., Dalla Fontana, M., & Musco, F. (2020). Mapping Heat Stress Vulnerability and Risk Assessment at the Neighborhood Scale to Drive Urban Adaptation Planning. *Sustainability*, 12, 1056. https://doi.org/10.3390/su12031056

Ministry of Home Affairs (MHA). (2011). Census of India, 2011. The Registrar General & Census Commissioner, Government of India. https://www.censusindia.gov.in/2011common/census_2011.html

Mills, G., Ching, J., See, L., Bechtel, B., & Foley, M. (2015). An introduction to the WUDAPT project. In *Proceedings of the 9th International Conference on Urban Climate* (pp. 20–24).

Mohite, S., & Surawar, M. (2024). Assessing pedestrian thermal comfort to improve walkability in the urban tropical environment of Nagpur city. *Geographica Pannonica*, 28(1). https://doi.org/10.5937/gp28-48166

Nanda, L., Chakraborty, S., Mishra, S. K., Dutta, A., & Rathi, S. K. (2022). Characteristics of Households' Vulnerability to Extreme Heat: An Analytical Cross-Sectional Study from India. *International journal of environmental research and public health*, 19(22), 15334. https://doi.org/10.3390/ijerph192215334

National Disaster Management Authority (NDMA). (2019). *National guidelines for preparation of action plan – Prevention and management of heat wave, 2019.* Ministry of Home Affairs, Government of India. https://ndma.gov.in

Navarro-Estupiñan, J., Robles-Morua, A., Díaz-Caravantes, R., & Vivoni, E. R. (2020). Heat risk mapping through spatial analysis of remotely-sensed data and socioeconomic vulnerability in Hermosillo, México. *Urban Climate*, 31, 100576. https://doi.org/10.1016/j.uclim.2019.100576

Nayak, S. G., Shrestha, S., Kinney, P. L., Ross, Z., Sheridan, S. C., Pantea, C. I., ... & Hwang, S. A. (2018). Development of a heat vulnerability index for New York State. *Public Health*, 161, 127–137. 10.1016/j.puhe.2017.09.006

Oke, T. R. (2004). *Initial guidance to obtain representative meteorological observations at urban sites* (IOM Report No. 81, WMO/TD-No. 1250, 47 pp.). World Meteorological Organization. https://www.wmo.int/pages/prog/www/IMOP/publications/IOM-81/IOM-81UrbanMetObs.pdf

Pascal, M., Lagarrigue, R., Tabai, A., Bonmarin, I., Camail, A., Laaidi, K., ... & Denys, S. (2021). Evolving heat waves characteristics challenge heat warning systems and prevention plans. *International Journal of Biometeorology*, 65, 1683–1694. https://doi.org/10.1007/s00484-021-02123-y

Raja, D. R., Hredoy, M. S. N., Islam, M. K., Islam, K. M. A., & Adnan, M. S. G. (2021). Spatial distribution of heatwave vulnerability in a coastal city of Bangladesh. *Environmental Challenges*, 4, 100122. https://doi.org/10.1016/j.envc.2021.100122

Rathi, S. K., Chakraborty, S., Mishra, S. K., Dutta, A., & Nanda, L. (2021). A Heat Vulnerability Index: Spatial Patterns of Exposure, Sensitivity and Adaptive Capacity for Urbanites of Four Cities of India. *International journal of environmental research and public health*, 19(1), 283. https://doi.org/10.3390/ijerph19010283

Reckien, D. (2018). What is in an index? Construction method, data metric, and weighting scheme determine the outcome of composite social vulnerability indices in New York City. Regional *Environmental Change*, 18(5), 1439–1451. 10.1007/s10113-017-1273-7

Reid, C., O'Neill, M., Gronlund, C., Brines, S., Brown, D., Diez-Roux, A., & Schwartz, J. (2009). Mapping Community Determinants of Heat Vulnerability. *Environmental Health Perspectives*, 117(1). 10.1289/ehp.0900683

Ren, J., Yang, J., Zhang, Y., Xiao, X., Xia, J. C., Li, X., & Wang, S. (2022). Exploring thermal comfort of urban buildings based on local climate zones. *Journal of Cleaner Production*, 340, 130744. https://doi.org/10.1016/j.jclepro.2022.130744

Rinner, C., Patychuk, D., Bassil, K., Nasr, S., Gower, S., & Campbell, M. (2010). The Role of Maps in Neighborhood-level Heat Vulnerability Assessment for the City of Toronto. Cartography and Geographic *Information Science*, 37(1), 31–44. 10.1559/152304010790588089

Romero-Lankao, P., Qin, H., & Dickinson, K. (2012). Urban vulnerability to temperature-related hazards: A meta-analysis and meta-knowledge approach. *Global Environmental Change*, 22(3), 670-683. 10.1016/j.gloenvcha.2012.04.002

Runnalls, K. E., & Oke, T. R. (2006). A Technique to Detect Microclimatic Inhomogeneities in Historical Records of Screen-Level Air Temperature. *Journal of Climate*, 19, 959–978. https://doi.org/10.1175/JCLI3663.1

Santamouris, M. (2019). Recent Progress on Urban Overheating and Heat Island Research. Integrated Assessment of the Energy, Environmental, Vulnerability and Health Impact Synergies with the Global Climate Change. *Energy and Buildings*, 207(1), 109482. 10.1016/j.enbuild.2019.109482

Schmidtlein, M. C., Deutsch, R. C., Piegorsch, W. W., & Cutter, S. L. (2008). A Sensitivity Analysis of the Social Vulnerability Index. *Risk Analysis*, 28(4), 1099–1114. https://doi.org/10.1111/j.1539-6924.2008.01072.x

Sharma, J., & Ravindranath, N. H. (2019). Applying IPCC 2014 framework for hazard-specific vulnerability assessment under climate change. *Environmental Research Communications*, 1(5). 10.1088/2515-7620/ab24ed

Shih, W.-Y., & Mabon, L. (2021). Understanding heat vulnerability in the subtropics: Insights from expert judgements. *International Journal of Disaster*

Risk Reduction, 63, 102463. https://doi.org/10.1016/j.ijdrr.2021.102463

Stewart, I. D., & Oke, T. R. (2012). Local climate zones for urban temperature studies. *Bulletin of the American Meteorological Society*, 93(12), 1879–1900. https://doi.org/10.1175/BAMS-D-11- 00019.1

Uejio, C. K., Wilhelmi, O. V., Golden, J. S., Mills, D. M., Gulino, S. P., & Samenow, J. P. (2011). Intra-urban societal vulnerability to extreme heat: The role of heat exposure and the built environment, socioeconomics, and neighborhood stability. *Health & Place*, 17(2), 498–507. 10.1016/j.healthplace.2010.12.005

Verdonck, M. -L., Demuzere, M., Hooyberghs, H., Beck, C., Cyrys, J., Schneider, A., Dewulf, R., & Van Coillie, F. (2018). The potential of local climate zones maps as a heat stress assessment tool, supported by simulated air temperature data. *Landscape and Urban Planning*, 178, 183–197. https://doi.org/10.1016/j.landurbplan.2018.06.004

Verdonck, M. L., Okujeni, A., van der Linden, S., Demuzere, M., De Wulf, R., & Van Coillie, F. (2017). Influence of neighbourhood information on 'Local Climate Zone'mapping in heterogeneous cities. *International Journal of Applied Earth Observation and Geoinformation*, 62, 102–113. 10.1016/j.jag.2017.05.017

Wehner, M., Stone, D., Krishnan, H., AchutaRao, K., & Castillo, F. (2016). The Deadly Combination of Heat and Humidity in India and Pakistan in Summer 2015. *Bulletin of the American Meteorological Society*, 97(12), 81–86. https://doi.org/10.1175/bams-d-16-0145.1

Wilhelmi, O. V., & Hayden, M. H (2010). Connecting people and place: a new framework for reducing urban vulnerability to extreme heat. *Environmental Research Letters*, 5(1), 014021. https://doi.org/10.1088/1748-9326/5/1/014021

Wolf, T., & McGregor, G. (2013). The development of a heat wave vulnerability index for London, United Kingdom. *Weather and Climate Extremes*, 1, 59–68. https://doi.org/10.1016/j.wace.2013.07.004

World Meteorological Organization. (2021). *State of the global climate 2020* (WMO-No. 1264). World Meteorological Organization. https://library.wmo.int/doc_num.php?explnum_id=10618

Wouters, H., De Ridder, K., Poelmans, L., Willems, P., Brouwers, J., Hosseinzadehtalaei, P., … & Demuzere, M. (2017). Heat stress increase under climate change twice as large in cities as in rural areas: A study for a densely populated midlatitude maritime region. *Geophysical Research Letters*, 44(17), 8997–9007. https://doi.org/10.1002/2017GL074889

Wu, J., Liu, C., & Wang, H. (2022). Analysis of Spatio-temporal patterns and related factors of thermal comfort in subtropical coastal cities based on local climate zones. *Building and Environment*, 207, 108568. https://doi.org/10.1016/j.buildenv.2021.108568

Zanter, K. (2016). *Landsat 8 data users handbook*. U.S. Geological Survey. https://landsat.usgs.gov/landsat-8-l8-data-users-handbook

Zhou, Y., Zhang, G., Jiang, L., Chen, X., Xie, T., Wei, Y., … & Lun, F. (2021). Mapping local climate zones and their associated heat risk issues in Beijing: Based on open data. *Sustainable Cities and Society*, 74(4), 103174. 10.1016/j.scs.2021.103174

Zou, Q., Yang, J., Zhang, Y., Bai, Y., & Wang, J. (2025). Variation in community heat vulnerability for Shenyang City under local climate zone perspective. *Building and Environment*, 267, 112242. https://doi.org/10.1016/j.buildenv.2024.112242

Zuhra, S. S., Tabinda, A. B., & Yasar, A. (2019). Appraisal of the heat vulnerability index in Punjab: a case study of spatial pattern for exposure, sensitivity, and adaptive capacity in megacity Lahore, Pakistan. *International Journal of Biometeorology*, 63(12). 10.1007/s00484-019-01784-0

Annexure I. Indicators of adaptive capacity, sensitivity and exposure

Variables	Indicators	Definition/method to quantify	Source
Adaptive Capacity (A_c)	1. Electricity supply (ES)	Ward-wise household per hectare that have electricity supply	Census of India-2011
	2. Water supply (WS)	Ward-wise household per hectare having water facility	
	3. Communication facilities (CF)	Ward-wise household per hectare that has landline and mobile phone	
	4. Health facilities (HF)	The distance of centroid of the continuous urban area in each ward to the nearest government hospitals	Remote Sensing & Nagpur Municipal Corporation
	5. Social facilities: religious facilities & schools (SF)	The distance of centroid of the continuous urban area in each ward to the nearest social facilities.	
	6. Personal vehicle (PV)	Ward-wise household per hectare having personal vehicle	Census of India-2011
	7. Bank account (BA)	Ward-wise household per hectare availing banking facilities	
	8. Normalized Difference Vegetation Index (NDVI)	An index for quantifying the health and density of vegetation	LANDSAT-8 imagery
Sensitivity (S)	9. Illiterate Population (IP)	Inhabitants per hectare who are illiterate	Census of India-2011
	10. Female population (FP)	Ward-wise female population per hectare	
	11. Population aged under 6 years (YP)	Inhabitants per hectare below six years age	
	12. Population aged over 60 years (OP)	Inhabitants per hectare with age equal to or greater than 60	
	13. Population of Scheduled Caste (SC)/Scheduled Tribe (ST)	Ward-wise population of SC/ST per hectare	
	14. Population density (PD)	Ward-wise population density per hectare	
	15. Typology of houses (TYP)	Ward-wise number of katcha/pucca houses per hectare	
	16. Single household size (SH)	Inhabitants per hectares who live alone	
	17. Average number of people per household (HH)	Ward-wise number of person per household	
	18. Rented housing (RH)	Ward-wise rented household per hectare	
	19. Roof material (RM)	Ward-wise household per hectare with roof material as asbestos/ metal/GI	
	20. Population with disability 18-64 years (DIS)	Ward-wise population that has disability 18-64 years	
Exposure (E)	21. Land Surface Temperature (LST)	An index which estimates radiative skin temperature of the land surface	LANDSAT-8 imagery

Annexure II. Ward-wise values for HVI

Name	Normalized values				
	adp_sc	exp_sc	sen_sc	hvi_total	hvi (out of 1)
WARD NO 1	0.626	0.461	0.339	1.426	0.484
WARD NO 2	0.463	0.555	0.471	1.489	0.512
WARD NO 3	0.115	0.426	0.363	0.905	0.255
WARD NO 4	0.130	0.338	0.680	1.147	0.361
WARD NO 5	0.102	0.626	1.000	1.728	0.617
WARD NO 6	0.041	0.665	0.866	1.572	0.548
WARD NO 7	0.631	0.092	0.255	0.979	0.287
WARD NO 8	0.431	0.091	0.176	0.698	0.164

Name	Normalized values				
	adp_sc	exp_sc	sen_sc	hvi_total	hvi (out of 1)
WARD NO 9	0.333	0.000	0.157	0.490	0.072
WARD NO 10	0.287	0.079	0.055	0.422	0.042
WARD NO 11	0.233	0.428	0.065	0.726	0.176
WARD NO 12	0.445	0.691	0.311	1.447	0.493
WARD NO 13	0.127	0.594	0.329	1.051	0.319
WARD NO 14	0.122	0.671	0.371	1.164	0.369
WARD NO 15	0.443	0.214	0.209	0.866	0.238
WARD NO 16	0.057	0.675	0.597	1.329	0.441
WARD NO 17	0.106	0.740	0.683	1.529	0.529
WARD NO 18	0.106	0.627	0.679	1.412	0.478
WARD NO 19	0.040	1.000	0.200	1.240	0.402
WARD NO 20	0.067	0.745	0.724	1.537	0.532
WARD NO 21	0.278	0.880	0.194	1.351	0.451
WARD NO 22	0.282	0.291	0.030	0.603	0.122
WARD NO 23	0.287	0.099	0.120	0.507	0.080
WARD NO 24	0.318	0.246	0.205	0.769	0.195
WARD NO 25	0.601	0.299	0.505	1.405	0.475
WARD NO 26	0.333	0.210	0.138	0.681	0.156
WARD NO 27	0.224	0.276	0.081	0.581	0.112
WARD NO 28	0.308	0.241	0.054	0.603	0.122
WARD NO 29	0.541	0.807	0.742	2.091	0.776
WARD NO 30	0.552	0.847	0.740	2.138	0.797
WARD NO 31	0.110	0.823	0.137	1.071	0.328
WARD NO 32	0.103	0.743	0.370	1.216	0.392
WARD NO 33	0.066	0.598	0.463	1.128	0.353
WARD NO 34	0.394	0.467	0.376	1.237	0.401
WARD NO 35	0.340	0.389	0.171	0.901	0.253
WARD NO 36	0.031	0.696	0.439	1.167	0.370
WARD NO 37	0.036	0.785	0.809	1.630	0.573
WARD NO 38	0.026	0.921	0.609	1.556	0.541
WARD NO 39	0.251	0.827	0.203	1.281	0.420
WARD NO 40	0.265	0.152	0.034	0.451	0.055
WARD NO 41	0.262	0.167	0.055	0.484	0.069
WARD NO 42	0.286	0.373	0.188	0.847	0.229
WARD NO 43	0.039	0.357	0.591	0.988	0.291
WARD NO 44	0.316	0.368	0.221	0.905	0.255
WARD NO 45	0.152	0.309	0.017	0.478	0.067
WARD NO 46	0.165	0.349	0.026	0.540	0.094
WARD NO 47	0.223	0.511	0.076	0.809	0.213
WARD NO 48	0.272	0.445	0.135	0.852	0.232
WARD NO 49	0.076	0.430	0.483	0.989	0.292
WARD NO 50	0.056	0.762	0.782	1.600	0.560
WARD NO 51	0.000	0.738	0.599	1.337	0.445

Name	Normalized values				
	adp_sc	exp_sc	sen_sc	hvi_total	hvi (out of 1)
WARD NO 52	0.509	0.243	0.204	0.955	0.277
WARD NO 53	0.649	0.283	0.358	1.290	0.424
WARD NO 54	0.606	0.430	0.380	1.416	0.480
WARD NO 55	0.435	0.510	0.305	1.250	0.407
WARD NO 56	0.649	0.709	0.615	1.972	0.724
WARD NO 57	0.588	0.442	0.613	1.643	0.579
WARD NO 58	0.320	0.545	0.201	1.065	0.325
WARD NO 59	0.504	0.617	0.332	1.453	0.496
WARD NO 60	0.306	0.465	0.000	0.771	0.196
WARD NO 61	0.286	0.511	0.014	0.811	0.213
WARD NO 62	0.396	0.237	0.031	0.664	0.149
WARD NO 63	0.265	0.409	0.023	0.697	0.163
WARD NO 64	0.330	0.441	0.177	0.948	0.273
WARD NO 65	0.340	0.213	0.445	0.999	0.296
WARD NO 66	0.659	0.355	0.500	1.513	0.522
WARD NO 67	0.125	0.496	0.722	1.344	0.448
WARD NO 68	0.568	0.315	0.163	1.046	0.317
WARD NO 69	0.353	0.434	0.183	0.970	0.283
WARD NO 70	0.219	0.201	0.260	0.679	0.155
WARD NO 71	0.272	0.448	0.263	0.983	0.289
WARD NO 72	0.076	0.447	0.261	0.784	0.202
WARD NO 73	0.056	0.446	0.259	0.761	0.191
WARD NO 74	0.000	0.446	0.257	0.703	0.166
WARD NO 75	0.509	0.445	0.255	1.209	0.388
WARD NO 76	0.649	0.444	0.253	1.346	0.449
WARD NO 77	0.606	0.444	0.251	1.301	0.429
WARD NO 78	0.435	0.443	0.248	1.126	0.352
WARD NO 79	0.649	0.443	0.246	1.338	0.445
WARD NO 80	0.588	0.442	0.244	1.274	0.417
WARD NO 81	0.320	0.441	0.242	1.003	0.298
WARD NO 82	0.504	0.441	0.240	1.185	0.378
WARD NO 83	0.306	0.440	0.238	0.984	0.289
WARD NO 84	0.286	0.439	0.236	0.961	0.280
WARD NO 85	0.396	0.439	0.234	1.068	0.327
WARD NO 86	0.265	0.438	0.232	0.934	0.268
WARD NO 87	0.330	0.437	0.229	0.996	0.295
WARD NO 88	0.340	0.437	0.227	1.004	0.298
WARD NO 89	0.659	0.436	0.225	1.320	0.437
WARD NO 90	0.125	0.435	0.223	0.784	0.201
WARD NO 91	0.568	0.435	0.221	1.224	0.395
WARD NO 92	0.353	0.434	0.219	1.006	0.299
WARD NO 93	0.219	0.433	0.217	0.869	0.239
WARD NO 94	0.272	0.433	0.215	0.920	0.261

Name	Normalized values				
	adp_sc	exp_sc	sen_sc	hvi_total	hvi (out of 1)
WARD NO 95	0.076	0.432	0.213	0.721	0.174
WARD NO 96	0.056	0.431	0.211	0.698	0.163
WARD NO 97	0.000	0.431	0.208	0.639	0.138
WARD NO 98	0.509	0.430	0.206	1.145	0.360
WARD NO 99	0.649	0.429	0.204	1.282	0.421
WARD NO 100	0.606	0.429	0.202	1.237	0.401
WARD NO 101	0.435	0.428	0.200	1.063	0.324
WARD NO 102	0.649	0.427	0.198	1.274	0.417
WARD NO 103	0.588	0.427	0.196	1.210	0.389
WARD NO 104	0.320	0.426	0.194	0.939	0.270
WARD NO 105	0.504	0.425	0.192	1.121	0.350
WARD NO 106	0.306	0.425	0.189	0.920	0.261
WARD NO 107	0.286	0.424	0.187	0.898	0.252
WARD NO 108	0.396	0.423	0.185	1.005	0.299
WARD NO 109	0.265	0.423	0.183	0.871	0.240
WARD NO 110	0.330	0.422	0.181	0.933	0.267
WARD NO 111	0.340	0.421	0.179	0.941	0.270
WARD NO 112	0.272	0.421	0.177	0.870	0.239
WARD NO 113	0.076	0.420	0.175	0.671	0.152
WARD NO 114	0.056	0.419	0.173	0.648	0.142
WARD NO 115	0.000	0.419	0.171	0.589	0.116
WARD NO 116	0.509	0.418	0.168	1.095	0.338
WARD NO 117	0.649	0.417	0.166	1.233	0.399
WARD NO 118	0.606	0.417	0.164	1.187	0.379
WARD NO 119	0.435	0.416	0.162	1.013	0.302
WARD NO 120	0.649	0.415	0.160	1.224	0.395
WARD NO 121	0.588	0.415	0.158	1.160	0.367
WARD NO 122	0.320	0.414	0.156	0.890	0.248
WARD NO 123	0.504	0.413	0.154	1.071	0.328
WARD NO 124	0.306	0.413	0.152	0.870	0.239
WARD NO 125	0.286	0.412	0.149	0.848	0.230
WARD NO 126	0.396	0.412	0.147	0.955	0.277
WARD NO 127	0.265	0.411	0.145	0.821	0.218
WARD NO 128	0.330	0.410	0.143	0.883	0.245
WARD NO 129	0.340	0.410	0.141	0.891	0.248
WARD NO 130	0.659	0.409	0.139	1.206	0.387
WARD NO 131	0.125	0.408	0.137	0.670	0.151
WARD NO 132	0.568	0.408	0.135	1.110	0.345
WARD NO 133	0.353	0.407	0.133	0.893	0.249
WARD NO 134	0.219	0.406	0.131	0.756	0.189
WARD NO 135	0.519	0.466	0.193	1.177	0.294
WARD NO 136	0.322	0.643	0.327	1.291	0.643

INTERNATIONAL SCIENTIFIC JOURNAL
GEOGRAPHICA PANNONICA
Volume 29, Issue 2, 108–120 (June 2025)
Journal homepage: http://www.dgt.uns.ac.rs/en/homepage/pannonica/

Hydrological Shifts in the Carpathian Basin: Climate Change Impacts on Summer Low-flows

Igor Leščešen[A]

[A] *Institute of Hydrology SAS, Dúbravská cesta 9, 841 04 Bratislava, Slovak Republic; ORCID IL: 0000-0001-9090-2662*

KEYWORDS

- hydrological trends
- climate change impacts
- Carpathian Basin
- low-flow regimes
- regionalization

ABSTRACT

To assess hydrological shifts in the Carpathian Basin, this study analyzes a 90-year summer minimum discharge dataset from 12 river stations. We reveal widespread, significant declines, with the most pronounced trends on the Danube showing an average decrease of (-8.9% per decade). Critically, we identify a systemic regime shift using Pettitt tests, with most changepoints occurring between 1968-1990. Self-Organizing Maps (SOMs) regionalize these trends into two clusters: a high-variability group (Danube/Sava) and a vulnerable, low-flow group (Tisza/Drava). These findings prove the region's growing drought vulnerability and highlight the urgent need for adaptive water management.

Introduction

The discharge of rivers plays a fundamental role in the formation of natural and human environments and directly affects extremes of water such as flooding and drought. High-pressure events have devastating human and socio-economic effects (Paprotny et al., 2018), while low-pressure events exacerbate droughts and drought conditions, affecting water supply and ecosystem sustainability (Feyen & Dankers, 2009). Changes in average discharge patterns further affect long-term availability of water resources and affect ecological integrity and agricultural productivity (Calzadilla et al., 2013; Jana-Capdevila et al, 2019). Understanding the temporal trends of river discharge is therefore essential for effective water management and climate adaptation strategies, especially in areas vulnerable to climate change.

The scientific community has undertaken significant research efforts to understand how river discharge patterns will evolve in response to climate change. Global and regional climate projections show significant changes in the hydrological system due to warming temperatures and changes in rainfall patterns (IPCC, 2021). In southern Europe and the Carpathian basin, advanced climate models predict a global drought trend that will increase precipitation and appear as a reduction in river low-flows (Kilifarska et al., 2025). Such changes will not only affect water availability, but also increase the intensity and frequency of extreme water situations. The interaction between climate change and human pressures such as land use changes and water management practices make the hydrological response of river basins even more complicated (Droll, 2014). These evolving risks require a strong understanding of flows trends to inform adaptation water management strategies and mitigate the potential negative impacts on society and ecosystems.

Several publications examine the impact of climate change on hydrological cycles at different levels, from individual river basins to continental and global assessments. Although global hydrological models provide valuable insights, their application to the regional context poses significant challenges due to calibration efforts and

* Corresponding author:Igor Leščešen; e-mail: lescesen@uh.savba.sk

doi: 10.5937/gp29-57090

Received: February 27, 2025| Revised: June 17, 2025| Accepted: June 19, 2025

data requirements. Studies on the long-term trends in the drainage of European rivers have revealed heterogeneous patterns throughout the continent. Many studies have shown that flows in southern and eastern Europe have declined, while flows in central and northern Europe have increased (Stahl et al. 2010, Caloiero & Veltri 2019). Some estimates suggest that river discharges in northern Europe have rised by 45% since 1962 (Tuling et al., 2019), while by 2050 the discharges in Northern parts of Europe will increase by 10% to 40% and while in Southern parts of Europe discharges will reduce by 10% to 30% under the A1B scenario (Milly et al., 2005). Likewise, Lehner et al. (2006), Feyen & Dankers (2009) project a significant reduction in drought-related emissions in southern and south-eastern Europe.

Seasonal discharge patterns have also been shown to be subject to substantial changes. In most European fisheries, a positive trend in discharge is observed in winter, while in spring and summer, a negative trend is evident (Bard and et al. 2015; Bormann & Pinter 2017; Leščešen et al., 2022; Gnjato et al., 2024). This trend reaches its peak in August, indicating an increase in the risk of summer droughts. Similarly, in the regions where the average monthly discharge is the lowest during the summer, the flow has declined, except in the areas where the groundwater reserves are substantial (Fleig et al. 2010; Laizé & Hannah 2010). A comprehensive review of European hydrological trends (Bates et al., 2008) confirmed these spatially explicit patterns, emphasizing the widespread reduction in summer discharge in Central and Eastern Europe.

Despite these extensive studies, significant research gaps remain with respect to robust detection of long-term discharge trends, especially in river basins in southern and southeastern Europe. Many existing studies are based on observational data from the second half of the 20th century (Piniewski, 2018; Fiala, 2010; Treuling, 2019), restricting the ability to capture extended historical trends. Furthermore, many studies focus on analysis of extreme event frequency data or validation of entire European hydrological models, but lack comprehensive studies to assess general trends in stream flows.

To address these shortcomings, our research aims to provide a long-term assessment of the trend in minimum monthly flow rates in the four main rivers in the Carpathia Basin during the summer of water (April to September). The aim of the study is to improve the understanding of the dynamics of regional flows, (i) to characterize monthly flows in the Carpathian basin with an extensive observation dataset, (ii) to conduct a detailed analysis of flows in the Carpathian basins, where water resources are increasingly under pressure due to climate change. (ii) Identification of potential inversion points in summer discharges using observation data; (iv) Comparing our results to existing literature to contextualize our results with wider European hydrological trends. This study uses long-term emission observations and robust statistical analyses to

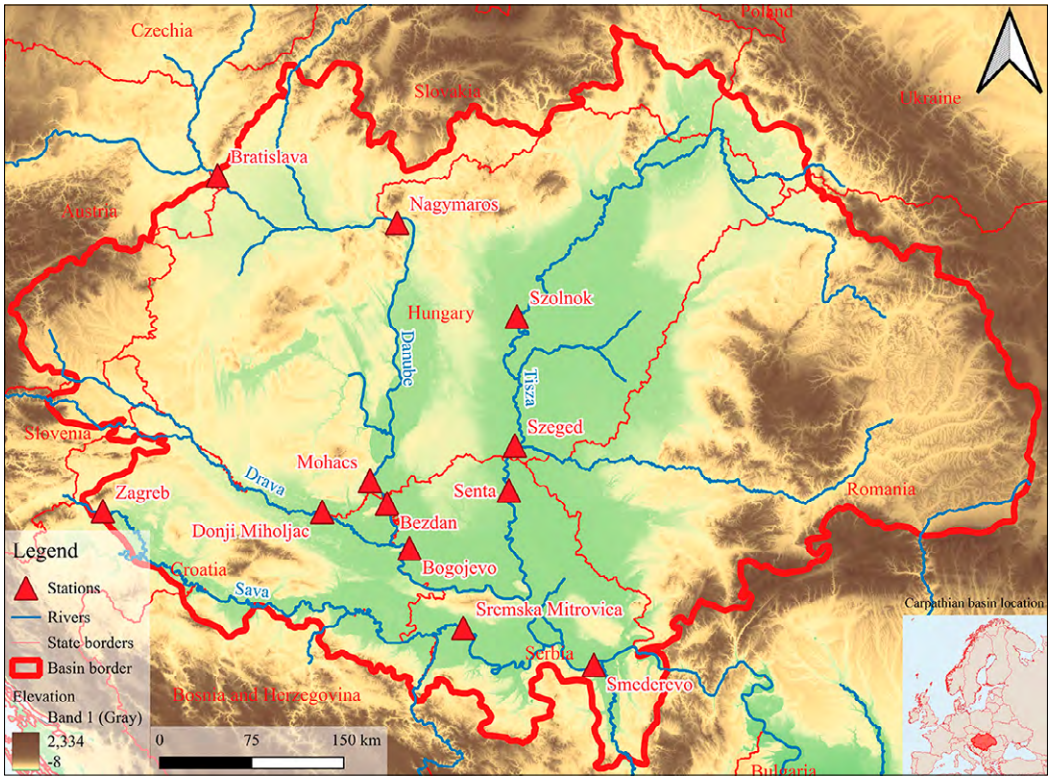

Figure 1. Study area of the Carpathian Basin, with the location of hydrological stations

Based on Gaudenyi & Mihajlovic (2022)

improve understanding of hydrological responses to climate change and inform water management strategies in vulnerable areas.

Study area

The Carpathian Basin, also known as the Pannonian Basin or Middle Danube Basin, is a large lowland basin in central and south-eastern Europe (Obreht 2019). Geographically, it is surrounded by the Alps to the west, the Carpathians to the north and east and the Dinaric Mountains, Šumadija, the Rhodope Mountains and the Balkans to the south (Gaudenyi & Mihajlović 2022). The basin stretches about 600 km from east to west and 500 km from north to south and forms a distinct geomorphologic and climatic region within the broader Alpine mountain belt in east-central Europe (Dolton, 2006). The hydrological characteristics of the region are influenced by three major climatic systems: the Atlantic, continental and Mediterranean climates. The presence of both humid oceanic and dry continental conditions further complicates the situation and leads to significant fluctuations in precipitation and temperature patterns (Mezősi, 2017). The basin is drained by four major rivers: the Danube, the Sava, the Tisza and the Drava. The Carpathian Basin spans multiple countries including Hungary, Croatia, Romania, and Serbia, extending into Austria, Slovakia, Ukraine, Bosnia and Herzegovina, and Slovenia. The present study focuses on the hydrological characteristics of Serbia, Croatia, Hungary, and Slovakia (Figure 1).

The Carpathian Basin is delineated by the ridges of mountain slopes that face the surrounding lowlands, including the Little Alföld, Alföld, Transylvanian Lowland, and Banat Plain (Gaudenyi & Mihajlović, 2022). This geomorphological configuration influences the basin's hydrology, affecting river discharge patterns, evapotranspiration, and regional water availability.

Data and methods

Data

In this work, a 90-year database (1931–2020) with daily discharge data for 12 stations in the Carpathian Basin is used (see Figure 1). The database is considered sufficiently extensive, as Kundzewicz & Robson (2000) point out that a minimum of 50 years of data is necessary to distinguish fluctuations from trends. The discharge data originate from four different national authorities (the Slovak Hydrometeorological Institute, the Meteorological and Hydrological Service of Croatia, the Hydrometeorological Service of the Republic of Serbia and the General Directorate for Water Management in Hungary). The data set was divided into hydrological summer (April–September) and hydrological winter (October–March) and the monthly minimum data for the summer season was used for further analysis. To ensure the integrity of the data, each national organization responsible for the collection and maintenance of hydrological data has taken strict measures to control data quality. These organizations adhered to stringent standards to guarantee the accuracy and consistency of the data series utilized in this study. In doing so, they followed their internal instructions, but also the recommendations of the World Meteorological Organization (WMO). To ensure the homogeneity of the data, the Mann–Kendall (MK) and Pettitt tests were applied.

Mann Kendall and Pettitt test

The Mann-Kendall (MK) test is a non-parametric statistical method that is very popular in the field of hydrological studies due to its efficiency in detecting trends in river discharge data. This approach has proven to be particularly valuable as it is highly resistant to non-normality and can effectively handle missing values. The MK test evaluates the monotonic trend in a time series by analyzing the ranks of the data points. This allows researchers to determine whether there is a significant upward or downward trend over time (Ferraz et al. 2022; Leščešen et al., 2024). Recent applications of the MK test have demonstrated its effectiveness in various contexts, including the analysis of long-term outflow trends in Afghanistan (Akhundzadah, 2024), Slovakia (Bačová Mitková et al., 2024), Serbia (Leščešen et al., 2022), Slovenija (Bezak et al., 2016). The MK test has also been used to assess trends in extreme floods and river fluctuations, providing important insights into hydrological changes under the influence of climate variability (Rydén, 2022). The ability of the MK test to detect trends at different confidence levels increases its usefulness in water resources management and planning and provides important information for adaptation to changing hydrological conditions (Bačová Mitková et al., 2024; Leščešen et al., 2022).

The Pettitt test is a non-parametric statistical method used to detect abrupt changes in time series data, which makes it particularly valuable for analyzing trends in river discharge (Pettitt, 1979). This test identifies points of change by comparing the ranks of observations before and after a potential change. This allows researchers to assess whether significant changes have occurred in the hydrological regime (Kocsis et al. 2020). The recent application of Pettitt tests has demonstrated its effectiveness in different water environments. For example, in a study of river flows in Ethiopia, the Pettitt test was used to identify significant changes in the pattern of monthly and seasonal river flows, and highlight changes that could affect wa-

ter resource management (Woldemarim et al., 2023). In the same way, studies conducted in Iran combine the Pettitt test and the Mann-Kendall test to analyze stream flow data. This analysis revealed critical changes corresponding to climate changes and anthropogenic influences (Deb 2024). This combination of tests improves the robustness of trend analysis and provides a comprehensive understanding of time changes in river discharge. By incorporating Pettitt tests into hydrological assessment, researchers can effectively inform water management strategies and adapt to the hydrological conditions changing under climate change (Gholami et al., 2022).

Self-organizing map

Self-Organizing Map (SOM) is an effective tool for hydrological regionalization and analyzes complex data according to the principles of artificial neural networks. Typically, SOMs are used to identify patterns and clusters in spatial and temporal data and allow researchers to effectively visualize and interpret hydrological phenomena. In hydrology, SOM is especially useful for the aggregation and visualization of high-dimensional data, which is essential for understanding the relationship between different hydrological parameters in different regions (Kohonen, 2001). The unsupervised nature of this method facilitates the extraction of interdependent relationships between inputs and enables the classification of these patterns into low-dimensional grids in which similar inputs are closely related (Vesanto & Alhoniemi 2000). This capability is crucial for hydrological research, as understanding the spatial distribution of parameters can improve model accuracy and resource management.

SOM can be used for regionalization in two ways: by creating a series of maps representing clusters at different time steps, or by creating a single map containing all available data. The latter method allows a temporal change to be visualized by using continuous data to represent the pattern of water pattern over time on a training map (Agarwal and al., 2016a). Recent studies have highlighted the effectiveness of SOMs in identifying precipitation patterns and their impact on the hydroelectric performance of Brazil (Ferreira & Reboita, 2022) and the regionalization of precipitation periods in Senegal (Faye et al., 2024). In addition, SOMs have been successfully used in environmental studies to assess pollution patterns (Licen et al., 2023), demonstrating their versatility in various fields. By integrating SOM into the framework of water modeling, researchers can improve parameter estimates and better understand complex water systems undergoing change (Guntu et al., 2020). Overall, the application of SOMs in hydrological regionalization is a significant advance in the field, providing solid tools for the analysis and interpretation of data that are essential for effective management of water resources.

Results and discussion

As shown in Table 1, a comprehensive set of key statistical parameters for the discharge of selected hydrological stations along the Danube, Tisza, Sava and Drava rivers in the Carpathian Basin is presented. The analysis provides insights into the spatial variations of discharge characteristics, focusing on the trends in mean, median and extreme discharge values at different locations.

The results presented in Table 1 demonstrate a general pattern of increasing minimum discharge values in the downstream direction along the Danube, Tisza, and Sava rivers, reflecting the cumulative effects of tributary inflows and river network expansion. Along the Danube, minimum discharges rise from 676 m^3/s at Bratislava to 1400 m^3/s at Smederevo. Notably, the value at Nagymaros (668 m^3/s) is marginally lower than that observed upstream at Bratislava. This counterintuitive pattern is likely attributable to the operational influence of the Gabčíkovo hydropower system, which diverts a substantial portion of the Danube's flow through an artificial navigation canal, bypassing the natural riverbed that leads toward Nagymaros. During low-flow periods, the regulated discharge regime and reduced inflow to the side arm feeding Nagymaros can produce lower observed minimum discharges, despite the location being downstream. Continuing downstream, minimum values show a steady increase: 718 m^3/s at Mohács, 742 m^3/s at Bezdan, 926 m^3/s at Bogojevo, and reaching 1400 m^3/s at Smederevo. This pattern underscores the additive contributions of major tributaries such as the Drava, Tisza, and Sava, as well as the influence of regulated hydropower reservoirs and channel morphology on baseflow maintenance. A similar increasing trend is evident along the Tisza River. Minimum discharge values increase from 61.3 m^3/s at Szolnok to 73.3 m^3/s at Szeged, and further to 90.0 m^3/s at Senta. These increases reflect the progressive accumulation of runoff from sub-catchments and the moderating effect of upstream reservoirs, which tend to maintain a regulated low-flow regime to satisfy ecological and socioeconomic needs. Along the Sava River, the pattern is likewise pronounced, beginning with a minimum of 48.7 m^3/s at Zagreb and rising substantially to 203 m^3/s at Sremska Mitrovica. This marked increase can be attributed to major tributaries such as the Kupa and Una, as well as contributions from catchments with relatively high baseflow due to karstic and mountainous hydrological settings in the western Balkans. It is also noteworthy that despite urban water use and local ab-

Table 1. Statistical Characteristics of River Discharge at Selected Hydrological Stations in the Carpathian Basin

	Bratislava (Danube)	Nagymaros (Danube)	Mohacs (Danube)	Bezdan (Danube)	Bogojevo (Danube)	Smederevo (Danube)
Mean (m^3/s)	1747.9	1968.3	2054.1	2028.5	2615.9	4444.1
Median (m^3/s)	1690	1903	1943.5	1913	2448	4094
Std. Dev. (m^3/s)	535.6	626.4	681.7	732.4	905.6	1905.9
Variance	286898.4	392417.5	464775.5	536524.5	820212.2	3632371
Skewness	1.288	0.999	1.119	1.269	1.075	1.06
Kurtosis	4.299	1.883	1.973	3.193	1.863	1.025
Range	4807	4868	5122	5939	6731	10700
Minimum (m^3/s)	676	668	718	742	926	1400
Maximum (m^3/s)	5483	5536	5840	6681	7657	12100
	Donji Miholjac (Drava)	**Szolnok (Tisza)**	**Szeged (Tisza)**	**Senta (Tisza)**	**Zagreb (Sava)**	**Sremska Mitrovica (Sava)**
Mean (m^3/s)	448.2	480.7	579.3	557.7	147.8	938.2
Median (m^3/s)	422.5	247	428	420	130	746.5
Std. Dev. (m^3/s)	152.9	424.7	471.3	452.1	70.3	658.2
Variance	23397.9	180403.9	222182.4	204392.6	4947.8	433304.5
Skewness	1.308	0.789	1.978	2.014	1.549	1.686
Kurtosis	3.634	-0.934	4.299	4.509	3.808	3.251
Range	1208	1848.7	2686.7	2745	528.3	3755
Minimum (m^3/s)	188	61.3	73.3	90	48.7	203
Maximum (m^3/s)	1396	1910	2760	2835	577	3958

stractions, the increasing trend remains robust, indicating that natural and semi-regulated hydrological processes dominate the observed extremes.

Figure 2 presented here shows the temporal variability of minimum summer flows (April–September) at several hydrological stations along the Danube, Tisza, Sava

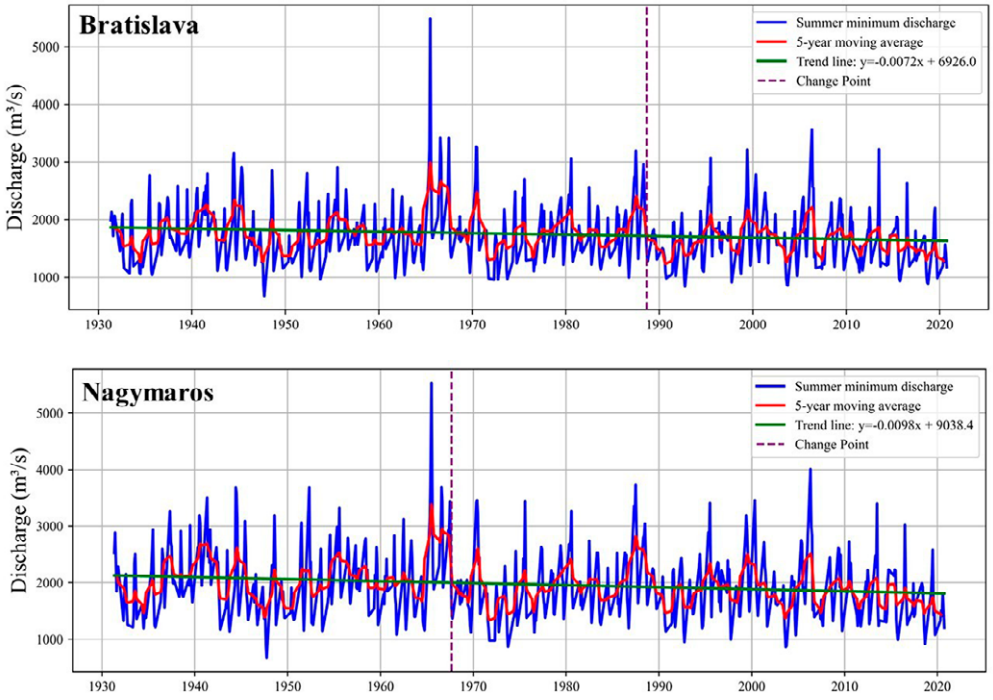

Figure 2. Spatiotemporal Variability of Summer Minimum Discharges

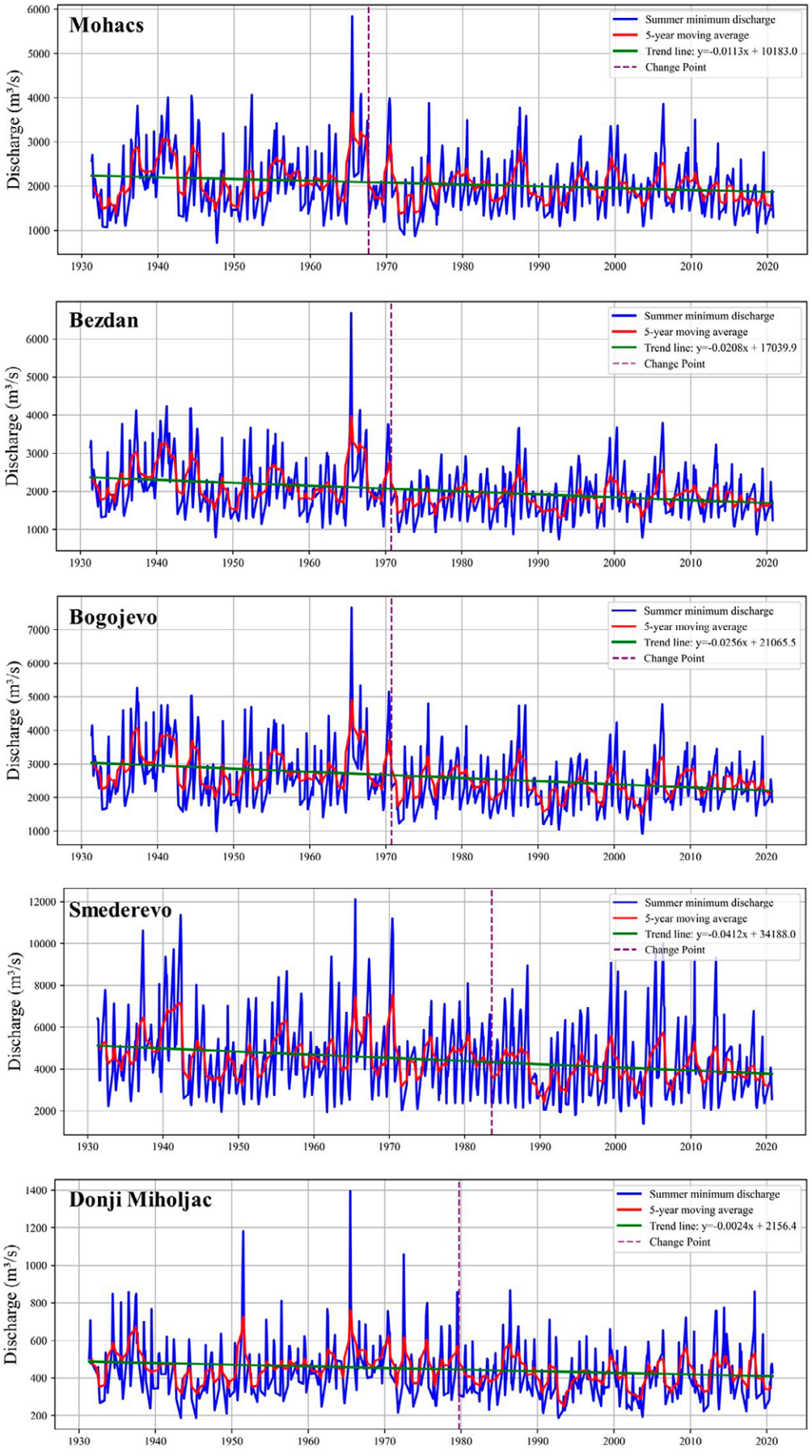

Figure 2. Spatiotemporal Variability of Summer Minimum Discharges (continued)

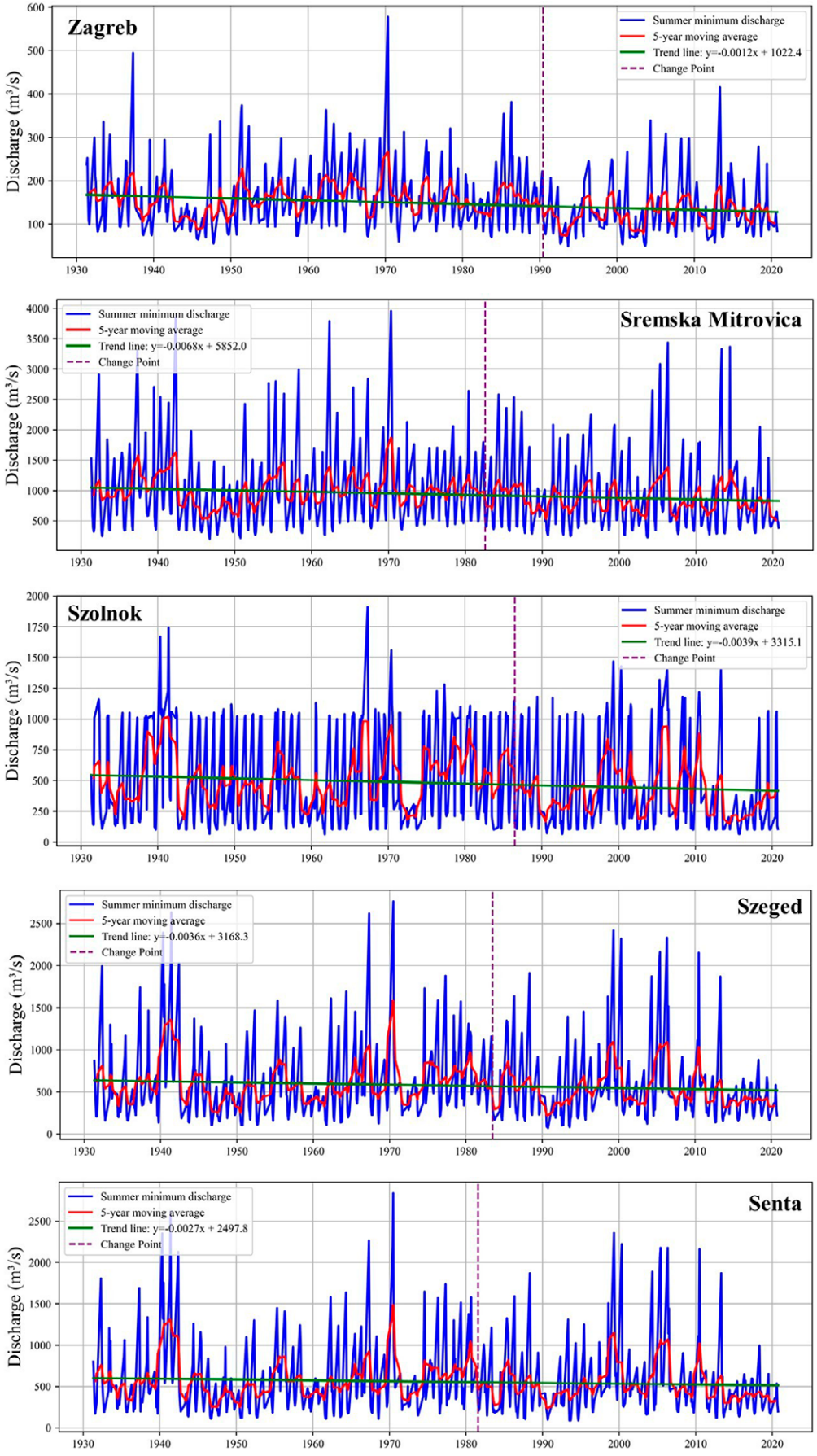

Figure 2. Spatiotemporal Variability of Summer Minimum Discharges (continued)

and Drava rivers. The stations on the Danube, which are arranged from upstream (Bratislava) to downstream (Smederevo), show a general trend towards decreasing summer low flows discharge, particularly noticeable in downstream sections. This indicates increasing hydrological stress due to cumulative water withdrawals, regulation and possible climatic influences. The variability of minimum flows is more pronounced in upstream sections such as Bratislava and Nagymaros, while downstream stations (e.g. Bezdan and Smederevo) show relatively weak fluctuations, probably due to flow regulation and groundwater interactions. This downstream dampening effect is attributable to the integration of flows within a larger catchment area, natural storage in extensive floodplains and alluvial aquifers, and the overarching influence of flow regulation structures (Poff et al., 1997; Tockner et al., 2009). A similar trend can be observed in the Tisza, where minimum flows in Szolnok are higher and more variable than in Seged and Senta, indicating a progressive decrease in groundwater supply downstream and increasing anthropogenic influences (Gocić & Trajković, 2013). A similar pattern can be observed on the Sava between Zagreb and Sremska Mitrovica, with extreme low water events being attenuated downstream. These results are consistent with established hydrological principles that flow regulation, inflows and groundwater exchange influence the downstream propagation of low flows. The Drava station (Donji Miholjac) shows pronounced interannual variability, indicating strong climatic control of minimum flows. The observed patterns indicate an increasing vulnerability of downstream river sections to prolonged periods of low flow. This phenomenon is of particular concern in the context of climate change and increasing water demand, as it can have significant environmental and socio-economic impacts The decrease in downstream variability underlines the impact of reservoirs and hydropower plants. While these anthropogenic activities can mitigate extreme low flow conditions, they also disrupt natural flow regimes. These results underline the need for integrated water management strategies that take into account both climatic and anthropogenic influences on low flow hydrology.

The results presented in Table 2 show a clear and statistically significant downward trend in summer minimum flows at most stations on the Danube, Tisza, Sava, and Drava rivers, as demonstrated by the Mann-Kendall test.

Table 2. Trend Analysis of Summer Minimum Discharges in the Danube, Tisza, Sava, and Drava Rivers Using the Mann-Kendall and Pettitt Tests

	Bratislava (Danube)	Nagymaros (Danube)	Mohacs (Danube)	Bezdan (Danube)	Bogojevo (Danube)	Smederevo (Danube)
Mann-Kendall Test						
Slope	0.449	-0.588	-0.581	-1.052	-1.321	-2.302
p-value	0.000	0.000	0.000	0.000	0.000	0.000
5-year moving average Mann-Kendall Test						
Slope	-0.380	-0.547	-0.603	-1.003	-1.314	-2.271
p-value	0.000	0.000	0.000	0.000	0.000	0.000
Pettitt Test Results:						
Change Point Year	1988	1967	1967	1970	1970	1983
Test Statistic (U)	14251.0	13875.0	14214.0	23704.0	23932.0	21403.0
p-value	0.000	0.000	0.000	0.000	0.000	0.000
	Donji Miholac (Drava)	**Szolnok (Tisza)**	**Szeged (Tisza)**	**Senta (Tisza)**	**Zagreb (Sava)**	**Sremska Mitrovica (Sava)**
Mann-Kendall Test						
Slope	-0.130	-0.065	-0.128	-0.096	-0.066	-0.302
p-value	0.000	0.017	0.084	0.164	0.000	0.011
5-year moving average Mann-Kendall Test						
Slope	-0.127	-0.268	-0.197	-0.155	-0.074	-0.417
p-value	0.000	0.000	0.000	0.001	0.000	0.000
Pettitt Test Results:						
Change Point Year	1979	1986	1983	1981	1990	1982
Test Statistic (U)	16434.0	11866.0	10657.0	8410.0	21446.0	11818.0
p-value	0.000	0.007	0.022	0.125	0.000	0.008

At the majority of locations, the associated p-values were below 0.001 (reported as $p < 0.001$), indicating strong evidence against the null hypothesis of no trend. The negative slopes of the trend lines, especially for the annual discharge and the double 5-year moving average discharge, indicate a long-term decline in summer low flows. This pattern is particularly evident on the Danube, where all stations from Bratislava to Smederevo show significantly decreasing trends. The results of the Pettitt test indicate that the turning points in the series of summer low flows are between the late 1960s and early 1980s, with most stations experiencing abrupt shifts around 1970–1980. Of particular interest is the observation that Bratislava, Nagymaros and Mohacs have similar years with change points (1967–1970), suggesting that the upstream sections of the Danube were affected by changes in the hydrological system earlier than the downstream sections, such as Smederevo (1983). This observation suggests the hypothesis that large-scale climatic drivers or anthropogenic interventions, such as dam construction and water management policies, have progressively altered discharge regimes over time.

A similar trend can be observed in the Tisza, where Szolnok and Seged show significant decreasing tendencies, while no clear trend can be seen in Senta. For both Szolnok and Seged, points of change were identified in the mid-1980s, indicating that the changes in hydrological conditions in the Tisza catchment occurred somewhat later than in the Danube.

A similar downward trend can be observed at the stations on the Sava (Zagreb and Sremska Mitrovica), where the changes occurred between 1982and 1990. This temporal consistency is consistent with broader hydrological shifts in the region that can be attributed to changing precipitation patterns, increased evapotranspiration due to rising temperatures or increased human-induced changes.

A similar trend can be observed at the Drava station (Donji Miholjac), where a change point occurred in 1979. This indicates that the hydrological shifts in the Western Balkans and Central Europe mainly occurred between the late 1960s and the late 1980s. The comprehensive results show that summer low flows have decreased over time due to a combination of climate change (reduced precipitation and increased temperature-induced evapotranspiration) and human activities (regulation of reservoirs, groundwater abstraction). These changes underline the increasing vulnerability of water resources in the region and highlight the need for adaptive water management strategies to mitigate the impacts of persistent low flow conditions on ecosystems and water availability.

The regionalization in this study is based on the monhly low-flow data for the warm season (April–September) in the Carpathian Basin. This period is crucial for the assessment of hydrological extremes such as droughts and low flows, which are increasingly influenced by climate change. The method of self-organising maps (SOMs) was applied to classify the hydrological stations based on important statistical parameters such as mean, median and standard deviation,

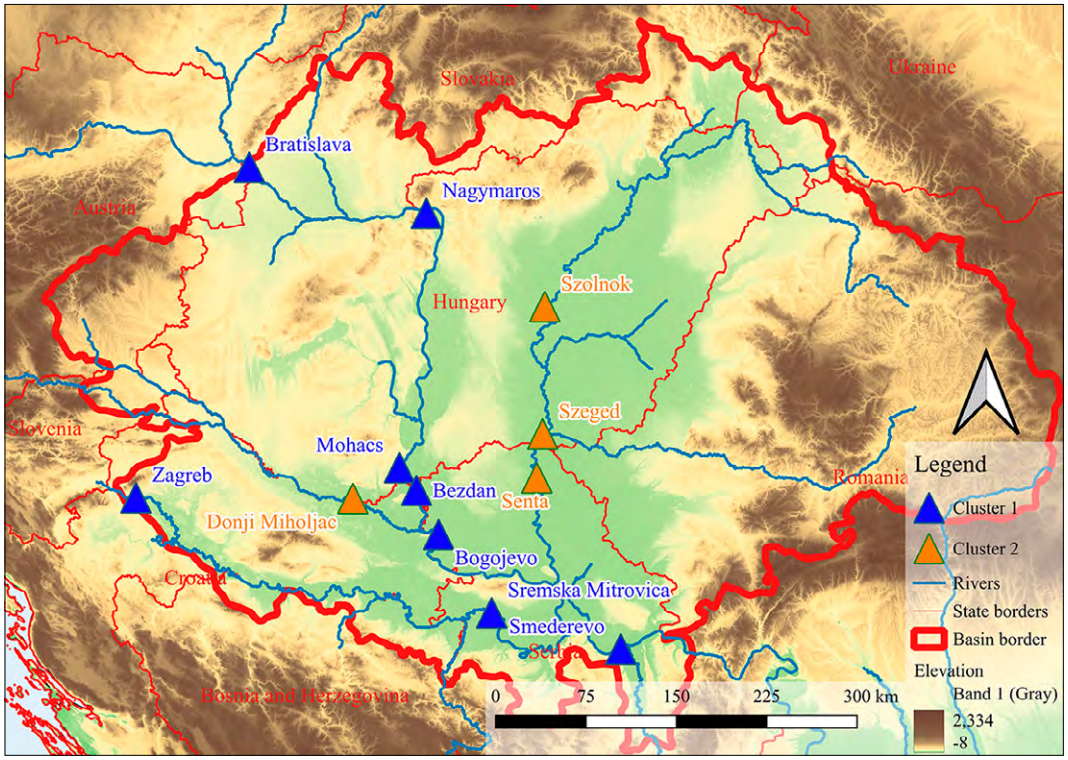

Figure 3. Regionalisation of Carpathian basin

variance, skewness, kurtosis, range, minimum, and maximum discharge values, along with trend indicators such as slope, p-values, and change point detection (Figure 3).

The stations were divided into clusters based on their hydrological behavior. Cluster 1 includes stations on the Danube (Bratislava, Nagymaros, Mohács, Bezdan, Bogojevo, Smederevo) and the Sava (Zagreb, Mitrovica), which are characterized by higher discharges, greater variability and significant hydrological changes. These results are supported by recent studies indicating that larger catchments lead to greater discharge variability and response to climatic events (Tadić et al., 2022). These stations are influenced by the larger catchment area of the Danube and its tributaries, leading to more pronounced responses to precipitation variability and snowmelt dynamics. In contrast, Cluster 2 consists of stations on the Tisza (Szolnok, Szeged, Senta) and the Drava (Miholjac), which have lower discharge, less variability and a pronounced low flow regime. Research has shown that such low flow regimes are increasingly vulnerable to the effects of climate change (Leščešen et al., 2022). The grouping was influenced by differences in trend slopes, statistical significance (p-values), and detected change points in flow behaviour.

Climate change is expected to exacerbate hydrological extremes in the region. Stations in Cluster 2 could experience a further decrease in low flows due to increased evaporation rates and longer dry periods, while stations in Cluster 1 could experience greater variability in flows due to changing precipitation patterns, more intense precipitation events and increasing temperatures. These changes are consistent with observed trends in other European river basins, where climate change is associated with altered hydrological regimes, including more frequent and severe droughts and floods (Blöschl et al., 2019; IPCC, 2021). Identifying these trends through statistical parameters ensures a data-driven understanding of regional hydrological responses and emphasizes the need for continuous monitoring and adaptive water management.

This classification provides a robust framework for assessing hydrological changes in the Carpathian Basin and highlights the evolving impacts of climate change on regional water resources. The findings are consistent with recent studies that have documented similar patterns of hydrological change in response to climate variability and anthropogenic influences (e.g., Hall et al., 2014; Lorenzo-Lacruz et al., 2010).

Conclusion

This study provides a comprehensive analysis of long-term trends in summer minimum flows across the Carpathian Basin, with a focus on the Danube, Tisza, Sava and Drava rivers. By using a 90-year data set and applying robust statistical methods, including the Mann-Kendall and Pettitt tests, we found a significant decrease in summer low flows at most stations. These trends are particularly pronounced in the Danube, where downstream stations show a greater reduction in minimum flow compared to upstream sections. Changes in the hydrological regime were observed between the late 1960s and the early 1990s, suggesting that climatic and anthropogenic factors have increasingly altered river discharge dynamics over the last fifty years.

Regionalization using self-organizing maps (SOMs) revealed different hydrological behavior, with Cluster 1 stations (Danube and Sava) characterized by higher discharge and greater variability, while Cluster 2 stations (Tisza and Drava) showed lower discharge and less variability. These results are consistent with broader European trends, where climate change increases low-flows variability in larger catchments and exacerbates low flow conditions in smaller catchments. The observed patterns highlight the dual influence of climate change — manifested in reduced precipitation and increased evapotranspiration — and human activities, such as reservoir regulation and water abstraction, on regional hydrology.

The study underlines the growing vulnerability of the Carpathian Basin to hydrological extremes, especially prolonged droughts and reduced water availability. These changes pose a major challenge for the management of water resources, the sustainability of ecosystems and socio-economic development. Our results emphasize the need for adaptive water management strategies that account for both climatic and anthropogenic drivers. Future research should focus on integrating climate projections with hydrological models to better predict and mitigate the impacts of climate change on regional water resources.

Acknowledgments

This research was supported by the "Streamflow Drought Through Time" project funded by the EU NextGenerationEU through the Recovery and Resilience Plan of the Slovak Republic within the framework of project no. 09I03-03-V04-00186.

References

Agarwal, A., Maheswaran, R., Sehgal, V., Khosa, R., Sivakumar, B., & Bernhofer, C. (2016). Hydrologic regionalization using wavelet-based multiscale entropy method. *Journal of Hydrology*, 538, 22–32. https://doi.org/10.1016/j.jhydrol.2016.03.023

Akhundzadah, N. A. (2024). Analyzing Temperature, Precipitation, and River Discharge Trends in Afghanistan's Main River Basins Using Innovative Trend Analysis, Mann–Kendall, and Sen's Slope Methods. *Climate*, 12(12), 196. https://doi.org/10.3390/cli12120196

Alfieri, L., Burek, P., Feyen, L., & Forzieri, G. (2015). Global warming increases the frequency of river floods in Europe. *Hydrology and Earth System Sciences*, 19(5), 2247–2260. http://dx.doi.org/10.5194/hess-19-2247-2015

Arnell, N.W., & Gosling, S.N. (2013). The impacts of climate change on river flow regimes at the global scale. *Journal of Hydrology*, 486, 351–364. http://dx.doi.org/10.1016/j.jhydrol.2013.02.010

Bard, A., Renard, B., Lang, M., Giuntoli, I., Korck, J., Koboltschnig, G., Janža, M., d'Amico, M., & Volken, D. (2015). Trends in the hydrologic regime of Alpine rivers. *Journal of Hydrology*, 529, 1823–1837. https://doi.org/10.1016/j.jhydrol.2015.07.052

Bates, B. C., Kundzewicz, Z. W., Wu, S., & Palutikof, J. P. (Eds.). (2008). *Climate change and water: Technical paper of the Intergovernmental Panel on Climate Change*. IPCC Secretariat.

Best, M.J., Pryor, M., Clark, D.B., Rooney, G.G., Essery, R.L.H., B.Menard, C., Edwards, J.M., Hendry, M.A., Porson, A., Gedney, N., Mercado, L.M., Sitch, S., Blyth, E., Boucher, O., Cox, P.M., Grimmond, C.S.B., & Harding, R.J. (2011). The joint UK land environment simulator (JULES), model description – part 1: energy and water fluxes. *Geosci. Model Dev. Discuss*, 4, 641–688. http://dx.doi.org/10.5194/gmdd-4-641-2011

Bezak N., Brilly M. & Šraj M. (2016). Flood frequency analyses, statistical trends and seasonality analyses of discharge data: a case study of the Litija station on the Sava River. *Journal of Flood Risk Management*, 9, 154–168. https://doi.org/10.1111/jfr3.12118.

Blöschl, G., Hall, J., Viglione, A., Perdigão, R. A. P., Parajka, J., Merz, B., Lun, D., Arheimer, B., Aronica, G. T., Bilibashi, A., Boháč, M., Bonacci, O., Borga, M., Čanjevac, I., Castellarin, A., Chirico, G. B., Claps, P., Frolova, N., Ganora, D., Gorbachova, L., Gül, A., Hannaford, J., Harrigan, S., Kireeva, M., Kiss, A., Kjeldsen, T. R., Kohnová, S., Koskela, J. J., Ledvinka, O., Macdonald, N., Mavrova-Guirguinova, M., Mediero, L., Merz, R., Molnar, P., Montanari, A., Murphy, C., Osuch, M., Ovcharuk, V., Radevski, I., Salinas, J. L., Sauquet, E., Šraj, M., Szolgay, J., Volpi, E., Wilson, D., Zaimi, K., and Živković, N. (2019). Changing climate both increases and decreases European river floods. *Nature*, 573, 108–111. https://doi.org/10.1038/s41586-019-1495-6

Bormann, H. & Pinter, N. (2017). Trends in low flows of German rivers since 1950: comparability of different low-flow indicators and their spatial patterns. *River Res. Appl.*, 33, 1191–1204. https://doi.org/10.1002/rra.3152

Caloiero, T., & Veltri, S. (2019). Drought assessment in the Sardinia Region (Italy) during 1922–2011 using the standardized precipitation index. *Pure Appl. Geophys.*, 176, 925–935. https://doi.org/10.1007/s00024-018-2008-5

Calzadilla, A., Rehdanz, K., Betts, R., Falloon, P., Wiltshire, A., & Tol, R.S.J. (2013). Climate change impacts on global agriculture. *Climatic Change*, 120, 357–374. https://doi.org/10.1007/s10584-013-0822-4

Deb, S. (2024). Analyzing trends and change points in hydro-meteorological parameters and groundwater level in the Barak river basin in India. *Physics and Chemistry of the Earth, Parts A/B/C*, 134, 103542. https://doi.org/10.1016/j.pce.2023.103542

Döll, P., Jiménez-Cisneros, B., Oki, T., Arnell, N.W., Benito, G., Cogley, J.G., Jiang, T., Kundzewicz, Z.W., Mwakalila, S., Nishijima, A. (2014). Integrating risks of climate change into water management. *Hydrological Sciences Journal*, 60, 4–13. http://dx.doi.org/10.1080/02626667.2014.967250

Dolton, G. L. (2006). *Pannonian Basin Province, Central Europe (Province 4808): Petroleum geology, total petroleum systems, and petroleum resource assessment* (U.S. Geological Survey Bulletin 2204-B, p. 47). U.S. Geological Survey. https://doi.org/10.3133/b2204B

Faye, D., Kaly, F., Dieng, A. L., Wane, D., Fall, C. M. N., Mignot, J., & Gaye, A. T. (2024). Regionalization of the Onset and Offset of the Rainy Season in Senegal Using Kohonen Self-Organizing Maps. *Atmosphere*, 15(3), 378. https://doi.org/10.3390/atmos15030378

Ferraz L. L., de Sousa L. F., da Silva L. S., de Jesus R. M., Santos C. A. S. & Rocha F. A. (2022). Land use changes and hydrological trend analysis in a Brazilian Cerrado basin. *International Journal of Environmental Science and Technology*, 19(8), 7469–7482. https://doi.org/10.1007/s13762-021-03666-8

Ferreira, G. W. S., & Reboita, M. S. (2022). A New Look into the South America Precipitation Regimes: Observation and Forecast. *Atmosphere*, 13(6), 873. https://doi.org/10.3390/atmos13060873

Feyen, L. & Dankers, R. (2009). Impact of global warming on streamflow drought in Europe, *Journal of Geophysical Research: Atmospheres*, 114, D17116. https://doi.org/10.1029/2008JD011438

Fiala, T., Ouarda, T. B. M. J., & Hladný, J. (2010). Evolution of low flows in the Czech Republic, *Journal of Hy-*

drology, 393, 206–218. https://doi.org/10.1016/j.jhydrol.2010.08.018

Fleig, A. K., Tallaksen, L. M., James, P., Hisdal, H., & Stahl, K. (2015). Attribution of European precipitation and temperature trends to changes in synoptic circulation. *Hydrology and Earth System Sciences*, 19(7), 3093–3107. https://doi.org/10.5194/hess-19-3093-2015

Gaudenyi, T., & Mihajlović, M. (2022). The Carpathian Basin: Denomination and Delineation. *European Journal of Environment and Earth Sciences*, 3(2), 1–6. https://doi.org/10.24018/ejgeo.2022.3.2.239

Gholami, H., Moradi, Y., Lotfirad, M., Gandomi, A.M., Bazgir, N., & Hajibehzad, M.S. (2022). Detection of abrupt shift and non-parametric analyses of trends in runoff time series in the Dez river basin. *Water Supply*, 22(2), 1216–1230. https://doi.org/10.2166/ws.2021.357

Gocić, M., Trajković, S. (2013) Analysis of changes in meteorological variables using Mann-Kendall and Sen's slope estimator statistical tests in Serbia. *Global and Planetary Change*, 100, 172-182. https://doi.org/10.1016/j.gloplacha.2012.10.014

Guntu, K. R., Maheswaran, R., Agarwal, A., & Singh, P. V. (2020) Accounting for temporal variability for improved precipitation regionalization based on self-organizing map coupled with information theory. *Journal of Hydrology*, 590. https://doi.org/10.1016/j.jhydrol.2020.125236

Gnjato, S., Leščešen, I., Basarin, B., & Popov, T. (2024). What is happening with frequency and occurrence of the maximum river discharges in Bosnia and Herzegovina?. *Acta geographica Slovenica*, 64(1). https://doi.org/10.3986/AGS.13461

Hall, J., Arheimer, B., Borga, M., Brázdil, R., Claps, P., Kiss, A., Kjeldsen, T. R., Kriaučiūnienė, J., Kundzewicz, Z. W., Lang, M., Llasat, M. C., Macdonald, N., McIntyre, N., Mediero, L., Merz, B., Merz, R., Molnar, P., Montanari, A., Neuhold, C., Parajka, J., Perdigão, R. A. P., Plavcová, L., Rogger, M., Salinas, J. L., Sauquet, E., Schär, C., Szolgay, J., Viglione, A., & Blöschl, G. (2014). Understanding flood regime changes in Europe: a state-of-the-art assessment. *Hydrology and Earth System Sciences*, 18(7), 2735–2772. https://doi.org/10.5194/hess-18-2735-2014

Hodgkins, G. A., Whitfield, P. H., Burn, D. H., Hannaford, J., Renard, B., Stahl, K., Fleig, A. K., Madsen, H., Mediero, L., Korhonen, J., Murphy, C., & Wilson, D. (2017). Climate driven variability in the occurrence of major floods across North America and Europe, *Journal of Hydrology*, 552, 704–717. https://doi.org/10.1016/j.jhydrol.2017.07.027

Intergovernmental Panel on Climate Change (IPCC). (2021). *Climate change 2021: The physical science basis*. IPCC. https://www.ipcc.ch/report/ar6/wg1/

Jorda-Capdevila, D., Gampe, D., Huber García, V., Ludwig, R., Sabater, S., Vergoñós, L., & Acuña, V. (2019). Impact and mitigation of global change on freshwater-related ecosystem services in Southern Europe. *Science of the Total Environment*, 651, 895–908. https://doi.org/10.1016/j.scitotenv.2018.09.228

Kilifarska, N.A., Metodieva, G.I., & Mokreva, A.C. (2025). Detection and Attribution of a Spatial Heterogeneity in the Temporal Evolution of Bulgarian River Discharge. *Geosciences*, 15(1), 12. https://doi.org/10.3390/geosciences15010012

Kocsis T., Kovács-Székely I. & Anda A. (2020). Homogeneity tests and non-parametric analyses of tendencies in precipitation time series in Keszthely, Western Hungary. *Theoretical and Applied Climatology*, 139 (3–4), 849–859. https://doi.org/10.1007/s00704-019-03014-4

Kohonen, T. (2001). *Self-organizing maps*. Springer.

Kundzewicz, Z. W., & Robson, A. (2000). *Detecting trend and other changes in hydrological data*. World Climate Programme Data and Monitoring, WMO/TD-No. 1013. World Meteorological Organization

Laizé, C. L. R. & Hannah, D. M. (2010). Modification of climate–river flow associations by basin properties. *Journal of Hydrology*, 389(1-2), 186–204. https://doi.org/10.1016/j.jhydrol.2010.05.048

Lehner, B., Döll, P., Alcamo, J., Henrichs, T., & Kaspar, F. (2006). Estimating the impact of global change on flood and drought risks in Europe: a continental, integrated analysis. *Climatic Change*, 75, 273–299. https://doi.org/10.1007/s10584-006-6338-4

Leščešen, I., Gnjato, S., Galinović, I., & Basarin, B. (2024). Hydrological drought assessment of the Sava River basin in South-Eastern Europe. *Journal of Water and Climate Change*, 15(8), 3902–3918. https://doi.org/10.2166/wcc.2024.157

Leščešen, I., Šraj, M., Basarin, B., Pavić, D., Mesaroš, M., & Mudelsee, M. (2022). Regional Flood Frequency Analysis of the Sava River in South-Eastern Europe. *Sustainability*, 14(15), 9282. https://doi.org/10.3390/su14159282

Leščešen, I., Šraj, M., Pantelić, M., & Dolinaj, D. (2022). Assessing the impact of climate on annual and seasonal discharges at the Sremska Mitrovica station on the Sava River, Serbia. *Water Supply*, 22(1), 195–207. https://doi.org/10.2166/ws.2021.277

Licen, S., Astel, A., & Tsakovski, S. (2023). Self-organizing map algorithm for assessing spatial and temporal patterns of pollutants in environmental compartments: A review. *Science of The Total Environment*, 878, 163084. https://doi.org/10.1016/j.scitotenv.2023.163084

Lorenzo-Lacruz, J., Vicente-Serrano, S. M., López-Moreno, J. I., Beguería, S., García-Ruiz, J. M., & Cuadrat, J. M. (2010). The impact of droughts and water management on various hydrological systems in the headwaters of the Tagus River (central Spain). *Journal of Hydrology*, 386(1–4), 13–26. https://doi.org/10.1016/j.jhydrol.2010.01.001

Mediero, L., Santillán, D., Garrote, L., & Granados, A. (2014). Detection and attribution of trends in magnitude, frequency and timing of floods in Spain, *Journal of Hydrology*, 517, 1072–1088. https://doi.org/10.1016/j.jhydrol.2014.06.040

Mezősi, G. (2017). *The Physical Geography of Hungary*. Springer International Publishing: Cham, Switzerland.

Milly, P. C. D., Dunne, K. A., & Vecchia, A. V. (2005). Global pattern of trends in streamflow and water availability in a changing climate. *Nature*, 438, 347–350. https://doi.org/10.1038/nature04312

Obreht, I., Zeeden, C., Hambach, U., Veres, D., Marković, B.S., & Lehmkuhl, F. (2019). A critical reevaluation of palaeoclimate proxy records from loess in the Carpathian Basin, *Earth-Science Reviews*, 190, 498-520. https://doi.org/10.1016/j.earscirev.2019.01.020

Papadimitriou, L.V., Koutroulis, A.G., Grillakis, M.G., Tsanis, I.K. (2016). High-end climate change impact on European runoff and low flows – exploring the effects of forcing biases. *Hydrology and Earth System Sciences*, 20(5), 1785–1808. http://dx.doi.org/10.5194/hess-20-1785-2016

Paprotny, D., Sebastian, A., Morales-Nápoles, O., Jonkman, S.N. (2018). Trends in flood losses in Europe over the past 150 years. *Nature communications*, 9, 1985. https://doi.org/10.1038/s41467-018-04253-1

Pettitt, A. N. (1979). A non-parametric approach to the change point problem. *Journal of the Royal Statistical Society. Series C. (Applied Statistics)*, 28(2), 126–135. https://doi.org/10.2307/2346729

Piniewski, M., Marcinkowski, P., & Kundzewicz, Z.W. (2018). Trend detection in river flow indices in Poland. *Acta Geophysica*, 66, 347–360. https://doi.org/10.1007/s11600-018-0116-3

Poff, N. L., Allan, J. D., Bain, M. B., Karr, J. R., Prestegaard, K. L., Richter, B. D., Sparks, R. E., Stromberg, J. (1997). The natural flow regime: A paradigm for river conservation and restoration. *BioScience*, 47(11), 769-784. https://doi.org/10.2307/1313099

Rydén, J. (2022). Statistical analysis of possible trends for extreme floods in northern Sweden. *River Research and Applications*, 38(6), 1041–1050. https://doi.org/10.1002/rra.3980

Schneider, C., Laizé, C.L.R., Acreman, M.C., & Flörke, M. (2013). How will climate change modify river flow regimes in Europe? *Hydrology and Earth System Sciences*, 17, 325–339. http://dx.doi.org/10.5194/hess-17-325-2013

Stahl, K., Hisdal, H., Hannaford, J., and Tallaksen, L. (2010). Streamflow trends in Europe: evidence from a dataset of nearnatural catchments. *Hydrology and Earth System Sciences*, 14(12), 2367–2382. https://doi.org/10.5194/hess-14-2367-2010

Tadić, L., Tamás, E. A., Mihaljević, M., & Janjić, J. (2022). Potential Climate Impacts of Hydrological Alterations and Discharge Variabilities of the Mura, Drava, and Danube Rivers on the Natural Resources of the MDD UNESCO Biosphere Reserve. *Climate*, 10(10), 139. https://doi.org/10.3390/cli10100139

Teuling, A. J., de Badts, E. A. G., Jansen, F. A., Fuchs, R., Buitink, J., Hoek van Dijke, A. J., & Sterling, S. M. (2019). Climate change, reforestation/afforestation, and urbanization impacts on evapotranspiration and streamflow in Europe. *Hydrology and Earth System Sciences*, 23(9), 3631–3652. https://doi.org/10.5194/hess-23-3631-2019

Uehlinger, U., Wantzen, M. K., Leuven, R. S. E. W., & Hartmut, A. (2009). The Rhine River. In K. Tockner, U. Uehlinger, & C. T. Robinson (Eds.), *Rivers of Europe* (pp. 199–246). Academic Press.

Vesanto, J., & Alhoniemi, E. (2000). Clustering of the self-organizing map. *IEEE Transactions on Neural Networks*, 11(3), 586–600. https://doi.org/10.1109/72.846731

Woldemarim, A., Getachew, T., & Chanie, T. (2023). Long-term trends of river flow, sediment yield and crop productivity of Andit tid watershed, central highland of Ethiopia. *All Earth*, 35(1), 3–15. https://doi.org/10.1080/27669645.2022.2154461

INTERNATIONAL SCIENTIFIC JOURNAL
GEOGRAPHICA PANNONICA
Volume 29, Issue 2, 121–136 (June 2025)
Journal homepage: http://www.dgt.uns.ac.rs/en/homepage/pannonica/

Intracountry Regional Inequalities in the Context of the Socioeconomic Status of Selected European Countries

Radoslav Klamár[A*], Monika Ivanová[A], Ján Kozoň[B]

[A] *Faculty of Humanities and Natural Sciences, University of Prešov, Prešov, Slovak Republic; ORCID RK: 0000-0002-5153-8412; MI: 0000-0002-2015-4918*

[B] *Statistical Office on the Slovak republic, Regional Statistical Office Prešov, Prešov, Slovak Republic; ORCID JK: 0000-0003-3848-8526*

KEYWORDS

- coefficient of variation
- Gini coefficient
- Gross Domestic Product
- Income of Household
- socioeconomic status
- intracountry regional inequalities

ABSTRACT

The paper deals with the issue of intracountry inequalities in selected European countries with attention paid to the analysis of potential connections between the level of identified regional inequalities in the assessed countries and their socioeconomic status. Two frequently employed indicators were chosen to assess regional inequalities: Gross Domestic Product per capita in PPS and Income of Households per capita in PPS, employing the Gini coefficient and the coefficient of variation as the basic statistical measures. The obtained results refer to the highest level of regional inequalities in the countries of the former Socialist Bloc, while the strong influence of capitals was also confirmed in these countries on the level of inequalities. At the same time, the presumption that the decreasing socioeconomic status of the countries caused the increasing level of intracountry regional inequalities was largely confirmed.

Introduction

Social development is significantly determined by the quality and the level of imbalance of social systems, particularly their subsystems, elements, nodes, and networks, the imbalance of their energies, inputs, outputs, etc. Development is mainly possible thanks to the existence of nonlinearities, asymmetries, contrasts, and imbalance. On one hand, we strive to put the social system in outer and inner balance but, on the other hand, we are aware, thanks to thermodynamic laws, that the disbalance of the system is a regular phenomenon, inevitable for a new movement, new arrangement, self-arrangement, for further system development (Ivanička et al., 2014).

If, however, the differences are too big, numerous authors recommend introducing to make measures to stop their increase (Gurgul & Lach, 2011), because big differences in regional development are not favourable for the socio-economic development of the whole country, and what is more, they are damaging (Czyż & Hauke, 2011). Excessive efforts made to reduce inequalities, however, may cause the stagnation of the socioeconomic development of the whole country (Blažek & Csank, 2007).

The paper focuses on intracountry regional inequalities in selected European countries and their assessment with regard to the socioeconomic status of the countries. Ezcurra (2019) states, that regional inequalities in development across the EU have drawn significant interest from both researchers and politicians over the past two decades. We were therefore curious about the extent to which

[*] Corresponding author:Radoslav Klamár; radoslav.klamar@unipo.sk

doi: 10.5937/gp29-56677

Received: February 10, 2025| Revised: June 20, 2025| Accepted: June 24, 2025

the socioeconomic status of the countries impacts the regional inequalities and their level; we paid particular attention to the capital cities with their specific positions in terms of spatial structure and their impact on the size of the regional inequalities.

Theoretical framework

Regional inequalities are a relatively frequently discussed topic and are looked at and characterised in different ways. They are defined by Kutscherauer et al. (2010) as divergence of characters, phenomena or processes, the identification and comparison of which make some rational sense (cognitive, psychological, social, economic, political, etc.). Matlovič & Matlovičová (2011) understand regional inequalities as differences in the degree of socioeconomic development of regions that are the consequences of its unevenness. Its manifest themselves through differences between the level of incomes per capita and determine, at a given moment, a chain reaction from public and private sector representatives, inhabitants, etc. aimed at counteracting their increase (Antonescu & Florescu, 2023). Regional inequalities arise when certain regions outperform others, resulting in an uneven distribution of well-being across different geographic areas. Consequently, regional inequalities are identified when researchers, through regional analysis, detect variations in comparable well-being indicators between regions, or when, after accounting for individual characteristics, disaggregated data still reveals persistent differences in well-being between people living in different regions (Maggino, 2023).

The issue of regional inequalities can be found in the works of many authors employing various approaches (for example the model proposed by Panzera & Postiglione (2021) extends the spatial specification of Mankiw-Romer-Weil by introducing regional income inequality as a determinant of economic growth while Boschma et al. (2023) deal with innovation, industrial dynamics and regional inequality) and assessment indicators in their evaluations. The basic and most frequently used indicator is Gross Domestic Product (GDP) and was used in the evaluations of regional inequalities by Paas & Schlitte (2007), Kallioras (2010), Klamár (2016), Arestis & Phelps (2019), Belinska et al. (2020), Klamár et al. (2020), Neszmélyi et al. (2022), Capello & Cerisola (2023) etc. Despite certain limitations when using this indicator (e.g. in works by Adler Braun, 2009, Buček et al., 2010, Laurent, 2017), the application of GDP per capita as the basic indicator of the social-economic level of a region may be ascribed to the availability of data on the regional level in the whole EU (Michálek, 2013). The second relevant socioeconomic indicator is disposable income per inhabitant, used when assessing inequalities by e.g. Källström (2012), Klamár (2016), Cörves & Mayhew (2021), Dauderstädt (2021), Neszmélyi et al. (2022), Savoia (2024), Bareith & Csizmadia (2025) etc.

Both above indicators are, together with their complexity and meaningfulness, also easily available for both individual European countries and their regions (Eurostat databases – identical methodologic procedure of processing statistical data), knowledge of which is an inevitable precondition for assessing regional inequalities on this hierarchic level (e.g. works by Wishlade & Yuill, 1997, Boldrin & Canova, 2001, Paas & Schlitte, 2007, Smętkowski & Wójcik, 2012, Källström, 2012, Iammarino et al., 2019, Fifeková et al., 2021, Neszmélyi et al., 2022).

The particular analyses and evaluations show that on one hand there are economically prosperous regions of the countries of Western and Northern Europe and on the other hand there are the countries of the former Eastern Bloc that, during the last three decades, have gone through a difficult transformation process and development within already "expanded" Europe. Iammarino et al. (2019) divided European regions based on the level of their development into four groups, specifically of low, medium, high, and very high development. Almost all the regions of the former Eastern Bloc countries (exclusive of the regions of their capitals) fell into the category of low development. In this context, Fifeková et al. (2021) pointed out the fact that the EU can be seen as a grouping of performance-differentiated countries, where the converging countries will no longer be able to narrow the performance gap with the rest of the EU with the passage of time. The above statement was also accepted by Boldrin & Canova (2001). In their opinion, the main reason for regional inequalities is the process of real convergence of the EU Cohesion countries compared to the Community average that has not always resulted in the reduction of regional inequalities. As the authors indicate, 50 of 211 regions (the number of EU NUTS 2 regions according to Eurostat) show an income per capita lower than 75% of the average. The ratio between the GDP per capita of the richest and the poorest US state is slightly less than 2, while in the EU it is more than 5. As presented by Fifeková et al. (2021), the studies of regional inequalities of converging European economies provide evidence that comply with Williamson´s hypothesis (Williamson, 1965) that the growing economic performance in the given European countries firstly led to the growth of regional inequalities, as a rule below the level of the middle income and then the regional inequalities tended to fall (Szörfi, 2007, Neszmélyi et al., 2016, Kisiała & Suszyńska, 2017).

The problem of intraregional and interregional inequalities within the context of the extending EU was dealt with by Szörfi (2007) who, apart from verifying the presumptions of Williamson´s hypothesis, found out that some factors have a larger impact on regional inequalities than the national income. He mentions EU accession, the process of transition to a new grouping (the speed of changing the economic structure, the ability to recover), eco-

nomic and monetary union involving the transparency of markets and increased competition, ability to use financial resources from the EU structural funds and the cohesion fund to build effective institutions that would enable more decentralized planning.

Regional inequalities can be seen not only between the regions but also within them (Boschma, 2022). Big cities are able to attract a relatively high number of highly and less qualified workers (Eeckhout et al., 2014). They may increase the demand for local services which can show itself in new vacancies with lower wages (Moretti, 2010). A particular influence on inequalities in this context is made by capitals. Szörfi (2007) pointed to a notable difference between the capital and the rest of the country in the countries of Central Europe and he also accented that Western European countries are more balanced in this respect. Matlovič & Matlovičová (2011), Psycharis et al. (2020), Klamár et al. (2020), Neszmélyi et al. (2022) etc. also discussed the effect of a capital city in their analyses and evaluations.

Meliciani (2016) also adds to the previous statements. She argues that the growing significance of innovation and human capital is a key factor contributing to the widening income and employment disparities among the older EU member states, particularly following the 2008 financial crisis. In contrast, she emphasizes that in the newer member states, regional disparities are primarily driven by broader socio-economic factors. While capital regions are increasingly aligning with Western European standards, other regions – especially former industrial and peripheral areas – continue to lag behind in terms of development.

Methodology

In the first step of the analyses, attention was paid to quantitative evaluation of the level of intracountry regional inequalities in the selected countries of Europe. As presented by Matlovič & Matlovičová (2011), when evaluating regional inequalities, it is important to define the evaluated territorial units, to determine the selection of adequate indicators and statistical measurement rates.

In the paper, attention is focused on 25 selected countries of Europe – Austria, Belgium, Bulgaria, Croatia, Czechia, Denmark, Finland, France, Germany, Greece, Hungary, Ireland, Italy, Lithuania, Netherlands, Norway, Poland, Portugal, Romania, Serbia, Slovakia, Slovenia, Spain, Sweden and Switzerland. Their selection depended on the availability of statistical data in the Eurostat databases on the NUTS 2 level that was determined as the observation level (the most data are available on this level) as well as on the country having a minimum of two or more NUTS 2 regions for the purposes of the comparison (that is why countries whose territory was represented by only one NUTS 2 region were excluded from the evaluation). In total, 254 regions were included in the analysis.

Another step to take was to choose suitable indicators. Considering availability, representativeness and complexity, two basic and frequently employed indicators were chosen – Gross Domestic Product (GDP) per capita in Purchasing Power Standards (PPS) and Income of Households per capita in PPS. GDP and Income of Households were also selected for analysis due to the availability of data at the NUTS 2 level and the uniform data collection methodology applied across all analysed European countries, which ensures cross-country comparability.

After defining territorial units and selecting the evaluation indicators we proceeded to select statistical measurement rates. Felsenstein & Portnov (2005), Matlovič & Matlovičová (2011), Ancuţa (2012), Hamada (2016), Klamár (2016), Klamár et al. (2020), Egri & Lengyel (2024), Kanó et al. (2025) mention more measurement rates such as the coefficient of variation, Gini coefficient, Theil index, Atkinson index, Hoover coefficient or the method of distance from a fictive object etc.

The most frequently used are the coefficient of variation and the Gini coefficient. Dauderstädt (2021) utilizes the coefficient of variation as a primary indicator to express relative income inequality both among EU member states and at the regional level (NUTS 1/NUTS 2). Savoia (2024) utilizes both the Gini coefficient and the coefficient of variation to analyse income inequality across EU regions. He reports descriptive statistics showing increases in both measures Gini and CV between 1990 and 2013. Balakrishnan et al. (2022) use the coefficient of variation as the main indicator for measuring regional inequalities among EU countries. Antonescu & Florescu (2023) explicitly utilize the Gini coefficient to measure regional income inequality at the NUTS 2 level during the COVID-19 period. This indicator is analysed in relation to GDP per capita in Purchasing Power Standards, which serves as a proxy for the economic development of EU regions. Borowski et al. (2025) in their analysis of inflation synchronization in the Eurozone, applied a range of indicators to measure inequality, including the Gini coefficient and the coefficient of variation.

In our analysis, we also used the Gini coefficient and the coefficient of variation, their application being justified due to both their statistical properties and their interpretative clarity. The Gini coefficient is particularly advantageous as it is independent of the number of observational units (e.g., regions) and takes into account differences between all possible pairs of values. The coefficient of varia-

tion, thanks to its dimensionless nature, is an ideal indicator for comparing inequalities across different types of indicators that may vary in scale or units of measurement. Both indicators offer a complementary perspective on regional differentiation. While the Gini coefficient captures overall inequality of the distributional within a dataset, the coefficient of variation reflects the dispersion of values around the mean. Compared to alternative measures such as the Theil index and Atkinson index, both the Gini coefficient and the coefficient of variation offer significant advantages in terms of lower computational complexity, more intuitive interpretation, and wide acceptance in international research.

The coefficient of variation (CV) is a tool for comparative analyses and is a relative rate of dispersion derived from a standard deviation σ (the ratio of the standard deviation and the average).

$$cv = \frac{\sigma}{\overline{x}} = \frac{\sqrt{\sum_{i=1}^{n}\left(x_i - \overline{x}\right)^2}}{\overline{x}}$$

The coefficient of variation enables mutual comparison of variability of variables with different values (reducing the standard deviation by the average value). The second used statistical rate was the Gini coefficient (GI) that originated as a tool to measure income inequality. It oscillates between 0 (maximal equality) and 1 (maximal inequality)

$$GI = \frac{1}{2n^2\overline{x}}\sum_{i=1}^{n}\sum_{j=1}^{n}\left(x_i - x_j\right)$$

n is the number of territorial units, x_i is the value of monitored indicator in i –territorial unit, x_j is the value of the monitored indicator in j - territorial unit and $\overline{x}$ is the arithmetic average of the monitored indicator x.

At this initial stage of the evaluation, we pronounced hypothesis H1 saying that the highest rate of intracountry regional inequalities will be recorded in the countries of the former Socialist Bloc. This is based on the fact, highlighted by Rauhut & Humer (2024), that mature economies display fewer regional inequalities and a higher degree of regional economic convergence than developing economies. According to Williamson (1965), regional inequality is generated during the early development stages, while mature growth produces regional convergence. In the next step, we were researching to what extent their capitals contributed to the level of the identified regional inequalities in the assessed countries. The impact of capitals on the size of regional inequalities was indicated by e.g. Smętkowski (2014), Matlovič et al. (2018), Klamár et al. (2020), Psycharis et al. (2020) etc. Based on the abovementioned, we present hypothesis H2 which presumes a significant decrease of regional inequalities in the countries after their capitals were excluded. The most significant decrease of inequalities after the exclusion of the capitals was expected again in the former socialist countries, which serves as hypothesis H3. This premise is based on the fact that the capital cities in these countries have had and continue to have a significantly dominant position within the settlement structure of the country with the cumulation of economic and decision-making functions. Reinl et al. (2023) state that the adjusted income per capita according to purchasing power of cities like Bratislava or Prague is comparable to incomes in Paris or the Oberbayern region (Germany), but peripheral regions of Czechia or Slovakia lag much further behind in term of income convergence than peripheral regions of France or Germany.

Finally we researched the connection between the level of established regional inequalities in the individual countries and their socioeconomic status. Following the work by Szörfi (2007), who assessed the relation between regional disparities and the development of the countries in the extended EU, we formulated hypothesis H4 stating that the growth of socioeconomic status of the countries would cause the decrease of their intracountry regional inequalities. Socioeconomic status presents a complex indicator in the evaluation (e.g. Klamár et al., 2019), whose construction comes out of the point method. As many as 13 global economic and social indexes were comprised in the assessment aiming to achieve maximum objectivity (the selected indexes are representative, have been monitored and evaluated over a long period, are methodologically well-defined and inherently quite complex – containing multiple sub-indicators, and most of these indexes evaluate almost every countries in the world): the KOF Globalisation Index (KGI), Global Competitiveness Index (GCI), Global Innovation Index (GII), Global Entrepreneurship Index (GEI), Inclusive Development Index (IDI), Easy Doing Business (EDB), Index of Economic Freedom (IEF), Digital Platform Economy Index (DPE), Corruption Perception Index (CPI), Human Development Index (HDI), Social Progress Index (SPI), Gross Happiness Index (GHI) and Legatum Prosperity Index (LPI). As the basis for comparison in each index the highest reached level in some of the countries was selected. The highest level was assigned 100 points and it represented the basic quantity in comparisons to other countries; the values reached within each index in the rest of the countries were compared to it. The value of each country was achieved by adding the values per individual indexes and the maximum was 1,300 points.

To express the relation (dependence) between the socioeconomic status of the countries and the level of their regional inequalities regression analysis and the correlation analysis, where the socioeconomic status of a country was

an independent variable and the size of regional inequalities (in both variants – Gini coefficient and coefficient of variation) was a dependent variable, were both used. The Pearson correlation coefficient R was the rate of considering the strength of linear dependence, whose absolute values approaching 1 indicated the increased strength of the relation between the status of a country and the size of regional inequalities. The determination coefficient R^2 expressed the percentage of the variability of the dependent variable expressible by the variability of the independent variable. Assessment of the suitability of the linear regression model was also part of the testing.

Research result

The level of intracountry regional inequalities in the countries

In the selected countries of Europe, regional inequalities were evaluated using two basic indicators, namely GDP per capita in PPS and Income of Households per capita in PPS.

In the case of the first evaluated indicator – GDP calculated for 2020 (Fig. 1), the highest inequalities were recorded in Slovakia (GI – 0.2579, CV – 0.6329). Slovakia together with Croatia, Serbia, Ireland, Romania and Hungary represented a group of countries with GI above 0.20 and CV around 0.50. It is evident from the summary of the countries that countries of the former Eastern Bloc prevailed here. The second group consisted of countries with a medium level of regional inequalities with GI from 0.10 to 0.20 and CV in most cases from 0.20 to 0.50. From the total of 11 countries in this group, slightly more than one third were represented by former socialist countries (Czechia, Bulgaria, Poland, Lithuania) and the level of their inequalities was in case of GI 0.14 and higher and as for CV around 0.40 and higher. Most of the remaining countries from this group recorded a lower level of inequalities (Italy, France, Denmark, Germany, Netherlands and Spain).

In the last group with the lowest level of inequalities (GI below 0.10, CV in most cases less than 0.20) the only country from the former socialist countries was Slovenia with

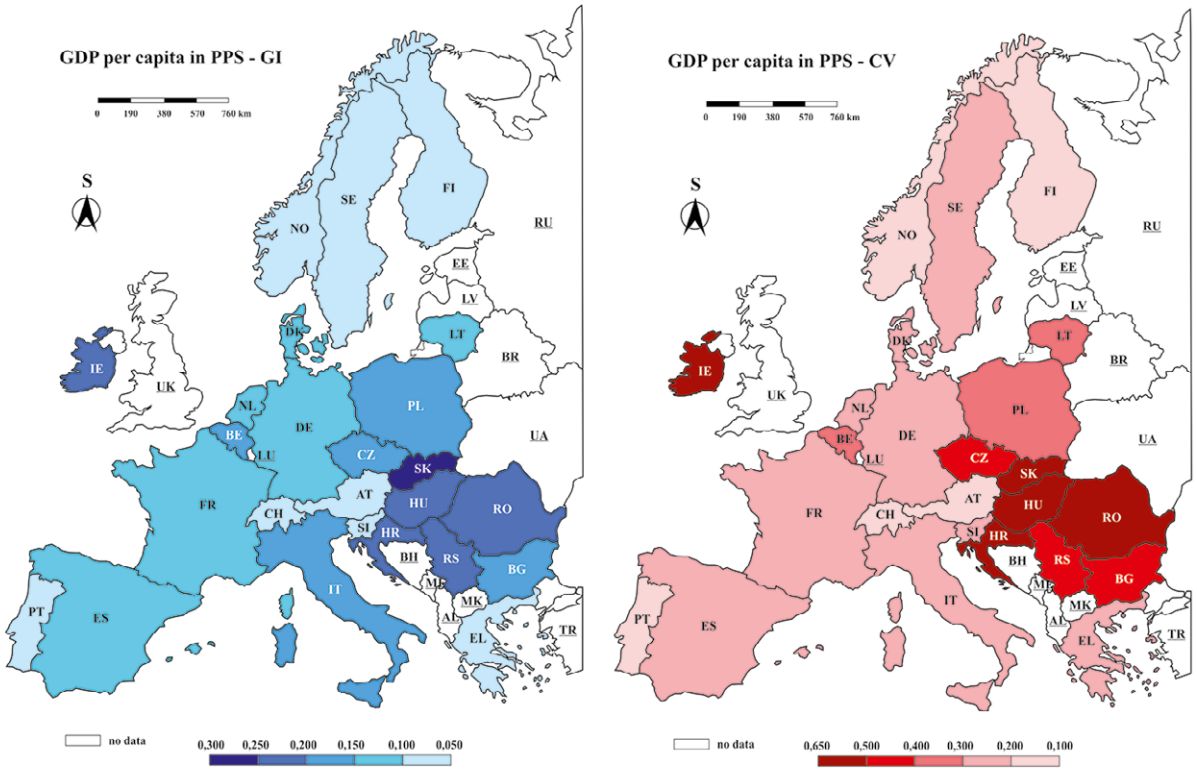

Figure 1. The Gini coefficient (GI) and the coefficient of variation (CV) within GDP per capita in PPS in the selected European countries in 2020

Note: Austria (AT), Belgium (BE), Bulgaria (BG), Croatia (HR), Czechia (CZ), Denmark (DK), Finland (FI), France (FR), Germany (DE), Greece (EL), Hungary (HU), Ireland (IE), Italy (IT), Lithuania (LT), Netherlands (NL), Norway (NO), Poland (PL), Portugal (PT), Romania (RO), Serbia (RS), Slovakia (SK), Slovenia (SI), Spain (ES), Sweden (SE), Switzerland (CH), LV – country without data

Source: Author's calculations based on the Eurostat data

GI 0.0907, but its CV was as high as 0.2567. This group was dominated by Scandinavian countries together with Austria, Portugal and Switzerland (GI – 0.0631, CV – 0.1257).

The second chosen indicator – Income of Household (Fig. 2) was, due to unavailable data for 2020, evaluated for 2019 and 23 countries participated in the evaluation (no data were available for Switzerland and Serbia). In total, the level of inequalities was lower in this indicator (GI up to 0.15 and CV up to 0.33) than in the case of GDP.

The highest level of regional inequalities was observed in the group of five countries whose GI was higher than 0.10 and CV higher than 0.19. As many as four former socialist countries, specifically Hungary, Bulgaria, Slovakia, and Romania, belonged to the group, while the last one recorded the highest regional inequalities (GI – 0.1406 and CV – 0.3280). The second group was formed by 10 countries with a medium level of disparities (GI from 0.05 to 0.10 and CV from 0.09 to 0.16). This group was represented by 4 former socialist countries, Croatia, Poland, Lithuania and Czechia, which recorded the lowest inequalities (GI – 0.0642, CV – 0.1406). The other countries were Ireland, Portugal, and Belgium.

The last group, the one with the lowest inequalities (GI below 0.05 and CV below 0.09) was created by the countries of Western Europe and Scandinavia. Slovenia was an exception, since it recorded the lowest inequalities, more precisely GI – 0.0086 and CV – 0.0243 (the level of regional inequalities was influenced by the fact that there are only two NUTS 2 regions in the country).

The level of intracountry regional inequalities after excluding capital cities

The level of regional inequalities is influenced by several factors one of the most significant being the influence of their capital cities. In most countries, capitals are not only the administrative centres of the particular countries, but at the same time the largest and economically most powerful city where strong economic subjects concentrate, and branches of foreign companies are located. For this reason, follow-up analyses addressed the level of inequalities after the exclusion of capitals.

In terms of the first indicator, GDP, we recorded a significant drop of inequalities (Fig. 3). The most notable drop was recorded in Bulgaria (GI dropped by 82.6%, CV by 87.0%), Slovakia (79.4%, 77.8%) and Czechia (72.8%, 80.1%). Only Finland approached the three former socialist countries with its drop by 74.8% (GI) and 77.8% (CV). It is

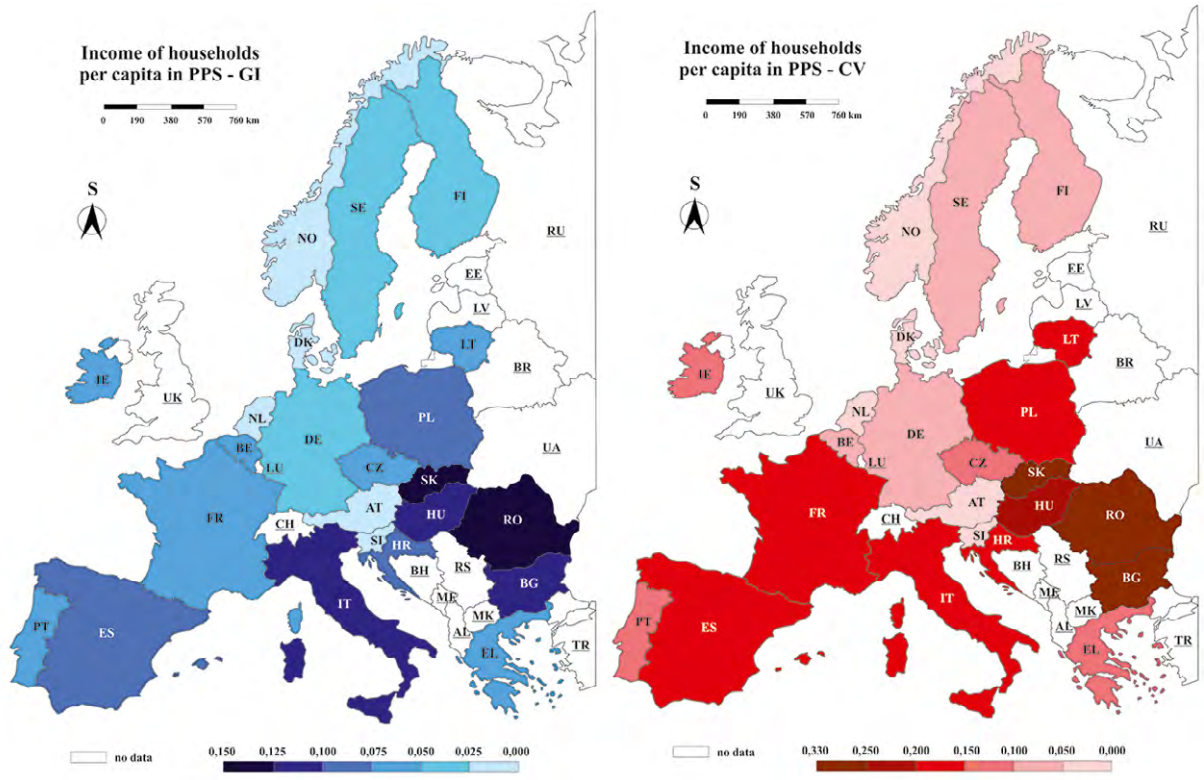

Figure 2. The Gini coefficient (GI) and the coefficient of variation (CV) within Income of household per capita in PPS in the selected European countries in 2019

Note: Austria (AT), Belgium (BE), Bulgaria (BG), Croatia (HR), Czechia (CZ), Denmark (DK), Finland (FI), France (FR), Germany (DE), Greece (EL), Hungary (HU), Ireland (IE), Italy (IT), Lithuania (LT), Netherlands (NL), Norway (NO), Poland (PL), Portugal (PT), Romania (RO), Serbia (RS), Slovakia (SK), Slovenia (SI), Spain (ES), Sweden (SE), Switzerland (CH), LV – country without data

Source: Author's calculations based on the Eurostat data

evident that metropolises such as Prague, Sofia, Bratislava and Helsinki enjoy an outstanding economic position in their countries.

In the next group of countries, the drop in inequalities was between 50 - 70%. Except for another Scandinavian country - Sweden (drop of 58.8%, 65.5%) and Portugal (63.8%, 66.4%) the group again consisted almost exclusively of the countries of the former Socialist Bloc, specifically Hungary (drop by 62.5%, 70.8%), Romania (61.9%, 70.5%), Croatia (67.0%, 67.6%) and Serbia (59.1%, 54.3%). The strong effect of a capital city again strongly manifested itself (Budapest, Bucharest, Ljubljana and Belgrade). This group also includes Poland (41.6%, 57.2%), where the impact of Warsaw was not that notable thanks to the polycentric structure of other big Polish cities such as Krakow, Katowice, Poznan, Wroclaw and Gdansk.

The third group consisted of the countries with a drop from 10 to 50%, represented by Denmark, Greece, Norway, France, Belgium, Netherlands and partially Spain, whose drop results were slightly below 10% (GI and CV by 9.2%). The fourth group was created by countries in which only a mild drop of inequalities was recorded, namely Switzerland (by 2.1%, 0.4%) and Austria (1.8%, 0.7%) or a slight growth as in the case of Germany (1.2%, 1.4%) and Italy (2.1%, 2.5%).

The only country, where a more notable growth of inequalities was recorded, was Ireland with 23.3% GI and 47.9% CV.

The second evaluated indicator Income of Household also confirmed the decrease of regional inequalities in most of the countries after excluding their capitals (Fig. 4). Also in this case there were two countries, Bulgaria (GI

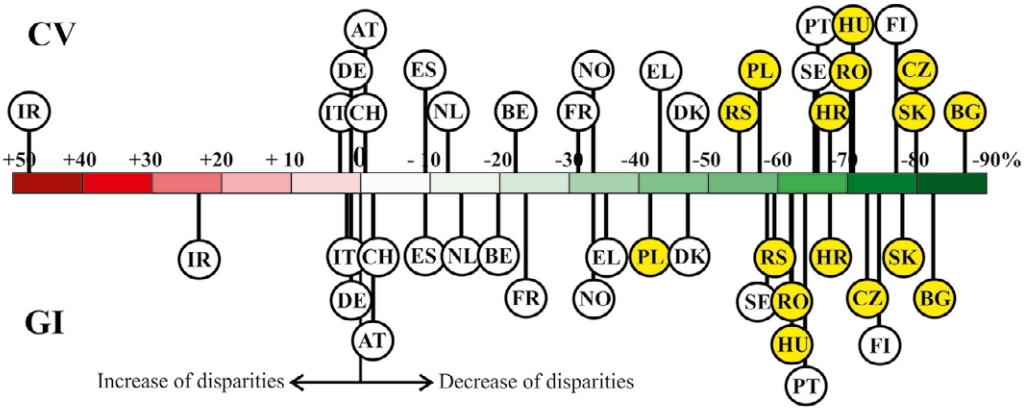

Figure 3. The increase or decrease (%) of the Gini coefficient (GI) and the coefficient of variation (CV) in GDP per capita in PPS after excluding capitals in 2020

Note: the yellow circles represent former socialist countries

Source: Author's calculations based on the Eurostat data

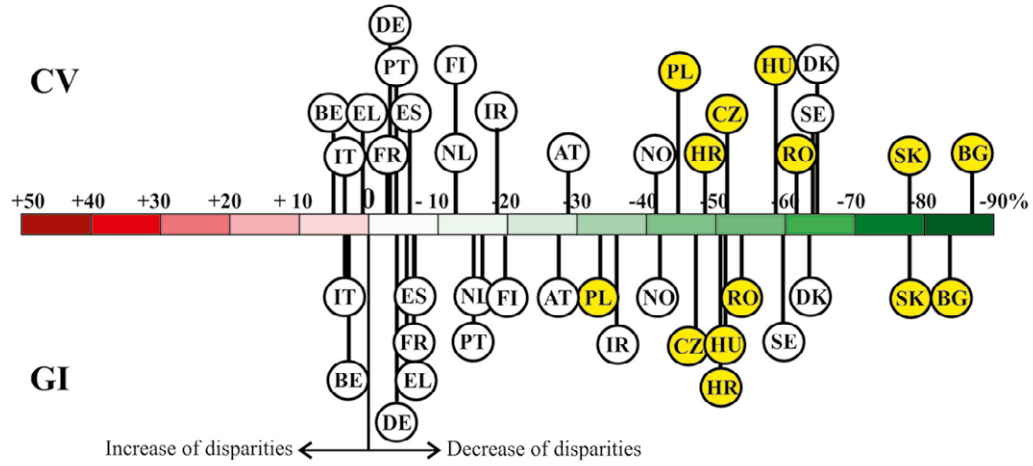

Figure 4. The increase or decrease (%) of the Gini coefficient (GI) and the coefficient of variation (CV) in Income per capita in PPS after excluding capitals in 2019

Note: the yellow circles represent the former socialist countries

Source: Author's calculations based on Eurostat data

drop of 83.9%, CV of 87.2%) and Slovakia (79.5%, 79.6%), which again confirmed the strong position of Sofia and Bratislava.

The second group with decreased inequalities from 40 to 65% is made up of three Nordic states, namely Denmark (63.5%, 64.1%), Sweden (59.2%, 64.0%) and Norway (41.9%, 41.3%) and five former socialist countries – Romania (53.7%, 61.4%), Czechia (46.9%, 51.4%), Hungary (51.2%, 58.9%), Croatia (50.5%, 48.1%) and Poland (33.1%, 44.5%). Together with Bulgaria and Slovakia, the dominant position of former socialist capitals was confirmed.

The third group was formed by Austria, Ireland, Finland and Netherland, whose decrease of inequalities is milder, in most cases from 10 to 35%.

The last group was represented by countries that recorded only a slight drop of inequalities (Spain, France, Germany, and Portugal) or only a mild drop (Belgium, Italy). Only in Greece did GI show decreased inequalities by 5.4% and CV increase by 0.4%.

Socioeconomic status and its connection with the level of regional inequalities

Socioeconomic status, as a result of evaluation of a set of 13 global indexes, is in the selected countries substantially differentiated (Table 1). The highest value within this complex indicator was reached by Switzerland (1271.4 points). Leaving aside the EDB (Easy Doing Business) index, it was

Table 1. Socioeconomic status in the assessed European countries in 2020

Country	KGI	GCI	GII	GEI	IDI	EDB	IEF	DPE	CPI	HDI	SPI	GHI	LPI	Σ points
Switzerland	100.0	99.9	100.0	100.0	99.5	89.7	100.0	92.6	96.6	99.8	98.6	96.0	98.7	1271.4
Denmark	96.7	98.5	87.0	96.5	95.6	100.0	95.5	86.3	100.0	98.2	99.3	93.9	100.0	1247.5
Sweden	97.8	98.5	94.6	85.4	94.7	96.0	91.3	93.2	96.6	99.0	98.8	94.4	98.5	1238.9
Netherlands	98.9	100.0	89.0	88.0	92.3	89.1	93.9	100.0	93.2	96.8	98.2	94.9	97.2	1231.4
Finland	95.6	97.3	86.2	85.4	87.7	93.9	92.3	83.6	96.6	98.0	99.1	100.0	98.5	1214.2
Norway	93.4	94.8	74.6	68.2	100.0	96.7	89.5	90.3	95.5	100.0	100.0	94.2	99.3	1196.5
Germany	96.7	99.3	85.6	81.1	86.7	93.3	89.6	78.2	90.9	99.0	97.7	89.9	96.1	1184.0
Ireland	94.5	91.1	80.3	86.7	89.5	90.0	98.7	80.1	81.8	99.8	97.4	90.0	95.0	1175.0
Austria	96.7	93.0	75.8	79.0	88.0	92.2	89.2	69.2	86.4	96.3	96.5	91.6	95.3	1149.0
Belgium	98.9	92.7	74.3	75.7	84.5	87.8	84.0	75.8	86.4	97.3	96.5	87.1	90.2	1131.3
France	95.6	95.6	81.2	81.6	83.1	89.7	80.5	77.2	78.4	94.1	95.7	85.5	90.6	1128.9
Spain	93.4	91.4	69.0	57.1	72.4	91.2	81.6	64.9	70.5	94.5	95.7	82.9	89.8	1054.4
Czechia	93.4	86.0	73.1	52.9	83.7	89.3	91.2	59.3	61.4	94.0	93.5	88.5	86.6	1053.0
Slovenia	87.9	85.2	64.9	79.7	81.1	89.6	82.7	54.7	68.2	95.8	64.6	84.8	88.4	1027.6
Lithuania	89.0	83.0	59.3	53.6	79.9	95.6	93.5	53.8	68.2	92.2	90.6	82.5	83.2	1024.3
Portugal	93.4	85.4	65.8	56.3	65.3	89.6	81.7	61.7	69.3	90.3	94.7	77.5	87.8	1018.8
Italy	91.2	86.8	69.1	54.9	70.9	85.4	77.8	55.9	60.2	93.2	94.2	82.7	85.1	1007.4
Poland	89.0	83.6	60.5	60.2	75.8	89.5	84.3	49.3	63.6	92.0	90.9	78.3	81.9	998.9
Slovakia	91.2	81.1	60.1	51.8	80.6	88.5	81.5	49.2	55.7	89.9	89.7	81.7	82.7	983.7
Hungary	92.3	79.0	62.8	56.2	78.0	85.9	81.0	46.6	50.0	89.2	87.4	77.9	78.3	964.6
Romania	86.8	78.2	54.5	47.0	72.9	85.8	85.0	40.0	50.0	86.5	84.2	82.9	76.9	930.7
Croatia	89.0	75.1	56.4	42.3	73.7	86.2	75.9	42.2	53.4	89.7	88.3	78.4	78.9	929.5
Greece	91.2	76.0	55.7	43.1	60.9	80.1	73.0	43.6	56.8	91.2	92.5	76.1	80.0	920.1
Bulgaria	86.8	78.8	60.5	36.6	72.5	84.3	85.6	42.5	50.0	85.3	86.1	68.7	76.3	914.0
Serbia	85.7	73.9	51.9	34.8	60.9	88.6	80.5	33.4	43.2	84.2	81.5	79.0	74.1	871.7

Note: dark colour – 5 countries with the highest index value, light colour – 5 countries with the lowest index value; KGI - KOF Globalisation Index, CGI - Global Competitiveness Index*, GII - Global Innovation Index, GEI - Global Entrepreneurship Index*, IDI - Inclusive Development Index**, EDB - Easy Doing Business, IEF - Index of Economic Freedom, DPE - Digital Platform Economy Index, CPI - Corruption Perception Index, HDI - Human Development Index, SPI - Social Progress Index, GHI - Gross Happiness Index, LPI - Legatum Prosperity Index; * - data available for 2019; ** - data available for 2018.

Source: Author's calculations based on the data of 13 selected global indexes (KOF Globalisation Index, 2020; Schwab, 2019; Dutta et al., 2020; Ács et al., 2019; Inclusive Development Index, 2018; World Bank, 2020; Miller et al., 2020; Ács et al., 2020; Corruption Perception Index, 2020; Human Development Report, 2020; Green et al., 2020; Helliwell et al., 2022; Legatum Prosperity Index, 2020)

always in the first "five" or in the TOP group of the best assessed countries. Other highly evaluated countries were the Scandinavian countries and the Netherlands. Denmark (1247.5 p.) was placed in the TOP group 11-times and Sweden (1238.9 p.) as many as 12-times. High positions were also reached by the Netherlands (1231.4 p., 8-times in TOP), Finland (1214.2 p., 6-times in TOP) and Norway (1196.5 p., 8-times in TOP).

Another group consisted of the countries of Western Europe (Germany, Ireland, Austria, Belgium and France), whose assessment of socioeconomic status reached 1100 points and more. Germany (1184.0 p.) appeared twice in the "five" of the best countries in indexes GCI, HDI, Ireland (1175.0 p.) was in TOP 3-times (GEI, IEF, HDI) and Belgium (1131.3 p.) once (KGI).

The next group (with socioeconomic status from 1000 to 1100 p.) was noticeably hybrid. It consisted not only of countries of Southern Europe, such as Spain (1054.4 p.), Portugal (1018.8 p.) and Italy (1007.4 p.), but also of the best assessed countries of the former Eastern Bloc – Czechia (1053.0 p.), Slovenia (1027.6 p.) and Lithuania (1024.3 p.) which was the only one of the countries in this group to reach the TOP group twice (EDB, IEF).

The weakest group (up to 1000 p.) was almost exclusively formed by former socialist countries. The best evaluated country was Poland (998.9 p.) followed by the other V4 countries (Slovakia – 983.7 p., Hungary – 964.6 p.), while the weakest ones were Bulgaria (914.0 p.) and Serbia (871.7 p.) which were in almost all indexes among the last five countries.

The only country in this group not part of the Socialist Bloc was Greece. It achieved only 920.1 p. and ended up in 23rd place.

In the last part we focused on the research of the dependence between the level of intracountry regional inequalities in the particular countries (expressed by CV and GI) and their socioeconomic status. The input values when calculating CV and GI were GDP data and information on the household income expressed in PPS for the EU countries. Since the values of the socioeconomic status of a country were calculated for the whole territory of the country, it was not possible to establish the dependence between the above-mentioned indicators with exclusion of the capitals.

When monitoring the correlation dependence between regional inequalities (calculated from GDP data) and socioeconomic status, strong negative correlation dependence was confirmed (R= -0.62 for CV calculated from GDP data for 25 EU countries) (Fig. 5). The best course of the dependence was represented by Sweden, France, and Poland. A remote value was achieved by Ireland. A similar situation happened when calculating the intensity of dependence between inequalities expressed by GI (Fig. 6). Also, in this case the hypothesis that higher socioeconomic status causes decreased value of regional inequalities (R= -0.58) was confirmed. The determination index was from 33% (in GI) to 35% (in CV). The abovementioned reveals that the change of an independent variable - in this case the level of socioeconomic status – influences the change of a dependent variable (inequalities) by more than 30%. The suitability of

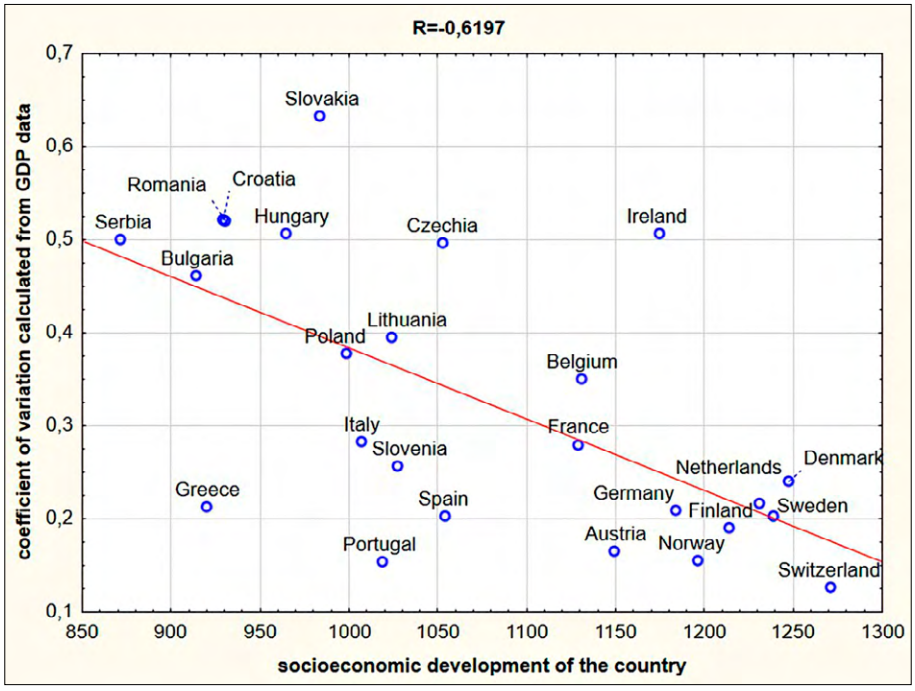

Figure 5. The degree of dependence between socioeconomic status and intracountry regional inequalities expressed by GDP per capita in PPS (coefficient of variation)

Source: Author's calculations based on the Eurostat data

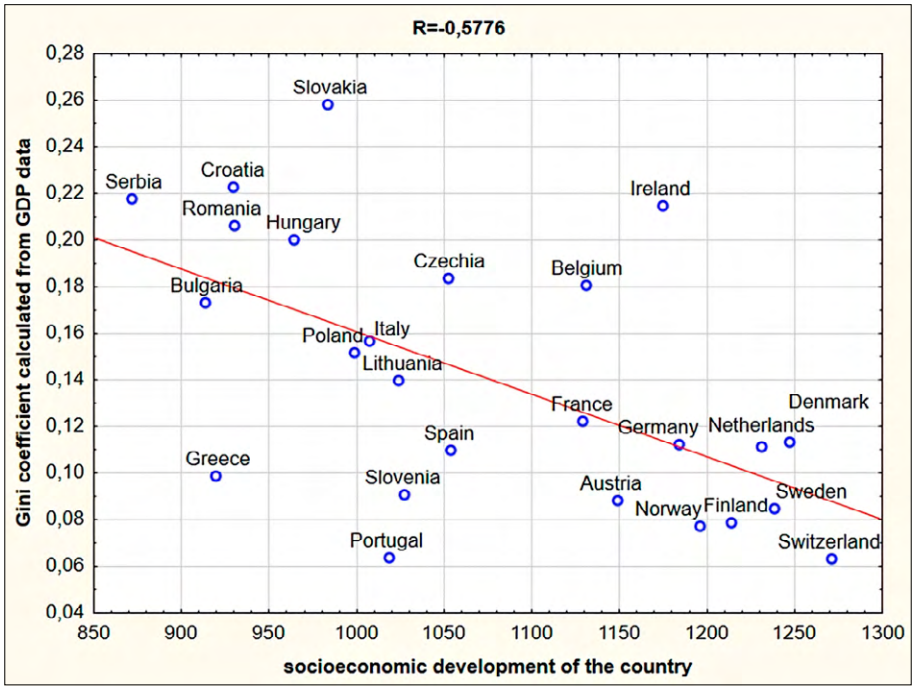

Figure 6 . The degree of dependence between socioeconomic status and intracountry regional inequalities expressed by GDP per capita in PPS (Gini coefficient)

Source: Author's calculations based on the Eurostat data

the linear regression model was confirmed in both inequalities expressed by CV and inequalities calculated by GI. The course of linear dependence for inequalities expressed using GI was best presented in the case of Germany and Italy. A remote value was again achieved by Ireland.

An efficient indicator to analyse inequalities also proved to be the differences in Income of Household per capita in individual countries expressed by Purchasing Power Standards. Since data for Serbia and Switzerland were not available for the year concerned, only 23 countries have been an-

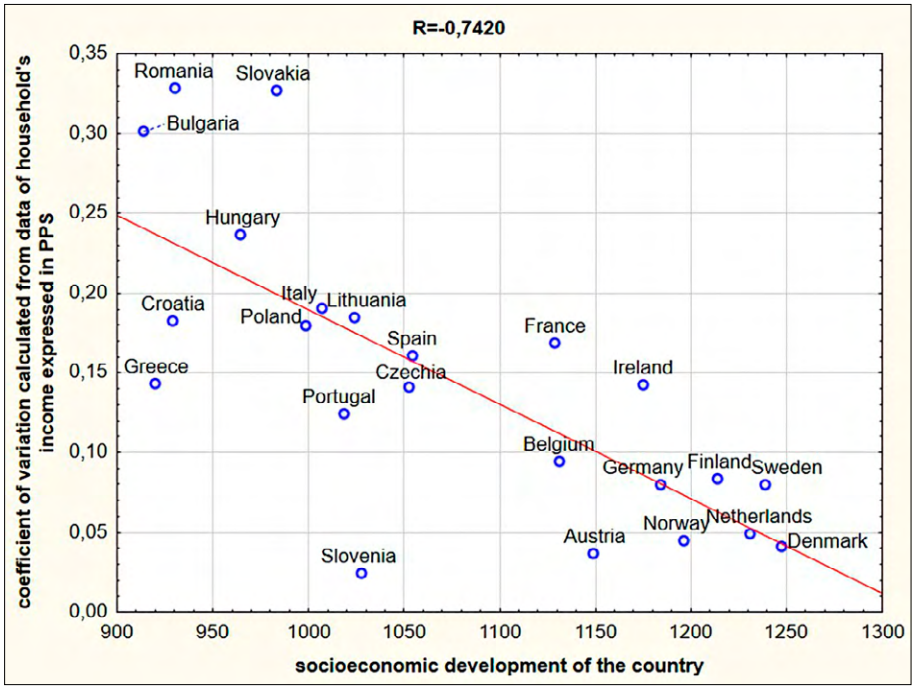

Figure 7. The degree of dependence between socioeconomic status and intracountry regional inequalities expressed by Income of Household per capita in PPS (coefficient of variation)

Source: Author's calculations based on the Eurostat data

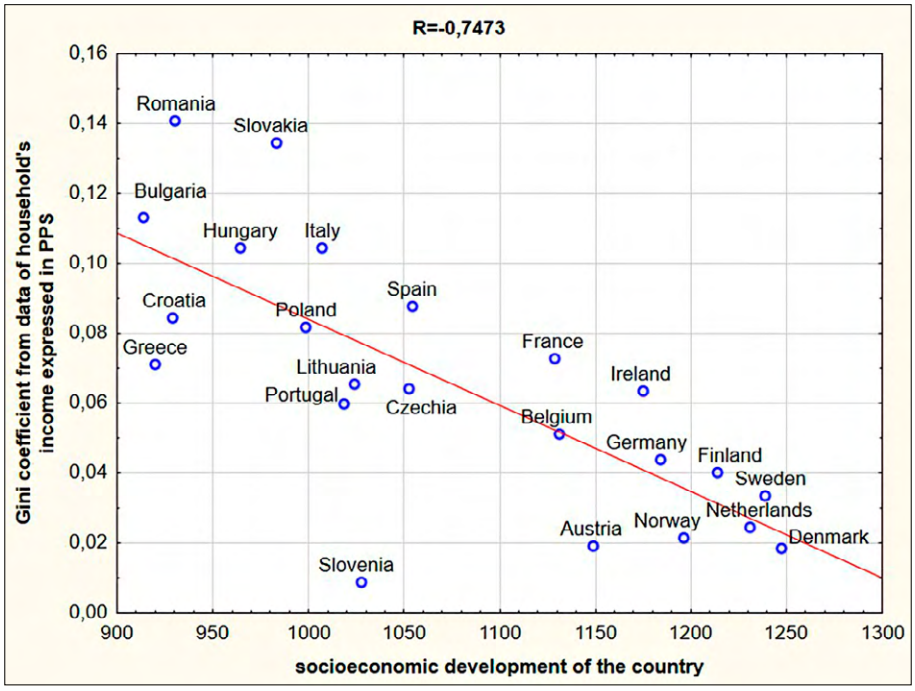

Figure 8. The degree of dependence between socioeconomic status and intracountry regional inequalities expressed by Income of Household per capita in PPS (Gini coefficient)

Source: Author's calculations based on the Eurostat data

alysed. The results of the correlation analysis confirmed even stronger correlation dependence than in the case of CV and GI calculated from GDP data (R= -0.74 for CV, R= -0.75 for GI, Fig. 7, 8). The hypothesis that a growth of socioeconomic status causes a decrease in regional inequalities was repeatedly confirmed. The graph of dependency between the socioeconomic status of a country and inequalities expressed by CV shows Slovenia and Slovakia as remote cases. Slovenia was the only country which showed dependency between socioeconomic status and inequalities expressed by GI. A suitability of the linear regression model was confirmed in disparities expressed by both, CV and GI. The determination index pointed to a distinctive influence of change in incomes on the change of regional inequalities (R^2=0.53 in the case of dependence between socioeconomic status and regional inequalities expressed by CV and R2= 0.54 in the case of dependence between socioeconomic status and regional inequalities expressed by GI).

Discussion

The assessment of regional inequalities within selected countries of Europe shows that the highest degree of regional differences was observed in the countries of the former Eastern Bloc (Fig. 1, 2). Rácz & Egyed (2023) also pointed out the following: they claim that the slow catching-up of Central and Eastern European countries with the EU average is evident at the national level (similarly Gianini & Martini, 2024), however, integration has resulted in fragmentation and increased heterogeneity at the subnational level. Also Scutariu (2017) states that the regional disparities in the Central and Eastern European countries are still quite high. Similar results are reported by Leško (2025), according to whom significant regional disparities persist among EU countries with the least developed areas located in Southern, Central and Eastern Europe.

The results of our research confirm that in the case of both monitored indicators, Slovakia, Hungary and Romania had the highest regional inequalities; in the case of GDP they were joined by Croatia, Serbia and in the case of Income by Bulgaria. Also, in the case of other former socialist countries such as Poland, Lithuania, and Czechia we recorded a relatively high level of regional inequalities. Based on the obtained results it is possible to declare that hypothesis H1 has been fully confirmed. Regional data on GDP per capita in the former socialist countries prove that the intensity of real convergence markedly differs in the regions (Tvrdoň & Skokan, 2011). With respect to the V4 countries, the named authors have proved that the existing regional inequalities increased after the admission of the new EU members, the main cause deemed to be the uneven pace of their economic development. In Belgrade

and Novi Sad further factors were the digital economy, opening scientific parks, financing start-ups and ineffective regional policy of subsidies for less developed regions (Uvalić & Bartlett, 2021), a finding already confirmed by Živanović & Gatarić (2017) in the sense that the level of development from north to south significantly decreases.

The above trend of growing regional inequalities is also confirmed by the research of Török (2019), from which it is evident that the economic development of Romania, conditioned by the admission to the EU (January 2007) and inflow of foreign investments, was accompanied by increasing polarisation. It showed that regional differences between Romanian counties intensified during the monitored period 1998-2015. While in 1998 the differences between the best (Bucharest) and the worst (Vaslui) assessed county according to GDP per capita and a share in the national average were threefold, by 2015 they were almost twice that amount. Concerning Hungary, significant regional inequalities were confirmed by Kebza et al. (2015). As for Slovakia, Rusnák et al. (2023) identified within the meaning of the Kuznets-Williamson´s inverted U-curve hypothesis growing inequalities in 1997-2008 with a significant spatial pattern of the east-west gradient; in 2012-2016 the previous phase continued after the outer shock caused by the economic crisis with selective dynamics in the regions successfully adapting and growing, while the last period 2016-2021 was accompanied by decreased inequalities.

Overall, growth in Central and East European countries is, territorially, significantly unbalanced, more so than in most other parts of the European Union. This polarised economic and territorial development within Central and East European countries poses challenges not only for the respective countries, but also for European cohesion (Smętkowski, 2013).

Similarly, when evaluating the impact of capital cities on intracountry regional inequalities (therefore on their drop too) hypothesis H2 has been confirmed, while only in one case, GDP in Ireland did we record a more significant increase in regional inequalities after excluding Dublin. The detailed assessment of the impact of the capitals (Fig. 3, 4) shows a drop of regional inequalities most visibly in Bulgaria and Slovakia, where the drop in both monitored indicators was as much as by 80% and more. Other former socialist countries also recorded a significant drop in inequalities, regarding GDP in Czechia (by more than 70%), Hungary, Romania, Croatia (by more than 60%) and Serbia by more than 50%. As for Income, the decrease in inequalities was slightly lower – from 50% and higher (Romania, Hungary, Czechia, and Croatia). As for the rest of the European countries, only Scandinavian countries (Finland, Sweden) and Portugal recorded a higher decrease in GDP and Sweden and Denmark in Income. It is evident from the above facts that mainly after excluding the former socialist metropolises Sofia, Bratislava, Prague, Budapest, Bucharest and Zagreb, the inequalities dropped most notably and so it is possible to state that hypothesis H3 has been confirmed to a large extent. The results for the strong influence of capitals on regional inequalities confirmed the conclusions reached in papers by Smętkowski (2014), Marošević & Sekur (2018), Matlovič et al. (2018), Klamár et al. (2020), Neszmélyi et al. (2022), etc. Szörfi (2007) mentioned the strong impact of metropolises in the countries of Central Europe, where a great difference can be seen between the capital and the rest of the country. While in the central part of Hungary the GDP level per capita was slightly above the EU average, in the poorest regions it was just a little more than 40%. Noticeable differences can be also seen in Slovakia, notably between the Bratislava region and the poorest Prešov region that was, according to numbers, three times poorer. In his opinion, it was also evident that the countries of Western Europe are more balanced in this way, a statement which has also been confirmed by our evaluation. The strong position of Prague and Bratislava as capital cities in terms of income per capita according to purchasing power was also pointed out by Reinl et al. (2023).

As the final step, we evaluated the connection between the established level of intracountry regional inequalities in the selected countries of Europe and their socioeconomic status. Within both evaluated indicators we have found medium strong or strong dependence, but in the case of GDP the Pearson correlation coefficient was -0.62 for CV and -0.58 for GI and in the case of Income as much as -0.74 for CV and -0.75 for GI. The negative values of the correlation coefficient show negative dependence which means that the growth of socioeconomic status decreases the level of their national regional inequalities which confirms the last H4 hypothesis. The connection between the level of regional inequalities and socioeconomic status was highlighted by Klamár et al. (2020) when assessing the V4 countries (Czechia, Poland, Hungary, Slovakia), Croatia and Serbia as well as by Neszmélyi et al. (2016), whose analyses confirmed that internal regional inequalities were higher in countries with lower GDP than in countries with higher GDP.

Ezcurra (2019) also confirms that within-country inequality is an important component of overall inequality across European regions with regional inequality having increased in most EU countries throughout the study period. Advances in national GDP per capita initially increase regional inequality, but beyond a certain threshold the link turns from positive to negative, with richer countries tending to experience lower levels of regional inequality. Fulterer & Lungu (2018) also state that the research results generally point to convergence at the country level but to increasing divergences between regions within countries.

Conclusion

The implemented analyses and assessments validated a notable socioeconomic differentiation of Europe in the form of highly developed regions in its northern and western part and, by contrast, the slower development of a considerable part of Southern Europe as well, notably, as the countries of the former Eastern Bloc. Duran et al. (2025), based on earlier work by Ertur & Koch (2006), state that regional disparities in the EU-15 were characterised by a persistent North-South direction (with a core comprising regions of the United Kingdom, France and Germany), while after the accession of the Central and Eastern European regions spatial orientation of disparities changed, creating a new North-West/East polarisation.

Socioeconomic maturity as an aggregate indicator based on a set of 13 global indexes confirmed this spatial polarisation, while pointing to the under-development of most of the former socialist countries. These countries mostly presented the highest level of domestic regional disparities (assessed using GDP and Income) with the regions of their capitals dominant. This was demonstrated by the most distinctive drop of regional disparities in all assessed European countries after excluding their capitals from the assessment. To conclude, it is possible to say that, to a large extent, the presumption has been confirmed that with decreasing socioeconomic maturity, the level of their domestic regional disparities has grown. Hopefully, there will be no more intensification of regional disparities within the countries in the period to come (mainly in the former socialist ones), as well as between the European countries themselves and the fear brought to our attention by Fifeková et al. (2021) that converging countries would not be able to narrow the performance gap in respect of the EU average, will not come true.

A positive finding in this regard at least is one of the conclusions of the study by Duran et al. (2025), which suggests that the spatial poles of prosperity are likely to change in the future. It is expected that most regions of Southern Europe will continue to lag behind, while many Eastern European regions will experience an increase in prosperity. Regions of Northern and Central Europe are likely to maintain their prosperous position.

References

Ács, Z. J., Szerb, L., Lafuente, E., & Márkus, G. (2019). *Global Entrepreneurship Index 2019.* The Global Entrepreneurship and Development Institute. https://thegedi.org/wp-content/uploads/2021/02/2019_GEI-2019_final_v2.pdf

Ács, Z. J., Szerb, L., Song, A., Komlósi, E., & Lafuente, E. (2020). *The Digital Platform Economy Index 2020.* The Global Entrepreneurship and Development Institute. https://thegedi.org/wp-content/uploads/2020/12/DPE-2020-Report-Final.pdf

Adler Braun, A. (2009). *Gross national happiness in Bhutan: A living example of an alternative approach to progress* (Wharton International Research Experience report). University of Pennsylvania.

Ancuţa, C. (2012). Aspects regarding the socio-economic indicators used in approaching the territorial disparities. *Geographica Pannonica*, 16(1), 26-34. https://doi.org/10.5937/GeoPan1201026A

Antonescu, D., & Florescu, I. C. (2023). *Spatial patterns of regional inequalities in the European Union in pandemic time: Empirical evidence from NUTS 2 regions* (MPRA Paper No. 120224). Munich Personal RePEc Archive. https://mpra.ub.uni-muenchen.de/120224/

Arestis, P. & Phelps, P. (2019). A Panel Analysis of Brazilian Regional Inequality. *Environment and Planning* A, 51(7), 1558-1585. https://doi.org.10.1177/0308518X19842584

Balakrishnan, R., Rabier, L., Ebeke, C. H., Firat, M., & Malacrino, D. (2022). *Regional disparities in Europe* (IMF Working Paper No. 22/198). International Monetary Fund. https://www.imf.org/en/Publications/WP/Issues/2022/09/23/Regional-Disparities-in-Europe-523252

Bareith, T. & Csizmadia, A. (2025). Are the determinants of per capita incomes spatially homogeneous? *Post – Communist Economies*, 1-16, https://doi.org/10.1080/14631377.2025.2487237

Belinska, S., Adamičková, I., Turčeková, N., Buliková, M. & Bieli, P. (2020). Regional disparities in the European Union from the perspective of environmental context indicators. *Visegrad Journal on Bioeconomy and Sustainable Development*, 9(2), 33-38. https://doi.org/10.2478/vjbsd-2020-0007

Blažek, J. & Csank, P. (2007). Nová fáze regionálního rozvoje v ČR? [A New Phase of Regional Development in the Czech Republic?]. *Sociologický časopis/Czech Sociological Review*, 43(5), 945-965. https://nbn-resolving.org/urn:nbn:de:0168-ssoar-53574 (in Czech)

Boldrin, M. & Canova, F. (2001). Inequality and Convergence in Europe's Regions: Reconsidering European Regional Policies. *Economic Policy*, 16(32), 205-253. https://doi.org/10.1111/1468-0327.00074

Borowski, J., Fidrmuc, J. & Jaworski, K. (2025). Convergence, inequality and inflation synchronization: Ev-

idence from the Eurozone. *Empirica*. https://doi.org/10.1007/s10663-025-09646-2

Boschma, R. (2022). Regional Diversification and Inequality between and within Regions. *EconPol Forum*, 5(23), 29-32. https://hdl.handle.net/10419/272130

Boschma, R., Pardy, M. & Petralia, S. (2023). Innovation, industrial dynamics and regional inequalities. *Economics 2023*, 151-164. https://doi.org/10.4337/9781800379091.00018

Buček, M., Rehák, Š., & Tvrdoň, J. (2010). *Regionálna ekonómia a politika* [*Regional economy and politics*]. Wolters Kluwer: Iura Edition. (in Slovak)

Capello, R. & Cerisola, S. (2023). Industrial transformations and regional inequalities in Europe. *The Annals of Regional Science*, 70, 15-28. https://doi.org/10.1007/s00168-021-01097-4

Görvers, F. & Mayhew, K. (2021). Regional inequalities: causes and cures. *Oxford Review of Economic Policy*, 37(1), 1-16. https://doi.org/10.1093/oxrep/graa067

Czyż, T. & Hauke, J. (2011). Evolution of regional disparities in Poland. *Quaestiones Geographicae*, 30(2), 35-48. 10.2478/v10117-011-0016-y

Dauderstädt, M. (2021). Cohesive Growth in Europe: A Tale of Two Peripheries. *Intereconomics: Review of European Economic Policy*, 56(2), 120-126. https://doi.org/10.1007/s10272-021-0964-y

Duran, H.E., Elburz, Z. & Çifçi, B.D. (2025). The Future of European Regional Inequalities: Box-Cox Transformed ARMA Process Trend Smoothing (BATS) Forecasting. *Growth and Change*, 56(2), e70031. 10.1111/grow.70031

Dutta, S., Lanvin, B., & Wunsch-Vincent, S. (Eds.). (2020). *Global Innovation Index 2020* (13th ed.). World Intellectual Property Organization. https://www.wipo.int/global_innovation_index/en/2020/

Eeckhout, J., R. Pinheiro, R. & Schmidheiny, K. (2014). Spatial Sorting. *Journal of Political Economy*, 122(3), 554-562. https://doi.org/10.1086/676141

Egri, Z. & Lengyel, I. (2024). Convergence and Catch-Up of the Region Types in the Central and Eastern European Countries. *Applied Spatial Analysis and Policy*, 17, 393-415, https://doi.org/10.1007/s12061-023-09551-w

Ertur, C. & Koch, W. (2006). Regional Disparities in the European Union and the Enlargement Process: An Exploratory Spatial Data Analysis, 1995–2000. *Annals of Regional Science*, 40(4), 723-765. https://doi.org/10.1007/s00168-006-0062-x

Ezcurra, R. (2019). Regional disparities and within-country inequality in the European Union. *Revista de economía mundial*, 51, 139-162.

Felsenstein, D., & Portnov, B. A. (Eds.). (2005). *Regional disparities in small countries*. Springer.

Fifeková, E., Nežinský, E., & Nemcová, E. (2021). Disparities in EU regions: First take. In *Proceedings of the International Scientific Conference Economic and Social Policy* (pp. 103–115). Ostrava: Vysoká škola PRIGO. https://www.narodacek.cz/wp-content/uploads/2022/01/66665v_Proceedings-of-the-International-Scientific_-Conference_202180-2-115-127.pdf

Fulterer, R., & Lungu, I. (2018). The speeds of Europe – An analysis of regional disparities across the EU. *EconStor Open Access Articles and Book Chapters*, ZBW – Leibniz Information Centre for Economics, 169–190.

Gianini, M., Martini, B. (2024). Regional disparities in the European Union. A machine learning approach. *Papers in Regional Science*, 103(4), 100033. https://doi.org/10.1016/j.pirs.2024.100033

Green, M., Harmacek, J., & Krylova, P. (2020). *2020 Social Progress Index: Executive summary* (17 pp.). Social Progress Imperative. https://www.socialprogress.org/static/37348b3ecb088518a945fa4c83d9b9f4/2020-social-progress-index-executive-summary.pdf

Gurgul, H. & Lach, Ł. (2011). The impact of regional disparities on economic growth. *Operations Research and Decisions*, 22(2), 37-63.

Hamada, R. (2016). Selected process and methods measurement and evaluation of regional disparities. *Regionální rozvoj mezi teorií a praxí*, 1. http://www.regionalnirozvoj.eu/201401/vybrane-sposoby-metody-merania-hodnotenia-regionalnych-disparit

Helliwell, J. F., Layard, R., Sachs, J. D., De Neve, J. E., Aknin, L. B., & Wang, S. (Eds.). (2022). *World Happiness Report 2022* (155 pp.). Sustainable Development Solutions Network. https://worldhappiness.report/ed/2022/

Iammarino, S., Rodriguez-Pose, A. & Storper, M. (2019). Regional inequality in Europe: evidence, theory and policy implications. *Journal of Economic Geography*, 19(2), 273-298. https://doi.org/10.1093/jeg/lby021

Ivanička, K., Barič, O., Filo, M., Gašparíková, J., Ivanička, K., Kadlečíková, M., Kapsdorferová, Z., Korček, Ľ., Matúšová, S., Mongiello, A., Ninášová, V., Strážovská, Ľ., Viestová, K., & Volner, Š. (2014). *Trvalá udržateľnosť inovácií v rozvoji Slovenska* [Sustainability of innovations in the development of Slovakia]. Wolters Kluwer. (in Slovak)

Kallioras, D. (2010). Regional inequalities in the new member European Union member-states: Is there a "population size" effect? *European Spatial Research and Policy*, 17(2), 107-116. https://doi.org.10.2478/s10105-010-0013-5

Källström, J. (2012). *An empirical study of regional convergence, inequality and spatial dependence in the enlarged European Union* (Bachelor's thesis, Lund University, NEKN01, 58 pp.). Lund University.

Kanó, I.S., Vas, Z., Lengyel, I., Sávai., M. & Vida, G. (2025). Spatial Disparities in Economic Structural Change in Central and Eastern Europe During Integration. *Intereconomics*, 60(2), 126-134. https://www.intereconomics.eu/contents/year/2025/number/2/article/spatial-disparities-in-economic-structur-

al-change-in-central-and-eastern-europe-during-integration.html

Kebza, M., Kubeš, J., & Nováček, A. (2015). Východo-západní gradient sociální a ekonomické prostorové diferenciace Maďarska [East-west gradient of social and economic space differentiation in Hungary]. In V. Klímová & V. Žítek (Eds.), *Proceedings of the 18th International Colloquium on Regional Sciences* (pp. 41–48). Masaryk University. https://doi.org/10.5817/CZ.MUNI.P210-7861-2015-4 (in Czech)

Kisiała, W., & Suszyńska, K. (2017). *The dynamics of regional inequalities and economic growth in Central and Eastern Europe* (Institute of Economic Research Working Papers No. 122, 10 pp.). Institute of Economic Research.

Klamár, R. (2016). Development tendencies of regional disparities in the Slovak Republic. *Geographica Pannonica*, 20(3), 127-135. https://doi.org/10.18421/GP20.03-02

Klamár, R., Kozoň, J. & Ivanová, M. (2020). Regional inequalities in the Visegrad group countries, Serbia and Croatia. *Geographica Pannonica*, 24(3), 187-204. https://doi.org/10.5937/gp24-26038

Klamár, R., Matlovič, R., Ivanová, M., Ištok, R. & Kozoň, J. (2019). Local Action Group as a Tool of Inter-municipal Cooperation: Case Study of Slovakia. *Folia Geographica*, 61(1), 36-67.

KOF Swiss Economic Institute. (2020). *KOF Globalisation Index*. https://kof.ethz.ch/en/forecasts-and-indicators/indicators/kof-globalisation-index.html

Kutscherauer, A., Fachinelli, H., Hučka, M., Skokan, K., Sucháček, J., Tománek, P., & Tuleja, P. (2010). *Regional disparities: Disparities in country regional development – Concept, theory, identification and assessment*. VŠB – Technical University of Ostrava. http://disparity.vsb.cz/edice_cd/cd11_regdis_mono_angl/pdf/Regional%20disparities.pdf

Laurent, É. (2017). *Measuring tomorrow: Accounting for well-being, resilience, and sustainability in the twenty-first century*. Princeton University Press.

Legatum Institute. (2020). *Legatum Prosperity Index 2020: Prosperity in lockdown*. https://knoema.com/infographics/gxumfad/legatum-prosperity-index-2020-prosperity-in-lockdown

Leško, P. (2025). European Regional Disparities and Application of EU Cohesion Policy - The Case of Slovakia. *Athens Journal of Business & Economics*, 11, 1-15 https://doi.org/10.30958/ajbe.X-Y-Z

Maggino, F. (Ed.). (2023). *Encyclopedia of quality of life and well-being research*. Springer. https://doi.org/10.1007/978-3-031-17299-1

Marošević, K., & Sekur, T. (2018). Comparative analysis of Croatian and Czech lagging regions. *European Scientific Journal, Special Edition*, 63–74. https://doi.org/10.19044/esj.2018.c4p5

Matlovič, R., Klamár, R., Kozoň, J., Ivanová, M. & Michalko, M. (2018). Spatial polarity and spatial polarization in the context of supranational and national scales: regions of Visegrad countries after their accession to the EU. *Bulletin of geography: Socio-economic series*, 41(3), 59-78. http://doi.org/10.2478/bog-2018-0026

Matlovič, R., & Matlovičová, K. (2011). Regionálne disparity a ich riešenie na Slovensku v rozličných kontextoch [Regional disparities and their solution in Slovakia in the various contexts]. *Folia Geographica*, 18, 8–88. (*in Slovak*)

Meliciani, V. (2016). *Regional disparities in the enlarged European Union: Geography, innovation and structural change*. Routledge.

Michálek, A. (2013). Indikátory identifikácie a merania regionálnych disparít: niekoľko poznámok k výberu indikátorov [Identification and measurement indicators of regional disparities: Some remarks on selection of indicators]. *Geografický časopis*, 65(4), 363–381. (*in Slovak*)

Miller, T., Kim, A. B., Roberts, J. M., & Tyrrell, P. (2020). *Highlights of the 2020 Index of Economic Freedom* (17 pp.). The Heritage Foundation. https://www.heritage.org/index/pdf/2020/book/2020_IndexofEconomicFreedom_Highlights.pdf

Moretti, E. (2010). Local Multipliers. *American Economic Review*, 100(2), 373-377. https://doi.org.10.1257/aer.100.2.373

Neszmélyi, G.I., Akócsi, I.L. & Bruder, E. (2016). The evolution of the regional disparities in the Visegrad group in the years 1995 – 2014. *Geografický časopis*, 68(4), 283-299.

Neszmélyi, G.I., Vinogradov, S. & Nagy, H. (2022). Regional inequalities within the Visegrad Group over the years 2000-2018. *European Spatial Research and Policy*, 29(1), 5-24. https://doi.org/10.18778/1231-1952.29.1.01

Paas, T., & Schlitte, F. (2007). *Regional income inequality and convergence processes in the EU-25* (HWWI Research Paper, 29 pp.). Hamburg Institute of International Economics.

Panzera, D. & Postiglione, P. (2021). The impact of regional inequality on economic growth: a spatial econometric approach. *Regional Studies*, 56(5), 687-702, https://doi.org/10.1080/00343404.2021.1910228

Psycharis, Y., Kalioras, D., & Pantazis, P. (2020). Regional inequalities in Central and Eastern European countries: The role of capital regions and metropolitan areas. In A. Śliwiński, P. Polychronidou, & A. Karasavvoglou (Eds.), *Economic development and financial markets* (pp. 3–20). https://doi.org/10.1007/978-3-030-32426-1_1

Rácz, S. & Egyed, I. (2023). From the "West of the East" to the "East of the West": The post-socialist economic and structural transition of Central and South-Eastern Europe. *Deturope*, 15(2), 9-27. https://doi.org.10.32725/det.2023.010

Rauhut, D., & Humer, A. (2024). Regional inequalities. In M. Lundahl, D. Rauhut, & N. Hatti (Eds.), *Inequality: Economic and social issues*. Routledge.

Reinl, A.K., Nicoli, F. & Kuhn, T. (2023). Regional inequalities and transnational solidarity in the European Union. *Political Geography*, 104, 102903. https://doi.org/10.1016/j.polgeo.2023.102903

Rusnák, J., Korec, P. & Plešivčák, M. (2023). The trade-off between national growth and interregional inequality: Three decades of regional development in Slovakia. *Geografický časopis*, 75(3), 291-311. https://doi.org/10.31577/geogrcas.2023.75.3.15

Savoia, F. (2024). Income inequality convergence among EU regions. *Socio-Economic Planning Sciences*, 92, 101803, https://doi.org/10.1016/j.seps.2024.101803

Schwab, K. (Ed.). (2019). *Global competitiveness report 2019*. World Economic Forum. https://www.weforum.org/reports/how-to-end-a-decade-of-lost-productivity-growth

Scutariu, A. L. (2017). The evolution of regional disparities in the Central and Eastern European countries of European Union. In C. Ignatescu, A. Sandu, & T. Ciulei (Eds.), *Rethinking social action. Core values in practice* (pp. 795–807). LUMEN Proceedings. https://doi.org/10.18662/lumproc.rsacvp2017.73

Smętkowski, M. (2013). Regional Disparities in Central and Eastern European Countries: Trends, Drivers and Prospects. *Europe-Asia Studies*, 65(8), 1529-1554. https://doi.org/10.1080/09668136.2013.833038

Smętkowski, M. (2014). Regional disparities and development dynamics of CEE regions in the period of prosperity and austerity. *Working Paper Series GRINCOH*, (6), 1–19.

Smętkowski, M. & Wójcik, P. (2012). Regional Convergence in Central and eastern European Countries: A Multidimensional Approach. *European Planning Studies*, 20(6), 923-939. https://doi.org/10.1080/09654313.2012.673560

Szörfi, B. (2007). Development and regional disparities – Testing the Williamson curve hypothesis in the European Union. *Focus on European Economic Integration*, 2, 100–121.

Török, I. (2019). Regional inequalities in Romania before and after the EU accession. *IOP Conference Series: Earth and Environmental Science*, 221, 1–8. https://doi.org/10.1088/1755-1315/221/1/012151

Transparency International. (2020). *Corruption Perceptions Index 2020*. Transparency International. https://www.transparency.org/en/cpi/2020

Tvrdoň, M. & Skokan, K. (2011). Regional disparities and the ways of their measurement: the case of the Visegrad four countries. *Technological and economic development of economy*, 17(3), 501-518. https://doi.org/10.3846/20294913.2011.603485

United Nations Development Programme. (2000). *Human development report 2000*. https://hdr.undp.org/content/human-development-report-2020

Uvalić, M., & Bartlett, W. (2021). *Regional disparities and regional development policies in Serbia*. Friedrich-Ebert-Stiftung.

Williamson, J.G. (1965). Regional Inequality and the Process of National Development: A Description of the Patterns. *Economic Development and Cultural Change*, 13(4), 3-45. https://doi.org/10.1086/450136

Wishlade, F., & Yuill, D. (1997). *Measuring disparities for area designation purposes: Issues for the European Union* (Regional and Industrial Policy Research Paper No. 24, 33 pp.). University of Strathclyde.

World Bank. (2020). *Doing business 2020: Comparing business regulation in 190 economies*. World Bank Group. https://documents1.worldbank.org/curated/en/688761571934946384/pdf/Doing-Business-2020-Comparing-Business-Regulation-in-190-Economies.pdf

World Economic Forum. (2018). *The Inclusive Development Index 2018: Summary and data highlights* (26 pp.). https://www3.weforum.org/docs/WEF_Forum_IncGrwth_2018.pdf

Živanović, Z. & Gatarić, D.R. (2017). Differences in regional development on the territory of the Republic of Serbia. *Bulletin of Geography: socio-economic series*, 35, 145-154. http://dx.doi.org/10.1515/bog-2017-0010

INTERNATIONAL SCIENTIFIC JOURNAL
GEOGRAPHICA PANNONICA
Volume 29, Issue 2, 137–148 (June 2025)
Journal homepage: http://www.dgt.uns.ac.rs/en/homepage/pannonica/

Seasonal Variations in Thermal Perception of Urban Environments: Summer and Winter In-situ Assessment from a Central European Town

Veronika Květoňová[A], Jiří Pánek[B], Miloslav Šerý[A], Michal Lehnert[A*]

[A] *Palacký University Olomouc, Faculty of Science, Department of Geography, Olomouc, Czech Republic; ORCID VK: 0000-0002-6391-6011; MŠ: 0000-0002-5805-2669; ML: 0000-0001-7691-1618*

[B] *Palacký University Olomouc, Faculty of Science, Department of Development and Environmental Studies, 17. listopadu 12, 771 46 Olomouc, Czech Republic; ORCID JP: 0000-0002-6390-3149*

KEYWORDS

- urban place
- thermal environment
- perception
- sketch mapping
- adaptation measures
- Czechia

ABSTRACT

Growing urbanisation, together with extreme weather events, negatively affects urban populations worldwide. Recent urban climate studies demonstrate that people-oriented approaches are needed to effectively target adaptation measures and thus improve urban populations' well-being. In this study we used the in-situ approach of sketch mapping to identify thermally pleasant and unpleasant places during two seasons, summer and winter, in Ústí nad Orlicí, a Czech town. Generally, places perceived as the most thermally unpleasant, regardless of season, are parking lots near shopping centres, and these require priority attention from urban planners. Respondents consistently identified the planting of high greenery and the construction of shelters as preferred adaptation measures across both seasons. Our findings also point to a clear preference for more enclosed places.

Introduction

Manifestations of climate change combined with accelerating urbanisation significantly impact both the physical and mental health and well-being of urban populations worldwide, and this requires urgent and effective solutions (IPCC, 2023). In the broader context of climate change, urban climate research is gaining increased attention (Nazarian et al., 2024). Traditionally, such studies have focused on analysing Urban Heat Islands (UHI) and Surface Urban Heat Islands (SUHI) respectively, as well as the numerical modelling of thermal exposure (Lehnert et al., 2023a). However, recent paradigm shifts in urban climate studies increasingly emphasise human-oriented approaches. Researchers nowadays advocate holistic and personalised approaches that consider how people experience diverse urban environments, with the aim of developing more effective adaptation and mitigation strategies that directly enhance urban dwellers' quality of life (Aucliems, 1981; Chen & Ng, 2012; Kuras et al., 2017; Schnell et al., 2021; Guzman-Echavarria et al., 2022). Within this holistic framework, local knowledge is essential for contextual understanding, and effective planning of climate adaptation measures demands site-specific analyses that take into account the unique geographic, geometric, and especially the microclimate characteristics of each (urban) neighbourhood or location (Lenzholzer & van der Wulp, 2010; Fagerholm et al., 2021; Lehnert et al., 2023a).

[*] Corresponding author:Michal Lehnert; m.lehnert@upol.cz

doi: 10.5937/gp29-59002

Received: May 21, 2025| Revised: June 23, 2025| Accepted: June 24, 2025

Both heat and cold extremes can negatively affect human health, leading to increased morbidity and mortality rates (Urban et al., 2014; Son et al., 2019; Masselot et al., 2025). Mortality and morbidity rates can particularly increase in urban environments with higher thermal exposure (Huang et al., 2022; Arsenović et al., 2019; 2024). Nevertheless, human thermal comfort is affected not only by thermal exposure (such as air temperature, radiation, humidity, and wind speed), but also by psychological, physiological, and social/behavioural aspects (Nikolopoulou & Steemers, 2003).

Thermal perception, which can never be separated from the overall perception of the environment (Knez et al., 2009; Lenzholzer, 2010), is of crucial importance in this context. People perceive places differently (Siwek, 2011), as Tuan (1974:45) notes, outward physical variations among individuals are striking yet relatively minor when compared to internal differences. Various environmental factors also influence individual thermal perception. From this perspective, it is essential to understand how the urban environment shapes thermal perception, as such knowledge is vital for designing thermally comfortable spaces that respond to human needs (Lenzholzer et al., 2018; Lai et al., 2020).

The urban environment is inherently structured into places. Place is one of the two or three fundamental geographical concepts that has long been studied; however, as Cresswell (2015) points out, this has often occurred with very little understanding of what the concept actually means. For the purposes of this paper, we draw on the conceptualisations of authors such as Tuan (1976) and Relph (1976), understanding place as something created through location, physical structure and, above all, individuals' relationships to these places. This approach allows places to be attributed with subjective dimensions, which may underlie attempts to answer questions concerning how people form relationships with places, their intentions and experiences within them, the meanings that places carry and, not least, the emotional bonds people develop with them.

The nature of emotional bonds between people and place is closely linked to two fundamental concepts: topophilia and topophobia. Topophilic places are those that evoke positive emotional responses and are therefore often understood as safe, pleasant, desirable, or well-liked (Tuan, 1974). The dichotomous counterpart to topophilic places are topophobic places—those associated with negative emotions (Ruan & Hogben, 2007). As a result of forming such negative attachments, people may perceive these places as unsafe, unpleasant, or repellent, and may deliberately avoid them. However, people do not necessarily form purely positive or purely negative emotional connections to specific places. It is evident that many places can elicit both types of emotional response. Beyond topophilia and topophobia, it is therefore useful to analytically distinguish topo-ambivalence—a situation in which a place is perceived simultaneously in both positive and negative terms. In the urban context, parks are frequently cited as examples of such ambivalent spaces (Daniel & Jirmus, 2023). Topophilic places may typically include urban greenery (Capineri et al., 2018), historical centres (Brisudová et al., 2020), and places featuring blue infrastructure (Völker & Kistemann, 2013; Doležal et al., 2024; Grzyb, 2024). In contrast, topophobic areas often encompass vacant and neglected urban places or buildings, high-traffic corridors or public transport hubs, areas of social disorder, and poorly lit alleys (Cucu et al., 2011; Brisudová et al., 2020; Šimáček et al., 2020; Doležal, 2022).

It should be noted that topophilia and topophobia are based on inherently subjective experiences shaped by cultural backgrounds and individual differences (Hashemnezhad et al., 2013). What one person finds appealing, another might perceive as threatening or uncomfortable. The same is also true specifically for thermal perception (Knez & Thorsson, et al. 2006; Květoňová et al., 2024). These perceptions are further modulated by temporal factors such as time of day (Lehnert et al., 2023a), seasonal variations (Lenzholzer & van der Wulp, 2010; Wei et al., 2022), prevailing weather conditions (Knez et al., 2009), culture (Aljawabra & Nikolopoulou, 2010), social dynamics, an individual's personal history and associations with similar environments (Knez, 2005), and the resulting thermal expectation (Nikolopoulou et al., 2001). Understanding these nuanced responses to urban spaces can significantly inform human-oriented approaches (not only) in urban planning (Brown et al., 2019).

Current research unfortunately does not adequately reflect the role that thermal (dis)comfort may play in shaping topophilia, topophobia, and topo-ambivalence. For this reason, the aim of this paper is to contribute new insights to the relationship between thermal (dis)comfort and urban places. Hence, the main objectives of this study are: i) to identify the seasonal variations in human perception of thermal comfort in urban environments based on in situ assessments of urban places during representative summer and winter days; ii) to explore and contextualise spatial aspects of urban places in which thermal (dis)comfort was perceived. By meeting these objectives, the study also contributes to a holistic understanding of the effect of urban environments on human thermal comfort and related cold and heat stress.

Data and methods

Study area

Ústí nad Orlicí is a town located in Eastern Bohemia, Czechia, situated in the Orlické Mountains foothills (49°58'N, 16°24'E) (Fig. 1). The town covers an area of approximately 36 km² (CZSO, 2017) and supports a population exceeding 14,000 inhabitants (CZSO, 2024), classifying it as a medium-sized town. This town serves as a district town and is characterised by regional importance, a functional typology classification as diversified, and the embodiment of characteristics typical of Czech settlements. For this study, the cadastre of Ústí nad Orlicí was selected.

The climate of Ústí nad Orlicí is classified as a temperate oceanic (Cfb), characterised by moderate summers and cold winters (Kottek et al., 2006). The elevation of the town centre ranges from 320 to 379 metres above sea level (ČÚZK, 2024). Located at the confluence of the Tichá Orlice and Třebovka Rivers, the town's topography and hydrological setting significantly influence its local climate. Historically, Ústí nad Orlicí served as an important agrarian centre before evolving into an industrial hub, earning the nickname "East Bohemian Manchester". Over recent decades, the town has undergone further transformation from its industrial heritage to become a contemporary administrative and service centre, featuring a distinctive blend of historical architecture and modern urban development. The surrounding landscape is characterised by rolling hills, forests, and agricultural lands, providing a scenic backdrop to the urban environment.

Methodology of this study and research methods used

This study employed participatory mapping as the primary research approach. The rationale behind this methodological approach lies in the feasibility and effectiveness of participatory mapping in gathering data related to research into residents' perceptions of urban environments and their local knowledge (see Šerý et al., 2025a). Apart from that, participatory approaches and community involvement are crucial for effective urban planning and the improvement of public urban environments. Implementing these approaches lays the foundation for more sustainable solutions. Participatory mapping encompasses three distinct approaches: Public Participation Geographic Information Systems (PPGIS), mental mapping, and sketch mapping (Brown & Kyttä, 2018; Denwood et al., 2022). For this investigation, we utilised sketch mapping, which involves data collection on paper with a base map. The re-

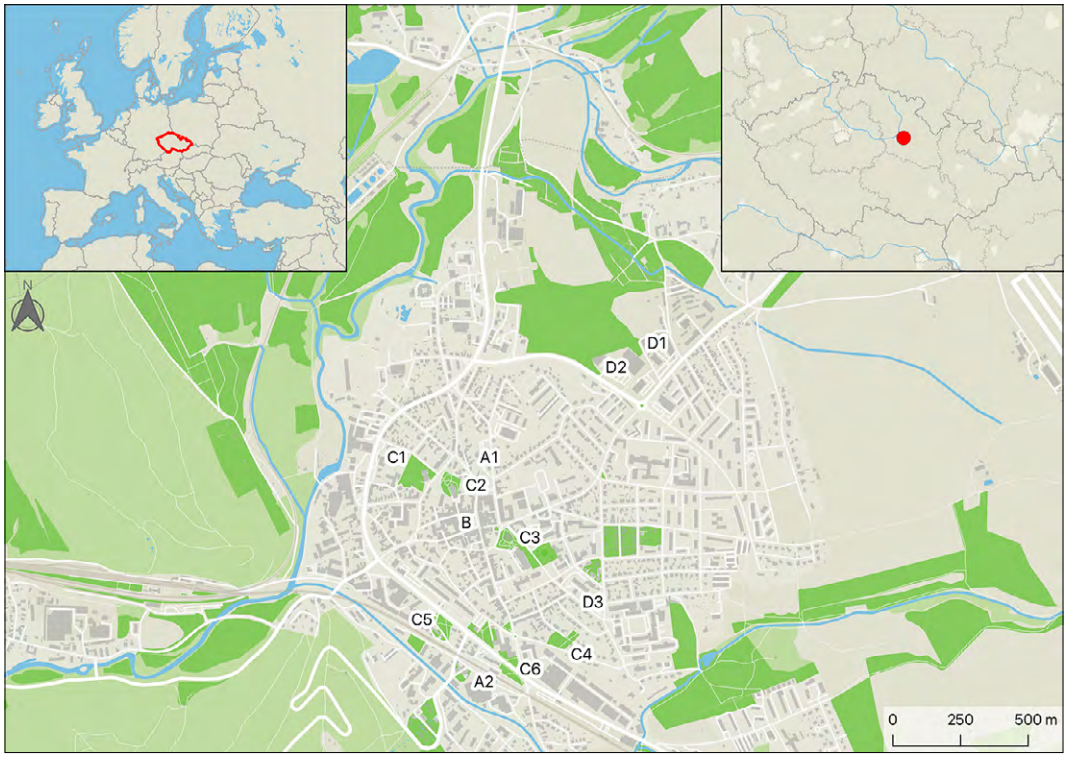

Figure 1. Location of the study area, map background: © MapTiler © OpenStreetMap contributors
A = public transport hubs; A1 = bus station, A2 = railway station
B = main square
C = parks; C1 = Park by the Theatre, C2 = Park by the Church, C3 = Kociánka Park, C4 = Czechoslovak Legions Park, C5 = Smetana Gardens, C6 = Park by the railway station
D = parking lots; D1 + D2 = Parking lots at the shopping zone, D3 = Parking lot near the hospital

search employed the *SketchMap Tool* developed at Heidelberg University (https://sketch-map-tool.heigit.org/). This tool integrates analogue data collection with digital processing via OpenStreetMap, allowing participant-marked sketch maps to be georeferenced automatically upon upload. The data can then be downloaded for use in GIS. The tool may be combined with questionnaires to provide contextual participant information and remains accessible to users with limited technical expertise due to its automated processes. As open-source software, it is particularly suitable for resource-constrained communities, though users must adhere to data protection regulations and ethical standards (Klonner & Norze, 2023).

The data collection took place in situ, allowing for real-time perception data while participants were physically present at locations ("here and now"). This method yields more precise data by capturing participants' spontaneous cognitive and emotional responses with minimal external influence. This contrasts with retrospective methods, where responses may be coloured by accumulated experiences, second-hand information, emotional states, or contextual variables at recall time (Brisudová et al., 2024).

Data collection

In this study, we performed three thermal walks with the same 10 participants (5 women and 5 men) aged between 18 and 28, all physically fit with no health issues, who were not residents but were familiar with the town as occasional visitors, ensuring they were not directly influenced by strong previous experiences with specific places. Thermal walks provide a method for pedestrians to analyse, identify, and perceive thermal conditions as they move through complex (urban) environments (Vasilikou & Nikolopoulou, 2013; Dzyuban et al., 2022; Květoňová et al., 2024). The first walk was conducted on 20 August 2023, a tropical day that was mostly cloudless and windless, with a mean daily air temperature of 22.9 °C and a maximum daily air temperature of 31.0 °C (according to the Ústí nad Orlicí station; WMO ID 11679). This thermal walk took place from 1:15 p.m. until 3:15 p.m., chosen as the time of the most extreme and simultaneously stable weather conditions. Before starting the walk, short-term thermal history was controlled with a half-hour acclimatisation period, during which respondents were acquainted with the methodology, which was adapted from Květoňová et al. (2024). The second and third thermal walks were held on 28 January 2024, a frost day that was mostly cloudless and almost windless, with an average daily temperature of -0.7 °C and a daily minimum of -3.0 °C (according to the Ústí nad Orlicí station; WMO ID 11679). Since research of this nature had not been previously conducted in winter, the authors organised two walks: one in the early morning (from 7:15 a.m.) when cold conditions are most extreme, and the second at the same time as the summer walk (from 1:15 p.m.). These thermal walks also lasted 2 hours, with the same acclimatisation procedure. For all walks, respondents were instructed to walk through the entire study area and visit several varied locations. No specific route was prescribed, enabling participants to explore the area according to their preferences, though they were specifically directed to visit key places, such as the main square, public transport hubs, parks, parking lots, main streets, etc. Research has shown that a two-hour duration is adequate to cover the study area comprehensively. Participants marked polygons on two maps – one for thermally unpleasant locations (in summer, "hot" locations marked in red; in winter, "cold" locations marked in blue) and another for thermally pleasant locations (in summer, "cool" locations marked in blue; in winter, "warm" locations marked in red). After each walk, an hour-long discussion was conducted with respondents about all the polygons they had marked, their reasons for selecting these locations, and the improvement measures they would suggest for each location.

Data processing and visualisation

Once the paper maps were collected, the SketchMap tool was used to automatically digitise the responses into a georeferenced vector layer. The polygons were then edited (topology check) in QGIS and converted into a hexagonal grid (10 m grid size) by calculating the number of overlapping polygons for each hexagonal cell. Isolines representing 50% overall agreement and the boundaries of all responses were created, simplified, and smoothed for final visualisation. The follow-up discussions with respondents were subjected to thematic analysis to identify key patterns in terms of thermal perception of the marked polygons, reasons for respondents' selection, and suggested measures.

Results

Winter thermal perception

At least half of the respondents identified several places which they perceived to be cold during winter, including both public transport hubs (Fig. 1,2 – A1, A2), the main square (B), various parks (C1, C3, C4), and the parking lots (D1–D3). The primary reasons (Fig. 3) for perceiving these places as cold were related to them being "open spaces". Additionally, all respondents mentioned that parking lots are too open and thus unpleasant. Squares, public transport hubs, and parking lots were perceived as cold due to their "cold and concrete" surfaces, while public transport hubs and parks were considered draughty areas. Respond-

ents also described public transport hubs and parking lots as depressing places. To reduce topophobia in these places, at least half of the respondents suggested planting high greenery, building shelters, and enclosing them with barriers.

Conversely, during winter, respondents also reported feeling thermally pleasant at the same public transport hubs (Fig. 1,2 – A1, A2), the main square (and part of the street leading to the main square) (B), and the parking lot near the hospital (D3), making these areas thermally ambivalent during winter. Sunlight and the presence of people contributed to thermal comfort at the square and the parking lot (Fig. 3). The square was also more pleasant due to its arcades and its compactness. The public transport hubs were more pleasant due to their shelters. Respondents who marked parks as thermally pleasant during winter attributed this to the presence of high greenery.

Summer thermal perception

Respondents identified several thermally unpleasant places where they perceived heat during summer, including both public transport hubs (Fig. 1,2 – A1, A2), the main square (B), the parking lots (D1–D3), and some parks (C3–C5); however, two parks (C3–C4) were also perceived as thermally pleasant during summer, rendering them thermally ambivalent. The primary reasons for perceiving all these places as thermally unpleasant were the absence or lack of shade and direct sunlight (Fig. 3). Furthermore, the square was considered unpleasant due to its overheated surface, lack of greenery, smell, and overcrowding. The public transport hubs were deemed unpleasant for the same reasons, plus the presence of homeless people, heavy traffic, and heat from vehicles and buildings. Parking lots were also characterised by overheated surfaces, overcrowding, absence of greenery, and openness. All respondents (10) suggested planting high greenery to improve thermally unpleasant areas. Half suggested building shelters and gazebos. Some respondents also suggested establishing blue elements, using less impervious surfaces, enclosing more space, and implementing water sprinkling on roads.

Thermally pleasant places during summer included almost all the parks (Fig. 1,2 – C1–C4, C6) due to their high greenery, shade, blue elements, and low greenery (Fig. 3). Respondents also noted that the square could sometimes be pleasant during summer due to its arcades, while public transport hubs could be perceived as pleasant due to the shade provided by buildings.

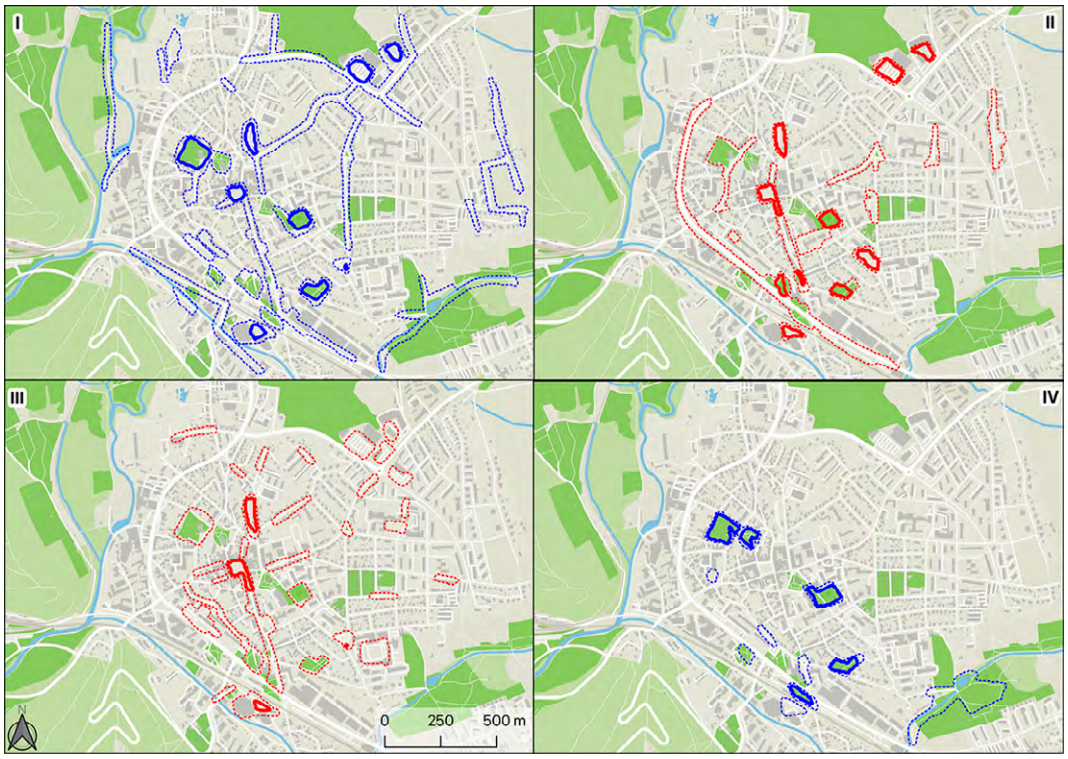

Figure 2. Thermally pleasant, resp. thermally unpleasant places in summer and winter in the study area, map background: © MapTiler © OpenStreetMap contributors

I = winter, blue colour = thermally unpleasant locations ("cold"),
II = summer, red colour = thermally unpleasant locations ("hot")
III = winter, red colour = thermally pleasant locations ("warm"), IV = summer, blue colour = thermally pleasant locations ("cool")
Solid lines indicate places identified by ≥5 participants; dotted lines indicate places identified by 1–4 participants.

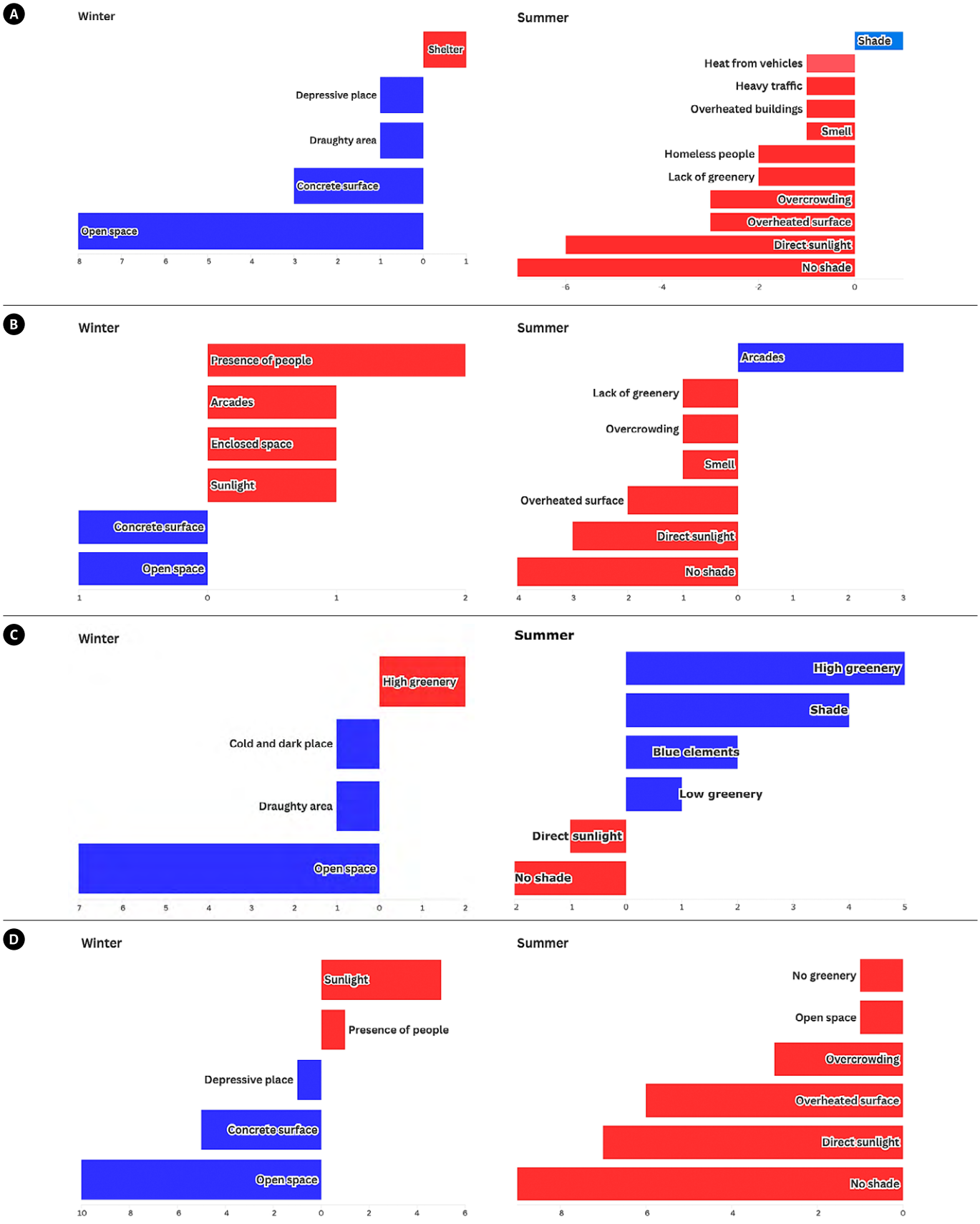

Figure 3. Reasons for perceiving places as (un)pleasant in summer and winter;
A) public transport hubs; B) main square; C) parks; D) parking lots;
Winter, blue colour = thermally unpleasant ("cold") locations, red colour = thermally pleasant ("warm") locations;
Summer, red colour = thermally unpleasant ("hot") locations, blue colour = thermally pleasant ("cool") locations.

Interseasonal differences in thermal perception

In terms of thermal perception, places have been generally categorised as thermally pleasant (comfortable), thermally unpleasant (uncomfortable), or thermally ambivalent. Our study examined the marked places and how they were perceived across two seasons, investigating whether the perception of thermal (dis)comfort in specific places remains consistent across seasons and whether any patterns emerge (Fig. 4).

The results reveal several distinct patterns. First, places perceived as unpleasant during both summer and winter include parking lots in the shopping zones (D1, D2). The second category consists of places that are thermally unpleasant during summer but are perceived as thermally ambivalent during winter, and this includes both public transport hubs (A1, A2), the main square (B), and the parking lot near the hospital (D3). One park was perceived as thermally pleasant during summer but unpleasant and cold during winter (C1), while some parks (C3, C4) were perceived as cold in winter but were perceived ambivalently during summer. Some places were marked only during summer, such as the park near the church (C2) and the park near the train station (C6), both perceived as pleasant, and Smetana Gardens (C5), which were perceived as unpleasant. Notably, no places were perceived as thermally pleasant during both summer and winter (Fig. 4).

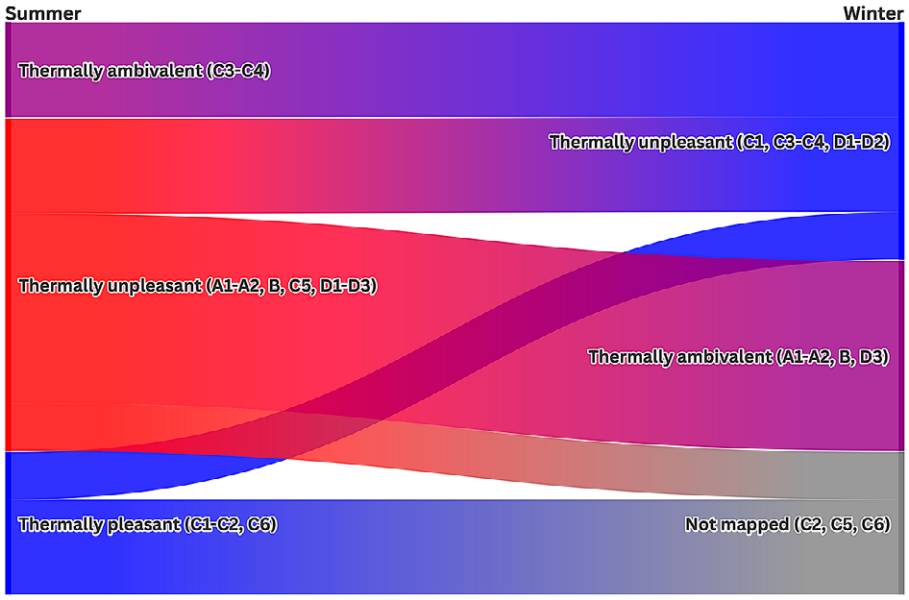

Figure 4. Interseasonal differences in the perception of thermally (un)pleasant places in the study area

A = public transport hubs; A1 = bus station, A2 = railway station
B = main square
C = parks; C1 = Park by the Theatre, C2 = Park by the Church, C3 = Kociánka Park, C4 = Czechoslovak Legions Park, C5 = Smetana Gardens, C6 = Park by the railway station
D = parking lots; D1 + D2 = Parking lots at the shopping zone, D3 = Parking lot near the hospital

Discussion

This study is unique in investigating the seasonal differences in thermal perception across different urban places in Ústí nad Orlicí, revealing spatial patterns of thermal (dis)comfort that extend beyond traditional urban climate research methods, such as temperature measurements, LST analyses, and numerical modelling. Our findings demonstrate that thermal perception is highly context-dependent, with significant differences between types of urban places and across seasons, as well as among individuals with varying (thermal) backgrounds and physiological characteristics (Aucliems, 1981; Tseliou et al., 2017; Schweiker et al., 2018). In this context, future research could investigate whether and how people with strong previous experiences of specific places may develop distinct patterns of (thermal) perception.

In this study, we suggest that certain urban places may be considered fundamentally problematic from a thermal comfort perspective, regardless of seasonal conditions. The most striking pattern to emerge from our approach was the consistent thermal discomfort associated with parking lots in shopping zones; these were perceived as thermally unpleasant places in both summer and winter. Květoňová et al. (2024), using the example of Prague, suggest that parking lots are considered unpleasant dur-

ing hot summer days. In this study we found that parking lots are perceived as thermally unpleasant not only during hot summer days, but also during winter days. Persistently experienced thermal discomfort may contribute to the year-round presence of negative associations individuals have with these places, thereby reinforcing the reproduction of topophobia associated with them. Therefore parking lots deserve considerably more attention from urban planners and local policymakers. Solutions could include, for instance, implementing more greenery with appropriate spacing and crown shape (Milosević et al., 2017). Furthermore, in accordance with previous studies from Czech cities (Lehnert et al., 2021; 2023b), public transport hubs during summer were perceived as thermally uncomfortable. However, by focusing on winter in this study in Ústí nad Orlicí, we found that transport hubs can be thermally ambivalent; this is in contrast to a simultaneous study carried out in Olomouc (Czechia) (Květoňová et al., 2025), where some transport hubs were even considered thermally comfortable by most respondents. With regard to urban squares, in this case study from Ústí nad Orlicí, we found ambivalent thermal perception in winter, similar to Květoňová et al. (2025) in Olomouc. Parks demonstrated the most pronounced seasonal dependency in thermal perception, being generally pleasant during summer but unpleasant during winter, particularly in more exposed locations. This finding aligns with previous research by Klemm et al. (2015), who noted the significant role of vegetation in creating pleasant microclimates during warmer months, while potentially exacerbating thermal discomfort during colder periods through increased shading and wind channelling effects. It should also be noted that the predominant type of deciduous trees could contribute to this perception.

The findings of our research highlight the ambiguous role of perceived thermal comfort and discomfort in the reproduction of people's topophilic and topophobic relationships to urban places. This role varies both in relation to the specific places unveiled in the study and in accordance with seasonal dynamics. This initial insight should serve as a rationale for further research aimed at achieving a deeper understanding of this ambiguity.

Concerning the reasons for their choices, respondents indicated that, especially in winter, some places were perceived as unpleasant due to their openness and sometimes due to the presence of "cold and concrete surfaces", which aligns with Lenzholzer & van der Wulp (2010). However, open spaces can also be perceived positively when there is, for example, sunlight in a pleasant place (Krüger et al., 2017; Lehnert et al., 2021). Furthermore, it should be emphasised that some places perceived as thermally unpleasant are unpleasant for other reasons beyond thermal perception, as seen in this study in the case of public transport hubs where participants cited the "presence of homeless people," suggesting that social stress could serve as a more significant stressor than the thermal load. Similarly, the commonly mentioned "heavy traffic" can negatively affect both thermal comfort (Schnell et al., 2016) and overall perception (Brisudová et al., 2020; Šerý et al., 2023).

Regarding the measures to improve their perceptions of places, in summer respondents most often suggested planting tall greenery, which is in line with Lehnert et al. (2023), while in winter, to improve thermal conditions, at least half of the respondents suggested, in addition to greenery, more enclosure of the places and the construction of shelters, which is consistent with the study by Květoňová et al. (2025). However, it should be taken into account that greenery should be appropriately placed in the environment (Geletič et al., 2023; Janků et al., 2024).

The results obtained have the potential not only to enrich existing knowledge on thermal (dis)comfort in urban environments, but also to be applied in urban planning policies aimed at mitigation measures. Indeed, all the identified proposed measures may serve as a basis for the deliberate evidence-based re-design of the physical settings of places with regard to mitigation. In this context, reconfiguring the spatial arrangements of problematic places could strengthen those aspects that render such places considerably more topophilic. In other words, as Šerý et al. (2025b) state, only such guided placemaking efforts can meaningfully contribute to shaping public places that effectively meet the needs of 21st-century urban residents.

Limits of the study

The study is based on the same homogenous group of 10 respondents across all three thermal walks. While this qualitative method is inherently subjective and the sample size is relatively small, we suggest using methods based on qualitative data as supplementary assessment in combination with quantitative data analysis. Future research could employ alternative methods, such as participatory mapping based on long-term thermal experiences or another in-situ approach, such as the analysis of thermal sensation votes using a mobile app (Květoňová et al., 2024). When conducting such research, care must be taken as respondents may become overly preoccupied with the research itself, such that the results might not accurately reflect reality (Lewis & Gutzwiller, 2023). Additionally, when mapping public spaces, the underlying research reason partially reveals itself through the mapping process (McLean, 2017). Moreover, the resulting map may differ when based on responses from local residents (Koukal, 2025). This research was specifically conducted during afternoon hours in summer and winter, with an additional morning session in winter to capture extreme weather conditions; however, it is important to note that the effects of blue(grey)green infrastructure can vary throughout the day (Lehnert et al., 2021).

Conclusion

The present study addressed the perception of urban environments across two different seasons, identifying key places with thermal (dis)comfort. Our findings indicate that parking lots are consistently perceived as the least thermally pleasant urban places, regardless of the season. Public transport hubs and the main square were perceived as thermally unpleasant during summer, but thermally ambivalent during winter. Furthermore, the research demonstrates a clear preference for more enclosed places over open places. Thermally pleasant places during summer included almost all the urban parks; however, most of these same parks were perceived as cold during winter. This seasonal contrast may be attributed to the species composition of the trees, which are predominantly deciduous. Nonetheless, respondents suggested several adaptation measures, with the most frequently mentioned being the planting of high greenery and the construction of shelters, regardless of season. This study contributes to a complex understanding of seasonal variations in human thermal comfort and the related cold and heat stress. Additionally, our findings emphasise the practical significance of considering seasonal thermal perception in the planning of urban places, particularly in the context of climate change and the creation of more liveable urban environments.

Acknowledgements

This work was supported by the Faculty of Science, Palacký University Olomouc internal grant IGA_PrF_2024_022–Novel approaches to studying the human thermal environment in urban areas. The authors thank all respondents involved in this research and are especially grateful to Sára Hurytová for her valuable contribution. We would also like to thank David Richardson who helped with the English.

References

Aljawabra, F., & Nikolopoulou, M. (2010). Influence of hot arid climate on the use of outdoor urban spaces and thermal comfort: Do cultural and social backgrounds matter? *Intelligent Buildings International*, 2(3), 198–207. 10.3763/inbi.2010.0046

Arsenović, D., Savić, S., Lužanin, Z., Radić, I., Milošević, D., & Arsić, M. (2019). Heat-related mortality as an indicator of population vulnerability in a mid-sized Central European city (Novi Sad, Serbia, summer 2015). *Geographica Pannonica*, 23(4), 204–216. https://doi.org/10.5937/gp23-22680

Arsenović, D., Savić, S., Milošević, D., Lužanin, Z., Kojić, M., Radić, I., Harhaji, S., & Arsić, M. (2024). Impact of urban outdoor thermal conditions on selected hospital admissions in Novi Sad, Serbia. *Vienna Yearbook of Population Research*, 22, 149–163. https://doi.org/10.1553/p-m53z-m2eh

Auliciems, A. (1981). Towards a psycho-physiological model of thermal perception. *International Journal of Biometeorology*, 25(2), 109–122. https://doi.org/10.1007/BF02184458

Brisudová, L., Šimáček, P., & Šerý, M. (2020). Mapping topo-ambivalent places for the purposes of strategic planning of urban space: The case of Šternberk, the Czech Republic. *Journal of Maps*, 16(1), 203–209. https://doi.org/10.1080/17445647.2020.1844087

Brisudová, L., Huck, J. J., & Solymosi, R. (2024). Does real time experience matter? Comparison of retrospective and in-situ spatial data in participatory mapping. *Computers, Environment and Urban Systems*, 113, 102159. https://doi.org/10.1016/j.compenvurbsys.2024.102159

Brown, G., & Kyttä, M. (2018). Key issues and priorities in participatory mapping: Toward integration or increased specialization? *Applied Geography*, 95, 1–8. https://doi.org/10.1016/j.apgeog.2018.04.002

Brown, R. D., Vanos, J., Kenny, N., & Lenzholzer, S. (2019). Designing urban parks that ameliorate the effects of climate change. *Landscape and Urban Planning*, 138, 118–131. https://doi.org/10.1016/j.landurbplan.2015.02.006

Capineri, C., Huang, H., & Gartner, G. (2018). Tracking emotions in urban space: Two experiments in Vienna and Siena. *Rivista Geografica Italiana*, 125(3), 273–288.

Chen, L., & Ng, E. (2012). Outdoor thermal comfort and outdoor activities: A review of research in the past decade. *Cities*, 29(2), 118–125. https://doi.org/10.1016/j.cities.2011.08.006

Cresswell, T. (2015). *Place: An introduction* (2nd ed.). Wiley Blackwell.

Cucu, L. A., Ciocănea, C. M., & Onose, D. A. (2011). Distribution of urban green spaces - an indicator of topophobia-topophilia of urban residential neighborhoods. Case study of 5th district of Bucharest, Romania. *Forum Geografic*, 10(2), 276–286. http://doi.org/10.5775/fg.2067-4635.2011.012.d

CZSO (Czech Statistical Office). (2017). *Small lexicon of municipalities of the Czech Republic – 2017.* Retrieved

April 14, 2025, from https://vdb.czso.cz/vdbvo2/faces/cs/index.jsf?page=vystup-objekt&z=T&f=TABULKA&skupId=2119&katalog=32225&pvo=MLO201709&pvo=MLO201709&pvokc=101&pvoch=40649

CZSO (Czech Statistical Office). (2024). *Population by permanent residence by 01.01.2024*. Retrieved April 14, 2025, from https://csu.gov.cz/produkty/pocet-obyvatel-v-obcich-9vln2prayv

Daniel, J., & Jirmus, R. (2023). Stávání se parkem: asambláž olomouckých parků v 19. a v první polovině 20. století. *Geografie*, 128(4), 459–481. https://doi.org/10.37040/geografie.2023.018

Denwood, T., Huck, J. J., & Lindley, S. (2022). Participatory Mapping: A Systematic Review and Open Science Framework for Future Research. Annals of the American *Association of Geographers*, 112(8), 2324–2343. https://doi.org/10.1080/24694452.2022.2065964

Doležal, D. (2022). Místa strachu z kriminality v Přerově. *Informace ČGS*, 41(1), 1–13.

Doležal, D., Šimáček, P., & Šerý, M. (2024). Attractive places in an ostensibly unattractive town: Přerov through the eyes of its inhabitants. *Geografie*, 129(3), 357–382. https://doi.org/10.37040/geografie.2024.011

Dzyuban, Y., Hondula, D. M., Vanos, J. K., Middel, A., Coseo, P. J., Kuras, E. R., & Redman, C. L. (2022). Evidence of alliesthesia during a neighborhood thermal walk in a hot and dry city. *Science of The Total Environment*, 834, 155294. https://doi.org/10.1016/j.scitotenv.2022.155294

Fagerholm, N., Raymond, C. M., Olafsson, A. S., Brown, G., Rinne, T., Hasanzadeh, K., Broberg, A., & Kyttä, M. (2021). A methodological framework for analysis of participatory mapping data in research, planning, and management. International *Journal of Geographical Information Science*, 35(9), 1848–1875. https://doi.org/10.1080/13658816.2020.1869747

Geletič, J., Lehnert, M., Resler, J., Krč, P., Bureš, M., Urban, A., & Krayenhoff, E. S. (2023). Heat exposure variations and mitigation in a densely populated neighborhood during a hot day: Towards a people-oriented approach to urban climate management. *Building & Environment*, 242(2). https://doi.org/10.1016/j.buildenv.2023.110564

Grzyb, T. (2024). Recreational use of the urban riverscape: What brings people to the river? *Moravian Geographical Reports*, 32(1), 14–25. https://doi.org/10.2478/mgr-2024-0002

Guzman-Echavarria, G., Middel, A., & Vanos, J. (2023). Beyond heat exposure—new methods to quantify and link personal heat exposure, stress, and strain in diverse populations and climates: The journal Temperature toolbox. *Temperature*, 10(3), 358–378. https://doi.org/10.1080/23328940.2022.2149024

Hashemnezhad, H., Heidari, A. A., & Mohammad Hoseini, P. (2013). Sense of place and place attachment. *International Journal of Architecture and Urban Development*, 3(1), 5–12.

Huang, Z., Chan, E. Y. Y., Wong, C. S., Liu, S., & Zee, B. C. Y. (2022). Health disparity resulting from the effect of built environment on temperature-related mortality in a subtropical urban setting. *International Journal of Environmental Research and Public Health*, 19(14), 8506. https://doi.org/10.3390/ijerph19148506

IPCC. (2023). *Climate change 2023: Synthesis report. Contribution of Working Groups I, II and III to the Sixth Assessment Report of the Intergovernmental Panel on Climate Change* [Core Writing Team, H. Lee & J. Romero (Eds.)]. IPCC. https://doi.org/10.59327/IPCC/AR6-9789291691647

Janků, Z., Belda, M., Bureš, M., Krč, P., Lehnert, M., Resler, J., Řezníček, H., Krayenhoff, E. S., Krüger, E., & Geletič, J. (2024). Towards climate-responsible tree positioning: Detailed effects of trees on heat exposure in complex urban environments. *Urban Forestry & Urban Greening*, 101. https://doi.org/10.1016/j.ufug.2024.128500

Klemm, W., Heusinkveld, B. G., Lenzholzer, S., Jacobs, M. H., & Van Hove, B. (2015). Psychological and physical impact of urban green spaces on outdoor thermal comfort during summertime in The Netherlands. *Building and Environment*, 83, 120–128. https://doi.org/10.1016/j.buildenv.2014.05.013

Klonner, C., & Norze, J. (2023). Sketch Map Tool. In *Evaluating participatory mapping software* (pp. 149–166). Springer International Publishing. https://doi.org/10.1007/978-3-031-18513-7_10

Knez, I. (2005). Attachment and identity as related to a place and its perceived climate. *Journal of Environmental Psychology*, 25(2), 207–218. https://doi.org/10.1016/j.jenvp.2005.03.003

Knez, I., & Thorsson, S. (2006). Influences of culture and environmental attitude on thermal, emotional and perceptual evaluations of a public square. *International Journal of Biometeorology*, 50(5), 258–268. https://doi.org/10.1007/s00484-006-0024-0

Knez, I., Thorsson, S., Eliasson, I., & Lindberg, F. (2009). Psychological mechanisms in outdoor place and weather assessment: towards a conceptual model. International *Journal of Biometeorology*, 53(1), 101–111. https://doi.org/10.1007/s00484-008-0194-z

Kottek, M., Grieser, J., Beck, C., Rudolf, B., & Rubel, F. (2006). World map of the Köppen-Geiger climate classification updated. *Meteorologische Zeitschrift*, 15(3), 259–263. https://doi.org/10.1127/0941-2948/2006/0130

Koukal, J. (2025). *Perception of odours in the city of Kroměříž* [Diploma thesis, Palacký University]. Palacký University, Olomouc, Czechia.

Krüger, E., Drach, P., & Broede, P. (2017). Outdoor comfort study in Rio de Janeiro: site-related context effects on reported thermal sensation. *International Journal*

of Biometeorology, 61, 463–475. https://doi.org/10.1007/s00484-016-1226-8

Kuras, E. R., Richardson, M. B., Calkins, M. M., Ebi, K. L., Hess, J. J., Kintziger, K. W., Jagger, M. A., Middel, A., Sailor, D. J., Sarnat, J. E., Vanos, J. K., Wee, B., Wenger, C. B., & Hondula, D. M. (2017). Opportunities and challenges for personal heat exposure research. *Environmental Health Perspectives*, 125(8), 085001. https://doi.org/10.1289/EHP556

Květoňová, V., Pánek, J., Geletič, J., Šimáček, P., & Lehnert, M. (2024). Where is the heat threat in a city? Different perspectives on people-oriented and remote sensing methods: The case of Prague. *Heliyon*, 10(16), e36101. https://doi.org/10.1016/j.heliyon.2024.e36101

Květoňová, V., Pánek, J., Koníček, J., & Lehnert, M. (2025). Wintertime thermal perception in a Central European city: The case of Olomouc, Czechia [Manuscript submitted for publication]. *Journal of Maps*.

Lai, D., Lian, Z., Liu, W., Guo, C., Liu, W., Liu, K., & Chen, Q. (2020). A comprehensive review of thermal comfort studies in urban open spaces. *Science of the Total Environment*, 742, 140092. https://doi.org/10.1016/j.scitotenv.2020.140092

Lehnert, M., Brabec, M., Jurek, M., Tokar, V., & Geletič, J. (2021). The role of blue and green infrastructure in thermal sensation in public urban areas: A case study of summer days in four Czech cities. *Sustainable Cities and Society*, 66, 102683. https://doi.org/10.1016/j.scs.2020.102683

Lehnert, M., Geletič, J., & Jurek, M. (2023a). Tradiční a nové přístupy ke studiu tepelného prostředí člověka ve městě: Kritické shrnutí současného stavu poznání [Traditional and new approaches to studying the human thermal environment in the city: A critical summary of the current state of knowledge]. *Geografie*, 128(3), 351–377. https://doi.org/10.37040/geografie.2023.012

Lehnert, M., Pánek, J., Kopp, J., Geletič, J., Květoňová, V., & Jurek, M. (2023b). Thermal comfort in urban areas on hot summer days and its improvement through participatory mapping: A case study of two Central European cities. *Landscape and Urban Planning*, 233, 104713. https://doi.org/10.1016/j.landurbplan.2023.104713

Lenzholzer, S. (2010). Thermal comfort and psychological adaptation as a guide for designing urban spaces. *Landscape and Urban Planning*, 98(3-4), 130–142. https://doi.org/10.1016/j.landurbplan.2010.08.006

Lenzholzer, S., & van der Wulp, N. Y. (2010). Thermal experience and perception of the built environment in Dutch urban squares. *Journal of Urban Design*, 15(3), 375–401. https://doi.org/10.1080/13574809.2010.488030

Lenzholzer, S., Klemm, W., & Vasilikou, C. (2018). Qualitative methods to explore thermo-spatial perception in outdoor urban spaces. *Urban Climate*, 23, 231–249. https://doi.org/10.1016/j.uclim.2016.10.003

Lewis, C. M., & Gutzwiller, R. S. (2023). Examining post-error performance in a complex multitasking environment. Cognitive Research: *Principles and Implications*, 8, 65. https://doi.org/10.1186/s41235-023-00512-y

Masselot, P., Mistry, M., Rao., S., Huber, V., Monteiro, A., Samoli, E., Stafoggia, M., Donato, F., García-León, D., Ciscar, J.-C., Feyen, L., Schneider, A., Katsouyanni, K., Vicedo-Cabrera, A. M., Aunan, K., & Gasparrini, A. (2025). Estimating future heat-related and cold-related mortality under climate change, demographic and adaptation scenarios in 854 European cities. *Nature Medicine*, 31, 1294–1302. https://doi.org/10.1038/s41591-024-03452-2

McLean, K. (2017). Smellmap: Amsterdam – olfactory art and smell visualization. *Leonardo*, 50(1), 92–93. https://doi.org/10.1162/LEON_a_01225

Milošević, D. D., Bajšanski, I. V., & Savić, S. M. (2017). Influence of changing trees locations on thermal comfort on street parking lot and footways. *Urban Forestry & Urban Greening*, 23, 113–124. https://doi.org/10.1016/j.ufug.2017.03.011

Nazarian, N., Bechtel, B., Mills, G., Hart, M. A., Middel, A., Krayenhoff, E. S., Jackson, T. L., Martilli, A., Brousse, O., Demuzere, M., Lipson, M. J., Sharma, A., & Chow, W. (2024). Integration of urban climate research within the global climate change discourse. *PLoS Climate*, 3(8), e0000473. https://doi.org/10.1371/journal.pclm.0000473

Nikolopoulou, M., Baker, N., & Steemers, K. (2001). Thermal comfort in outdoor urban spaces: understanding the human parameter. *Solar Energy*, 70(3), 227–235. https://doi.org/10.1016/S0038-092X(00)00093-1

Nikolopoulou, M., & Steemers, K. (2003). Thermal comfort and psychological adaptation as a guide for designing urban spaces. *Energy and Buildings*, 35(1), 95–101. https://doi.org/10.1016/S0378-7788(02)00084-1

Relph, E. (1976). *Place and placelessness*. Pion Limited.

Ruan, X., & Hogben, P. (2007). *Topophilia and topophobia: Reflections on twentieth-century human habitat*. Routledge.

Schnell, I., Cohen, P., Mandelmilch, M., & Potchter, O. (2021). Portable-trackable methodologies for measuring personal and place exposure to nuisances in urban environments: Towards a people oriented paradigm. *Computers, Environment and Urban Systems*, 86, 101589. https://doi.org/10.1016/j.compenvurbsys.2020.101589

Schnell, I., Potchter, O., Yaakov, Y., & Epstein, Y. (2016). Human exposure to environmental health concern by types of urban environment: The case of Tel Aviv. *Environmental Pollution*, 208, 58–65. https://doi.org/10.1016/j.envpol.2015.08.040

Schweiker, M., Huebner, G. M., Kingma, B. R. M., Kramer, R., & Pallubinsky, H. (2018). Drivers of diversity in human thermal perception – A review for holistic comfort models. *Temperature*, 5(4), 308–342. https://doi.org/10.1080/23328940.2018.1534490

Siwek, T. (2011). *Percepce geografického prostoru* [Perception of geographic space]. Česká geografická společnost.

Son, J.-Y., Liu, J. C., & Bell, M. L. (2019). Temperature-related mortality: a systematic review and investigation of effect modifiers. *Environmental Research Letters*, 14(7), 073004. 10.1088/1748-9326/ab1cdb

Šerý, M., Brisudová, L., Buil-Gil, D., Kimic, K., Polko, P., & Solymosi, R. (2023). The perception of personal security in urban parks: A comparative analysis of research methods. In *Placemaking in practice* (Vol. 1, pp. 290–308). https://doi.org/10.1163/9789004542389_017

Šerý, M., Burini, F., Consolandi, E., Desbiens, C., Doležal, D., Rodeschini, M., & Šimáček, P. (2025a). Participatory approaches to placemaking: Methodological outlines for public spaces in Bergamo (Italy), for Indigenous communities in Québec (Canada) and for popular places in Přerov (Czech Republic). In A. Delgado-Jiménez, T. Ruchinskaya, & C. Palmese (Eds.), Dynamics of placemaking volume 3: *The future of placemaking and digitization. Emerging challenges and research agenda* (pp. 87–107). Brill.

Šerý, M., Burini, F., Gartner, G., Rodeschini, M., & Šimáček, P. (2025b). Digital collaborative mapping tools for engaging residents in placemaking. In F. Rotondo et al. (Eds.), *Dynamics of placemaking volume 2: Engagement in placemaking: Methods, strategies and approaches* (pp. 213–234). Brill.

Šimáček, P., Šerý, M., Fiedor, D., & Brisudová, L. (2020). To fear or not to fear? Exploring the temporality of topophobia in urban environments. *Moravian Geographical Reports*, 28(4), 308–321. https://doi.org/10.2478/mgr-2020-0023

Tseliou, A., Tsiros, I. X., & Nikolopoulou, M. (2017). Seasonal differences in thermal sensation in the outdoor urban environment of Mediterranean climates – the example of Athens, Greece. *International Journal of Biometeorology*, 61(7), 1191–1208. https://doi.org/10.1007/s00484-016-1298-5

Tuan, Y. F. (1974). *Topophilia: A study of environmental perception, attitudes, and values*. Prentice-Hall.

Tuan, Y. F. (1976). Humanistic Geography. A*nnals of the Association of American Geographers*, 66(2), 266–276. https://doi.org/10.1111/j.1467-8306.1976.tb01089.x

Urban, A., Davídková, H., & Kyselý, J. (2014). Heat- and cold-stress effects on cardiovascular mortality and morbidity among urban and rural populations in the Czech Republic. *International Journal of Biometeorology*, 58(6), 1057–68. https://doi.org/10.1007/s00484-013-0693-4

Vasilikou, C., & Nikolopoulou, M. (2013, September 10–12). Thermal walks: Identifying pedestrian thermal comfort variations in the urban continuum of historic city centres. Paper presented at *PLEA 2013 - 29th Conference, Sustainable Architecture for a Renewable Future*, Munich.

Völker, S., & Kistemann, T. (2013). "I'm always entirely happy when I'm here!" Urban blue enhancing human health and well-being in Cologne and Düsseldorf, Germany. *Social Science & Medicine*, 78, 113–124. https://doi.org/10.1016/j.socscimed.2012.09.047

Wei, D., Lian, Z., & Liu, B. (2022). A field study of outdoor human thermal perception in three seasons in Shanghai, China. *Buildings*, 12(9), 1453. https://doi.org/10.3390/buildings12091453

INTERNATIONAL SCIENTIFIC JOURNAL
GEOGRAPHICA PANNONICA
Volume 29, Issue 2, 149–171 (June 2025)
Journal homepage: http://www.dgt.uns.ac.rs/en/homepage/pannonica/

Multiscale Analysis of Green Infrastructure Impacts on PM2.5 and PM10 Pollution in Delhi, India

Atul Kumar[A*], Mahua Mukherjee[A], Ajanta Goswami[A], Nishant Saxena[A], Aditya Rahul[B]

[A] *Indian Institute of Technology Roorkee; Roorkee, Uttarakhand, Republic of India*
[B] *Trinity College Dublin, the University of Dublin, College Green, Dublin, Republic of Ireland*

KEYWORDS

- Green Infrastructure (GI)
- PM2.5
- PM10
- Green Infrastructure Characteristics
- Urban Air Quality
- NDVI
- PCA
- FRAGSTAT

ABSTRACT

Urban air pollution, particularly from fine particulate matter (PM2.5 and PM10), poses critical environmental and public health challenges in rapidly urbanizing regions. This study presents a multiscale, seasonal analysis of the relationship between Green Infrastructure (GI) landscape characteristics and PM concentrations in Delhi, India. Using high-resolution Sentinel-2 imagery (2019–2021) and air quality data from 39 Central Pollution Control Board (CPCB) monitoring stations, we quantified 15 GI characteristics across five spatial scales (0.5–2.5 km) using NDVI. Empirical Bayesian Kriging was applied for spatial interpolation of PM values, and Otsu's thresholding was used to delineate vegetated areas. Principal Component Analysis (PCA) and regression models revealed that compositional metrics—such as Class Area (CA) and Percentage of Landscape (PLAND)—showed consistent negative correlations with PM2.5 and PM10 levels across all scales and seasons. Configuration metrics, including Largest Patch Index (LPI), Edge Density (ED), and Aggregation Index (AI), exhibited scale- and season-specific influences, with stronger effects observed at broader spatial scales during winter and autumn. The findings suggest that both the quantity and spatial arrangement of urban vegetation significantly affect local air quality. The study underscores the need for scale-aware, evidence-based GI planning as a nature-based solution, supporting India's airshed-level approach to urban pollution management. These insights offer practical guidance for urban policymakers and planners aiming to enhance air quality through strategic green infrastructure design.

Introduction

The globe saw an upsurge in human populations during the Industrial Revolution in the nineteenth century, which has exacerbated the pace of urbanization since then (Grimm et al., 2008; Singh et al., 2020). Countries' population projections report that over 95% of the global population's net growth occurs in the cities of developing countries (Jiang & O'Neill, 2017; UNDESA, 2019). In addition, nearly all of the world's new megacities (defined as having a population of more than 10 million people) are located in the developing world (UNDESA, 2019). Globally, rapid economic expansion and unregulated urbanisation have altered land surface attributes, including roughness, thermal inertia, and albedo (AlKhaled et al., 2020; Zhou et al., 2019). Such factors further impact regional meteorological parameters like temperature, wind speed, and air quality (Agarwal & Tandon, 2010; Grimm et al., 2008). In recent decades, fast economic expansion and unregulated urbanization have brought unprecedented negative an-

* Corresponding author:Atul Kumar; e-mail: akumar5@ar.iitr.ac.in
doi: 10.5937/gp29-53959
Received: October 10, 2024| Revised: June 2, 2025| Accepted: June 26, 2025

thropogenic stress in the urban environment regarding air quality, which has become a growing concern in densely populated regions of developed as well as developing countries (Singh et al., 2020; Song et al., 2018; Molina et al., 2012; Impacts, n.d.; Mathers et al., 1999). Megacities usually have significant PM10 and PM2.5 levels from fossil fuel combustion, fugitive dust, and biomass burning from industry, transportation, and densely populated areas. The WHO reported that outdoor air pollution (PM) kills about 4 million people yearly, accounting for 11.65% of worldwide deaths (WHO, 2018). Air pollution, the most significant health concern posed by the environment, is costing the world a total of $8.1 trillion, which is comparable to 6.1% of the global GDP (Li, 2016; UNEP, 2018; Li, 2017; Molina et al., 2012). Throughout the 1950s and 1960s, Particulate Matter (PM) pollution experienced a notable expansion in European and North American locations. Its severity, meanwhile, has been rising in developing countries, including India and China (Rohde & Muller, 2015; Yale & Columbia Universities, 2022). In India, during the last decades, air pollution in urban regions has become a major urban environmental issue (Gulia et al., 2015a; Chelani et al., 2001; Ramani et al., 2019; Central Pollution Control Board, 2003; Gupta, 2008; Ministry of Environment & Forests, 1987; Kushwaha & Nithiyanandam, 2019; Menon & Sharma, 2021; Ramaiah & Avtar, 2019; Kotharkar & Bagade, 2018). The 2021 assessment by IQAir, a Swiss organisation that assesses air quality by measuring PM concentration, placed India as the fifth most polluted nation out of 117 countries. It also identified Delhi as the most significant metropolitan agglomeration with the most hazardous air in the world (IQAir, 2021). In India, it has been estimated that the average economic impact of PM air pollution alone amounts to 5.4 per cent of the country's yearly GDP (Greenpeace, 2020). Furthermore, it is accountable for roughly one million deaths each year and contributes to 980,000 preterm births (Chatterji, 2020). It is estimated that in 2021, the deaths of 40,000 children under the age of five were directly linked to PM pollution (IQAir, 2021). According to studies conducted during the COVID-19 pandemic, being exposed to particulate matter (PM2.5 & PM10) increases the likelihood of acquiring the virus and experiencing more severe symptoms, including mortality, if infected (Role, 2021; Soni, 2021). The effects of urban issues extend to the urban, regional, continental, and global scales. Large cities pose challenges in managing a rising population, yet they also pose potential opportunities to manage environmental issues such as air pollution sustainably.

In the last 20 years, extensive research has been conducted on PM10 and PM2.5, which are typically considered harmful to people's health (Kumar et al., 2019; Mannucci et al., 2015; Leão et al., 2023; Ramadan et al., 2025). A number of studies examined the relationship between PM pollution and human health, finding that it was associated with sharp rises in respiratory and cardiovascular diseases (Morelli et al., 2016; Lavigne et al., 2016; Peters, 2011; Sangkham et al., 2024). Numerous studies have examined the spatial distribution of particulate matter of varying sizes at regional or national scales, along with the influencing variables (Sharma et al., 2014; Luo et al., 2020). Source apportionment of particles is another crucial field of study focused on characterizing different sources of fine-particulate air pollution (Banerjee et al., 2015; Sharma et al., 2014; Guttikunda et al., 2014; Nautiyal et al., 2025; Meng et al., 2025). Global cities have studied and suggested many ways to lower PM pollution. These include using cleaner energy, changing the way the economy grows, limiting driving, and working together at the regional or national level (Guttikunda et al., 2019; Gulia et al., 2015b; Dhingra, 2020; Wu et al., 2017). Identifying sustainable approaches by using nature-based solutions by which PM pollution can be reduced nowadays has become a priority for researchers and urban planners (Zhang et al., 2024; Power et al., 2023; Tomson et al., 2025). For example, research in 10 US cities found that trees eliminated 4.7 t to 64.5 t of PM2.5 yearly (Nowak et al., 2006). Similarly, Leicester, UK, research found that trees and grasses remove 14 tons of PM2.5 annually (Jeanjean et al., 2016; Jeanjean et al., 2017). Local PM declines were detected in Sydney's urban woodlands by Irga et al. (2015). Mcdonald et al. (2007) simulated PM10 concentrations in the West Midlands and Glasgow (UK) and showed that tree cover might cut PM by 10%. Kumar et al. (2019) suggested in their study that green infrastructure (GI) as a physical barrier may lower PM10 by 60%, 59%, 16%, 63%, and 77% compared to control circumstances. Due to the preponderance of qualitative research and the scarcity of quantitative studies, much of the attention is placed on a micro-scale configuration and species typology of green infrastructure (Yu & Jingyi, 2019; Im, 2019; Bartesaghi-Koc et al., 2018; Ouyang et al., 2021; Urban Climate Lab, 2016). Recently, there has been growing interest in understanding how the landscape level or urban macro scale composition and configuration of green infrastructure (GI) affect the delivery of ecosystem services, including pollution control (Andersson-Sköld et al., 2018; Selmi et al., 2016; Wu et al., 2018; Lei et al., 2018; Lei et al., 2021; Ramyar & Zarghami, 2017; Tomson et al., 2025; Barwise, 2023; Yao et al., 2025). "Green Infrastructure" (GI) is a natural and semi-natural open place around cities that provides ecological services to the surroundings (Calfapietra et al., 2019; Bartesaghi-Koc et al., 2019; NWGITT, 2008; Ramyar & Zarghami, 2017). GI is a novel name, but its concept originates in planning and conservation initiatives dating back 150 years. The concept was prompted by two precedents: integrating parks and other green spaces for people and linking natural areas to improve biodiversity and reduce habitat fragmentation (Benedict et al., 2006; Schneekloth, 2000; US EPA, OW, 2010;

Tallis et al., 2015; Sinnett et al., 2015; Calfapietra & Cherubini, 2019). To investigate and quantify the effects of GI on many sustainability advantages, researchers have attempted to develop a general categorisation of GI based on multiple benefits through quantitative and qualitative studies at local to regional scales. GI at the regional scale can have substantial spatial heterogeneity because various land cover and land-use types exhibit distinctive surface features. In urban form and urban landscape study, landscape metrics are algorithms that measure patches, classes, and aggregation of landscape patterns (Zheng et al., 2020; Wu et al., 2015; Lei et al., 2018; Ahern, 2007; Fan et al., 2015; Guo et al., 2021). Landscape metrics may efficiently illustrate the GI characteristics (Mcgarigal, 2015). They have been extensively utilised to explore the patterns of greenspace landscapes and their effects on PM reduction (Lei et al., 2021; Guo et al., 2021; Lei et al., 2018; Wu et al., 2015; Myint et al., 2015).

Recent studies have shown that the fragmentation of urban greenspace has a significant impact on particulate matter pollution. An investigation conducted by Lei et al. in a Chinese metropolis indicated that the composition of greenspace had a more significant impact on lowering PM pollution at shorter distances. In contrast, the configuration of greenspace was more significant at longer distances (Lei et al., 2018; Lei et al., 2021; Barwise, 2023). Further, a study demonstrated, that PM2.5 concentration and landscape evenness/fragmentation are strongly connected (Wu et al., 2015; Barwise, 2023; Zhang et al., 2024). There are limited or no studies on particulate matter pollution in relation to green infrastructure landscape patterns in Indian cities. Most, if not all, of these studies, adopted a FRAGSTAT model, which represents a landscape in three levels of matrices, i.e., patch, class, and landscape metrics, with further segmentation in area-edge, shape, and aggregations (Forman, 1995; McGarigal, 1995; McGarigal et al., 2002; Cao et al., 2024; Jiang et al., 2023). This study aims to propose landscape-level Green Infrastructure (GI) as a potentially sustainable approach to explain the variation of the seasonal PM concentration in an urban area. The study has direct alignment with the government approach of managing air quality and urban risk at the air-shed level contrary to the local scale by integrating green infrastructure as a potential nature-based solutions (CleanAirAsia, 2016; CPCB, 2013). The objectives of this study were to investigate the relationship between the landscape pattern of GI and PM concentration at multiple scales. The contributions of this study include the following: it investigates the role of green infrastructure composition and configuration in indicating particulate matter concentration in Delhi; it offers recommendations for the green infrastructure planning of urban redevelopment in the city.

Materials and Methodology

Study Area

The city is noted for its air pollution, with air quality levels routinely surpassing the World Health Organization's recommended thresholds, creating significant health hazards for its inhabitants (REF: IQ Air 2023). The World Health Organization (WHO) produced a report in 2014 identifying Delhi as the most polluted city in the world, citing air pollution as the city's most pressing problem (Saraswat et al., 2017; Jalan, 2019; Jain et al., 2021; Guttikunda & Calori, 2013). The Delhi government has taken various initiatives for long-term and seasonal measures to combat air pollution. For example, the Graded Response Action Plan (GRAP) developed by the Central Pollution Control Board (CPCB), the odd-even vehicle policy in 2016. The government also periodically shut down coal-based thermal power facilities and developed real-time air monitoring devices and the Green Delhi App for citizens to report pollution levels. In addition to regulatory and technological measures, the Delhi government has increasingly adopted nature-based solutions to combat air pollution and improve urban resilience. The Delhi Development Authority (DDA) and Forest Department have created additional city forests and green belts to filter air and cool the city. They have also pushed vertical gardens and green walls along flyovers and metro pillars to provide vegetation to crowded urban areas. The government intended to maximise the potential of green infrastructure by implementing several programmes like the smart city mission, the India Forum for Nature-based Solutions, the AMRUT project, etc. Delhi has undergone unprecedented urbanisation over the past few decades and manifested high GI and air pollution heterogeneity. Thus, Delhi serves as a good model for addressing the following questions: (1) Do the GI landscape patterns affect the Particulate matter concentration level? Furthermore, (2) if so, how do the PM10 or PM2.5 vary by different GI spatial patterns and scales?

Data

PM2.5/10 Measurements: 39 Air Quality Monitoring Stations (AQMS) are deployed throughout the city, as shown in Figure 1. All the stations are uniformly distributed in the city. These monitoring stations provide hourly and daily mean PM2.5/10 pollution concentration data. The data protocol suggests that each monitoring station has a spatially representative radius of 1 to 5 sq. km (CPCB, 2015). These AQMS are located at a height of 3 to 15 m on the street or roadsides. PM2.5/10 concentration and weather data at all 39 AQMS from the year 2019 to 2021 were obtained from

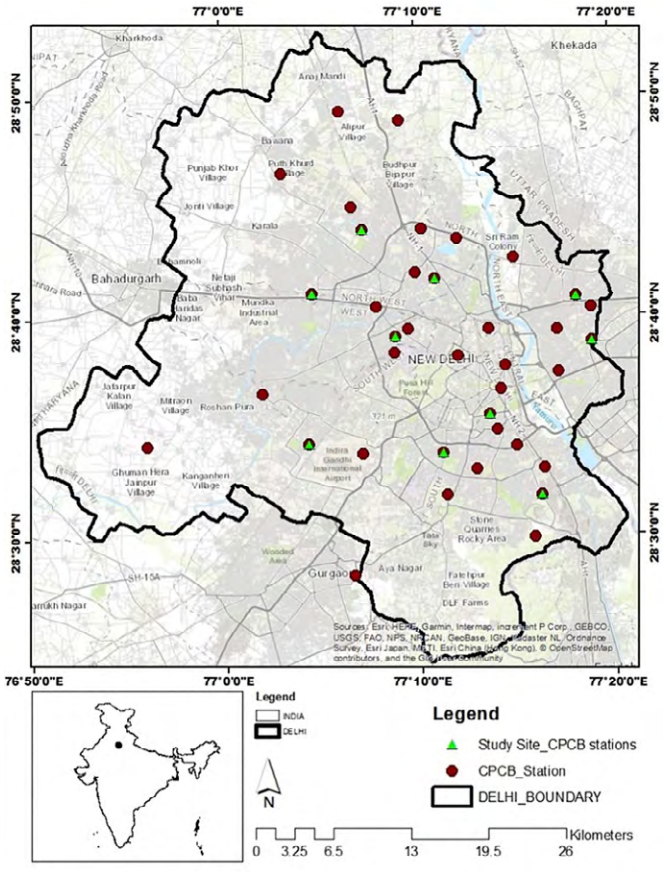

Figure 1. Delhi city Boundary and Location of all CPCB monitoring stations in Delhi and Location of monitoring stations selected for the study

the Central Pollution Control Board (https://app.cpcbccr.com/ccr/#/caaqm-dashboard-all/caaqm-landing). Seasonal mean data sets for the PM concentration were calculated based on the respective months of the seasons. Geographical Information System (GIS) based interpolation techniques have been used to map the concentration of particulate matter in interest. The interpolation technique is used to predict values in the cells in a raster when there are limited sample data points (Shareef et al., 2016; Bezyk et al., 2021; Singh & Tyagi, 2013a; Londoño-Ciro & Cañón-Barriga, 2015).The study used geostatic analysis interpolation techniques called Empirical Bayesian kriging; this method estimates cell values by averaging the sample point value in the neighbourhood of each processing cell. The standardised R square value for the maps is between 0.94 and 0.99. Data-driven traditional Empirical Bayesian kriging predicts unsampled locations. Parallel processing helps Empirical Bayesian kriging forecast large datasets and improve prediction accuracy. The method can provide accurate and reliable predictions of geographical data.

Green Infrastructure (GI) characterization

GI in an urban region, including land surfaces covered by trees, shrubs, and herbaceous vegetation, has long been known to influence local atmospheric PM concentrations and Temperature. GI changes PM concentrations through direct and indirect ways (Hofman et al., 2016) at plant level and landscape level, including capturing particulates on leaf surfaces (Zhang et al., 2021b)cities are implementing greening plans to satisfy the demands of residents for a more habitable environment. Because the relationship between the supply and demand of ecosystem services (ESs and altering urban temperature, atmospheric turbulence, and wind flow through "evapotranspiration" (Soydan, 2020; Liu & Shen, 2014). To obtain the landscape patterns of GI, which are reported in several scholarly works, 10 m spatial resolution data of Sentinel-2 (Year 2019, 20202 and 2021) from the Google Earth engine repository is used to delineate normalized difference vegetation index (NDVI) for 2019, 2020, and 2021; the study used the mean season-wise data for the specific month of the respective years. NDVI is a popular way to measure the cover and condition of vegetation in urban areas using remote sensing (Thiis et al., 2018). The threshold values of the seasonal NDVI maps were calculated using Otsu's thresholding technique, defining the condition of vegetative cover (Grover & Singh, 2015; Gašparović & Dobrinić, 2021; Ashok et al., 2021). Otsu's approach minimises vegetation and non-vegetation pixel variation (Dissanayake et al., 2018)(Sathyakumar et al., 2020). The difference between near-infrared and red-light reflectance is used to calculate NDVI values ranging from -1 to 1. Otsu's approach analyses histograms of NDVI values to identify an appropriate threshold t that divides pixel values into vegetation and non-vegetation classes. This is done by finding a threshold value that maximizes class variance $\sigma^2_b(t)$, defined as $\sigma^2_b(t) = \omega_1(t)\omega_2(t)[\mu_1(t)-\mu_2(t)]^2$, where $\omega_i(t)$ and $\mu_i(t)$ are the class probabilities and means of the two classes separated by threshold t. Finally, the resulting binary classification designates non-vegetation as pixels with NDVI < t and vegetation as pixels with NDVI ≥ t. It adjusts to the data patterns of each scene, making it strong for extensive or automated vegetation mapping without needing manual set limits for NDVI-based land cover analysis. After selecting the optimal threshold value mentioned in Table 1, binaries the image by putting all pixels with intensity levels over the threshold into the vegetation while converting all other pixels into the non-vegetation class (Sathyakumar et al., 2020). Finally, landscape-level metrics measured GI landscape composition and configuration features. Landscape-level metrics were widely used to describe GI patterns (Lei et al., 2018; Heather R. McCarthy, 2011; Mcgarigal, 2015). In this study, fifteen landscape-level metrics were used to measure landscape patterns of GI, as listed in Table 2. The landscape patterns included five composition metrics and ten configuration metrics (McGarigal, 1995). These metrics have been utilised in various landscape pattern-ecological process articles (Zhou et al., 2011; Li et al.,

2013; Chen et al., 2019; Wu et al., 2018; Liang & Gong, 2020; Soydan, 2020). These parameters were selected based on three criteria: (1) theoretically and practically significant; (2) readily computed and explained; and (3) minimum repetition.

FRAGSTATS was used to quantify landscape metrics using NDVI maps for ten plots. In this study, we used CPCB's ten air quality monitoring stations (AQMS) as central points to create five square plots per site ranging in size from 0.5 km x 0.5 km to 2.5 km x 2.5 km for each monitoring site, as shown in Figure 2. The following were taken into consideration while choosing the locations: (i) choosing monitoring sites with consistently high pollution levels (all seasons), (ii) avoiding areas with water bodies or other potential modifiers, (iii) Unique Local Climate Zone (built-up morphology) with variables land use and (iv) there was no primary emission source present. The smallest sample plot is 0.5 km x 0.5 km, which is ideal for urban micro-scale urban forestry study, while 2.5 km x 2.5 km is ideal for urban local scale. NDVI maps were validated using 100 randomly chosen points and reference data from Google images; the confusion matrix suggests 92% seasonal average accuracy with a seasonal average kappa coefficient value of 94% for the vegetation classifications. Finally, the seasonal data sets of the PM (PM10, PM2.5) concentration, along with the quantified GI landscape characteristics, were employed in the Principal Component Analysis (PCA) to analyse the variation of variables. PCA is a statistical technique commonly used in environmental studies to identify key factors by isolating those that account for the most variance in the data.

Table 1. Season-wise threshold value for Binarization of NDVI Image

Season	Threshold value for Binarization of NDVI Image
Summer (April to June)	0.29
Monsoon (July to August)	0.17
Autumn (September to October)	0.29
Winter (November to January)	0.17
Spring (February to March)	0.24

Data analysis

Green infrastructure features that have similar properties are clustered together using a hierarchical cluster analysis method (Yu et al., 2017; Grafius et al., 2018). Then, at first, we performed a one-way analysis of variance (ANO-

Table 2. Green Infrastructure characterization at landscape level

Typology	Metrics Type	GI Characterization	Equation (Unit)
Composition	Area	CA	$CA = \sum_{j=1}^{n} a_{ij}\left(\frac{1}{10{,}000}\right)$
		PLAND	$PLAND = P_i \frac{\sum_{j=1}^{n} a_{ij}}{A}(100)$
		LPI	$LPI = \frac{max\left(a_{ij}\right)}{A}(100)$
	Shape	SH_MN	$SH\_MN = \frac{1}{n} X \sum_{i=1}^{n} \frac{e_i}{min e_i}$
		LSI	$LSI = \frac{.25E^*}{\sqrt{A}}$
Configuration	Aggregation	COH	$COH = \left[1 - \frac{\sum_{j=1}^{n} P_{ij}^*}{\sum_{j=1}^{n} P_{ij}^* \sqrt{a_{ij}^*}}\right]\left[1 - \frac{1}{\sqrt{Z}}\right]^{-1} \cdot (100)$
		NP	$NP = n_i$
		PD	$PD = \frac{N}{A}(10{,}000)(100)$

Typology	Metrics Type	GI Characterization	Equation (Unit)
Configuration	Aggregation	CLUMPY	$CLUMPY = \begin{cases} \frac{G_i - P_i}{1 - P_i} \; for \; G_i \geq P_i \\ \frac{G_i - P_i}{1 - P_i} \; for \; G_i < Pi; P_i \geq 0.5 \\ \frac{P_i - G_i}{-P_i} \; for \; G_i < Pi; P_i \geq 0.5 \end{cases}$
		ENN_MN	$ENN\_MN = d(in\ km)$
		AI	$AI = \left[\sum_{i=1}^{m}\left(\frac{g_{ii}}{max\ g_{ii}}\right)P_i\right](100)$
		SDI	$SDI = -\sum_{i=1}^{m}(P_i \cdot \ln P_i)$
		SEI	$SEI = \frac{-\sum_{i=1}^{m}(P_i \cdot \ln P_i)}{\ln m}$
		ED	$ED = \frac{E}{A}(10{,}000)$
		TE	$TE = E$

Note: TOTAL AREA (CA); PERCENTAGE OF LANDSCAPE (PLAND); LARGEST PATCH INDEX (LPI); MEAN SHAPE INDEX (SH_MN); LARGEST SHAPE INDEX (LSI); PATCH COHESION INDEX (COH); NUMBER OF PATCH (NP); PATCH DENSITY (PD); CLUMPINESS (CLUMPY); MEAN NEAREST NEIGHBOR DISTANCE (ENN_MN); AGGREGATION INDEX (AI); SHANNON'S DIVERSITY INDEX (SDI); SHANNON'S EVENNESS INDEX (SEI); TOTAL EDGE (TE); EDGE DENSITY (ED); (ref: McGarigal, 1995; McGarigal, 2003)

VA) to examine whether there were significant differences among the PM2.5 and PM10 concentrations among the four seasons (Ginevan & Splistone, 2004; Vieira et al., 2018; Wu et al., 2018). We compared the PM2.5 and PM10 concentrations using the least significant difference test, with a significance level of $p < 0.05$. All values were reported as mean ± standard error. Second, we used the principal component analysis (PCA) to investigate the relationship between the PM2.5/10 concentration with the characterise and quantified green infrastructure at landscape level at scale variation from micro (0.5 km x 0.5 km) to local (2.5 km x 2.5 km) urban scale. PCA is the preferred approach for studying variation in environmental parameters with vegetation (Zhang et al., 2016; Yang et al., 2011; Ou et al., 2017; Andrew et al., 2012; Wu et al., 2018; Elhaik, 2022). It can help researchers understand the underlying ecological processes that drive these interactions. In addition, it can help to assess the GI composition and configuration impact on environmental variables such as PM2.5/10 (Chen & Dai, 2022; Heo et al., 2020), and assist in determining environmental factors variation in relation to quantified GI patterns (Wu et al., 2018; Jolliffe et al., 2016). It has been utilised in ecological research in tropical forests, grasslands, and wetlands to examine the link between GI and environmental factors (Kenkel, 2006; Yang et al., 2011; Rezaei & Millard-Ball, 2023). Climate change, land use change, and other anthropogenic disturbances have also been studied using it (Franklin et al., 1995; Jolliffe et al., 2016; Vieira et al., 2015). Finally, PCA regression was used to evaluate the relative impact of the five-composition measures and ten-configuration metrics of explanatory variables on PM2.5/10 concentration at each scale.

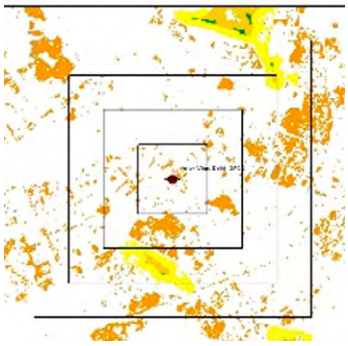

(A-1)

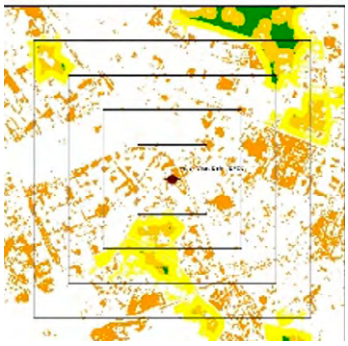

(B-1)

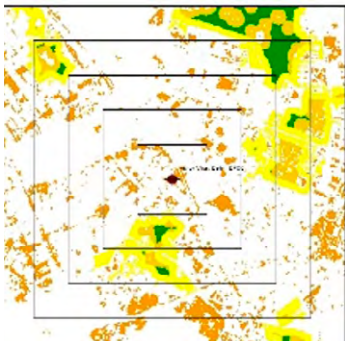

(C-1)

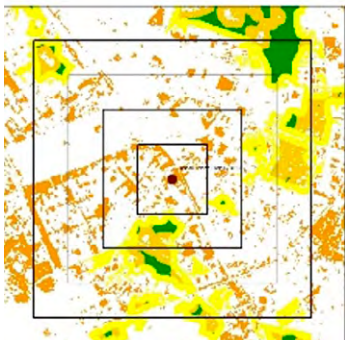

(D-1)

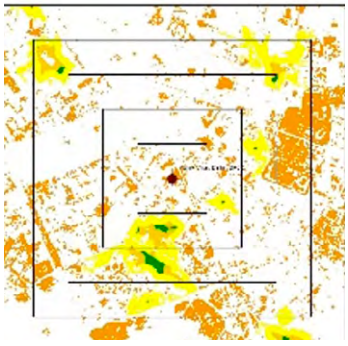

(E-1)

Google Earth Image of the site Ashok Vihar (Delhi) Monitoring Stations

Green Infrastructure Characterization mapping for all the seasons and multiscale buffer at Ashok Vihar (Delhi) Monitoring Stations

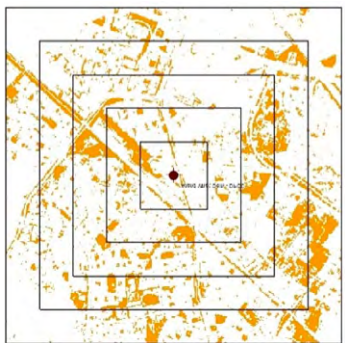

(A-2)

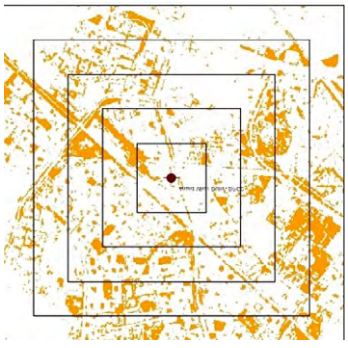

(B-2)

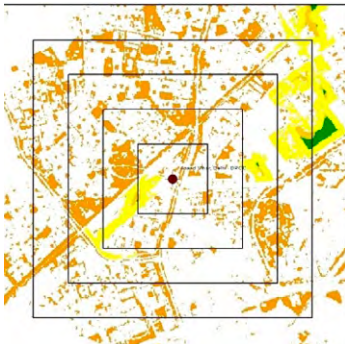

(C-2)

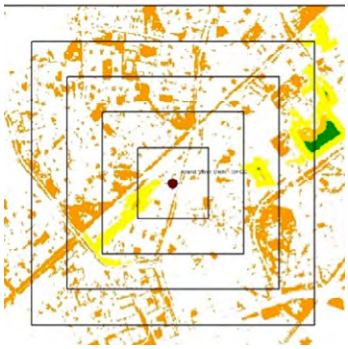

(D-2)

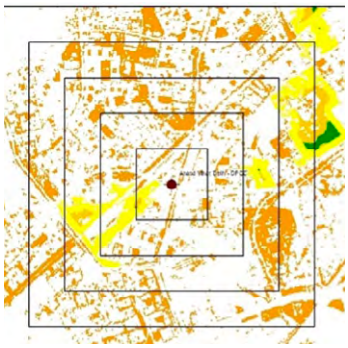

(E-2)

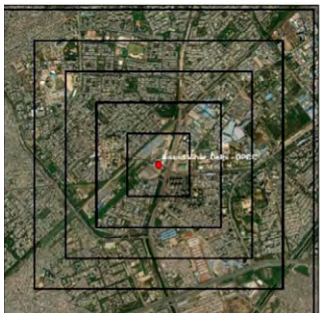

Google Earth Image of the site Anand Vihar (Delhi) Monitoring Stations

Green Infrastructure Characterization mapping for all the seasons and multiscale buffer at Anand Vihar (Delhi) Monitoring Stations

Figure 2. GI characterisation mapping for the selected study site in Delhi and buffer region depicting 0.5km (the inner square plot), 1km, 1.5km, 1.5km, 2km, and 2.5km (the outer square plot), A1-10: Spring Season; B1-10: Summer Season; C1-10: Monsoon Season; D1-10: Autumn Season; E1-10: Winter Season

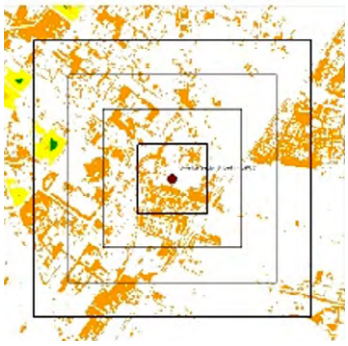

(A-3)

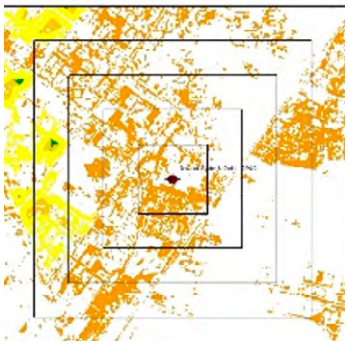

(B-3)

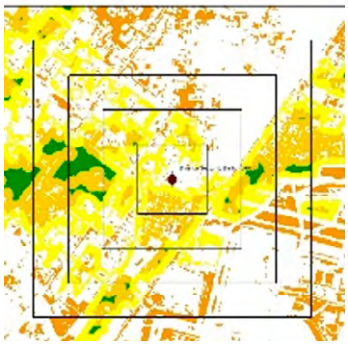

(C-3)

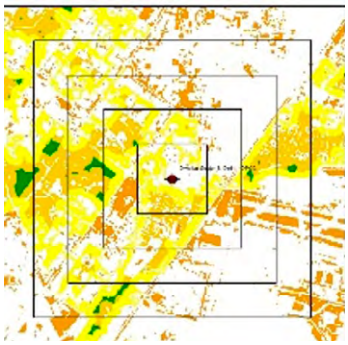

(D-3)

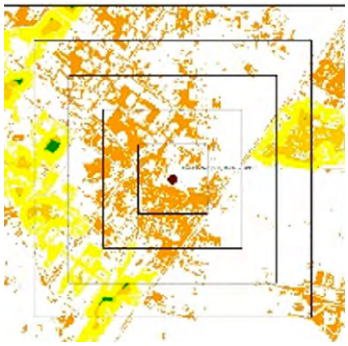

(E-3)

Google Earth Image of the site Dwarka-Sector 8 (Delhi) Monitoring Stations

Green Infrastructure Characterization mapping for all the seasons and multiscale buffer at Dwarka-Sector 8 (Delhi) Monitoring Stations

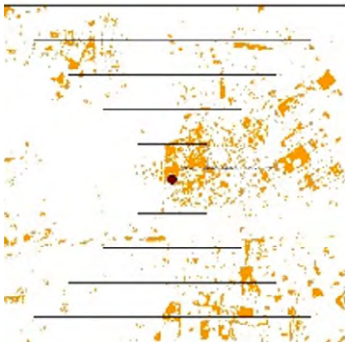

(A-4)

(B-4)

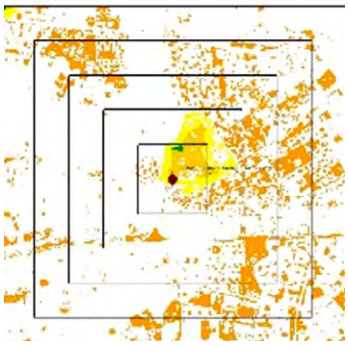

(C-4)

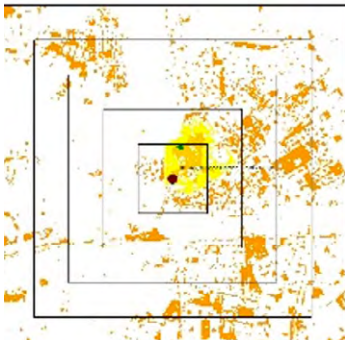

(D-4)

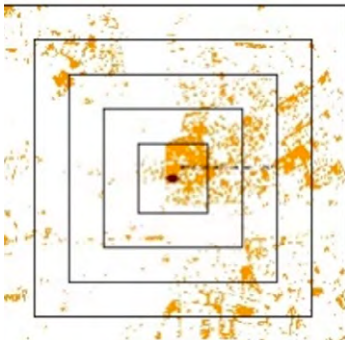

(E-4)

Google Earth Image of the site IHBAS, Dilshad Garden (Delhi) Monitoring Stations

Green Infrastructure Characterization mapping for all the seasons and multiscale buffer at IHBAS, Dilshad Garden (Delhi) Monitoring Stations

Figure 2. GI characterisation mapping for the selected study site in Delhi and buffer region depicting 0.5km (the inner square plot), 1km, 1.5km, 1.5km, 2km, and 2.5km (the outer square plot), A1-10: Spring Season; B1-10: Summer Season; C1-10: Monsoon Season; D1-10: Autumn Season; E1-10: Winter Season (continued)

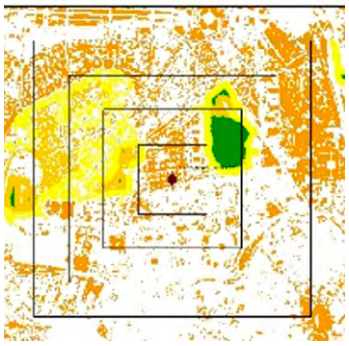

(A-5)

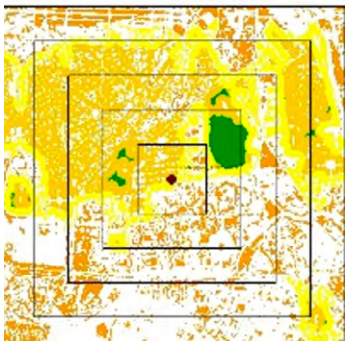

(B-5)

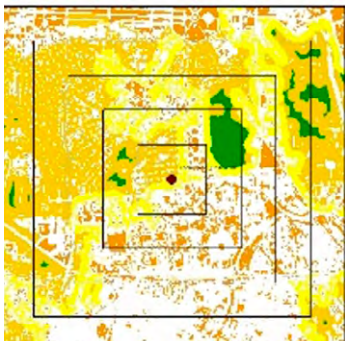

(C-5)

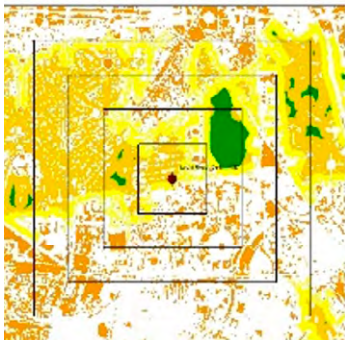

(D-5)

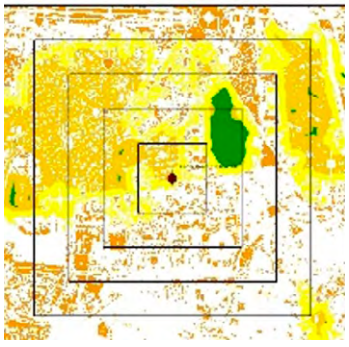

(E-5)

Google Earth Image of the site Lodhi Road (Delhi) Monitoring Stations

Green Infrastructure Characterization mapping for all the seasons and multiscale buffer at Lodhi Road (Delhi) Monitoring Stations

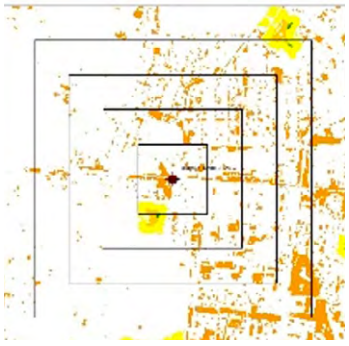

(A-6)

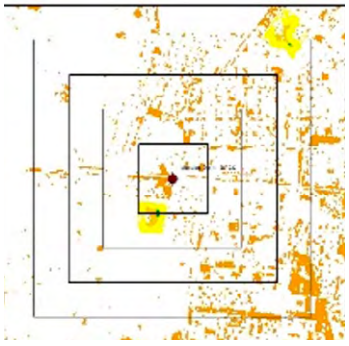

(B-6)

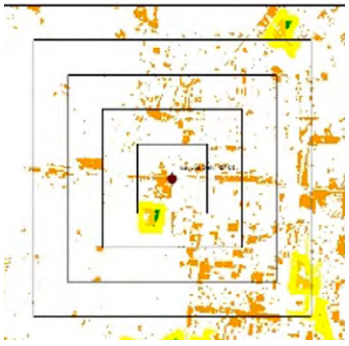

(C-6)

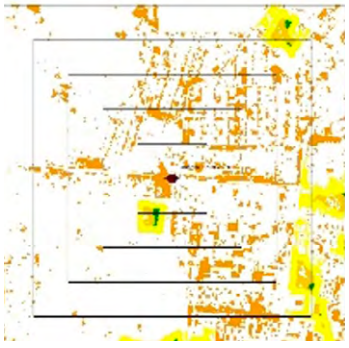

(D-6)

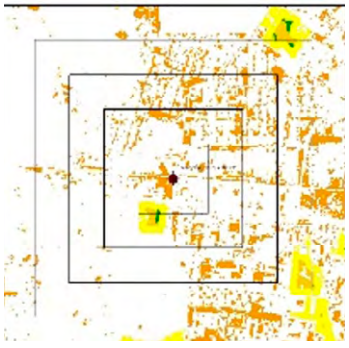

(E-6)

Google Earth Image of the site Mundka (Delhi) Monitoring Stations

Green Infrastructure Characterization mapping for all the seasons and multiscale buffer at Mundka (Delhi) Monitoring Stations

Figure 2. GI characterisation mapping for the selected study site in Delhi and buffer region depicting 0.5km (the inner square plot), 1km, 1.5km, 1.5km, 2km, and 2.5km (the outer square plot), A1-10: Spring Season; B1-10: Summer Season; C1-10: Monsoon Season; D1-10: Autumn Season; E1-10: Winter Season (continued)

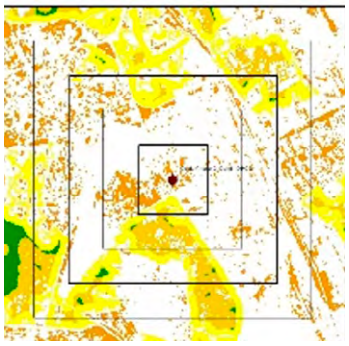

(A-7)

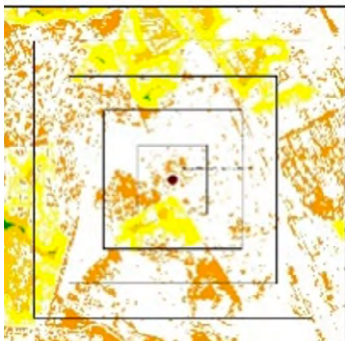

(B-7)

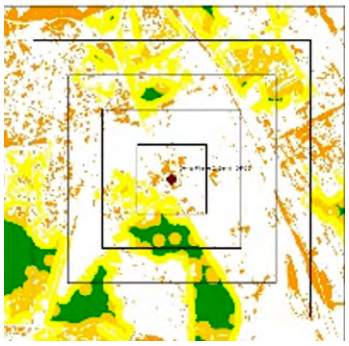

(C-7)

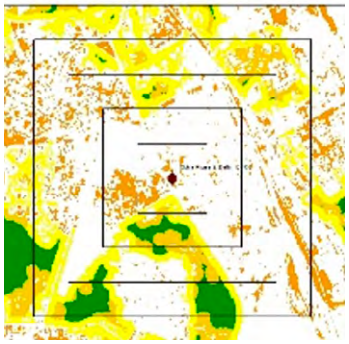

(D-7)

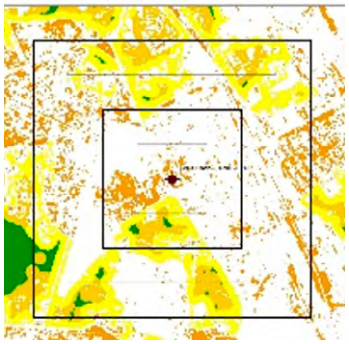

(E-7)

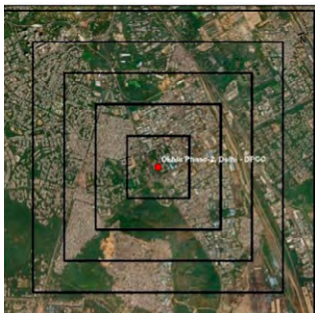

Google Earth Image of the site Okhla Phase-2 (Delhi) Monitoring Stations

Green Infrastructure Characterization mapping for all the seasons and multiscale buffer at Okhla Phase-2 (Delhi) Monitoring Stations

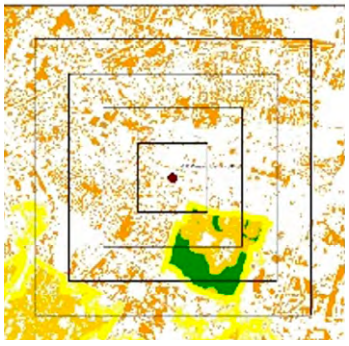

(A-8)

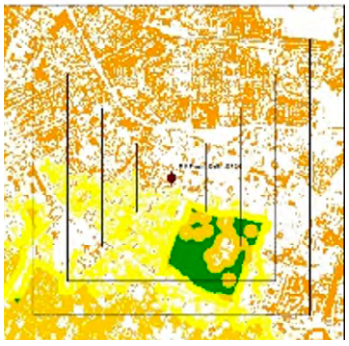

(B-8)

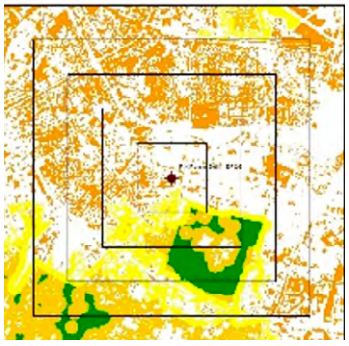

(C-8)

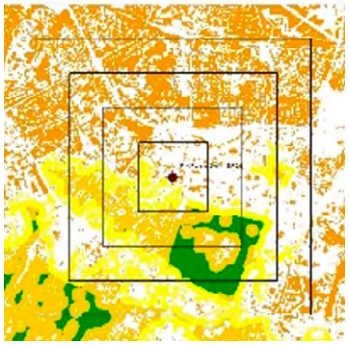

(D-8)

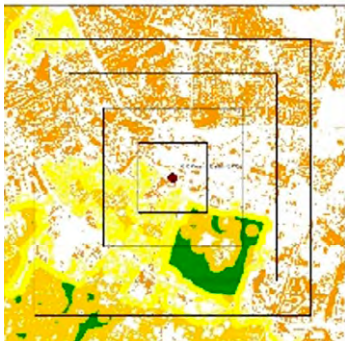

(E-8)

Google Earth Image of the site R K Puram (Delhi) Monitoring Stations

Green Infrastructure Characterization mapping for all the seasons and multiscale buffer at R K Puram (Delhi) Monitoring Stations

Figure 2. GI characterisation mapping for the selected study site in Delhi and buffer region depicting 0.5km (the inner square plot), 1km, 1.5km, 1.5km, 2km, and 2.5km (the outer square plot), A1-10: Spring Season; B1-10: Summer Season; C1-10: Monsoon Season; D1-10: Autumn Season; E1-10: Winter Season (continued)

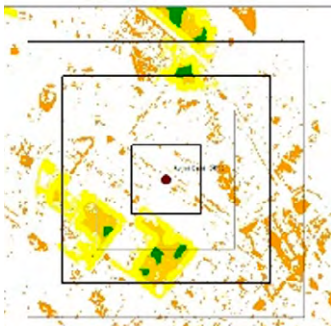

(A-9)

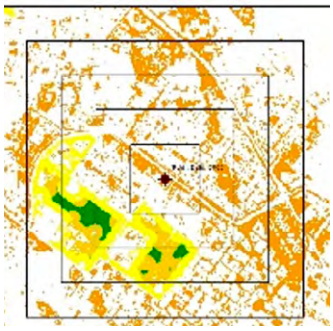

(B-9)

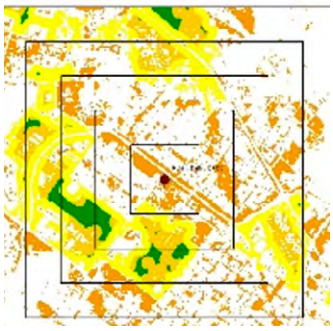

(C-9)

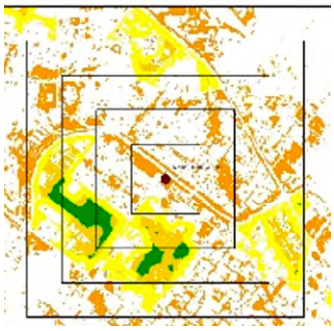

(D-9)

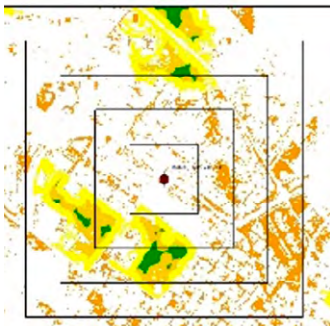

(E-9)

Google Earth Image of the site Rohini (Delhi) Monitoring Stations

Green Infrastructure Characterization mapping for all the seasons and multiscale buffer at Rohini (Delhi) Monitoring Stations

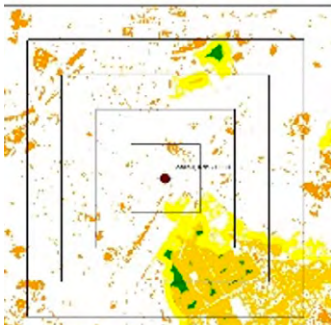

(A-10)

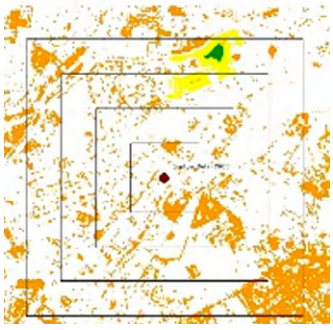

(B-10)

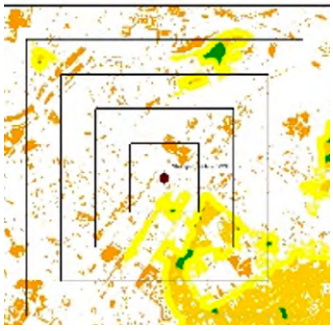

(C-10)

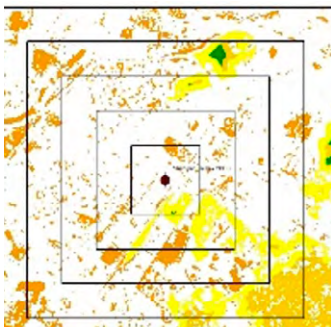

(D-10)

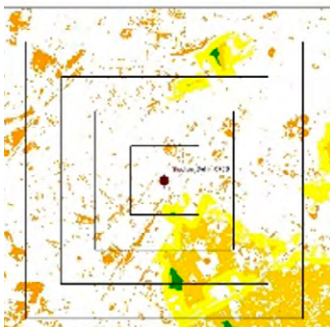

(E-10)

Google Earth Image of the Shadipur (Delhi) Monitoring Stations

Green Infrastructure Characterization mapping for all the seasons and multiscale buffer at Shadipur (Delhi) Monitoring Stations

Figure 2. GI characterisation mapping for the selected study site in Delhi and buffer region depicting 0.5km (the inner square plot), 1km, 1.5km, 1.5km, 2km, and 2.5km (the outer square plot), A1-10: Spring Season; B1-10: Summer Season; C1-10: Monsoon Season; D1-10: Autumn Season; E1-10: Winter Season (continued)

Result

Clustering GI characteristics

Landscape metrics are often directly deployed as independent variables to explore the effects of landscape patterns on air pollution. Many of these metrics exhibit strong correlations; therefore, certain metrics must be excluded from the full model to prevent multicollinearity. Hierarchical Cluster Analysis (HCA) helps identify uncorrelated landscape descriptors without requiring a priori decisions about which metrics to include or exclude. Figure 3 shows a dendrogram depicting the hierarchical clustering of GI characteristics. The variables were grouped via a distance-based method to find fundamental structural links. Metrics with comparable spatial patterns have been shown to cluster at reduced linkage distances, as demonstrated with CA and PLAND, as well as ENN_MN (Euclidean Nearest Neighbour Mean Distance) and CLUMPY, which form compact clusters. As the distance between clusters grows, they gradually merge, which shows that measure groups are less alike overall. It has been observed that highly correlated clusters contain CA–PLAND, TE-ED and NP-PD. A relatively mid-level correlated cluster contains ENN_MN-CLUMPY and SH_MN-{LSI-(TE-ED)} as shown in dendrogram Figure 3.

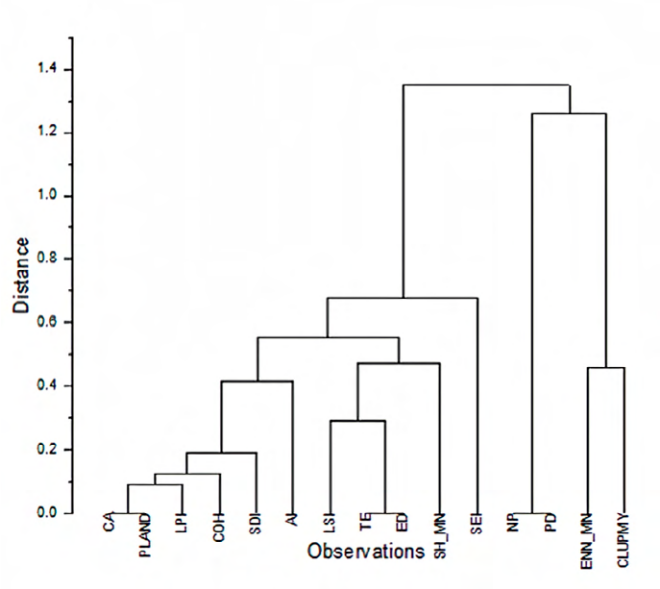

Figure 3. HCA of Green Infrastructure Landscape metrics

Seasonal Differences in Particulate Matter (PM) Pollution

The findings of an analysis of variance (ANOVA) revealed that there were significant differences ($p < 0.05$) between the PM10/2.5 concentrations during four distinct seasons. Both PM2.5 and PM10 concentrations were at their highest during the winter season, whereas both PM2.5 and PM10 concentrations were at their lowest level during the summer. It was discovered that the PM10/2.5 concentration in autumn was much higher than what was recorded in the spring. Possible reasons for significant fluctuations during the four seasons may include variations in air temperatures, humidity levels, wind direction and speed, presence or absence of leaves on vegetation, and patterns of fossil energy consumption. The winter season in Delhi is characterised by elevated pollution levels, which can be attributed to a combination of factors such as low temperatures, elevated humidity, and stagnant airflow. The circumstances are conducive to the trapping of pollutants in the atmosphere. In addition, the practice of burning agricultural residue in neighbouring states significantly contributes to the increased levels of pollution in Delhi during the winter months, as the area falls within the same boundary level airshed.

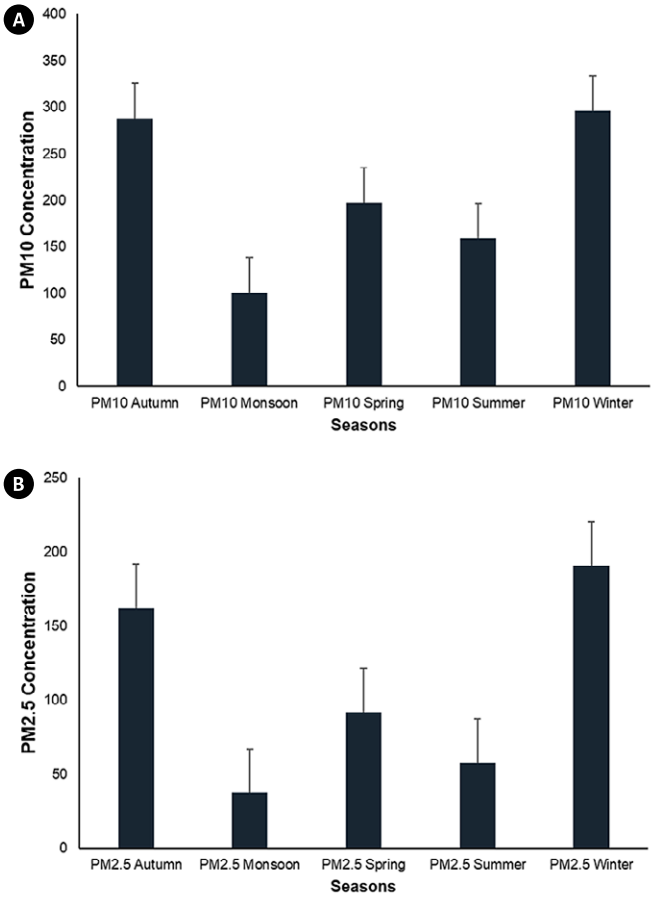

Figure 4. Analysis of variance (ANOVA) of PM2.5 and PM10 concentrations in four seasons. (A) seasonal ANOVA of PM10 concentration; (B) seasonal ANOVA of PM2.5 concentration

Principal Component Analysis (PCA)

Using PCA, we simplify the GI landscape-characterised data set by lowering its dimension. First, the predictor (response) variables (including PM2.5/10 value) and GI land-

scape characterise value defined as explanatory variables employed a centralised and standardised transformation, respectively. Then, the predictor variables are transformed into an equal number of principal components (PCs) to obtain a small number of components that could explain most (approximately 60%–90%) of the total variation in the predictor variables (Singh et al., 2013b; Wu et al., 2018). The percentage explained of variance and the cumulative proportion of variance are measures of the extent to which variation in PM pollution can be attributed to the presence of respective GI landscape characteristics along the first two principal component analysis (PCA) axes. The eigenvalues represent data variance along the principal component axis. The significant component with the highest eigenvalue explains the most data variation. In a PCA analysis, eigenvalues decide how many principal components must be retained. PCA explained 0.8204, 0.8626, 0.8668, 0.8429 and 0.8609 of the total variation in PM2.5, from scale 0.5 to scale 2.5. In contrast, the same axes explained 0.8377, 0.8392, 0.8477, 0.8518 and 0.8609 of the total variances in PM10 (Table. 3). Which suggested that the first two axes of PCA explain 82% to 86% of the variation for PM2.5 and 83% to 87% for PM10 with all the explanatory variables. Table 4. F-Ratio was used to test whether the multiscale GI characteristics affect PM pollution significantly, and R^2 represents the significance of PCA regression for the first seven PC axes, which explain more than 90% variance of PM pollution by GI characteristics in the PCA model, and the R^2adj was the adjusted or real value of the explained proportion. R^2 of PM2.5 from scale 0.5 km to scale 2.5 km were 0.9164, 0.9434, 0.8609, 0.9645, 0.9316, and R^2 of PM10 0.9502, 0.9287, 0.9717, 0.8566, 0.9753 respectively (Table 4). The tests indicated that landscape metrics of GI at all scales significantly explained the total variance of PM2.5 and PM10. Each scale included all the fifteen GI characterise metrics: CA, PLAND, SHAPE_MN, LSI, TE, COHESION, LPI, NP, PD, CLUMPY, ENN_MN, AI, SDI, ED, SEI. Positive and negative correlations with PCA axes indicate the direction and magnitude of the association between the features and the variables. By interpreting the PCA coefficients, we can gain insight into the underlying structure of the data and the relationships between the variables. The correlation between GI characteristics and the top two PCA axes of both PM2.5 and PM10 at a scale of 0.5 km × 0.5 km to 2.5 km × 2.5 km has been shown in Table 5. We selected the scales at which correlations between the PCA axes and PM concentration were significant based on the correlation that existed between the landscape metrics and the PCA axes seasonally.

PM2.5, CA (negative), PLAND (negative), TE (negative), and ED (negative) related to the first axis at all scales with minimal variation in the correlation coefficient, whereas all these GI characteristics showed relatively high negative relation at 0.5 to 1.5 km scale. NP (positive) and PD (positive) are significantly related to the first axis at all scales, whereas these are negatively related to PM2.5 at 2 km and 2.5 km. LPI (negative) and LSI (negative) were on a 1 km and 2.5 km scale, respectively. SH_MN (positive), ENN_MN (positive) and CLUMPY (positive) at 1.5 km scale with the second axis, 2.5 km scale with the first axis and 0.5 km scale with the first axis, respectively. COH (negative) at 2 km was significantly related to the second axis, whereas AI (positive) was significantly related at 0.5 km scale with the first axis. SDI (negative) and SEI (negative) with first and second axes, respectively, at 0.5 km and 1 km with first and second axes, respectively.

Table 3. PCA of PM2.5PM2.5 and PM10PM10 concentration on multiscale plots

Scale	Parameters	PCA1-PM2.5	PCA2-PM2.5	PCA1-PM10	PCA2-PM10
0.5	Eigenvalues	5.528	2.774	5.567	2.895
	Proportion explained of variance	0.618	0.307	0.609	0.322
	Cumulative proportion of variance	0.618	0.820	0.609	0.838
1	Eigenvalues	5.413	2.549	5.375	2.536
	Proportion explained of variance	0.595	0.283	0.590	0.284
	Cumulative proportion of variance	0.595	0.862	0.590	0.839
1.5	Eigenvalues	5.685	2.268	5.531	2.202
	Proportion explained of variance	0.634	0.262	0.623	0.257
	Cumulative proportion of variance	0.634	0.866	0.622	0.847
2	Eigenvalues	5.385	3.052	5.549	3.048
	Proportion explained of variance	0.643	0.346	0.652	0.344
	Cumulative proportion of variance	0.643	0.842	0.652	0.851
2.5	Eigenvalues	4.834	2.499	4.871	2.370
	Proportion explained of variance	0.623	0.279	0.622	0.275
	Cumulative proportion of variance	0.623	0.860	0.622	0.860

PM10, CA (negative), PLAND (negative), TE (negative), and ED (negative) are related to the first axis at all scales, with minimal variation having relatively high negative significant relation at a lower scale that is from 0.5 km to 1.5 km. NP (positive) and PD (positive) are significantly related to the first axis at 0.5 km scale. LPI (negative) and LSI (positive) at 2.5 km with the second axis. SH_MN (negative) at 1.5 km, ENN_MN (positive) significant relation at 2.5 km, CLUMPY (positive) at 1 km with first axis. COH (negative) at 0.5 km is significantly related to the second axis, whereas AI (positive) is significantly related at 0.5 km scale with the first axis. SDI (negative) and SEI (negative) with first and second axes, respectively, at 0.5 km and 1.5 km with first and second axes, respectively.

Table 4. Significance Test at $p < 0.05^*$

Test of Significance of all Canonical Axes	F-Ratio	R^2	R^2adj
PM2.5-0.5	0.0261	0.9164	0.8997
PM2.5-1	0.0171	0.9434	0.9321
PM2.5-1.5	0.0462	0.8609	0.8330
PM2.5-2	0.0105	0.9645	0.9574
PM2.5-2.5	0.0210	0.9316	0.9179
PM10-0.5	0.0025	0.9502	0.9403
PM10-1	0.0038	0.9287	0.9144
PM10-1.5	0.0049	0.9717	0.9660
PM10-2	0.0478	0.8566	0.8279
PM10-2.5	0.0072	0.9753	0.9703

Table 5. Correlation between Green Infrastructure characterise metrics and Principal Component Analysis (PCA) axes of scale and PM2.5/10 and Graphical representation respectively, $p < 0.05^*$.

Axes	CA	PLAND	NP	PD	LPI	LSI	SH_MN	ENN_MN	CLUMPY	COH	AI	SDI	SEI	TE	ED
PCA1-PM2.5-0.5	-2.05	-2.05	3.35	3.36	-2.03	-0.81	-1.12	3.71	3.83	-1.86	2.93	-1.87	0.66	-2.02	-2.02
PCA2-PM2.5-0.5	-0.19	-0.19	-1.95	-1.94	0.44	-2.45	1.76	1.07	-0.39	0.30	1.34	-0.07	-1.98	-0.53	-0.53
PCA1-PM2.5-1	-1.92	-1.92	3.10	3.10	0.57	-0.43	-1.50	4.21	3.82	-1.43	2.63	-1.65	-0.78	-2.11	-2.11
PCA2-PM2.5-1	-0.01	-0.01	1.73	1.73	-2.17	-2.64	1.70	-0.56	-1.29	-1.93	-1.38	0.02	-2.99	-0.01	-0.01
PCA1-PM2.5-1.5	-2.08	-2.08	3.29	3.28	-2.03	-0.81	-1.35	4.16	3.39	1.04	-1.29	-1.82	0.50	-1.96	-1.96
PCA2-PM2.5-1.5	0.01	0.01	0.87	0.86	0.49	-2.76	1.91	-0.01	-0.68	-1.77	2.08	0.64	2.79	-0.33	-0.33
PCA1-PM2.5-2	-1.92	-1.92	3.13	3.14	-1.83	-0.28	-1.49	4.31	3.64	0.82	-0.59	-1.70	0.69	-1.88	-1.88
PCA2-PM2.5-2	0.32	0.32	-1.85	-1.85	0.00	-2.66	-0.96	0.49	-0.43	-2.00	2.53	0.73	2.00	0.14	0.14
PCA1-PM2.5-2.5	-1.92	-1.97	2.46	2.45	-2.02	-0.81	-0.81	4.46	2.98	-0.15	-0.60	-1.85	0.04	-1.94	-1.84
PCA2-PM2.5-2.5	0.44	0.38	-2.11	-2.11	0.21	-2.79	1.57	0.85	2.25	-1.71	2.43	-0.61	-1.52	-0.45	-0.45
Significant negative Relation	-2.08	-2.08	-2.11	-2.11	-2.17	-2.79	-1.50	-0.56	-1.29	-2.00	-1.38	-1.87	-2.99	-2.11	-2.11
Significant Positive Relation	0.44	0.38	3.35	3.36	0.57	-0.28	1.91	4.46	3.83	1.04	2.93	0.73	2.79	0.14	0.14

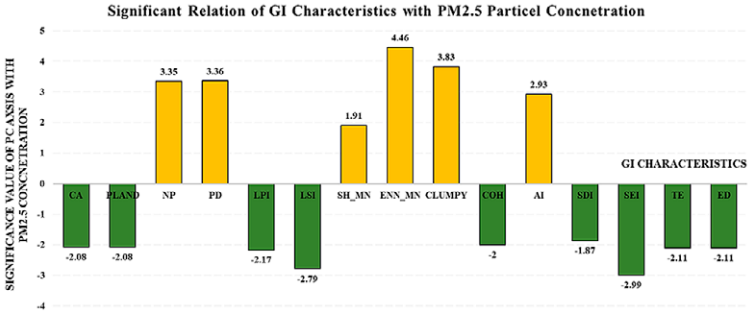

Axes	CA	PLAND	NP	PD	LPI	LSI	SH_MN	ENN_MN	CLUMPY	COH	AI	SDI	SEI	TE	ED
PCA1-PM10-0.5	-2.06	-2.06	3.22	3.22	-1.99	-0.01	-1.57	3.86	3.50	-0.29	2.92	-1.84	0.70	-2.05	-2.05
PCA2-PM10-0.5	-0.18	-0.18	2.36	2.35	-0.11	2.69	-1.58	-0.72	1.46	-2.33	1.46	-0.16	-1.84	-0.57	-0.57
PCA1-PM10-1	-1.89	-1.89	1.05	1.05	0.62	-0.40	-1.64	4.26	3.91	1.53	2.60	-1.63	-0.31	-2.06	-2.06
PCA2-PM10-1	-0.22	-0.22	3.08	3.08	-2.10	2.62	0.32	-0.20	-0.92	-1.72	-1.63	-0.40	-2.13	0.00	0.00
PCA1-PM10-1.5	-2.05	-2.04	3.21	3.21	-1.95	-0.58	-1.12	4.21	3.43	1.00	-1.07	-1.73	1.00	-2.00	-2.00
PCA2-PM10-1.5	-0.12	-0.12	1.17	1.16	-0.62	2.77	-2.14	0.02	-1.38	-1.80	-2.09	-0.69	-2.51	0.45	0.45
PCA1-PM10-2	-1.89	-1.89	3.07	3.08	-1.86	-0.73	-1.56	4.28	3.61	0.77	-0.19	-1.54	0.84	-1.96	-1.96
PCA2-PM10-2	-0.47	-0.46	-1.93	-1.93	-0.07	2.61	0.71	0.07	-0.55	-1.97	-2.51	-0.92	-1.73	0.75	0.75
PCA1-PM10-2.5	-2.00	-2.00	2.29	2.28	-2.11	-1.11	-0.93	4.44	3.66	-0.16	-0.29	-1.81	0.06	-1.94	-1.88
PCA2-PM10-2.5	0.77	0.76	2.37	2.37	0.21	2.17	-1.51	0.78	-1.26	-1.70	-2.34	-0.68	-1.66	0.70	0.69
Significant negative Relation	-2.06	-2.06	-1.93	-1.93	-2.11	-1.11	-2.14	-0.72	-1.38	-2.33	-2.51	-1.84	-2.51	-2.06	-2.06
Significant Positive Relation	0.77	0.76	3.22	3.22	0.62	2.77	0.71	4.44	3.91	1.53	2.92	-0.16	1.00	0.75	0.75

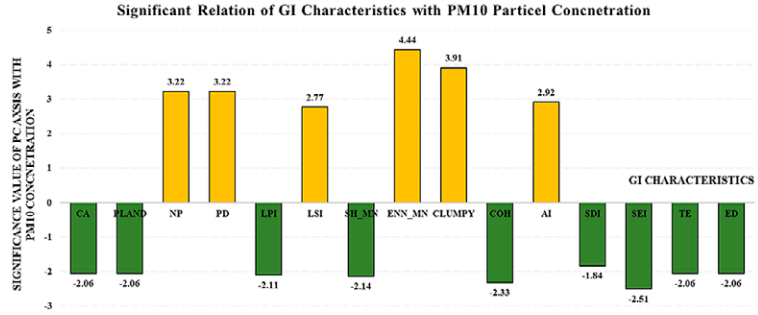

Discussion

In this study, we took PM pollution as the targeted urban environmental issue to be solved by the planning of GI. The study addresses the solution at the local level from 0.5 km to 2.5 km in alignment with the government approach of air quality management at the airshed level (Ganguly et al., 2020). The results provide the complex connections between GI design and PM pollution levels, as well as effective solutions for improving air quality via urban green space planning.

Season and scale-wise Effects of Green Infrastructure Characteristics on PM Pollution

ANOVA results revealed significant seasonal differences in PM concentrations, with the highest levels in winter and the lowest in summer. This variation is consistent with previous studies, which attribute winter pollution peaks to lower temperatures, stagnant air, higher humidity, and regional agricultural residue burning. PCA demonstrated that a considerable proportion of PM concentration variance (82%–87%) could be explained by the first two principal components, confirming the strong relationship between GI characteristics and air pollution. Scale sensitivity was evident, with smaller spatial scales (0.5–1.5 km) favoring compositional metrics like CA and PLAND since the vegetation cover serves as a sink for pollution (Liu et al., 2017; Zhang et al., 2021a) and promotes pollutant deposition (Hirabayashi et al., 2015; Hirabayashi et al., 2012; Tiwari & Kumar, 2020). At larger scales (2–2.5 km) configurational metrics such as LPI and ED favored, as the high ED zone of GI behaves as an air filter by creating a buffer or protective green boundary as the high ED zone of GI behaves as an air filter by creating a buffer or protective green boundary as the high ED zone of GI behaves as an air filter by creating a buffer or protective green boundary. These findings align with existing literature emphasizing that vegetative coverage impacts local air quality more directly at smaller scales, while spatial configuration plays a greater role at broader urban landscape levelsThe shape matrices of GI characteristics do not directly impact PM pollution reduction (Lei et al., 2018). High COH values in the landscape can be a tangible obstacle that intercepts and captures suspended particulate matter from the atmosphere (Li et al., 2021). The process of interception helps in the removal of particulate matter (PM) from the atmosphere, thereby leading to a reduction in its concentration. A high coefficient of COH supports the formation of microenvironments that facilitate the accumulation of settled dust, thereby mitigating its dispersion into the atmosphere (Ge et al., 2021). The spatial distribution of GI characteristics in a given area can impact the direction and flow of air movements across the terrain. The phenomenon of wind encountering an obstacle can result in a reduction of its velocity and a change in its direction, leading to the occurrence of turbulence. The phenomenon of turbulence helps in the dispersion and attenuation of particulate matter and other airborne pollutants by impeding their accumulation in specific regions. The process facilitates the amalgamation of uncontaminated air with contaminated air, decreasing the collective level of particulate matter (PM). AI significantly impacts PM10 reduction at higher scales of 1.5 km to 2.5 km. The findings were consistent with prior research, which suggested that the ability of urban green spaces to mitigate fine particulate matter was positively correlated with the proximity and contiguity of their landscape patches (Liu & Shen, 2014). Moreover, the escalating intricacy of the GI terrain typically amplifies the edge effects of GI landscapes, thereby aiding in the interception of particulate matter. SDI and SEI show significant reduction potential during summer at 0.5 km scale and during Autumn at 1.5 km. The SDI and SEI have the potential to demonstrate the heterogeneity of landscape patches, and their efficacy is based on the distribution of diverse patches. A higher index value indicates a landscape that is more evenly distributed. A higher degree of landscape distribution results in a stronger correlation between land use and increased interaction between “sink” and “source” landscapes, leading to a more frequent reduction of PM pollution (Łowicki, 2019). However, six configuration GI characteristics increase PM pollution during certain seasons at several scales.

Comparison of compositional and configurational GI on PM pollution variation

A comparative analysis revealed that compositional characteristics (e.g., CA, PLAND) are more effective in PM reduction at smaller spatial scales, where vegetation density directly contributes to pollutant deposition. On the other hand, configurational metrics (e.g., LPI, ED, COH, AI) played a stronger role at larger scales, influencing airflow patterns, turbulence, and pollutant dispersion. This reinforces the importance of a scale-sensitive GI design, as certain benefits—such as aerodynamic interactions and pollutant interception—become more pronounced with increasing spatial extent (Lei et al., 2018). The results also underscore the complex role of shape and spatial configuration metrics like LSI, SH_MN, COH, and AI. While high COH values were associated with PM reduction by forming barriers to airborne particulates, other metrics exhibited season-dependent or pollutant-specific effects. For instance, LSI showed a stronger association with PM2.5 reduction, while SH_MN was more relevant for PM10, highlighting the need for pollutant-specific GI design

strategies. The observed heterogeneity in GI–PM relationships across scales and seasons suggests that a one-size-fits-all approach to green space planning is insufficient. Instead, contextual design strategies are required. For example, denser vegetation patches (high CA/PLAND) should be prioritized in residential neighborhoods to improve local air quality, while connectivity and edge complexity (high ED/LPI/AI) should be enhanced in larger parks or peri-urban buffers to leverage wind interactions and pollutant dispersion.The presence of a greater number of trees within a street canyon may result in decreased ventilation and an overall rise in air pollution levels (Chen et al, 2018; Zhou et al., 2019). Additionally, studies have also shown that the existence of high-level vegetation canopies, such as trees, can lead to a decline in air quality. In contrast, low-level green infrastructure, such as hedges, can enhance air-quality conditions (Wu et al., 2018b; Hirabayashi et al., 2012; Srbinovska et al., 2021). The correlation between spatial configurations and PM concentration exhibited heterogeneity across various seasons and scales. Additionally, the landscape metrics of green space exhibited both positive and negative impacts on PM concentration. Therefore, the efficacy of green space in mitigating PM concentration is contingent upon the equilibrium between these advantages and disadvantages.

Limitation

This study increased our understanding of PM pollution and urban green space spatial patterns, but it had some constraints, though the following assumptions and conditions were adopted to try to minimise the constraints. Based on the conditions and assumptions, this study picked the most significant number of plots possible for the study. Future research may benefit from more sample plot data. The following criteria and presumptions were used to choose monitoring stations for study: (i) Major modifiers like substantial bodies of water are absent from AOI; (ii) Data on PM concentrations on rainy days were excluded from the research; (iii) Monitoring stations were located in certain local climatic zones (LCZs) so as to have the least amount of disagreement owing to built-up morphology in the research. Interpolated PM concentration map data was used to calculate each plot's PM concentration value, which was verified statistically, and the mean value was estimated at each scale. In future studies, more monitoring stations may be used to achieve a more accurate concentration value. High-resolution geospatial data may help map green infrastructure landscape patterns more accurately. The association between PM pollution and greenspace patterns must be examined with respect to wind speed and direction. Other weather-related characteristics are also required.

Conclusion

The relationship between PM pollution and the greenspace pattern was not as straightforward as anticipated. In this study, we took Delhi as an example, one of the most polluted cities in India.This study provides a comprehensive multiscale and seasonal assessment of the influence of GI landscape characteristics on particulate matter (PM2.5 and PM10) pollution in an urban context. Key findings indicate that compositional metrics such as CA and PLAND consistently show strong negative correlations with PM concentrations across all seasons and spatial scales, underscoring the role of vegetation cover in pollutant deposition. Similarly, TE and ED metrics contribute significantly to PM reduction, particularly during the autumn and winter months at lower scales, by enhancing the buffering capacity of green spaces. Configurational metrics such as LPI, LSI, and COH also exhibited scale- and season-specific effectiveness. Their influence on PM pollution was more pronounced at larger spatial scales, highlighting the importance of spatial arrangement and connectivity of GI patches. The study also emphasizes the dual role of GI: while certain configurations reduce PM through improved dispersion and deposition, others—especially dense, high-canopy vegetation in confined spaces—may hinder air circulation and increase PM accumulation. This reinforces the need for context-specific GI design strategies that balance aerodynamic and deposition effects for optimal air quality outcomes. The research perfectly aligns with the government's strategy for reducing air pollution by focusing on airsheds. Overall, the findings provide actionable insights for urban planners and policymakers. By tailoring GI interventions to scale, configuration, and seasonal dynamics, cities can enhance the effectiveness of green infrastructure as a nature-based solution for urban air quality management. Future research incorporating more monitoring stations, high-resolution spatial data, and additional meteorological variables will further refine the understanding of GI–PM dynamics.

Acknowledgements

The authors sincerely thank the Indian Institute of Technology Roorkee for providing the necessary facilities and assistance for this study. The authors express gratitude to the Central Pollution Control Board (CPCB) for providing access to the air quality data used in this study. The authors express gratitude for the support and motivation from colleagues and mentors, whose advice significantly enhanced our study.

References

Agarwal, M., & Tandon, A. (2010). Modeling of the urban heat island in the form of mesoscale wind and of its effect on air pollution dispersal. *Applied Mathematical Modelling*, 34(9), 2520–2530. https://doi.org/10.1016/j.apm.2009.11.016

Ahern, J. (2007). Green infrastructure for cities: The spatial dimension. In *Cities ofthe Future Towards Integrated Sustainable Water and Landscape Management* (pp. 267–283). http://citeseerx.ist.psu.edu/viewdoc/download;jsessionid=E549A4EF0DF3B927AD82A5B40BA1C2B1?doi=10.1.1.558.8386&rep=rep1&type=pdf

AlKhaled, S., Coseo, P., Brazel, A., Cheng, C., & Sailor, D. (2020). Between aspiration and actuality: A systematic review of morphological heat mitigation strategies in hot urban deserts. *Urban Climate*, 31, 100570. https://doi.org/10.1016/j.uclim.2019.100570

Andersson-Sköld, Y., Klingberg, J., Gunnarsson, B., Cullinane, K., Gustafsson, I., Hedblom, M., Knez, I., Lindberg, F., Ode Sang, Å., Pleijel, H., Thorsson, P., & Thorsson, S. (2018). A framework for assessing urban greenery's effects and valuing its ecosystem services. *Journal of Environmental Management*, 205, 274–285. https://doi.org/10.1016/j.jenvman.2017.09.071

Andrew, S. M., Moe, S. R., Totland, Ø., & Munishi, P. K. T. (2012). Species composition and functional structure of herbaceous vegetation in a tropical wetland system. *Biodiversity and Conservation*, 21(11), 2865–2885. https://doi.org/10.1007/s10531-012-0342-y

Ashok, A., Rani, H. P., & Jayakumar, K. V. (2021). Monitoring of dynamic wetland changes using NDVI and NDWI based landsat imagery. *Remote Sensing Applications: Society and Environment*, 23, 100547. https://doi.org/10.1016/j.rsase.2021.100547

Banerjee, T., Murari, V., Kumar, M., & Raju, M. P. (2015). Source apportionment of airborne particulates through receptor modeling: Indian scenario. *Atmospheric Research*, 164–165, 167–187. https://doi.org/10.1016/j.atmosres.2015.04.017

Bartesaghi-Koc, C., Osmond, P., & Peters, A. (2019). Mapping and classifying green infrastructure typologies for climate-related studies based on remote sensing data. *Urban Forestry and Urban Greening*, 37(July 2017), 154–167. https://doi.org/10.1016/j.ufug.2018.11.008

Bartesaghi Koc, C., Osmond, P., & Peters, A. (2018). Evaluating the cooling effects of green infrastructure: A systematic review of methods, indicators and data sources. *Solar Energy*, 166(April), 486–508. https://doi.org/10.1016/j.solener.2018.03.008

Barwise, E. Y. (2023). *Developing a design framework for enhanced air pollution mitigation by urban green infrastructure* [University of Surrey Guildford, Surrey, GU2 7XH, United Kingdom]. https://openresearch.surrey.ac.uk/esploro/outputs/doctoral/Developing-a-design-framework-for-enhanced/99890066602346

Benedict, M. A., McMahon, E., & Conservation Fund (Arlington, V. . (2006). *Green infrastructure : linking landscapes and communities*. Island Press.

Bezyk, Y., Sówka, I., Górka, M., & Blachowski, J. (2021). Gis-based approach to spatio-temporal interpolation of atmospheric co2 concentrations in limited monitoring dataset. *Atmosphere*, 12(3), 1–25. https://doi.org/10.3390/atmos12030384

Calfapietra, C., & Cherubini, L. (2019). Green Infrastructure: Nature-Based Solutions for sustainable and resilient cities. *Urban Forestry and Urban Greening*, 37, 1–2. https://doi.org/10.1016/J.UFUG.2018.09.012

Cao, W., Zhou, W., Yu, W., & Wu, T. (2024). Combined effects of urban forests on land surface temperature and PM2.5 pollution in the winter and summer. *Sustainable Cities and Society*, 104(February), 105309. https://doi.org/10.1016/j.scs.2024.105309

Central Pollution Control Board. (2003). Guidelines for Ambient Air Quality Monitoring. *National Ambient Air Quality Monitoring, NAAQMS*, 2003–2004. https://doi.org/10.1080/15265160903581718

Chatterji, A. (2020). Air Pollution in Delhi: Filling the Policy Gaps. *Observer Research Foundation, December*. https://www.orfonline.org/research/air-pollution-delhi-filling-policy-gaps/

Chelani, A. B., Gajghate, D. G., Tamhane, S. M., & Hasan, M. Z. (2001). Statistical modeling of ambient air pollutants in Delhi. *Water, Air, and Soil Pollution*, 132(3–4), 315–331. https://doi.org/10.1023/A:1013204120867

Chen, M., & Dai, F. (2022). PCA-Based Identification of Built Environment Factors Reducing PM2.5 Pollution in Neighborhoods of Five Chinese Megacities. *Atmosphere*, 13(1). https://doi.org/10.3390/atmos13010115

Chen, M., Dai, F., Yang, B., & Zhu, S. (2019). Effects of neighborhood green space on PM 2 . 5 mitigation : Evidence from five megacities in China. *Building and Environment*, 156(March), 33–45. https://doi.org/10.1016/j.buildenv.2019.03.007

Chen, M., Dai, F., & Zhu, S. (2018). Effects of spatial forms of green infrastructure in block scale on PM10 and PM2.5 removal - A case study of the main city of Wuhan. *Landscape Research Record*, 7.

CleanAirAsia. (2016). *Guidance Framework for Better Air Quality in Asian Cities*.

CPCB. (2013). News Letter CPCB. *Cpcbenvis*, 53(9), 1689–1699.

CPCB. (2015). *CPCB Data Protocol*.

Dhingra, C. (2020). *Assessment of AIR Quality Index for Delhi region_* A comparison between odd-even policy 2019 and Lock Down Period.

Dissanayake, D., Morimoto, T., & Murayama, Y. (2018). Impact of Urban Surface Characteristics and Socio-Economic Variables on the Spatial Variation of Land Surface Temperature in Lagos City, Nigeria. *Sustainability*, 11(25). https://doi.org/10.3390/su11010025

Elhaik, E. (2022). Principal Component Analyses (PCA)-based findings in population genetic studies are highly biased and must be reevaluated. In *Scientific Reports* (Vol. 12, Issue 1). Nature Publishing Group UK. https://doi.org/10.1038/s41598-022-14395-4

Fan, C., Myint, S. W., & Zheng, B. (2015). Measuring the spatial arrangement of urban vegetation and its impacts on seasonal surface temperatures. *Progress in Physical Geography*, 39(2), 199–219. https://doi.org/10.1177/0309133314567583

Forman, R. T. T. (1995). *Some general principles of landscape and regional ecology*. 10(3), 133–142.

Franklin, S. B., Gibson, D. J., Robertson, P. A., Pohlmann, J. T., Fralish, J. S., Scott, B., David, J., Philip, A., John, T., & James, S. (1995). Parallel Analysis : a Method for Determining Significant Principal Components significant principal components. *Journal of Vegetation Scienc*, 6(1), 99–106.

Ganguly, T., Selvaraj, K. L., & Guttikunda, S. K. (2020). National Clean Air Programme (NCAP) for Indian cities: Review and outlook of clean air action plans. *Atmospheric Environment*: X, 8, 100096. https://doi.org/10.1016/j.aeaoa.2020.100096

Gašparović, M., & Dobrinić, D. (2021). Green infrastructure mapping in urban areas using sentinel-1 imagery. *Croatian Journal of Forest Engineering*, 42(2), 337–356. https://doi.org/10.5552/crojfe.2021.859

Ge, M., Fang, S., Gong, Y., Tao, P., Yang, G., & Gong, W. (2021). Understanding the Correlation between Landscape Pattern and Vertical Urban Volume by Time-Series Remote Sensing Data: A Case Study of Melbourne. *ISPRS International Journal of Geo-Information*, 10(1), 14. https://doi.org/10.3390/ijgi10010014

Ginevan, M. E., & Splistone, D. E. (2004). Statistical Tools for Environemntal Quality Measurement. In *Applied Environemntal Statistics* (Vol. 59).

Grafius, D. R., Corstanje, R., & Harris, J. A. (2018). Linking ecosystem services, urban form and green space configuration using multivariate landscape metric analysis. *Landscape Ecology*, 33(4), 557–573. https://doi.org/10.1007/s10980-018-0618-z

Greenpeace. (2020). Toxiz Air: The Price of Fossil Fules (Issue February).

Grimm, N. B., Faeth, S. H., Golubiewski, N. E., Redman, C. L., Wu, J., Bai, X., & Briggs, J. M. (2008). Global Change and the Ecology of Cities. *Science*, 319(February).

Grover, A., & Singh, R. B. (2015). Analysis of urban heat island (UHI) in relation to normalized difference vegetation index (NDVI): A comparative study of delhi and mumbai. *Environments - MDPI*, 2(2), 125–138. https://doi.org/10.3390/environments2020125

Gulia, S., Shiva Nagendra, S. M., Khare, M., & Khanna, I. (2015a). Urban air quality management-A review. *Atmospheric Pollution Research*, 6(2), 286–304. https://doi.org/10.5094/APR.2015.033

Gulia, S., Shiva Nagendra, S. M., Khare, M., & Khanna, I. (2015b). Urban air quality management-A review. *Atmospheric Pollution Research*, 6(2), 286–304. https://doi.org/10.5094/APR.2015.033

Guo, G., Wu, Z., Cao, Z., Chen, Y., & Zheng, Z. (2021). Location of greenspace matters: a new approach to investigating the effect of the greenspace spatial pattern on urban heat environment. *Landscape Ecology*, 0123456789. https://doi.org/10.1007/s10980-021-01230-w

Gupta, U. (2008). Valuation of urban air pollution: A case study of Kanpur City in India. In *Environmental and Resource Economics* (Vol. 41, Issue 3). https://doi.org/10.1007/s10640-008-9193-0

Guttikunda, S. K., & Calori, G. (2013). A GIS based emissions inventory at 1 km × 1 km spatial resolution for air pollution analysis in Delhi, India. *Atmospheric Environment*, 67, 101–111. https://doi.org/10.1016/j.atmosenv.2012.10.040

Guttikunda, S. K., Goel, R., & Pant, P. (2014). Nature of air pollution, emission sources, and management in the Indian cities. *Atmospheric Environment*, 95, 501–510. https://doi.org/10.1016/j.atmosenv.2014.07.006

Guttikunda, S. K., Nishadh, K. A., & Jawahar, P. (2019). Air pollution knowledge assessments (APnA) for 20 Indian cities. *Urban Climate*, 27(November 2018), 124–141. https://doi.org/10.1016/j.uclim.2018.11.005

Heo, S., Bell, M. L., Haven, N., & States, U. (2020). The Influence of Green Space on the Short-term Effects of Particulate Matter on Hospitalization in the U.S. for

2000–2013. *Environment Research*, 174, 61–68. https://doi.org/10.1016/j.envres.2019.04.019

Hirabayashi, S., Kroll, C. N., & Nowak, D. J. (2012). Development of a distributed air pollutant dry deposition modeling framework. *Environmental Pollution*, 171, 9–17. https://doi.org/10.1016/j.envpol.2012.07.002

Hirabayashi, S., Kroll, C. N., & Nowak, D. J. (2015). *i-Tree Eco Dry Deposition Model Descriptions*. http://www.itreetools.org/eco/resources/iTree_Eco_Dry_Deposition_Model_Descriptions.pdf

Hofman, J., Bartholomeus, H., Janssen, S., Calders, K., Wuyts, K., Van Wittenberghe, S., & Samson, R. (2016). Influence of tree crown characteristics on the local PM10 distribution inside an urban street canyon in Antwerp (Belgium): A model and experimental approach. *Urban Forestry and Urban Greening*, 20(2016), 265–276. https://doi.org/10.1016/j.ufug.2016.09.013

Im, J. (2019). Green streets to serve urban sustainability: Benefits and typology. *Sustainability (Switzerland)*, 11(22). https://doi.org/10.3390/su11226483

Impacts, E. (n.d.). *AIR*.

IQAir. (2021). *World Air Qualtiy Report*.

Irga, P. J., Burchett, M. D., & Torpy, F. R. (2015). Does urban forestry have a quantitative effect on ambient air quality in an urban environment? *Atmospheric Environment*, 120, 173–181. https://doi.org/10.1016/j.atmosenv.2015.08.050

Jain, D., Bhatnagar, S., Rathi, V., Sharma, D., & Sachdeva, K. (2021). Mainstreaming Built Environment for Air Pollution Management Plan in Delhi. *Economic and Political Weekly*, 2019, 19–22. https://www.epw.in/journal/2021/6/commentary/mainstreaming-built-environment-air-pollution.html%0Ahttps://www.epw.in/system/files/pdf/2021_56/5/CM_LVI_06_060221_DeeptyJain_6Feb2021_Pages 19-22.pdf

Jalan, I. (2019). *What is Polluting Delhi ' s Air ? Understanding Uncertainties in Emissions Inventories* (Issue March).

Jeanjean, A., Buccolieri, R., Eddy, J., Monks, P., & Leigh, R. (2017). Air quality affected by trees in real street canyons: The case of Marylebone neighbourhood in central London. *Urban Forestry and Urban Greening*, 22, 41–53. https://doi.org/10.1016/j.ufug.2017.01.009

Jeanjean, A. P. R., Monks, P. S., & Leigh, R. J. (2016). Modelling the effectiveness of urban trees and grass on PM2.5 reduction via dispersion and deposition at a city scale. *Atmospheric Environment*, 147, 1–10. https://doi.org/10.1016/j.atmosenv.2016.09.033

Jiang, L., & O'Neill, B. C. (2017). Global urbanization projections for the Shared Socioeconomic Pathways. *Global Environmental Change*, 42, 193–199. https://doi.org/10.1016/j.gloenvcha.2015.03.008

Jiang, R., Xie, C., Man, Z., Afshari, A., & Che, S. (2023). LCZ method is more effective than traditional LUCC method in interpreting the relationship between urban landscape and atmospheric particles. *Science of the Total Environment*, 869(October 2022), 161677. https://doi.org/10.1016/j.scitotenv.2023.161677

Jolliffe, I. T., Cadima, J., & Cadima, J. (2016). Principal component analysis : a review and recent developments Subject Areas. *The Royal Society*, 374.

Kenkel, N. C. (2006). On selecting an appropriate multivariate analysis. *Canadian Journal of Plant Science*, 86(3), 663–676. https://doi.org/10.4141/P05-164

Kotharkar, R., & Bagade, A. (2018). Evaluating urban heat island in the critical local climate zones of an Indian city. *Landscape and Urban Planning*, 169, 92–104. https://doi.org/10.1016/J.LANDURBPLAN.2017.08.009

Kumar, P., Abhijith, K. V., & Barwise, Y. (2019). *Implementing Green Infrastructure for Air Pollution Abatement: General Recommendations for Management and Plant Species Selection. August*. https://doi.org/doi.org/10.6084/m9.figshare.8198261.v1

Kumar, P., Druckman, A., Gallagher, J., Gatersleben, B., Allison, S., Eisenman, T. S., Hoang, U., Hama, S., Tiwari, A., Sharma, A., Abhijith, K. V., Adlakha, D., McNabola, A., Astell-Burt, T., Feng, X., Skeldon, A. C., de Lusignan, S., & Morawska, L. (2019). The nexus between air pollution, green infrastructure and human health. *Environment International*, 133(September). https://doi.org/10.1016/j.envint.2019.105181

Kushwaha, S., & Nithiyanandam, Y. (2019). The study of heat island and its relation with urbanization in Gurugram, Delhi NCR for the period of 1990 to 2018. *International Archives of the Photogrammetry, Remote Sensing and Spatial Information Sciences - ISPRS Archives*, 42(5/W3), 49–56. https://doi.org/10.5194/isprs-archives-XLII-5-W3-49-2019

Lavigne, E., Yasseen, A. S., Stieb, D. M., Hystad, P., Donkelaar, A. Van, Martin, R. V, Brook, J. R., Crouse, D. L., Burnett, R. T., Chen, H., Weichenthal, S., Johnson, M., Villeneuve, P. J., & Walker, M. (2016). Ambient air pollution and adverse birth outcomes : Differences by maternal comorbidities. *Environmental Research*, 148, 457–466. https://doi.org/10.1016/j.envres.2016.04.026

Leão, M. L. P., Zhang, L., & da Silva Júnior, F. M. R. (2023). Effect of particulate matter (PM2.5 and PM10) on health indicators: climate change scenarios in a Brazilian metropolis. *Environmental Geochemistry and Health*, 45(5), 2229–2240. https://doi.org/10.1007/s10653-022-01331-8

Lei, Y., Davies, G. M., Jin, H., Tian, G., & Kim, G. (2021). Scale-dependent effects of urban greenspace on particulate matter air pollution. *Urban Forestry & Urban Greening*, 61(March), 127089. https://doi.org/10.1016/j.ufug.2021.127089

Lei, Y., Duan, Y., He, D., Zhang, X., Chen, L., Li, Y., Gao, Y. G., Tian, G., & Zheng, J. (2018). Effects of urban greenspace patterns on particulate matter pollution in metropolitan Zhengzhou in Henan, China. *Atmosphere*, 9(5), 1–15. https://doi.org/10.3390/ATMOS9050199

Li, K., Li, C., Liu, M., Hu, Y., Wang, H., & Wu, W. (2021). Multiscale analysis of the effects of urban green infrastructure landscape patterns on PM2.5 concentrations in an area of rapid urbanization. *Journal of Cleaner Production*, 325(October), 129324. https://doi.org/10.1016/j.jclepro.2021.129324

Li, X. (2017). Air Pollution: a global Problem Needs local Fixes. *Springer Nature*, 5, 9–11.

Li, X., Zhou, W., & Ouyang, Z. (2013). Relationship between land surface temperature and spatial pattern of greenspace: What are the effects of spatial resolution? *Landscape and Urban Planning*, 114, 1–8. https://doi.org/10.1016/j.landurbplan.2013.02.005

Li, Y. (2016). A Review of Air Pollution Control Policy Development and Effectiveness in China. *Intech*, *i*(tourism), 13.

Liang, L., & Gong, P. (2020). Urban and air pollution: a multi-city study of long-term effects of urban landscape patterns on air quality trends. *Scientific Reports*, 10(1), 1–13. https://doi.org/10.1038/s41598-020-74524-9

Liu, H., & Shen, Y. (2014). *The Impact of Green Space Changes on Air Pollution and Microclimates: A Case Study of the Taipei Metropolitan Area*. 8827–8855. https://doi.org/10.3390/su6128827

Liu, Y., Wu, J., & Yu, D. (2017). Characterizing spatiotemporal patterns of air pollution in China: A multiscale landscape approach. *Ecological Indicators*, 76, 344–356. https://doi.org/10.1016/j.ecolind.2017.01.027

Londoño-Ciro, L. A., & Cañón-Barriga, J. E. (2015). Imputation of spatial air quality data using gis-spline and the index of agreement in sparse urban monitoring networks. In *Revista Facultad de Ingenieria*, 76, 73–81. https://doi.org/10.17533/udea.redin.n76a09

Łowicki, D. (2019). Landscape pattern as an indicator of urban air pollution of particulate matter in Poland. *Ecological Indicators*, 97(September 2018), 17–24. https://doi.org/10.1016/j.ecolind.2018.09.050

Luo, H., Han, Y., Cheng, X., Lu, C., & Wu, Y. (2020). Spatiotemporal Variations in Particulate Matter and Air Quality over China: National, Regional and Urban Scales. *Atmosphere*, 12(1), 43. https://doi.org/10.3390/atmos12010043

Mannucci, P. M., Harari, S., Martinelli, I., & Franchini, M. (2015). Effects on health of air pollution: a narrative review. *Internal and Emergency Medicine*, 10(6), 657–662. https://doi.org/10.1007/s11739-015-1276-7

Mathers, C., Vos, T., & Stevenson, C. (1999). *The burden of disease and injury in Australia* (pp. 216–222).

Mcdonald, A. G., Bealey, W. J., Fowler, D., Dragosits, U., Skiba, U., Smith, R. I., Donovan, R. G., Brett, H. E., Hewitt, C. N., & Nemitz, E. (2007). *Quantifying the effect of urban tree planting on concentrations and depositions of PM 10 in two UK conurbations*. 41, 8455–8467. https://doi.org/10.1016/j.atmosenv.2007.07.025

Mcgarigal, K. (2015). Fragstats. *Fragstats*, April, 1–182.

McGarigal, K. (1995). *FRAGSTATS : Spatial Pattern Analysis Program for Quantifying Landscape Structure*. *August*.

McGarigal, K., Cushman, S. A., Neel, M. C., & Ene, E. (2002). *FRAGSTATS: spatial pattern analysis program for categorical maps* [internet].[cited 2009 October 12]. January 2002.

Meng, F., Tang, W., Gao, J., Ma, T., Li, Y., Du, X., Liu, J., Yang, Y., & Yu, Y. (2025). A Receptor Model and CTM Integrated PM2.5 Source Apportionment Approach and Its Application in 2 + 26 Cities Region of China Apportionment Approach and Its Application in 2 + 26 Cities Region of China. *Atmospheric Science and Meteorology*, 0–15. https://doi.org/10.20944/preprints202503.2207.v1

Menon, J. S., & Sharma, R. (2021). Nature-Based Solutions for Co-mitigation of Air Pollution and Urban Heat in Indian Cities. *Frontiers in Sustainable Cities*, 3(October), 1–11. https://doi.org/10.3389/frsc.2021.705185

Ministry Of Environment & Forests. (1987). *Air pollution control areas in various ut (s)* (Issue February, p. 14012).

Molina, M. J., Molina, L. T., Molina, M. J., & Molina, L. T. (2012). *Megacities and Atmospheric Pollution Megacities and Atmospheric Pollution*. 2247(2004). https://doi.org/10.1080/10473289.2004.10470936

Morelli, X., Rieux, C., Cyrys, J., Forsberg, B., & Slama, R. (2016). *Air pollution , health and social deprivation : A fine-scale risk assessment*. 147, 59–70. https://doi.org/10.1016/j.envres.2016.01.030

Myint, S. W., Zheng, B., Talen, E., Fan, C., Kaplan, S., Middel, A., Smith, M., Huang, H. ping, & Brazel, A. (2015). Does the spatial arrangement of urban landscape matter? examples of urban warming and cooling in phoenix and las vegas. *Ecosystem Health and Sustainability*, 1(4), 1–15. https://doi.org/10.1890/EHS14-0028.1

Nations, U., Programme, E., This, R., United, T., Environment, N., Nations, U., Programme, E., The, D., Nations, U., Programme, E., Nations, U., Programme, E., Nations, U., Programme, E., Nations, U., Programme, E., Pollution, A., This, S. S., Pacific, A., … Coalition, C. A. (2018). Air Pollution in Asia and the Pacific: Science-based solutions. In *United Nations Environment Programme*. http://www.ccacoalition.org/en/resources/air-pollution-asia-and-pacific-science-based-solutions

Nautiyal, S. N., Joshi, V., Gautam, A. S., Kumar, R., Kumar, S., Singh, K., & Gautam, S. (2025). Characterization and source apportionment of PM2.5 and PM10 in a Mountain Valley: seasonal variations, morphology, and elemental composition. *Journal of Atmospheric Chemistry*, 82(1). https://doi.org/10.1007/s10874-025-09469-2

Nowak, D. J., Crane, D. E., & Stevens, J. C. (2006). Air pollution removal by urban trees and shrubs in the United States. *Urban Forestry and Urban Greening*, 4(3–4), 115–123. https://doi.org/10.1016/j.ufug.2006.01.007

NWGITT. (2008). *Green Infrastructure Guide*.

Ou, Y., Rousseau, A. N., Wang, L., & Yan, B. (2017). Spatio-temporal patterns of soil organic carbon and pH in relation to environmental factors—A case study of the Black Soil Region of Northeastern China. *Agriculture, Ecosystems and Environment*, 245(May), 22–31. https://doi.org/10.1016/j.agee.2017.05.003

Ouyang, W., Morakinyo, T. E., Ren, C., Liu, S., & Ng, E. (2021). Thermal-irradiant performance of green infrastructure typologies: Field measurement study in a subtropical climate city. *Science of the Total Environment*, 764, 144635. https://doi.org/10.1016/j.scitotenv.2020.144635

Peters, A. (2011). Ambient Particulate Matter and the Risk for Cardiovascular Disease. *Progress in Cardiovascular Diseases*, 53, 327–333. https://doi.org/10.1016/j.pcad.2011.02.002

Power, A. L., Tennant, R. K., Stewart, A. G., Gosden, C., Worsley, A. T., Jones, R., & Love, J. (2023). The evolution of atmospheric particulate matter in an urban landscape since the Industrial Revolution. *Scientific Reports*, 13(1), 1–15. https://doi.org/10.1038/s41598-023-35679-3

Ramadan, B. S., Budihardjo, M. A., Syafrudin, Huboyo, H. S., & Sari, S. A. (2025). Analysis of particulate matter (PM10 and PM2.5) emissions from Jatibarang landfill: implications for air quality and health. *IOP Conference Series: Earth and Environmental Science*, 1477(1). https://doi.org/10.1088/1755-1315/1477/1/012033

Ramaiah, M., & Avtar, R. (2019). Urban Green Spaces and Their Need in Cities of Rapidly Urbanizing India: A Review. *Urban Science*, 3(3), 94. https://doi.org/10.3390/urbansci3030094

Ramani, P., Shah, C., Parikh, D., & Dadhaniya, B. (2019). Air pollution effect on urban areas. *Pramana Research Journal*, 9(9), 1–12.

Ramyar, R., & Zarghami, E. (2017). Green infrastructure contribution for climate change adaptation in urban landscape context. *Applied Ecology and Environmental Research*, 15(3), 1193–1209. https://doi.org/10.15666/aeer/1503_11931209

Rezaei, N., & Millard-Ball, A. (2023). Urban form and its impacts on air pollution and access to green space: A global analysis of 462 cities. *PLoS ONE*, 18(1 January), 1–26. https://doi.org/10.1371/journal.pone.0278265

Rohde, R. A., & Muller, R. A. (2015). Air Pollution in China : Mapping of Concentrations and Sources. *PLoS ONE*, 2, 1–14. https://doi.org/10.1371/journal.pone.0135749

Role, T. (2021). *Integrating Clean Air* , Climate , and Health Policies in the COVID-19 Era. March.

Sangkham, S., Phairuang, W., Sherchan, S. P., Pansakun, N., Munkong, N., Sarndhong, K., Islam, M. A., & Sakunkoo, P. (2024). An update on adverse health effects from exposure to PM2.5. *Environmental Advances*, 18(September), 100603. https://doi.org/10.1016/j.envadv.2024.100603

Saraswat, I., Mishra, R. K., & Kumar, A. (2017). Estimation of PM10 concentration from Landsat 8 OLI satellite imagery over Delhi, India. *Remote Sensing Applications: Society and Environment*, 8(April), 251–257. https://doi.org/10.1016/j.rsase.2017.10.006

Sathyakumar, V., Ramsankaran, R. A. A. J., & Bardhan, R. (2020). Geospatial approach for assessing spatiotemporal dynamics of urban green space distribution among neighbourhoods: A demonstration in Mumbai. *Urban Forestry and Urban Greening*, 48(December 2019), 126585. https://doi.org/10.1016/j.ufug.2020.126585

Schneekloth, L. H. (2000). Urban green infrastructure. In *Time-Saver Standards for Urban* Design (Issue 1987).

Selmi, W., Weber, C., Rivière, E., Blond, N., Mehdi, L., & Nowak, D. (2016). Air pollution removal by trees in public green spaces in Strasbourg city, France. *Urban Forestry and Urban Greening*, 17(2), 192–201. https://doi.org/10.1016/j.ufug.2016.04.010

Shareef, M. M., Husain, T., & Alharbi, B. (2016). Optimization of Air Quality Monitoring Network Using GIS Based Interpolation Techniques. *Journal of Environmental Protection*, 7(6), 895–911. https://doi.org/10.4236/jep.2016.76080

Sharma, S. K., Mandal, T. K., Saxena, M., Rashmi, Rohtash, Sharma, A., & Gautam, R. (2014). Source apportionment of PM10 by using positive matrix factorization at an urban site of Delhi, India. *Urban Climate*, 10, 656–670. https://doi.org/10.1016/j.uclim.2013.11.002

Singh, N., Singh, S., & Mall, R. K. (2020). Urban ecology and human health: implications of urban heat island, air pollution and climate change nexus. In *Urban Ecology*. Elsevier Inc. https://doi.org/10.1016/b978-0-12-820730-7.00017-3

Singh, P., & Tyagi, A. (2013a). Applying Kriging Approach on Pollution Data Using GIS Software. *International Journal of Environmental Engineering and Management*, 4(3), 185–190. http://www.ripublication.com/ijeem.htm

Singh, V., Guizani, N., Al-Alawi, A., Claereboudt, M., & Rahman, M. S. (2013b). Instrumental texture profile analysis (TPA) of date fruits as a function of its physico-chemical properties. *Industrial Crops and Products*, 50, 866–873. https://doi.org/10.1016/j.indcrop.2013.08.039

Sinnett, D., Smith, N., & Burgess, S. (2015). Handbook on green infrastructure: Planning, design and implementation. *Handbook on Green Infrastructure: Planning, Design and Implementation*, 1–474. https://doi.org/10.4337/9781783474004

Song, Z., Li, R., Qiu, R., Liu, S., Tan, C., Li, Q., Ge, W., Han, X., Tang, X., Shi, W., Song, L., Yu, W., Yang, H., & Ma, M. (2018). Global land surface temperature influenced by vegetation cover and PM 2.5 from 2001 to 2016. *Remote Sensing*, 10(12), 1–18. https://doi.org/10.3390/rs10122034

Soni, P. (2021). Effects of COVID-19 lockdown phases in India: an atmospheric perspective. *Environment, Development and Sustainability*, 0123456789. https://doi.org/10.1007/s10668-020-01156-4

Soydan, O. (2020). Effects of landscape composition and patterns on land surface temperature: Urban heat island case study for Nigde, Turkey. *Urban Climate*, 34(December 2019), 100688. https://doi.org/10.1016/j.uclim.2020.100688

Srbinovska, M., Andova, V., Mateska, A. K., & Krstevska, M. C. (2021). The effect of small green walls on reduction of particulate matter concentration in open areas. *Journal of Cleaner Production*, 279, 123306. https://doi.org/10.1016/j.jclepro.2020.123306

Tallis, M. J., Amorim, J. H., Calfapietra, C., & Smith, P. F. (2015). The impacts of green infrastructure on air quality and temperature. In *Handbook on Green Infrastructure: Planning, design and implementation* (Issue January 2016). https://doi.org/10.4337/9781783474004.00008

Thiis, T. K., Gaitani, N., Burud, I., & Engan, J. A. (2018). Classification of urban blue green structures with aerial measurements. *International Journal of Sustainable Development and Planning*, 13(4), 506–515. https://doi.org/10.2495/SDP-V13-N4-506-515

Tiwari, A., & Kumar, P. (2020). Integrated dispersion-deposition modelling for air pollutant reduction via green infrastructure at an urban scale. *Science of the Total Environment*, 723, 138078. https://doi.org/10.1016/j.scitotenv.2020.138078

Tomson, N., Michael, R. N., & Agranovski, I. E. (2025). Classic Theory of Aerosol Filtration for Application to Urban Green Infrastructure. *Water, Air, and Soil Pollution*, 236(3), 1–9. https://doi.org/10.1007/s11270-025-07829-y

UNDESA. (2019). World population prospects 2019. In *Department of Economic and Social Affairs. World Population Prospects* 2019. (Issue 141).

Urban Climate Lab. (2016). *The benefits of green infrastructure for heat mitigation and emissions reductions in cities*. June.

US EPA, OW, O. (2010). *What is Green Infrastructure?*

Vieira, J., Matos, P., Mexia, T., Silva, P., Lopes, N., Freitas, C., Correia, O., Santos-Reis, M., Branquinho, C., & Pinho, P. (2018). Green spaces are not all the same for the provision of air purification and climate regulation services: The case of urban parks. *Environmental Research*, 160(October 2017), 306–313. https://doi.org/10.1016/j.envres.2017.10.006

Vieira, L., Polisel, R., Ivanauskas, N., Shepherd, G., Waechter, J., Yamamoto, K., & Martins, F. (2015). Geographical patterns of terrestrial herbs : a new component in planning the conservation of the Brazilian. *Biodivers Conserv*, 24, 2181–2198. https://doi.org/10.1007/s10531-015-0967-8

WHO. (2018). *World Health Organization releases new global air pollution data | Climate & Clean Air Coalition*. 1–11. https://www.ccacoalition.org/en/news/world-health-organization-releases-new-global-air-pollution-data

Wu, H., Yang, C., Chen, J., Yang, S., Lu, T., & Lin, X. (2018). Effects of Green space landscape patterns on particulate matter in Zhejiang Province, China. *Atmospheric Pollution Research*, 9(5), 923–933. https://doi.org/10.1016/j.apr.2018.03.004

Wu, J., Xie, W., Li, W., & Li, J. (2015). Effects of urban landscape pattern on PM2.5 Pollution-A Beijing Case Study. *PLoS ONE*, 10(11), 1–20. https://doi.org/10.1371/journal.pone.0142449

Wu, X., Chen, Y., Guo, J., Wang, G., & Gong, Y. (2017). Spatial concentration, impact factors and prevention-control measures of PM2.5 pollution in China. *Natural Hazards*, 86(1), 393–410. https://doi.org/10.1007/s11069-016-2697-y

Yale and Columbia Universities. (2022). *Environmental Performance Index* (Vol. 1, Issue June).

Yang, H., Wu, M., Liu, W., Zhang, Z., Zhang, N., & Wan, S. (2011). Community structure and composition in response to climate change in a temperate steppe. *Global Change Biology*, 17(1), 452–465. https://doi.org/10.1111/j.1365-2486.2010.02253.x

Yao, M., Smith, M., & Peng, C. (2025). Modelling the effects of vegetation and urban form on air quality in real urban environments: A systematic review of measurements, methods, and predictions. In *Urban Forestry and Urban Greening* (Vol. 105). https://doi.org/10.1016/j.ufug.2025.128693

Yu, X., & Jingyi L, Y. H. (2019). A Review of the Relationship Between Urban Green Morphology and Urban Climate. *Urban Morphology Theory*, 23(10), 835–846.

Yu, Z., Wang, Y., Deng, J., Shen, Z., Wang, K., Zhu, J., & Gan, M. (2017). Dynamics of hierarchical urban green space patches and implications for management policy. *Sensors (Switzerland)*, 17(6). https://doi.org/10.3390/s17061304

Zhang, R., Chen, G., Yin, Z., Zhang, Y., & Ma, K. (2021a). Urban greening based on the supply and demand of atmospheric. *Ecological Indicators*, 126, 107696. https://doi.org/10.1016/j.ecolind.2021.107696

Zhang, R., Chen, G., Yin, Z., Zhang, Y., & Ma, K. (2021b). Urban greening based on the supply and demand of atmospheric PM2.5 removal. *Ecological Indicators*, 126, 107696. https://doi.org/10.1016/j.ecolind.2021.107696

Zhang, S., Ban, Y., Xu, Z., Cheng, J., & Li, M. (2016). Comparative evaluation of influencing factors on aquaculture wastewater treatment by various constructed wetlands. *Ecological Engineering*, 93, 221–225. https://doi.org/10.1016/j.ecoleng.2016.05.029

Zhang, X., Xi, Z., Li, X., Wang, C., Qiu, L., & Gao, T. (2024). Urban green space influencing air particulate matter concentration at different spatial scales base on land use regression model Urban green space influencing

air particulate matter concentration at different 2 spatial scales base on land use regression m. *Sustainability*, 3. https://ssrn.com/abstract=4684225

Zheng, D., Zhang, G., Shan, H., Tu, Q., Wu, H., & Li, S. (2020). Spatio-temporal evolution of urban morphology in the Yangtze River Middle Reaches Megalopolis, China. *Sustainability (Switzerland)*, 12(5), 1–15. https://doi.org/10.3390/su12051738

Zhou, W., Huang, G., & Cadenasso, M. L. (2011). Does spatial configuration matter? Understanding the effects of land cover pattern on land surface temperature in urban landscapes. *Landscape and Urban Planning*, 102(1), 54–63. https://doi.org/10.1016/j.landurbplan.2011.03.009

Zhou, W., Shen, X., Cao, F., Sun, Y., & Ph, D. (2019). *Effects of Area and Shape of Greenspace on Urban Cooling in Nanjing* , China. 145(4), 1–9. https://doi.org/10.1061/(ASCE)UP.1943-5444.0000520

Zhou, Y., Liu, H., Zhou, J., & Xia, M. (2019). GIS-based urban afforestation spatial patterns and a strategy for PM2.5 removal. *Forests*, 10(10), 1–17. https://doi.org/10.3390/f10100875